

Biphasic influence of *Staphylococcus aureus* and  
*Staphylococcus epidermidis* on epidermal Tight  
Junctions in submerged and 3D tissue culture

**Dissertation**

with the aim of achieving the doctoral degree

Doctor rerum naturalium (Dr. rer. nat)

at the Faculty of Mathematics, Informatics and Natural Sciences

Department of Biology of

University Hamburg

submitted by

**Katja Bäsler**

2017 in Hamburg

**Day of oral defense: December 15<sup>th</sup>, 2017**

**Evaluators**

Prof. Dr. Johanna M. Brandner

Prof. Dr. Thorsten Burmester

**Lists of abbreviations and symbols..... IV**

<b>1</b>	<b>Introduction .....</b>	<b>1</b>
1.1	The skin.....	1
1.2	Epidermal modelling .....	3
1.3	Tight Junctions (TJs) .....	5
1.4	Tight Junctions in the epidermis .....	8
1.4.1	Tight Junctions and other skin barrier components .....	10
1.5	The cutaneous microbiome – boon and bane .....	13
1.6	<i>Staphylococcus</i> .....	14
1.7	The accessory gene regulator ( <i>agr</i> ).....	17
1.8	Tight Junctions and skin infections in diseased skin .....	19
1.8.1	Atopic Dermatitis (AD) .....	20
1.9	Aim of the thesis.....	25
<b>2</b>	<b>Material and methods .....</b>	<b>26</b>
2.1	Chemicals and media .....	26
2.2	Devices .....	28
2.3	Antibodies and Primer.....	29
2.4	Software .....	30
2.5	Cells and tissue .....	30
2.6	Bacterial strains .....	30
2.7	Cell and tissue culture .....	31
2.7.1	Primary culture of human keratinocytes and fibroblasts .....	31
2.7.2	Keratinocyte submerged culture.....	35
2.7.3	3D models.....	37
2.7.4	Bacterial culture and inoculation .....	40
2.7.5	Barrier assays .....	45
2.8	Molecular biological and biochemical analyses .....	48
2.8.1	Protein analyses by Western Blotting .....	48
2.8.2	mRNA analyses by quantitative real-time PCR .....	51
2.8.3	Analyses of protein levels of cytokines .....	52
2.9	Stainings/histological methods .....	52
2.9.1	Tissue-MTT .....	52
2.9.2	Fixation in formalin and embedding in paraffin.....	53

2.9.3	Haematoxylin and Eosine (H&E) staining.....	54
2.9.4	Immunohistochemical stainings.....	54
2.10	Statistical analyses.....	56
<b>3</b>	<b>Results.....</b>	<b>57</b>
3.1	Results, Part 1: Investigation of different model systems in order to find those suited best for Tight Junction analyses and staphylococcal treatment.....	57
3.1.1	Submerged model .....	57
3.1.2	3D reconstruction.....	59
3.2	Results, Part 2: Investigation of the effect of staphylococcal inoculation on Tight Junctions in submerged models.....	69
3.2.1	<i>S. epidermidis</i> and <i>S. aureus</i> first increase and later on decrease Tight Junction barrier function in submerged models .....	69
3.2.2	Cell death is not the cause for decreased barrier function .....	71
3.2.3	Investigations on Tight Junction protein localisation patterns.....	72
3.2.4	Investigations on Tight Junction protein expression and protein levels .....	74
3.2.5	Investigations of antimicrobial peptides and proinflammatory cytokines.....	78
3.2.6	Investigations on bacterial virulence factors .....	82
3.3	Results, Part 3: Investigation of the effect of staphylococcal treatment on Tight Junctions in reconstructed human epidermis (PFe3D).....	84
3.3.1	<i>S. aureus</i> and <i>S. epidermidis</i> grow and live on top of the models .....	84
3.3.2	The growth of <i>S. aureus</i> can be reduced by <i>S. epidermidis</i> .....	85
3.3.3	Morphological investigations of PFe3D after <i>S. epidermidis</i> or <i>S. aureus</i> inoculation.....	86
3.3.4	Investigations on overall barrier function of PFe3D after <i>S. epidermidis</i> and <i>S. aureus</i> inoculation.....	86
3.3.5	Investigations on Tight Junction functionality of PFe3D after <i>S. epidermidis</i> and <i>S. aureus</i> inoculation .....	87
3.3.6	Infection of PFe3D with <i>S. aureus</i> did not result in cell death.....	89
3.3.7	Investigations on Tight Junction protein localisation patterns.....	90
3.3.8	Investigations on Tight Junction protein levels.....	93
3.4	Results, Part 4: Atopic dermatitis mimicking conditions .....	96
<b>4</b>	<b>Discussion.....</b>	<b>100</b>
4.1	Results, Part 1: Finding the right model system .....	100
4.2	Suitability of submerged and PFe3D models for bacterial infection approaches .	105
4.3	Results, Parts 2 and 3: Biphasic influence of live <i>S. aureus</i> and <i>S. epidermidis</i> on epidermal Tight Junctions .....	107



4.3.1	<i>S. aureus</i> and <i>S. epidermidis</i> strengthen Tight Junction barrier function during short-term inoculation via different mechanisms .....	107
4.3.2	Live <i>S. epidermidis</i> and <i>S. aureus</i> impair Tight Junction barrier function after long-term inoculation.....	114
4.3.3	<i>S. epidermidis</i> – commensal or not? .....	120
4.3.4	The occludin discrepancies .....	120
4.3.5	Summary and future prospective of Results, Part 2 and 3 .....	122
4.4	Results, Part 4: Atopic dermatitis mimicking conditions .....	124
<b>Abstract .....</b>		<b>127</b>
<b>Zusammenfassung .....</b>		<b>128</b>
<b>References .....</b>		<b>130</b>
<b>Lists of Figures and Tables .....</b>		<b>150</b>
<b>Danksagung .....</b>		<b>154</b>
<b>Certificate of Language Proof .....</b>		<b>155</b>
<b>Declaration of authorship .....</b>		<b>156</b>
<b>Eidesstattliche Versicherung .....</b>		<b>156</b>

## LISTS OF ABBREVIATIONS AND SYMBOLS

A detailed List of abbreviations used within this work can be found in Table 1.

**Table 1: List of abbreviations used in this work.**

Abbreviation	Meaning
3D	3-Dimensional
AB	Antibiotics
AD	Atopic Dermatitis
<i>agr</i>	Accessory gene regulator
AIP	Autoinducing peptide
ALI	Air-liquid-interface
AMP	Antimicrobial peptide
ANOVA	Analysis of variance
APS	Ammonium persulfate
Aqua dest.	Distilled water (Latin: <i>aqua destillata</i> )
BHI	Brain heart infusion
BSA	Bovine serum albumin
cDNA	Complementary deoxyribonucleic acid
CFU	Colony forming units
CH	Switzerland
Cldn	Claudin
CnTe3D	Reconstructed human epidermis according to the protocol of CellnTec
CTM	Cytokine-Toll-like-receptor-agonist-Mix
DE	Germany
DMEM	Dulbecco's Modified Eagle Medium
DMSO	Dimethyl sulfoxide
DNA	Deoxyribonucleic acid
e.g.	For example (Latin: <i>exempli gratia</i> )
EDTA	Ethylenediaminetetraacetic acid
et al.	And others (Latin: <i>et alii</i> )
F	France
FCS	Fetal calf serum
FD4	Fluorescein isothiocyanate dextran (4 kDa)
GFP	Green fluorescent protein
GM-CSF	Granulocyte-macrophage colony-stimulating factor
HaCaT	Human adult low calcium high temperature keratinocytes (keratinocyte cell line)
HBSS	Hanks' Balanced Salt Solution
HKGS	Human keratinocyte growth supplement
h $\beta$ D3	Human Beta defensin 3
IFN	Interferon
IgE	Immunoglobulin E
IHC	Immunohistochemical
IL	Interleukin
JAM	Junctional adhesion molecule
KGF/FGF-7	Keratinocyte growth factor, also known as fibroblast growth factor-7
KGM2	Keratinocyte growth medium 2
MDCK	Madin-Darby canine kidney cells (epithelial cell line)
mRNA	Messenger ribonucleic acid
MTT	3-(4,5-dimethylthiazol-2-yl)-2,5-diphenyltetrazolium bromide
NHEKs	Normal human epidermal keratinocytes

Abbreviation	Meaning
NL	Netherlands
Ocln	Occludin
OD <sub>600</sub>	Optical density measured at a wavelength of 600 nm
p	Probability value
Pam3CSK4	Toll-like receptor 1/2 (TLR1/2) agonist (synthetic triacylated lipopeptide: Pam <sub>3</sub> - Cys-Ser-Lys-Lys-Lys-Lys)
PBS	Phosphate-buffered saline
PCF	Polycarbonate-filter
PCR	Polymerase chain reaction
PFe3D	Reconstructed human epidermis according to the protocol of Pierre Fabre
Poly I:C	Toll-like receptor 3 agonist (Polyinosinic:polycytidylic acid)
PRR	Pattern recognition receptor
RFP	Red fluorescent protein
RHE	Reconstructed human epidermis
RHS	Reconstructed human skin
RNA	Ribonucleic acid
ROI	Region of interest
RPMI	Roswell Park Memorial Institute medium
S.	<i>Staphylococcus</i>
SB	<i>Stratum basale</i>
SC	<i>Stratum corneum</i>
SDS	Sodium dodecyl sulfate
SEM	Standard Error of the Mean
SG	<i>Stratum granulosum</i>
SKDM	Supplemented keratinocyte defined medium
SNP	Single-nucleotide polymorphism
spp.	Species
SS	<i>Stratum spinosum</i>
SSL	Staphylococcal superantigen-like protein
TAMP	Tight junction-associated marvel protein
TBST	Tris-buffered saline and tween 20
TEC	Tris-EDTA-citrat
TER	Transepithelial electrical resistance
Th2	T helper cells type 2
TJ	Tight junction
TLR	Toll-like receptor
TMED	Tetramethylethylenediamine
TNF	Tumor necrosis factor
UK	United kingdom
USA	United states of america
w/o	Without
WB	Western blot
WT	Wil-type
ZO	Zonula occludens

A detailed list of measurement units and symbols used within this work can be found in Table 2.

**Table 2: List of measurement units and symbols used in this work.**

Measurement unit / Symbol	Meaning
%	Percent
~	Approximately
<	Less than
>	Greater than
°C	Degree Celsius
μg	Microgram
μl	Microliter
μm	Micrometer
μM	Micromolar
Å	Ångström
cm	Centimeter
Da	Dalton
g	Gravitational force
h	Hour/Hours
kDa	Kilo dalton
l	Liter
mg	Milligram
min	Minute/Minutes
ml	Milliliter
mM	Millimolar
mm	Millimeter
mmol	Millimol
N	Normal
ng	Nanogram
nm	Nanometer
P	Permeability
pH	Potential of hydrogen
pmol	Picomol
s	Seconds
V	Volt
W	Watt
α	Alpha
β	Beta
γ	Gamma
Δ	Delta
Ω	Ohm

# 1 INTRODUCTION

---

## 1.1 The skin

The skin, our largest organ, is the first line of defence to protect the body from external factors. It interfaces with the environment and therefore provides a barrier against different kinds of disturbances such as physical disruption, allergens, and bacterial, fungal or viral infection. It not only presents an outside-in barrier but also an inside-out barrier to maintain water and nutrient homeostasis, and therefore protects the organism from dehydration. Nevertheless, the skin not only functions as a barrier, further responsibilities are: sensation, thermoregulation and control of evaporation and absorption of gases (Kenshalo, 1970; Scheuplein and Blank, 1971).

The mammalian skin consists of three fundamental layers (Figure 1). The lowermost layer is the subcutaneous tissue where subcutaneous fat is most widely distributed to act as padding, energy reservoir and provides some thermoregulation. The next layer is the dermis, which mainly consists of elastin and collagen (produced by fibroblasts), elastic fibres and extrafibrillar matrix. This connective tissue hosts mechano- and thermoreceptors, hair follicles and diverse types of glands. Blood vessels cross the dermal structure and provide nourishment and waste removal for both dermal and epidermal cells (Figure 1). Being tightly connected to the dermis via a basement membrane, the uppermost layer, the epidermis, is formed by different strata, which means from inside out: *Stratum basale* (SB), *Stratum spinosum* (SS), *Stratum granulosum* (SG) and *Stratum corneum* (SC) (Figure 1). Maintaining the epidermal scaffold, keratinocytes represent about 90% of cellular proportion (Moll, 2016). Other important cell types are present as well, such as melanocytes that provide the pigment melanin, local immune cells (e.g. Langerhans cells), neuroendocrine Merkel cells and lymphocytes (Moll, 2016). In addition, nerve fibres also find their way through the outermost layer of the body. Epidermal structuring is highly organised. Keratinocyte stem cells within the SB proliferate continuously to regenerate the epidermis and produce progenitors that go on to terminally differentiate (Li et al., 1998). During the differentiation process, keratinocytes undergo distinct changes and each layer/stratum can be characterised by its expression pattern of typical differentiation markers. These are mainly proteins that are restricted to one or more defined layers as shown in Figure 1 (e.g. Keratins 5 or 14 in SB or Keratins 1 or 10 in the suprabasal layers of SS and SG). They can be visualized

for example by fluorescent antibody staining and subsequent fluorescent light microscopy, but also under normal light microscopic conditions, e.g. with Haematoxylin and Eosin staining, the epidermal structuring can be easily seen. Whereas in SB the keratinocytes are structured in palisades, they become more and more flattened from SS to SG when they finally end as dead and totally flattened cells in SC.

Directly beneath the SC, in SG, the typical tight junction (TJ) structures are found providing an additional physical barrier (see below) (Brandner et al., 2002; Kirschner et al., 2010) e.g. for a 557 Da tracer (Figure 1).

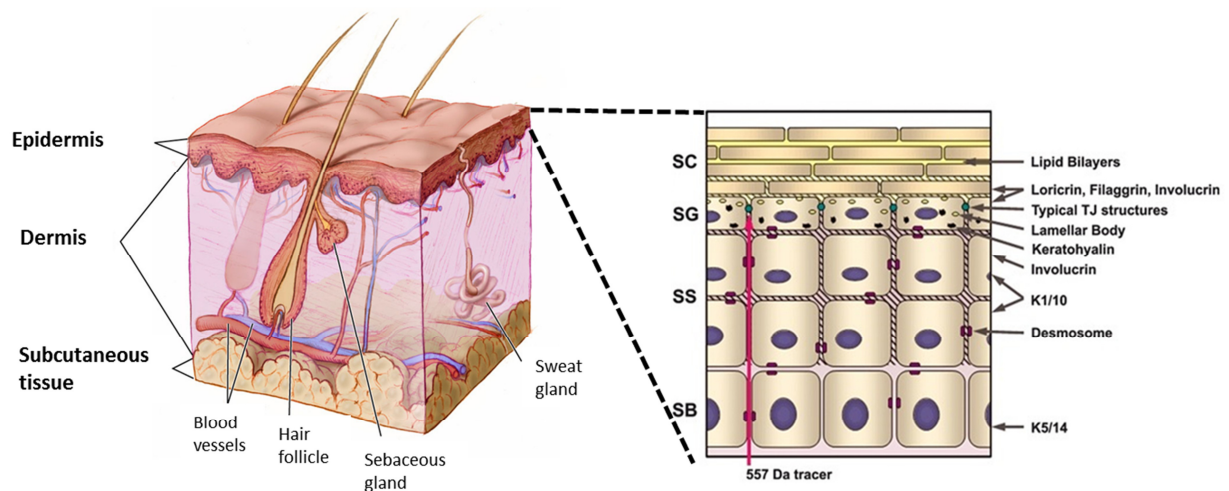


**Figure 1: Schematic overview on the skin composition, in particular the epidermal composition.** SB – *Stratum basale*; SS – *Stratum spinosum*; SG – *Stratum granulosum*; SC – *Stratum corneum*; K – keratin; TJ – tight junction (Modified from an original (ID: 4604) of Don Bliss, 2010 for the National Cancer Institute, Public Domain and with permission from Kirschner et al., 2012).

The process of terminal differentiation, resulting in cornification of keratinocytes, is essential for building a SC and thereby fulfilling the barrier function of the skin (Candi et al., 2005). Briefly, the first step of terminal differentiation is the initiation phase, which starts in the first suprabasal layer in SS where structural proteins and lipids of the SC are synthesised. Transglutaminases -1 and -5 connect envoplakin and periplakin, and anchor them to the desmosomes. The second step is the reinforcement phase, which takes place in the SG, and entails the covalent attachment of some lipids to the cornified-envelope proteins. Concomitantly for reinforcement of terminal differentiation, lipid-envelope-formation steps take place. Finally, cornification ends in the SC where the flattened and dead corneocytes (formed as flattened tetrakaidecahedrons (Feuchter et al., 2006)) combine together with an insoluble lipid scaffold and form the horny layer. These corneocytes mostly consist of keratin intermediate filaments embedded in a filaggrin (filament-aggregating-protein) matrix. Corneocytes are tightly attached to each other by corneodesmosomes, which are modified

desmosomal structures. These are proteolytically degraded in the uppermost layers of the cornified envelope to allow desquamation (Serre et al., 1991; Candi et al., 2005).

Concerning skin research, as most research on human health and disease, it is not possible to investigate all fields of interest with *in vivo* or *ex vivo* human or animal skin due to limitations on donation as well as for ethical considerations. Therefore *in vitro* approaches are a necessary tool when investigating skin biology.

## 1.2 Epidermal modelling

Growing large numbers of keratinocytes was a problem for a long time which was solved over 40 years ago by Rheinwald and Green (1975). They described culture conditions that induced maturation of a teratogenic cell line, which mimicked epidermal keratinisation (Rheinwald and Green, 1975a) indicating that the same conditions might be favourable for growing normal human epidermal keratinocytes (NHEKs) as well. Indeed, from then on NHEKs were grown easily (Rheinwald and Green, 1975b). This first model medium contained serum, the epidermal growth factor, insulin and cholera toxin (for its positive effect on cyclic adenosine monophosphate production) as well as a feeder-layer of irritated fibroblasts. Over the years culture media were improved and serum-free conditions were developed in order to reduce variability within experiments, to reduce the risk of disease transmissions and for ethical reasons. The next important step in the development of epidermal modelling was the discovery of different calcium concentrations to regulate growth and differentiation in mouse keratinocytes (Hennings et al., 1980), which was later on adapted to NHEKs as well and showed the influence of calcium on cell-cell interactions in particular on stratification of keratinocytes through the formation of desmosomes (Boyce and Ham, 1983). However, not only high calcium conditions but also the cell density (being confluent) as well as the cell detachment from the culture substrate are important regulators of epidermal differentiation (Radoja et al., 2006). Culturing keratinocytes as monolayers already is a highly useful tool in basic research on this cell type. But under these conditions the development of a cornified layer does not occur (Madison et al., 1989; Eckhart et al., 2000), which is important for investigations that aim to mimic the *in vivo* situation.

Finally the ground-breaking process was developed in 1983 by Pruniéras et al., who achieved full differentiation *in vitro* by raising the keratinocytes up to the air-liquid-interface (ALI) and culturing the cells on a de-epidermised dermis (Pruniéras et al., 1983). The interface with air

stimulates the granular phenotype, which does not appear in submerged culture (Poumay and Coquette, 2007).

Subsequently, reconstruction of human epidermis or even skin became a highly useful tool to investigate epidermal properties. These reconstructs are continually developing, and more closely resemble the *in vivo* situation, making them an important alternative to animal models as they are built with human cells and avoid animal experiments. An example of a reconstructed human epidermis (RHE), with ALI-keratinocytes growing on a filter-membrane and reflecting *in vivo* epidermal structuring, is shown in Figure 2.

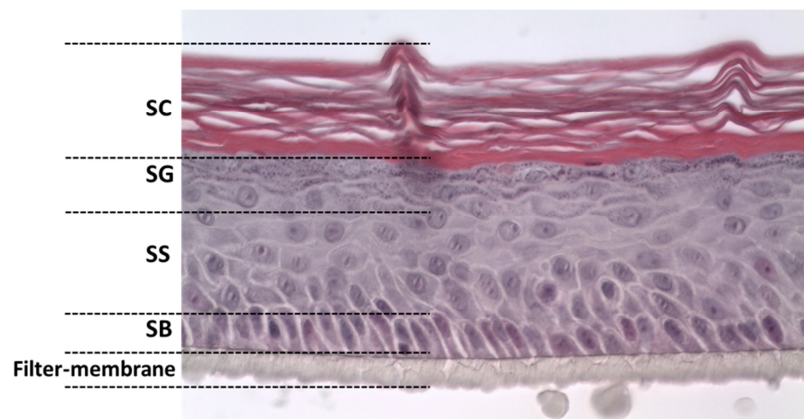


**Figure 2: Reconstructed human epidermis under air-liquid-interface (ALI) conditions.** Normal human epidermal keratinocytes grown on a filter-membrane provide a palisade-like structure in *Stratum basale* (SB), followed by several layers of *Stratum spinosum* (SS), as well as a *Stratum granulosum* (SG) composing keratohyalin granules, and several layers of dead and flattened cells in *Stratum corneum* (SC) (This exemplary model was built within this work after the protocol of CellnTec cultured for 14 days in ALI).

Another important aspect of using epidermal or skin reconstructions is the possibility to investigate specific diseased conditions as e.g. the influences of single cytokines or mixtures or other compounds of interest. However, as a lot of research was/is performed on epidermal modelling, it is clear, that over the years a lot of different models have been developed and one has to find the system being the most appropriate for the analyses of interest, as e.g. for this work the analysis of tight junctions.



### 1.3 Tight Junctions (TJs)

“For this study we have surveyed a number of epithelia, particularly those of the mucosae of cavitory organs, and in all cases investigated we have found a characteristic junctional complex between adjacent epithelial cells. The arrangement varies in detail from one epithelium to another but typically consists of three successive components to be described as tight junction (zonula occludens), intermediate junction (zonula or fascia adhaerens), and desmosome (macula adhaerens). The tight junction is located the closest to the lumen and the desmosome the farthest away from it.” (Farquhar and Palade, 1963)

In general, TJs are complex cell-cell junctions localized in the apical part of the lateral plasma membrane of cells in simple and multi-layered epithelia as well as endothelia (e.g. in lung, intestine, blood vessels, or epidermis). After the first recognition of TJs with transmission electron microscopy (Farquhar and Palade, 1963), for a long time TJs were believed to be a static, impermeable barrier. In electron microscopic images they appear as very narrow contacts of the plasma membranes of two neighbouring cells, so called “kissing points” (Figure 3 A and C) (Tsukita et al., 2001). With freeze-fracture electron microscopy it was shown that TJs are a network of anastomosing strands composed of small punctae (Figure 3 B and C).

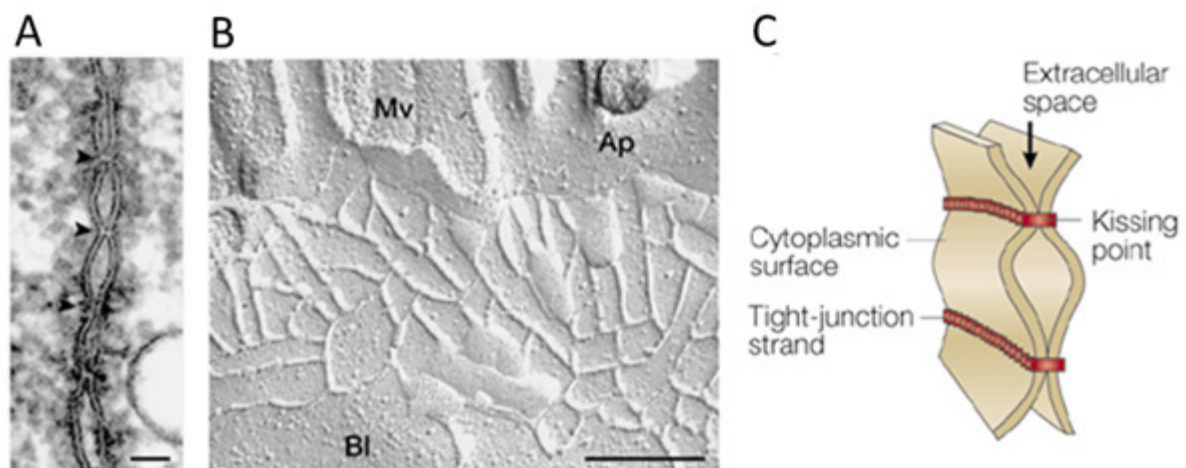


**Figure 3: Ultrathin sectional view of tight junctions (TJs).** Kissing points of TJs (arrowheads) obtained with transmission electron microscopy (Scale bar, 50 nm) (A). Freeze-fracture replica electron microscopy of intestinal epithelial cells. TJs appear as continuous, anastomosing intramembranous particle strands (Mv – microvilli; Ap – apical membrane; Bl – basolateral membrane) (Scale bar, 200 nm) (B). Schematic of three-dimensional structure of TJs (C) (modified with permission from Tsukita et al. (2001)).

For quite a long time two models existed to describe the chemical nature of these TJ strands. In the ‘protein model’, TJ strands were described as units of integral membrane proteins that are polymerized linearly between adjacent cells. Whereas the ‘lipid model’ proposed lipids that are organized in inverted cylindrical micelles to constitute the TJ strands (Kachar and Reese, 1982; Tsukita et al., 2001). However, the identification of several TJ-specific integral membrane proteins favoured the ‘protein model’.

In 1973, Claude and Goodenough positively correlated the number of strands in different epithelial tissues to their tightness (ohmic resistance) (Claude and Goodenough, 1973). Following this,

different mathematical models were investigated in order to describe a relationship between the strand number and barrier function. However, this failed. The independency of barrier function and strand number is e.g. supported by the existence of two Madin-Darby canine kidney (MDCK) cell lines with similar strand number and TJ ultrastructure, that have a greater than 30-fold difference in electrical resistance. This gave hint for a possibility in regulating the ion conductance without impacting morphology (Shen et al., 2011). Due to this it was suggested that different pores for anions and cations might be present.

Different TJ proteins have been identified and some of their functions provided new understanding of the molecular characteristics of a high-capacity pore pathway, that allows the passage of large quantities of small ions and molecules (with radii of  $\sim 4$  Å or less) (Van Itallie et al., 2008), and a low-capacity leak pathway, which allows the flux of small quantities of larger molecules (Van Itallie et al., 2008; Shen et al., 2011). In pig ileum also a third condition was described with an additional pore cut off at about 6.5 Å (Van Itallie et al., 2008).

After discovering zonula occludens-1 (ZO-1) as the first protein being associated with the TJs (Stevenson et al., 1986) - however not as a transmembrane protein - occludin (Ocln) was the first TJ-associated integral membrane protein to be described (Furuse et al., 1993). Meanwhile, tricellulin (MarvelD2) and MarvelD3 had been identified as well, as further TJ-specific tetraspanning proteins which, together with Ocln, form the TJ-associated marvel protein (TAMP) family, which share a conserved MARVEL (MAL and related proteins for vesicle trafficking and membrane link) domain of four transmembrane domains linked by two extracellular (ECL) and one intracellular loop (ICL) (Sánchez-Pulido et al., 2002; Dörfel and Huber, 2012) (Figure 4 A, B).

A second family of TJ integral membrane proteins is the claudin (Cldn) family, whereupon Cldn-1 and Cldn-2 had been discovered first (Furuse et al., 1998). Up to now at least 27 claudins were described in mouse and human (Mineta et al., 2011). They are important to regulate TJ ion selectivity (pore pathway) (Günzel and Yu, 2013). Just like the TAMPs, claudins are also tetraspanning membrane proteins that have two extracellular loops (Figure 4 A, C). Basically, two broad categories of claudins exist: pore forming and sealing that allow or deny passage of ions through TJs (Shen et al., 2011; Günzel and Yu, 2013).

The third family of transmembrane components of TJs are the junctional adhesion molecules (JAMs) (Figure 4 A, D). They belong to the immunoglobulin super family (Williams and Barclay, 1988) and the family is composed of seven members; three classical JAMs (JAM-A, B, C) and four related proteins (JAM-4, JAM-L, CAR, ESAM) (Garrido-Urbani et al., 2014). JAMs are involved in cell-

cell adhesion/junctional assembly of cells as well as in extravasation of monocytes (Tsukita et al., 2001). Furthermore, JAM-A is involved in proliferation, barrier function and also in regulation of barrier function (Monteiro and Parkos, 2012).

The TJ proteins are connected to the actin cytoskeleton via TJ plaque proteins. These contain several protein complexes, which are involved in scaffolding of membrane proteins, regulation of cytoskeletal organization, establishment of polarity, and signalling to and from the nucleus (e.g. ZO-1, ZO-2 and ZO-3, cingulin, membrane-associated guanylate kinase inverted proteins (MAGIs), multi-PDZ protein MUPP1, and small GTPases) (Figure 4 A) (reviewed in Guillemot et al. (2008)).

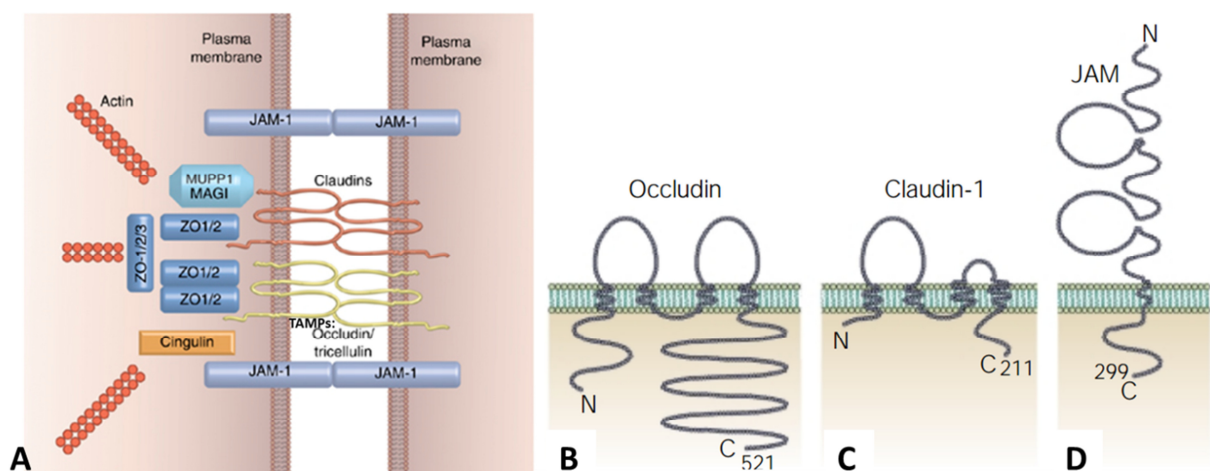


**Figure 4: Schematic overview of the basic structural transmembrane components of tight junctions (TJs).** Zonula occludens-1 (ZO-1) or ZO-2 are important for clustering of e.g. claudins and occludin, resulting in the formation of TJ strands. The ZOs and cingulin can give direct link to the actin cytoskeleton (A). Molecular structure of occludin (B), claudin-1 (C) and junctional adhesion molecule (JAM) (D) (modified with permission from Tsukita et al. (2001) and Niessen (2007)).

The exact composition of functional TJs strongly depends on the cell type, the differentiation status and on physiologic stimuli.

The main function of TJs is to seal the paracellular pathway to narrow and control the movement of molecules through the intercellular space in both directions (inside-out as well as outside-in) (Anderson, 2001). Furthermore, they also provide an additional barrier within the cells as they function as a fence between the proteins and lipids of the apical and the basolateral plasma membrane in cooperation with associating polarity complexes (Schneeberger and Lynch, 2004) and contribute therefore to cell polarity as well. Additionally, TJ proteins are involved in differentiation, proliferation, vesicular transport and signal transduction processes of cells (Matter et al., 2005; Kirschner and Brandner, 2012).

### 1.4 Tight Junctions in the epidermis

**“The impermeability of the skin to water and electrolytes is caused neither by the presence of a greasy-waxy cover of the skin nor by the presence of the horny layer. The seat of the absorption-barrier is to be placed in the transitional layers between cornified and non-cornified epithelium, i.e. in the stratum granulosum and stratum lucidum, which represent an electric double layer with positive hydrogen ions on the outside and negative hydroxyl ions on the inside.” (Rothman, 1944)**

The existence of a second physical barrier, next to SC, within the epidermis was speculated for a long time (Rothman, 1944; Hashimoto, 1971). However, certain verification of epidermal TJs in mammalian skin was just given at the turn of the century due to the availability of specific antibodies (Morita et al., 1998; Pummi et al., 2001; Yoshida et al., 2001; Brandner et al., 2002) and functional proof of epidermal TJs in barrier function was given in 2002 with a Cldn-1 knock-out mouse, which died within the first day of birth due to a tremendous trans-epidermal water loss (Furuse et al., 2002). Further investigations finally also described barrier-forming TJs within the human epidermis in SG (Kirschner et al., 2010). Meanwhile, it was also described in porcine skin (Herbig et al., 2015).

Up to now, in *in vivo/ex vivo* epidermis only an inside-out barrier function has been unambiguously shown for a 557 Da molecule (Biotin-SH) (Kirschner et al., 2010; Yuki et al., 2011a), larger molecules (1500 and 5000 Da, in mouse epidermis) (Yokouchi et al., 2015) and a 32 kDa protein (Yoshida et al., 2013) as well as for the ion tracer Lanthanum (Baek et al., 2013). Additionally, the TJ barrier function of NHEKs in submerged culture already has been investigated for intermediate-sized molecules, as fluorescein (332 Da) (De Benedetto et al., 2011a), as well as for macromolecules (3, 4 and 40 kDa FITC-Dextran) (Mertens et al., 2005; Yuki et al., 2007; Kirschner et al., 2011). It was also shown that TJs in NHEKs play an important role in controlling the paracellular pathway of ions such as  $\text{Na}^+$ ,  $\text{Cl}^-$  and  $\text{Ca}^{2+}$  (Kirschner et al., 2013). Additionally, it was shown that Cldn-1, Cldn-4, Occludin and ZO-1 contribute to the formation of these TJ barriers (Kirschner et al., 2013). However, the barrier function of undisturbed epidermal TJs from outside to inside could not be shown up to now. Tracer molecules are already stopped at or in the SC and when removing the SC, TJs are no longer undisturbed as SC and TJs are interconnected (see below). But commonly TJs are bidirectional structures (Anderson, 2001) and it is most likely that this also holds true for epidermal TJs even though evidence is missing. Furthermore, in assays with submerged NHEKs apically applied tracers (e.g. 4 and 40 kDa FITC Dextran) are commonly used to investigate TJ functionality. This indicates that if substances applied topically onto the skin were able to reach the SG they should likely be stopped at TJ structures.

Interestingly, not all TJ proteins are restricted to the functional TJ structures in SG, but some are also expressed in additional layers as shown by the schematic overview in Figure 5. This strongly argues for TJ structure-dependent as well as -independent functions of these proteins. For instance, involvement in proliferation and differentiation as well as apoptosis, cell-cell adhesion and cell signalling has been shown (Enikanolaiye et al., 2010; O'Neill and Garrod, 2011; Kirschner and Brandner, 2012; Rachow et al., 2013; Sugawara et al., 2013). Additionally, they are thought to contribute to desquamation (Igawa et al., 2011).

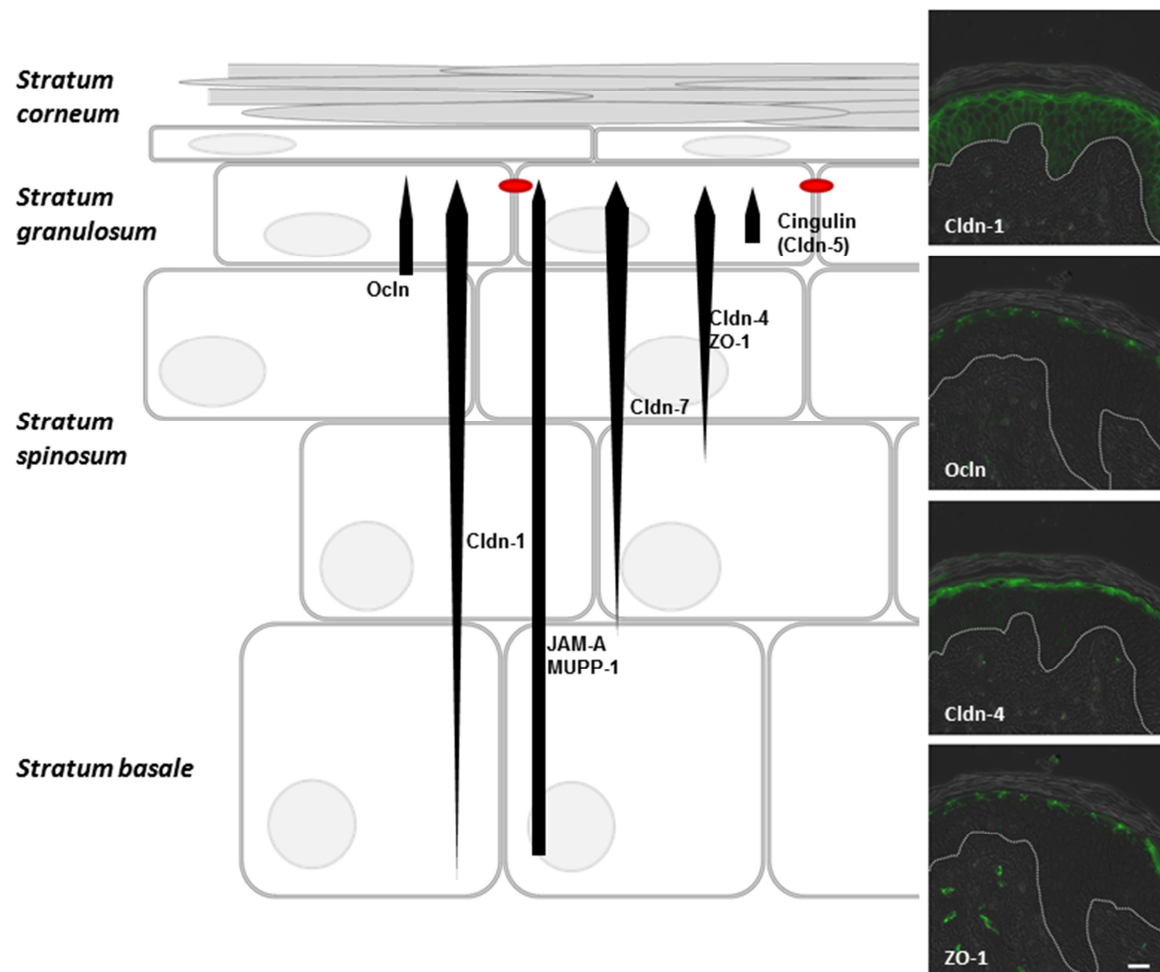


**Figure 5:** Schematic overview of distribution patterns of tight junction (TJ) proteins within the epidermis and immunohistochemical stainings (green) of claudin-1 (Cldn-1), occludin (Ocln), Cldn-4 and zonula-occludens-1 (ZO-1) in normal human skin. Red dots indicate functional TJ structures; the white dotted line indicates the basement membrane. JAM-A - junctional adhesion molecule A; MUPP-1 - Multi-PDZ domain protein 1. Bar = 50 µm (with permission from Bäsler and Brandner (2016)).

During analyses of epidermal TJ structures and function, it is important to keep in mind that also other components of the skin barrier may interact and it is important to know what interactions are possible in order to understand underlying mechanisms.

### 1.4.1 Tight Junctions and other skin barrier components

When looking deeper into the skin's barrier function, it becomes evident that this is provided by a complex system of different barriers that are all interconnected and work together closely in order to provide a secure shelter against environmental influences. These are: the two physical barriers (SC and the TJs), the cutaneous microbiome, a chemical barrier (provided by antimicrobial peptides (AMPs) and the skin surface pH), and the immunological barrier (provided by immune cells and cytokines). These barriers influence each other either directly or indirectly and can therefore react dynamically on changes within each other (Figure 6).

TJs play a central role in this system. In contrast to the SC, epidermal TJ integrity can be regulated immediately as part of the living cell signalling system, and therefore may contribute faster in order to improve or decrease physical barrier function than the SC. The interactions between TJs and the other skin barrier components are shown in the schematic overview of Figure 6.

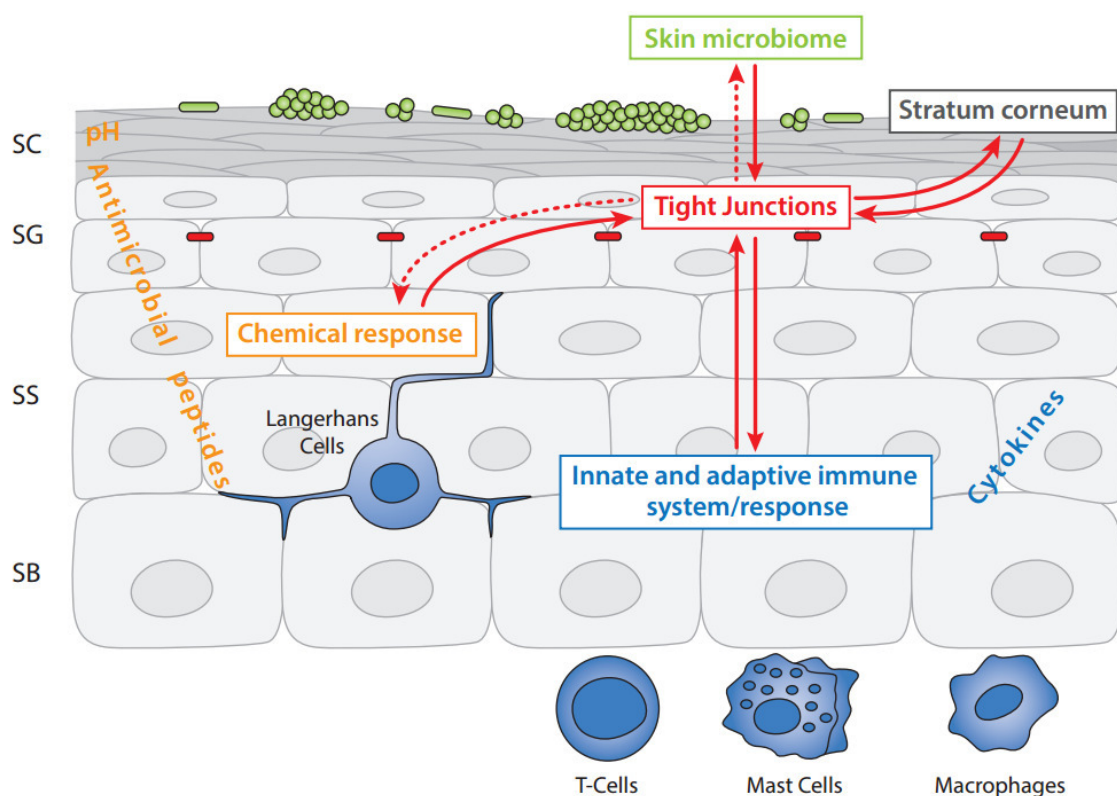


**Figure 6: Schematic drawing denoting the different barriers in the epidermis and their interaction with the tight junction barrier.** SB – Stratum basale; SC – Stratum corneum; SG – Stratum granulosum, SS – Stratum spinosum. Continuous arrows denote interactions already experimentally shown. Dotted arrows denote hypothetical interactions (modified with permission after Bäsler et al. (2016)).

*Tight Junctions influence other skin barrier components*

Within the last years evidence arose that TJs influence the **SC**. For example, knockdown of Cldn-1 in NHEKs and knockout of Cldn-1 in mice resulted in alterations of proteins important for SC formation (e.g. involucrin, loricrin, filaggrin and transglutaminase-1) (Kirschner et al., 2013; Sugawara et al., 2013; Gruber et al., 2015), and the latter was also shown to result in changes of SC morphology, filaggrin processing, lipid composition and an impaired SC water barrier (Sugawara et al., 2013). Additionally, knockdown of Occludin in NHEKs (Rachow et al., 2013) or overexpression of Cldn-6 in mice (Turksen and Troy, 2002) resulted in distinct changes in SC protein composition. Searching for the origin of these alterations, it could either be the consequence of changes in TJ barrier function or of TJ independent functions of TJ proteins.

Furthermore, the **immunological barrier** is influenced by TJs as the knock down of ZO-1 in NHEKs led to a release of the proinflammatory cytokine interleukin-1 $\beta$  (IL-1 $\beta$ ) (Bäsler and Brandner, 2016). Additionally, transgenic mice, expressing only low levels of Cldn-1, showed an increased IL-1 $\beta$  expression (Tokumasu et al., 2016). The influences of TJs on the **microbiome** or the **chemical barrier** still have to be elucidated. However, as TJs influence the SC, it seems logical to assume that microorganisms and skin surface pH could indirectly be affected.

*Tight Junctions are influenced by other skin barrier components*

Conversely, other skin barrier components have been shown to influence TJs. Within 1 h after mechanically disturbing murine **SC** (by tape stripping) an increase of Cldn-1 and Cldn-4 expression was reported (Kirschner et al., 2011; Baek et al., 2013). However, interestingly in this context timing was important, as shortly after tape stripping (15 and 30 min) a downregulation of Cldn-1 and -4 protein level was observed, which was accompanied by an impaired barrier for lanthanum (Baek et al., 2013).

A lot is known on the impact of the **immunological barrier** on epidermal TJs. Actually, TJs can be even defined as part of the innate immune system as TJ integrity is involved in limiting the contact of pattern recognition receptors (PRRs) to external ligands as well as the entry of viruses and the binding to their receptors (Guttman and Finlay, 2009; Rahn et al., 2017). In addition, different components of the immune system are able to influence TJs. The activation of several PRRs, especially Toll-like receptors (TLRs 2, 3, 4, 5, 6 and 9), enhanced TJ barrier function already after short time incubation (Yuki et al., 2011b; Kuo et al., 2013; Borkowski et al., 2015). Also, proinflammatory cytokines, another component of the immunological barrier, have been

demonstrated to influence TJ proteins and barrier function, respectively. Treatment of NHEKs with IL-1 $\beta$  or tumour necrosis factor  $\alpha$  (TNF $\alpha$ ) led to a time-dependent increase in TJ barrier function followed by a decrease after long-term treatment (Kirschner et al., 2009). Increase and decrease of barrier function were accompanied by TJ protein up or down regulation or relocalisation respectively (Kirschner et al., 2009). After dermal injection of IL-1 $\beta$  into healthy volunteers a downregulation of Cldn-1 was reported *in vivo* (Watson et al., 2007). *Ex vivo* skin, which was treated with IL-1 $\beta$ , showed a broader localization of OcIn and ZO-1 as well as an upregulation of ZO-1 protein level (Kirschner et al., 2009). Furthermore, after treatment of NHEKs with IL-4 and IL-13 Cldn-1 expression was upregulated (De Benedetto et al., 2011a). However, Treatment of RHE with cytokine mixture of IL-4, IL-13, and IL-31 resulted in a decrease of Cldn-1 in lower epidermal layers (Gruber et al., 2015). Additionally, IL 17 influenced Cldn-7 and ZO-2 in HaCaT (Human adult low calcium high temperature keratinocytes; immortal keratinocyte cell line) cells (Gutowska-Owsiak et al., 2012) and decreased TJ barrier function in RHE (Yuki et al., 2016). The inflammatory mediator histamine was shown to decrease Cldn-1, -4, OcIn, and ZO-1 levels and increase permeability for a 557-Da tracer in reconstructed human skin (RHS) (Gschwandtner et al., 2013). Not only the immunological barrier components PRRs and cytokines are interacting with TJs, but also immune cells. It has been demonstrated very elegantly that functional TJs are formed between the dendrites of activated Langerhans cells (LCs) and keratinocytes (Kubo et al., 2009; Yoshida et al., 2014). The dendrites find their way through the TJ structures but do not disturb barrier integrity by the formation of transient TJs. With this they are able to uptake antigens from above the TJ barrier that can be presented to T cells in the second lymphatic organs afterwards.

The **chemical barrier** has been described to influence the epidermal TJ barrier as well. The antimicrobial peptides cathelicidin (LL-37), human- $\beta$ -defensin-3 (h $\beta$ D3) and psoriasin have been shown to enhance TJ function (Akiyama et al., 2014; Hattori et al., 2014; Kiatsurayanon et al., 2014) which has been associated with increased TJ protein expression and/or increased relocalisation of OcIn and Cldn-4 to the cell borders.

Of special interest for this work is the influence of the **microbiome** on TJs (see below).



### 1.5 The cutaneous microbiome – boon and bane

The skin is an ecosystem colonized with a broad diversity of different microorganisms as there are aerobic as well as facultative anaerobic bacteria, viruses, fungi and mites, all together the residential microbes. During lifetime, the skin also comes into contact with so-called transient microbes, which are usually apathogenic and live in a symbiotic relationship with their human host. However, some transient and residential microorganisms can be pathogenic and lead to serious skin infections, especially when other skin barrier components are altered.

A classical definition of infection is the passive or active invasion of an organism's tissues by disease-causing pathogens (e.g. bacteria, fungi or virus), their residence and multiplication. The development of skin infections strongly depends on the pathogenic characteristic of the organism, on the status of the overall skin barrier and on the immune response (Jung et al., 2016). Some examples of infectious microorganisms (and their disease pattern) are: *Trichophyton* spec. or *Microsporum* spec. (Tinea) as dermatophytes, and *Candida albicans* (Candidiasis) as yeast in context of fungal infections as well as Herpes simplex virus or human papilloma virus in context of viral infection. The most prominent example for bacterial skin infections is *Staphylococcus aureus* (*S. aureus*) (*impetigo contagiosa*) (Rassner, 2009).

To better understand the interactions of the microbiome with the human host, a large project was started in 2007, called The Human Microbiome Project. Within this project not just the skin but the whole human body is going to be analysed genetically for microorganisms (as it is until now it only is possible to culture a small number of bacterial species in the lab) (Turnbaugh et al., 2007). The normal human skin microbiome strongly depends on the body site (topography), host factors such as age and sex as well as on environmental factors such as hygiene or clothing choice. For example, when investigating the 'head' bacteria (forehead, external nose, external ears and hair) the phylum of Propionibacterineae dominated, which were less abundant on the arms. In contrast, sites on the trunk and legs where dominated by *Staphylococcus* spp. (phylum Firmicutes) or *Corynebacterium* spp. (phylum Actinobacteria) (Costello et al., 2009).

Under healthy conditions the skin microbiome is thought to provide a barrier in order to inhibit the growth of pathogens due to occupying space and nutrients as well as due to the production of bactericidal compounds. Also, they are thought to educate and prime adaptive immunity and to enhance host innate immunity (Sanford and Gallo, 2013). One fascinating example

for the microbiome barrier function is *Propionibacterium acnes*. They hydrolyse the triglycerides present in sebum releasing free fatty acids that contribute to acidification of the skin surface to pH 5. Thereby the growth of many common pathogens, such as *S. aureus* and *Streptococcus pyogenes* is inhibited (reviewed in Grice and Segre (2011)). Another example was given with germ free mice, which were more susceptible to cutaneous infection with the protozoan *Leishmania major*, whereas colonisation with *S. epidermidis* supported protective immunity against *Leishmania major* (Naik et al., 2012).

In diseased skin, the microbiome can be changed dramatically, e.g. in atopic dermatitis a decrease in microbial diversity is reported going along with an increase in *Staphylococcus* spp. (Kong et al., 2012); discussed below in more detail).

## 1.6 *Staphylococcus*

“Micrococcus is met with in two distinct forms, chains and groups. They are often found together, yet the two are different, and the chain form does not pass into the grouped form, nor the grouped into the chain form. Throughout this paper the term *micrococcus* is used as embracing both forms; the chain coccus is often called *streptococcus* (Billroth), and I shall call the grouped form *staphylococcus* (from *σταφυλή*, a bunch of grapes).” (Ogston, 1882)

During his studies on ‘micrococcus poisoning’ Alexander Ogston was the first to describe the genus *Staphylococcus* in 1882 (Ogston, 1882). Two years later Anton J. Rosenbach distinguished between two strains of staphylococci, which he named after the pigmented appearance of their colonies: *Staphylococcus aureus* (Latin: aurum – gold) and *Staphylococcus albus* (now *epidermidis*; Latin: albus – white) (Rosenbach, 1884; Orenstein, 2011).

*Staphylococcus* in general is a gram positive and facultative anaerobic bacterial genus that includes at least 40 species. They typically grow as so called grape clusters, which is already indicated by their name (from the Greek: *σταφυλή*, *staphylē*, ‘grape’ and *κόκκος*, *kókkos*, ‘granule’). Staphylococci are common commensals as well as pathogens in/on human and animals. On human skin two species play a major role: *S. epidermidis* and *S. aureus*.

*S. epidermidis* usually belongs to the normal flora of the human body and colonises the skin as well as mucous membranes (Vuong and Otto, 2002). It is the most frequently isolated species from human epithelia, where it mostly colonizes the axillae, head and nares (Kloos and Musselwhite, 1975). However, if the host is predisposed, *S. epidermidis* can act as a pathogen and cause serious infections (Vuong and Otto, 2002). In particular, it represents the most common source of infections on indwelling medical devices (Otto, 2009). Therefore it has to be described as an

opportunistic pathogen. Nevertheless, *S. epidermidis* infections only rarely develop into life-threatening diseases, but infections are very common and difficult to treat due to the presence of antibiotic resistance and the formation of biofilms (Otto, 2009).

The more virulent cousin of *S. epidermidis*, *S. aureus* colonizes the human body in about 20% of healthy individuals (Wertheim et al., 2005). It can be isolated as a normal commensal mainly in nose and throat. However, *S. aureus* is associated with several diseases either in mediating or in worsening. Distinguishing *S. aureus* strains two main groups can be explored: Methicillin sensitive *S. aureus* (MSSA) and Methicillin resistant *S. aureus* (MRSA), which is also often referred to as multidrug resistant, as they are usually resistant against a broad spectrum of antibiotics, particularly  $\beta$ -lactam antibiotics (Otto, 2013). MRSA strains are becoming a major problem, especially in hospitals, where administration of antibiotics promotes the development of resistant strains. A hallmark of *S. aureus* infection is neutrophil abscess formation. This is mediated by proinflammatory cytokines (IL-1 $\beta$ , TNF $\alpha$  or IL-6) and especially by chemokines like CXCL2 or IL-8 (Miller and Cho, 2011).

The impact of *S. epidermidis* and *S. aureus* on TJ proteins has been basically elucidated in a previous work from our laboratory (Ohnemus et al., 2008). Immunohistochemical staining of human *in vivo* skin diagnosed with *impetigo contagiosa* revealed a downregulation of ZO-1, Cldn-1 and partly of Occludin at areas covered with bacteria (infected areas) and an upregulation of ZO-1 and especially Occludin at neighbouring areas as well as in some parts of infected areas (Ohnemus et al., 2008) (Figure 7 A). Treatment of porcine *ex vivo* skin with *S. aureus* resulted in a decreased immunointensity of Cldn-1 and ZO-1 (Figure 7 B). However, evaluation of Occludin revealed enhanced staining following *S. aureus* inoculation in certain areas indicating a special role of Occludin in this context (Figure 7 B). In the same work, inoculation of the immortalized keratinocyte cell line HaCaT with *S. epidermidis* resulted in a temporary increase in TJ function as measured by transepithelial electrical resistance (TER), whereas treatment with *S. aureus* resulted in a direct decrease in TER (Ohnemus et al., 2008) (Figure 7 C).

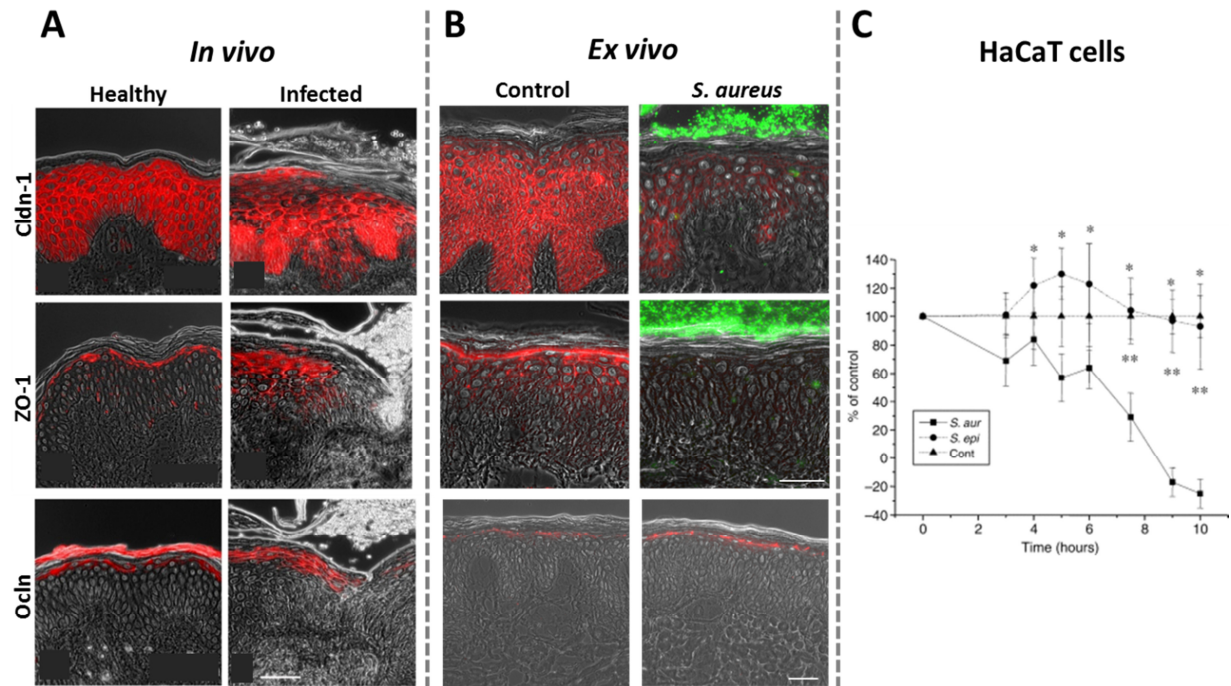


**Figure 7: The influence of Staphylococci on epidermal tight junctions (TJs).** Immunohistochemical staining of indicated TJ proteins (red) of healthy *in vivo* skin and infected *in vivo* skin diagnosed with *impetigo contagiosa* (A), as well as in a porcine *ex vivo* model uninfected and infected with *S. aureus* (green) (B). Transepithelial electrical resistance of HaCaT keratinocytes after inoculation with *S. epidermidis* (circles) and *S. aureus* (squares) normalized to the uninfected control (triangles) (C). Mean  $\pm$  SEM; \*  $p < 0.05$  between *S. aureus* and control; \*\*  $p < 0.05$  between *S. epidermidis* and *S. aureus*. Cldn-1 – claudin-1; ZO-1 – zonula occludens-1; Occludin – occludin. Bars = 50  $\mu$ m (Modified with permission from Ohnemus et al. (2008)).

Nevertheless, treatment of NHEKs with peptidoglycan derived from *S. aureus* (activation of TLR2) resulted in an increase in TER and decreased permeability, which was shown to be dependent on phosphorylation of Occludin via the atypical protein kinase C (aPKC) (Yuki et al., 2011b). This hints for differences in the reaction to *S. aureus* between the immortalized cell line HaCaT and NHEKs. However, also the difference between the usage of only peptidoglycan or live bacteria could be an explanation for different results. As not only other bacterial components than peptidoglycan, but also the generation of different virulence factors of live bacteria, could be involved. One essential regulator for the production of these virulence factors is the accessory gene regulator.

### 1.7 The accessory gene regulator (*agr*)

Many bacteria use chemical signals to assess their local population densities in a process called quorum sensing. This quorum sensing process enables the bacteria to “count” themselves and in case of high numbers to behave as a multicellular group. *S. aureus* but also *S. epidermidis* use quorum sensing to establish acute and chronic infections (Yarwood and Schlievert, 2003).

The ability of particularly *S. aureus* to invade host tissues and cause serious infections is dependent on a broad arsenal of virulence factors as there are: adhesins, toxins, tissue degrading enzymes or immune evasins. The expression of these effector molecules is controlled by several global regulators that often overlap in their regulating genes and thereby also regulate each other (Priest et al., 2012). This allows *S. aureus* to express appropriate virulence factors in response to a distinct environment. One essential regulator for skin and soft tissue infections is the accessory gene regulator (*agr*) (Painter et al., 2014). The *agr* operon is the comprehensive regulon that controls cell-density dependent virulence factor expression. Within the regulation of quorum sensing induced activation or inhibition of virulence genes, autoinducing peptides (AIPs) play an important role. These act extracellularly as the actual quorum sensing signalling molecule.

Different variants of these AIPs exist depending on the species or subgroups, which in general self activate *agr* response, whereas non-self AIPs inhibit the response. E.g. four allelic variants of AIP molecules are known in *S. aureus* (Dufour et al., 2002). Each of these AIP molecules functions as a specific ligand for their corresponding sensor transmembrane histidine kinase, while inhibiting other. At high population densities, the AIPs will reach an adequately high concentration to bind and activate their associated receptors enabling autophosphorylation (binding of heterologous AIP would prevent this). This then leads to phosphorylation and activation of the DNA-binding response regulator, upregulating the expression of an effector molecule (RNAIII), which regulates the production of many virulence factors and surface proteins associated with biofilm production (Tal-Gan et al., 2013; Painter et al., 2014).

Interestingly, the four different *S. aureus* allelic variants of AIP (Type I-IV) have been correlated with specific diseases: type-I and -II are associated with the majority of invasive infections (Jarraud et al., 2002; Holtfreter et al., 2007; Limbago et al., 2009), type-III *S. aureus* was mainly discovered in nasal carriage cases and is predominately responsible for human toxic shock

syndrome and type-IV is considered rare and limited to exfoliative toxin-related syndromes (Jarraud et al., 2002; Holtfreter et al., 2007).

The *agr* regulon is not only beneficial in order to recognize a high cell density, but is also required for *S. aureus* to kill neutrophils from inside. Once internalized by neutrophils, *agr* is able to detect enclosure of *S. aureus* in the phagosome and thereby act as a diffusion sensing system (Shompole et al., 2003). Now literarily, a fight between *S. aureus* and the neutrophils takes place. *Agr*-dependent production of several toxins leads to neutrophil lysis and killing of the granulocyte from inside. However, neutrophils produce reactive oxygen species within the phagosome that are able to inactivate AIPs and also cause dissociation of the response regulator. But, this dissociation also activates a gene promoting the oxidative stress response and resistance in *S. aureus* (Sun et al., 2012; Painter et al., 2014). On the other hand, neutrophils under attack also trigger strong proinflammatory response in order to recruit 'help' (Kobayashi et al., 2010; Painter et al., 2014).

The usage of therapeutics addressing the *agr* quorum sensing pathway in order to inhibit the production of secreted virulence factors provide good alternatives to antibiotic treatment, as these do not place a selective pressure on the bacterial community in order to develop resistance. This is of special interest in the case of *S. aureus*, which is known to rapidly develop resistance against antibiotics (Sully et al., 2014). Suppressing the *agr* regulon would help neutrophils fulfil their decontaminating function, especially in skin and soft tissue infections, which usually play an essential role in diseased skin.

### 1.8 Tight Junctions and skin infections in diseased skin

After the generation of conclusive evidence for the existence of TJ proteins and functional TJs in the skin in the early 21<sup>st</sup> century, many correlations have been made between skin diseases (especially inflammatory, e.g. Atopic Dermatitis or Psoriasis, but also skin tumours) and abnormal expression patterns of TJ proteins. Usually these skin diseases do not show influences on only one but on several skin barrier components and as the different skin barrier components are interconnected very tightly, it is often hard to distinguish whether the TJs influence other components or whether the other components influence the TJs.

Changes in TJ proteins or protein localisation in neonatal ichthyosis sclerosing cholangitis (NISCH) syndrome, Ichthyosis vulgaris (IV), Psoriasis and Atopic Dermatitis (AD; see below) are demonstrated in Figure 8 and have been reviewed in Bäsler et al. (2016).

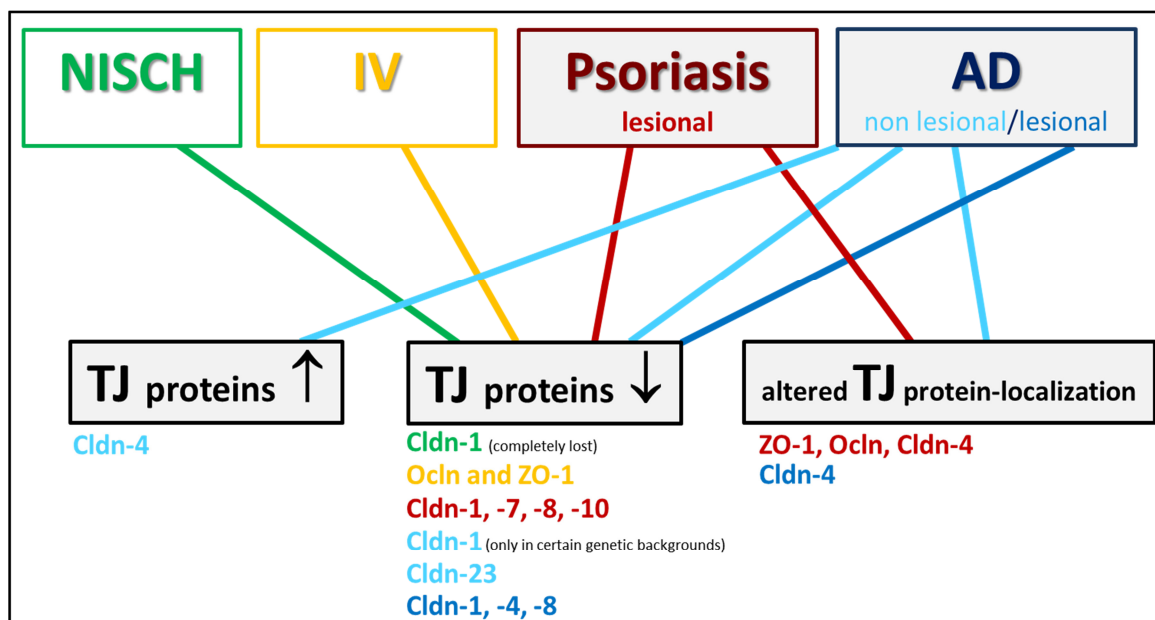


**Figure 8: Alteration of tight junction (TJ) proteins in skin diseases.** The different colors denote the different diseases and the corresponding TJ protein alterations. AD: atopic dermatitis; Cldn – claudin; IV – ichthyosis vulgaris; NISCH – neonatal ichthyosis sclerosing cholangitis; Ocln – occludin, ZO-1 – zonula occludens 1 (modified with permission from Bäsler et al. (2016)).

AD is the most common inflammatory skin disease and AD patients often suffer from serious skin infections. Thus, it is of special interest for this work and will therefore be introduced in more detail.

### 1.8.1 Atopic Dermatitis (AD)

As a chronic and non-contagious skin disorder AD is characterized by dry and scaly skin (non-lesional), which periodically exhibits severe, itchy eczema (lesional). Usually starting in infancy it affects up to 20% of school aged children (Leung et al., 2004; Winge et al., 2011). In 90% of cases the disease terminates during puberty, but in up to 10% of cases it persists into adulthood (Garnacho-Saucedo et al., 2013). In any cases it tremendously affects the quality of life, especially during disease flares.

AD is usually the first manifestation of an allergic disease. The AD-driven overactive T helper type 2 (Th2) immune response to environmental allergens is likely to be blamed for triggering further diseases such as asthma, allergic rhinitis and allergies against pollen, house dust mite or food. Increased serum Immunoglobulin E (IgE) levels and inflammatory infiltrates (e.g. lymphocytes and macrophages with rare eosinophil and neutrophil leukocytes) producing proinflammatory cytokines (e.g. IL-4, -13 and -31), which often represent inflammation in AD patients (Neis et al., 2006). Additionally, in correlation with the disease severity, high levels of IL-1 $\beta$  have been recorded in the serum of AD patients (Nutan et al., 2012). Histologically acute lesional sites showed intercellular edema (spongiosis) of the epidermis and a dermal inflammatory cell infiltrate (Soter, 1989).

Patients do not only show immunological variations but also disturbed physical barriers. A disturbed inside-out barrier could be measured by a slightly increased transepidermal water loss even in non-lesional skin, which was more distinct in lesional skin (Eberlein-König et al., 2000; Lee et al., 2006; Gruber et al., 2015). The outside-in barrier is disturbed as well in these patients. Analyses of *in vivo* skin showed increased diffusion coefficients into the SC for polyethylene glycols of various molecular sizes as well as sodium lauryl sulphate. This was more pronounced in lesional compared to non-lesional skin as well (Jakasa et al., 2006; Jakasa et al., 2007). Furthermore, changes in SC lipid composition have been linked to a decreased barrier function in non-lesional skin (Sator et al., 2003; van Smeden et al., 2014).

Regarding TJs, increasing evidence exist that they are also involved in the pathogenesis of AD. Investigations on non-lesional skin showed differences concerning different populations or population subgroups. In a northern American cohort, reduced expression of Cldn-1 and -23 have been reported and single nucleotide polymorphisms (SNPs) in the Cldn-1 gene were associated with AD (De Benedetto et al., 2011b). Furthermore in a Korean study a significant correlation between CLDN-1 SNPs and AD were found in a hospital based study group and in



an Ethiopian cohort, a significant correlation between a Cldn-1 SNP and the onset of AD before the age of 5 years has been reported (Asad et al., 2016). Nevertheless, this was not confirmed in a population based Korean study group (Yu et al., 2015) as well as in a population based Danish cohort (Ross-Hansen et al., 2013). Furthermore, immunointensity investigations of an Austrian cohort did not report changes in Cldn-1 expression in non-lesional skin (Gruber et al., 2015). This shows that concerning Cldn-1 distinct populations or population subgroups may have genetic differences. The investigation of Cldn-4 in non-lesional skin revealed an upregulation of immunointensity within two independent European cohorts ((Gruber et al., 2015) and lab intern unpublished data).

More consistent changes have been reported for TJ proteins in lesional skin. Different cohorts showed a clear downregulation of Cldn-1 immunointensity (Batista et al., 2015; Gruber et al., 2015). Also in different mouse models for AD a down-regulation of Cldn-1 was reported and was shown to likely be a consequence of the evoked inflammation (Gruber et al., 2015; Yu et al., 2015). In comparison to non-lesional skin, Cldn-4 immunointensity was downregulated as well and it appeared to be localized in a broader manner ((Kubo et al., 2014; Gruber et al., 2015) and lab intern unpublished data).

The microbiome of AD patients shows variations too. Microbial diversity is decreased dramatically in favour to an increased amount of *Staphylococcus spp.* in AD patients, especially during disease flares (Kong et al., 2012).

Concerning *S. aureus*, it was shown that it could be isolated from skin lesions in about 80-100% of AD cases, whereas, as already mentioned, only about 20% of healthy individuals are carrier (Breuer et al., 2002; Gong et al., 2006). The colonization density of *S. aureus* can reach up to  $10^7$  colony forming units (CFU) per  $\text{cm}^2$  (Leyden et al., 1974) and the density of *S. aureus* on AD lesions was correlated with cutaneous inflammation (Williams et al., 1990; Bunikowski et al., 2000) and treatment of *S. aureus* decreased disease severity (Huang et al., 2009).

Interestingly, a low diversity of gut bacteria in one month old infants was associated with the development of AD in later life (Abrahamsson et al., 2012) and another study showed that giving probiotics to pregnant women reduced the incidence of AD for their infants (Foolad et al., 2013). This study also showed that probiotic treatment of children with AD reduced disease severity (Foolad et al., 2013). However, the connection between AD and gut microbial diversity remains unknown but the gut microbiome may potentially help to tune the cutaneous immune system (Grice, 2014; van Rensburg et al., 2016).

The causes for the development of AD are not completely elucidated yet. For a long time it was believed, that an immune dysfunction is the cause for skin barrier defects, but now evidence is increasing that an impaired epidermal barrier might be the key feature of AD development (Eyerich and Novak, 2013). It is increasingly appreciated that affected skin barrier function by both genetic and environmental factors contribute to AD sensitivity (Barnes, 2010). The occurrence of AD in industrial countries is continuously increasing, which supports socioeconomic influences (Eyerich and Novak, 2013). Up to now the strongest genetically predisposing factor for the development of AD is a loss-of-function mutation in the filaggrin gene, which has been described in 2006 (Palmer et al., 2006). But still, only about one third of European patients show a homo- or heterozygote filaggrin mutation (Palmer et al., 2006). Being a key protein that supports terminal differentiation and formation of the skin barrier, filaggrin deficient patients show a significant increase in surface pH (Jungersted et al., 2010) and filaggrin knock-out mice showed increased penetration of antigens (Kawasaki et al., 2012). However, increased transepidermal water loss and skin permeability in AD patients were investigated to be independent from filaggrin mutations (Jakasa et al., 2011). Furthermore, RHEs built with keratinocytes of filaggrin negative patients, did not show differences in barrier function (Niehues et al., 2016).

These data collectively suggest the pathology of AD seems to be a vicious cycle of disrupted physical skin barrier and skin inflammation (Figure 9). A dysfunctional physical skin barrier results in an increased uptake of allergens, which activates an immune response and results in inflammation, which again influences physical barrier function. Interestingly, increased numbers of TJ penetrating Langerhans cells have been reported in AD patients, which is likely to contribute to an increased uptake of allergens (Yoshida et al., 2014). In turn, inflammation is able to reduce physical skin barrier function e.g. via altering keratinocyte differentiation. In particular, it is known that keratinocytes differentiating in the presence of IL-4 and IL-13 show reduced levels of filaggrin (Howell et al., 2007). Additionally, after treatment of epidermal models with Th2 cytokines and TNF $\alpha$  a reduction in filaggrin was recognized (Danso et al., 2014). These models also showed altered SC lipid compositions (Danso et al., 2014). AD patients most often suffer from severe pruritus which is likely to be stimulated by IL-31 or bacterial toxins (reviewed in Elias and Schmuth (2009)), leading to scratching, which disturbs the SC barrier as well and contributes to this vicious cycle.

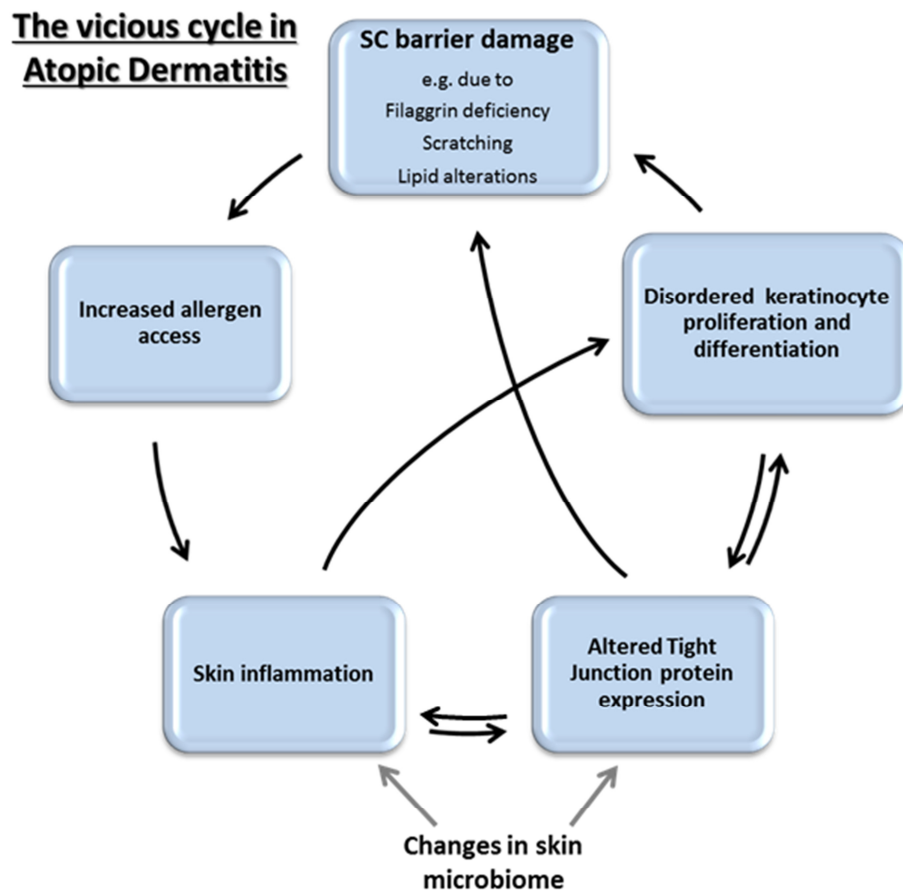


**Figure 9: The vicious cycle in atopic dermatitis.** *Stratum corneum* (SC) barrier disruption due to filaggrin deficiency, scratching, or lipid alterations leads to increased access of allergens. This results in skin inflammation, which can also be provoked by changes in the skin microbiome. Skin inflammation and changes in the skin microbiome lead to altered TJ protein expression. Disordered keratinocyte proliferation, which is provoked by skin inflammation and altered TJ protein expression, again leads to SC barrier damage. This also can be directly triggered by altered TJ protein expression (with permission from Bäsler and Brandner (2016)).

How do TJs actually fit into this cycle? The TJ sealing claudins, Cldn-1 and Cldn-4 (at least compared to non-lesional skin), appear to be decreased in lesional skin of AD, which is putatively the result of inflammation, but also genetic predisposition (at least for Cldn-1) might act as a part in some cohorts (see above). Additionally, alterations of the chemical or the microbial barrier might be involved in this downregulation (see above). Supposedly, does the decrease in sealing claudins on one hand result in further decreasing physical skin barrier function by impairment of TJ barrier function in cross-talk with the SC (see above and Bäsler et al. (2016)). On the other hand in an AD mouse model, the decrease of Cldn-1 independent from TJ-barrier forming structures has been significantly associated with increased proliferation and epidermal thickness as well as altered differentiation in eczema (Gruber et al., 2015), which might also contribute to the clinical features. This is also supported by data from Tokumasu et al. (2016) who invented mouse models with reduced levels of Cldn-1 expression. These models exhibited AD-like features like dry skin, epidermal thickness, invasion of

macrophages and increased levels of IFN $\gamma$  and IL-10. In addition, it was shown before that Cldn-1 down-regulation increased proliferation (De Benedetto et al., 2011a). Taken together it is thinkable that in those cohorts where a decrease of Cldn-1 already is observed in non-lesional skin TJs could be initiators of this vicious circle. However in other cohorts, where this is not the case, it even seems that TJs try to rescue the impaired SC barrier function by upregulating Cldn-4 (Gruber et al., 2015).

## 1.9 Aim of the thesis

The topic of the skin barrier is an intensely studied field and the understanding of the importance of TJs is continuously increasing. They form a mechanical barrier and interact with the other components of the skin barrier. This thesis is interested in the role of TJs in the course of bacterial skin infection, especially by the pathogen *Staphylococcus aureus* as being one of the most common examples causing serious skin and soft tissue infection. But also *S. epidermidis*, as a normal commensal (however, opportunistic pathogen), shall be investigated in this context as it is known that this microbe is involved on the one hand in preventing infections but can also cause on the other hand infections on its own under certain circumstances.

In a previous study, *in vivo* infection (*impetigo contagiosa*) and infection of an *ex vivo* porcine skin infection model revealed changes in TJ protein expression and localisation, but not investigations concerning TJ barrier function were performed with these specimen.

Investigation of the immortalised keratinocyte cell line HaCaT showed enhanced keratinocyte barrier function after inoculation with *S. epidermidis*, while decreased barrier function was found upon *S. aureus* treatment. However, it is known that HaCaT cells express different pattern recognition receptors compared to normal human primary keratinocytes (NHEKs). Furthermore, analyses with bacterial cell wall components of *S. aureus* resulted in TJ barrier enhancement in NHEKs, also hinting on putatively different effects in NHEKs. Therefore, the goal of this work was to analyse effects of Staphylococci on TJs in NHEKs and to analyse the putative mechanisms behind possible changes. In order to do so, TJ function of NHEKs after bacterial inoculation with *S. aureus* and *S. epidermidis* was examined in a submerged model, without a functional SC barrier to directly address the TJs, and in a 3D skin model to investigate additionally also interactions between bacteria, TJs and SC. An important prerequisite for these studies was to characterise different 3D skin model to identify the most suitable for my experiments.

Bacterial infections, in particular with *S. aureus*, are one of the most common complications in pathogenesis of Atopic dermatitis (AD). The skin of AD patients is colonised with a higher amount of Staphylococci while a decrease in microbial diversity is reported, especially during disease flares. Therefore, an additional aim of the work was to study the interaction of staphylococci and TJs in the context of AD mimicking models.

## 2 MATERIAL AND METHODS

### 2.1 Chemicals and media

A list of chemicals and purchased media that have been used in experimental procedures within this work can be found in Table 3.

**Table 3: Listing of chemicals and their origins used within this work.**

Chemical	Company	Location
1 N NaOH	Merck	Darmstadt, DE
2-Phospho-L-ascorbic acid	Sigma	Taufkirchen, DE
2-Propanol	Sigma	Taufkirchen, DE
4',6-diamidino-2-phenylindol (DAPI)	Roche	Mannheim, DE
Acetone	Geyer Hamburg GmbH	Hamburg, DE
Acrylamide	Serva	Heidelberg, DE
Ammonium persulfate (APS)	Serva	Heidelberg, DE
Ascorbic acid	Sigma	Taufkirchen, DE
Bacitracin	Sigma	Taufkirchen, DE
Bacto™ Agar	Becton Dickinson	Heidelberg, DE
BHI-Agar	Oxoid	Hampshire, UK
Bis	Serva	Heidelberg, DE
Boric acid	Merck	Darmstadt, DE
Bovine serum albumin (BSA)	Roche	Mannheim, DE
Bromphenol blue	Sigma	Taufkirchen, DE
CaCl <sub>2</sub> (Dihydrat)	Serva	Heidelberg, DE
CellnTec 3D medium kit: Basal medium: CnT-BM.3-500 3D supplements: CnT-02-3DP5.S	CellnTec	Bern, CH
Chloramphenicol	Sigma	Taufkirchen, DE
Columbia-Agar	Oxoid	Hampshire, UK
Coomassi brilliant blue	Fluka	Taufkirchen, DE
Cryomatrix	Roth	Karlsruhe, DE
Dimethylsulfoxid (DMSO)	Merck	Darmstadt, DE
Na <sub>2</sub> HPO <sub>4</sub> x 2 H <sub>2</sub> O	Merck	Darmstadt, DE
DNA size standard (F-303SD)	Thermo scientific	Schwerte, DE
ECL-system (chemiluminescent substrate)	Thermo scientific	Schwerte, DE
EDTA	Roth	Karlsruhe, DE
EDTA (1 %)	Biochrom AG	Berlin, DE
Eosin	Thermo scientific	Schwerte, DE
EpiLife and supplements (HKGS)	Thermo scientific	Schwerte, DE
Ethanol (99, 96, 80 and 70 %)	Merck	Darmstadt, DE
Eukitt	Kindler GmbH	Freiburg, DE
EZ-Link Sulfo-NHS-LC-Biotin (Biotin-SH)	Thermo scientific	Schwerte, DE
Fetal calf serum (FCS)	Invitrogen	Carlsbad, USA
FD4	Sigma	Taufkirchen, DE
Fluoromount-G	Southern Biotech	Eching, DE
Formafix	Grimm med. Logistik GmbH	Torgelow, DE
Glycerine	Roth	Karlsruhe, DE
Glycine	Roth	Karlsruhe, DE
Haematoxylin	Medite	Burgdorf, DE
Hanks buffered salt solution (HBSS)	Life Technologies	Darmstadt, DE
InstaGene Matrix	BioRad	München, DE
Interleukin-1β (IL-1β)	Tebu-bio	Le-Perray-en-Yvelines, F

Chemical	Company	Location
KH <sub>2</sub> PO <sub>4</sub>	Merck	Darmstadt, DE
KCl	Merck	Darmstadt, DE
Keratinocyte growth medium 2 (KGM2 kit)	Promocell	Heidelberg, DE
Leupeptin	Sigma	Taufkirchen, DE
L-Glutamine	Biochrom AG	Berlin, DE
Lysostaphin	Sigma	Taufkirchen, DE
Maxima first strand cDNA synthesis kit for RT-qPCR	Life Technologies	Carlsbad, USA
Methanol	Mallinckrodt Baker	Deventer, NL
3-(4,5-dimethylthiazol-2-yl)-2,5-diphenyltetrazolium bromide (MTT)	Sigma	Taufkirchen, DE
NaCl	Mallinckrodt Baker	Deventer, NL
Non-fat milk	Roth	Karlsruhe, DE
Normal goat Serum (NGS)	Jackson ImmunoResearch	Baltimore, USA
NP40	Sigma	Taufkirchen, DE
Nutrient broth 2	Oxoid	Hampshire, UK
Orthophosphoric acid (88 %)	Sigma	Taufkirchen, DE
Pam3CSK4	Invitrogen	Carlsbad, USA
Paraffin	MCCormick scientific	Richmond, USA
PBS (w/o Ca <sup>2+</sup> , Mg <sup>2+</sup> )	Biochrom AG	Berlin, DE
Penicillin/Streptomycin (10.000 U/ml / 10.000 U/ml)	Biochrom AG	Berlin, DE
Pepstatin	Sigma	Taufkirchen, DE
Phenylmethane sulfonyl fluorid (PMSF)	Sigma	Taufkirchen, DE
Phosphatase inhibitor	Cell Signalling Technology	Denver, USA
Phusion high-Fidelity PCR kit	Thermo scientific	Schwerte, DE
Poly I:C	R&D systems	Minneapolis, USA
Ponceau S solution	Sigma	Taufkirchen, DE
Prestained SDS molecular weight marker	Thermo scientific	Schwerte, DE
Proteinblock	DAKO	Carpinteria, USA
PureCol (bovine collagen)	Advanced BioMatrix	San Diego, USA
Recombinant human KGF/FGF-7	R&D systems	Minneapolis, USA
Red safe (nucleic acid staining solution)	Intron Biotechnologie	South Korea
RNeasy mini kit	Quiagen	Hilden, DE
RPMI 1640	Biochrom AG	Berlin, DE
Sodium dodecyl sulfate (SDS)	BioRad	München, DE
SeaKem LE-Agarose	Lonza	Basel, CH
Sodium citrate	Merck	Darmstadt, DE
Sodium deoxycholate	Sigma	Taufkirchen, DE
TEMED	Sigma	Taufkirchen, DE
Tetracycline	Sigma	Taufkirchen, DE
TNF $\alpha$	Biomol	Hamburg, DE
Tris	Sigma	Taufkirchen, DE
Tri-sodiumcitrate-dihydrate	Merck	Darmstadt, DE
Triton X-100	Sigma	Taufkirchen, DE
Trizama base	Sigma	Taufkirchen, DE
Trypsin	Sigma	Taufkirchen, DE
Tween 20	Merck	Darmstadt, DE
Xylol	Mallinckrodt Baker	Deventer, NL
$\beta$ -Mercaptoethanol	Fluka	Taufkirchen, DE
0.05 % Trypsin – 0.02 % EDTA solution	Biochrom	Berlin, DE
NaCl-solution (0.9 %)	Baxter Deutschland GmbH	Unterschleißheim, DE
Trypsin (2,5 %)	Biochrom AG	Berlin, DE
DMEM (3,7 g/l Glucose)	Biochrom AG	Berlin, DE

## 2.2 Devices

A list of devices used within this work can be found in Table 4.

**Table 4: Listing of the devices and their origins used within this work.**

Device	Type	Company	Location
Aqua dest. unit	PFXXM1	Elga labwater	Lane End, UK
Autoclave	Evo130	MediTech	Norderstedt, DE
Gel imaging system	ChemiDoc XRS	Bio-Rad	Hercules, USA
Benchtop aspiration system	Vacupip	Integra Biosciences	Biebertal, DE
Camera for Light Microscope	EC3	Leica	Wetzlar, DE
Cell counting machine	Countess	Invitrogen	Karlsruhe, DE
Centrifuge	Bifuge fresco	Heraeus Instruments	Hanau, DE
	Laborfuge 400R	Heraeus Instruments	Hanau, DE
	Multifuge1	Heraeus Instruments	Hanau, DE
	Centrifuge5424R	Eppendorf	Hamburg, DE
CO <sub>2</sub> -Incubator (cell culture)	Heracell <sup>TM</sup> 150i	Thermo Fischer Scientific	Schwerte, DE
	MCO-17AC	Sanyo	Osaka, Japan
Cryostat	CM 3050	Leica	Wetzlar, DE
Electrophoresis chamber and power supply	Mini PROTEAN3 system	Bio-Rad	Hercules, USA
Fluorescence Microscope	Axiophot2	Zeiss	Göttingen, DE
Fluorescence reader	Infinite M200	Tecan	Crailsheim, DE
Heat block	Ori-Block DB-3	Tecne	Cambridge, UK
Homogenizer	TissueLyser	Quiagn	Hilden, DE
Incubator without additional CO <sub>2</sub> in Air	B5090E	Heraeus Instruments	Hanau, DE
Laminar-flow working bench	T6030	Heraeus Instruments	Hanau, DE
	Hera Safe 12	Heraeus Instruments	Hanau, DE
Light microscope	CH-2	Olympus	Hamburg, DE
	DMIL/DMLS	Leica	Wetzlar, DE
Magnetic stirring hotplate	MR 3001	Heidolph	Schwabach, DE
Microtome	RM2165	Leica	Wetzlar, DE
Microwave oven	60	Bosch	Stuttgart, DE
	209	Bosch	Stuttgart, DE
Notebook	Latitude E5500	Dell	Round Rock, US
Paraffin embedding mashine	Citradel2000	Thermo Scientific	Schwerte, DE
pH meter	766 Calimatic	Knick	Berlin, DE
Photometer (OD <sub>600</sub> )	Smart Spec 3000	Bio-Rad	Hercules, USA
Photometer (well plates)	Sunrise	Tecan	Crailsheim, DE
Pipettes	Research <sup>®</sup>	Eppendorf	Hamburg, DE
Pouring station	EG1150H	Leica	Wetzlar, DE
Power supply	PS 3002	Life Technologies	Carlsbad, USA
Radiographic film developing machine	Curix60	Agfa	Berlin, DE
Real-Time PCR-Cycler	Light cycler 96	Roche	Rotkreuz, DE
Scales	BL3100	Sartorius	Hannover, DE
	PCB1000-2	Kern	Ballingen, DE
Semidry-Blot System	Trans-Blot <sup>®</sup> Turbo <sup>TM</sup>	Bio-Rad	München, DE
Shaker	KS250	IKA Labortechnik	Staufen, DE
Shrink-wrapping machine	Folio	Severin	Sundern, DE
Sonifier	Branson sonifier	G Heinemann	Schwäbisch Gmünd, DE
	Sonorex Super RK103H	Bandelin	Hagen, DE
Special accuracy weighing machine	ISO 9001	Sartorius	Hannover, DE



Device	Type	Company	Location
Spectrophotometer	NanoDrop 2000c	Thermo Fischer scientific	Schwerte, DE
Thermocycler	PeqSTAR	PeqLab	Erlangen, DE
Thermocycler (cDNA)	UNO-Thermoblock	Biometra GmbH	Göttingen, DE
Turning shaker	Tiny Turner	CTI	Idstein, DE
Voltohmmeter	EVOM	World Precision Instruments	Sarasota, USA
Vortexing machine	Vortex-Genie Z	Scientific Industries	Bohemia, USA

### 2.3 Antibodies and Primer

A detailed list of antibodies and their dilutions used for either Western Blots or immunofluorescence stainings can be found in Table 5. Antibody isotypes were used as negative controls for immunofluorescent stainings in equal protein concentrations to the used primary antibodies (guinea pig IgG, Santa Cruz Biotechnology, Heidelberg, DE; rabbit Ig-fraction, Dako, Hamburg, DE; mouse IgG1, R&D Systems, Wiesbaden, DE).

**Table 5: Antibodies and dilutions used within this work for Western Blot (WB) and immunohistochemical stainings (IHC).**

Antibody	Species/specification	Company	Dilution WB	Dilution IHC
Claudin-1	Rabbit /Jay.8	Invitrogen (Darmstadt, DE)	1:1500	1:900
Claudin-4	Mouse/3E2C1	Invitrogen (Darmstadt, DE)	1:200	1:500
Goat	Donkey/F(ab) 2 DyLiht 488	Bethyl Laboratories (Montgomery, USA)		1:500
Mouse	Goat/Alexa 488 F(ab') <sub>2</sub>	MoBiTec (Göttingen, DE)		1:600
Mouse	Goat/Alexa 594 F(ab') <sub>2</sub>	MoBiTec (Göttingen, DE)		1:1200
Mouse	Goat/HRP	Jackson ImmunoResearch (West Grove, USA)	1:5000	
Occludin	Goat/N-19	Santa Cruz (Dallas, USA)		1:500
Occludin	Mouse	Invitrogen (Darmstadt, DE)	1:100	
Rabbit	Goat/Alexa 488 F(ab') <sub>2</sub>	MoBiTec (Göttingen, DE)		1:600
Rabbit	Goat/Alexa 594 F(ab') <sub>2</sub>	MoBiTec (Göttingen, DE)		1:1200
Rabbit	Goat/HRP	Jackson ImmunoResearch (West Grove, USA)	1:5000	
β-Actin	Mouse/AC-15	Sigma-Aldrich (Darmstadt, DE)	1:30 000	

FAM dye-labeled real-time PCR (qRT-PCR) TaqMan MGB probes were purchased from Applied Biosystems (Carlsbad, CA) and are listed in Table 6.

**Table 6: FAM dye-labeled real-time PCR (qRT-PCR) TaqMan MGB probes and their catalogue numbers.**

Target mRNA	Catalogue number
Human 18S rRNA	Hs99999901_s1
Human claudin-1	Hs00221623_m1
Human claudin-4	Hs00533616_s1
Human interleukin-1β	Hs01555410_m1
Human interleukin-6	Hs00985639_m1
Human interleukin-8	Hs00174103_m1
Human occludin	Hs00170162_m1
Human tumor necrosis factor α	Hs001113624_g1
Human zonula occludens-1	Hs01551861_TJP1

## 2.4 Software

A listing of the different software that was used during this work can be found in Table 7.

**Table 7: Software and its origin used during this work.**

Software	Used for	Company	Location
Adobe Photoshop	Generation of Images	Adobe	Mountain View, USA
Endnote	Literature database	Clarivate Analytics	Philadelphia, USA
Fiji (ImageJ) ( <a href="http://imagej.net">http://imagej.net</a> )	1. Densitometrical evaluation of Western-Blot intensities 2. Evaluation of Immunointensities	Wayne Rasband	Madison, USA
i-control 1.5	Evaluation of fluorescence intensities	Tecan	Crailsheim, DE
LAS EZ 2.1.0	Taking pictures with the light microscope	Leica	Wetzlar, DE
LightCycler® 96 Systems 1.1	Quantitative Real-Time-PCR	Roche	Basel, CH
Magellan™ 6	Measurement of light extinction	Tecan	Crailsheim, DE
Microsoft Office	Generation of this work, Images and Graphs; Statistics	Microsoft	Redmond, USA
NanoDrop 2000	Evaluation of amount and purity of mRNA and bacterial DNA	Thermo Fisher Scientific	Schwerte, DE
OpenLab 5.0.2	Taking pictures with the fluorescence microscope	Improvision	Forchheim, DE
Quantity One 4.5.2	Gel imaging of PCR products	Bio-Rad	Hercules, USA
SPSS 21	Statistics	IBM	Armonk, USA

## 2.5 Cells and tissue

For *in vitro* assays infant primary human keratinocytes and fibroblasts were used. Skin samples for keratinocyte and fibroblast cultures were derived from circumcisions and obtained from the children's hospital in Hamburg-Altona. The utilisation of these samples was approved by the ethics committee of the Aerzteammer Hamburg (WF-61/12). Samples were used anonymously. All investigations were conducted according to the principles expressed in the Declaration of Helsinki.

## 2.6 Bacterial strains

All bacterial strains used within this project have been kindly provided by Prof. Dr. Holger Rohde from the institute of medical microbiology, virology and hygiene at the University Medical Center Hamburg-Eppendorf. Bacterial strains used in this study and their origins are listed in Table 8.

**Table 8: Listing of bacterial strains that have been used during this work.** *Agr* – accessory gene regulator; BHI – brain heart infusion; GFP – green fluorescent protein; RFP – red fluorescent protein; WT – wild-type

Bacterial species	Strain	Characteristics	Agar plates	Origin
<i>Staphylococcus aureus</i>	SH1000	WT	Columbia or BHI	Horsburgh et al. (2002)
	SH1000xpCM29	GFP positive	BHI + Chloramphenicol (10 µg/ml)	Generated by Dr. Thomas Volksdorf
	SH1000Δ <i>agr</i> ::tetM	Δ <i>agr</i>	BHI + Tetracycline (10 µg/ml)	This study
	RN6390Δ <i>agr</i> ::tetM	Δ <i>agr</i>	BHI + Tetracycline (10 µg/ml)	Novick et al. (1993)
	6820	WT, MRSA	Columbia	Clinical isolate, University Medical Center Hamburg-Eppendorf
<i>Staphylococcus epidermidis</i>	PIA97	WT	Columbia or BHI	Rohde et al. (2007)
	PIA97	RFP positive	BHI + Tetracycline (10 µg/ml)	Generated by Dr. Thomas Volksdorf
<i>Staphylococcus carnosus</i>	TM300	WT	Columbia	Rosenstein et al. (2009)

## 2.7 Cell and tissue culture

As far as not mentioned otherwise, all experimental procedures were performed under sterile conditions. This includes:

- Usage of sterilised material (tweezers, pipette tips etc.)
- Usage of working benches with laminar flow
- Usage of sterile media and solutions

As far as not mentioned otherwise, media and solutions were preheated to 37°C and all cells or tissues were maintained at 37°C in a humidified atmosphere of 5% carbon dioxide (CO<sub>2</sub>) in air.

### 2.7.1 Primary culture of human keratinocytes and fibroblasts

Isolated cells (keratinocytes as well as fibroblasts) were labelled with internal laboratory codes, dependent on donor and cell type.

#### Media:

##### Pre cultivation medium

Prepared with Dulbecco's Modified Eagle Medium (DMEM)

Penicillin/Streptomycin	100 units/ml
-------------------------	--------------

For primary tissue culture keratinocytes and fibroblasts were isolated from juvenile prepuces. Before usage, prepuces were incubated for at least 24 h at 4°C in pre cultivation medium to decontaminate the tissue.

### 2.7.1.1 Isolation and cultivation of normal human epidermal keratinocytes (NHEKs)

#### Media:

##### **Keratinocyte cultivation medium without antibiotics (KGM2)**

Keratinocyte basal medium 2 was prepared with supplements to obtain keratinocyte growth medium 2 (KGM2) according to manufacturer's specifications.

##### **Keratinocyte cultivation medium with antibiotics (KGM2 + AB)**

Prepared with KGM2 (see above)

Penicillin/Streptomycin	100 units / ml
-------------------------	----------------

KGM2 and KGM2 + AB were stored at 4°C for up to 4 weeks.

#### Solutions:

##### **0.25% trypsin-solution**

Prepared in Phosphate-buffered saline (PBS) (w/o  $\text{Ca}^{2+}$ ,  $\text{Mg}^{2+}$ ).

Aliquots were stored at -20°C.

##### **10% FCS-solution**

Prepared in PBS (w/o  $\text{Ca}^{2+}$ ,  $\text{Mg}^{2+}$ ).

The solution was stored at 4°C for up to 2 weeks.

##### **Trypsin-EDTA-solution**

Prepared in PBS (w/o  $\text{Ca}^{2+}$ ,  $\text{Mg}^{2+}$ ).

Trypsin	0.1%
Ethylenediaminetetraacetic acid (EDTA)	0.02%

Aliquots were stored at -20°C.

#### *Isolation*

For isolation of NHEKs, the prepuces were shortly washed in PBS (w/o  $\text{Ca}^{2+}$ ,  $\text{Mg}^{2+}$ ) and cut into about 1 mm<sup>2</sup> large pieces by dint of a scalpel and tweezers. After incubation for either 2 h at 37°C or over night at 4°C in 0.25% trypsin-solution the epidermis could easily be separated from the dermis. With a Pasteur-pipette the epidermal pieces were transferred into 5 ml 10% FCS-solution and strongly suspended to stop trypsin reaction and separate cells from each other. Cells were pelleted by centrifugation at 808 g for 5 min. Subsequently, the supernatant was discarded, cells were resuspended in an appropriate amount of KGM2 + AB and finally seeded at a density of about  $1 \times 10^6$  cells per petri dish (10 cm in diameter) with 10 ml KGM2 + AB and allowed to attach and proliferate for 5 days. Afterwards the medium was refreshed once and depending on the confluence, cells were incubated for another 1 to 2 days and either cryopreserved (see chapter: cryopreservation) or propagated to further passages (see below).

#### *Cultivation*

For further cultivation/sub cultivation, keratinocytes were split at a confluence of 60 – 80%. Starting from passage 1 it was resigned to use antibiotics in any experimental setting. After discarding the supernatant the cells were shortly washed with PBS (w/o  $\text{Ca}^{2+}$ ,  $\text{Mg}^{2+}$ ) at room

temperature and incubated with 2 ml trypsin-EDTA-solution per 10 cm dish (volume was adapted when using other sizes of culturing dish) for 5 min at 37°C. Due to this treatment cells were detached and could be rinsed off easily by a 10% FCS-solution (with at least twice of the amount of trypsin-EDTA-solution). Subsequently, cells were pelleted by centrifugation, resuspended in an appropriate amount of KGM2, and split in a ratio of about 1:3 or cells were counted and seeded in desired densities and desired culture items for experimental setup (see chapter: counting of cell suspensions). All NKEKs were cultured continuously up to a maximum of 4 passages.

### 2.7.1.2 Isolation and cultivation of primary human fibroblasts

#### Media:

##### **Fibroblast culture medium (RPMI-complete)**

Prepared in Roswell Park Memorial Institute medium (RPMI 1640)

FCS	10%
L-Glutamine	2 mM
Penicillin/Streptomycin	100 Units/ml

RPMI-complete medium was stored at 4°C for up to 4 weeks.

#### *Isolation*

For Isolation of primary human fibroblasts, the prepuces were shortly washed in PBS (w/o  $\text{Ca}^{2+}$ ,  $\text{Mg}^{2+}$ ) and cut into  $>1 \text{ mm}^2$  large pieces by dint of a scalpel and tweezers. These pieces were transferred into  $25 \text{ cm}^2$  cell culture flasks, filled with 2.5 ml RPMI-complete medium and incubated for at least 7 days. During this time the fibroblasts proliferated and migrated out of the tissue and attached on the bottom of the culture flask. After 7 days the medium was refreshed followed by refreshment every 2 days. When large numbers of fibroblasts were attached to the culture flask, the cells were either directly cryopreserved (see chapter: cryopreservation) or used for further cultivation (see below).

#### *Cultivation*

To passage the isolated fibroblasts, the medium was discarded and cells were washed with PBS (w/o  $\text{Ca}^{2+}$ ,  $\text{Mg}^{2+}$ ). In order to detach the fibroblasts, 3 ml of 0.05% trypsin-0.02% EDTA-solution per  $25 \text{ cm}^2$  culture flask (volume was adapted when using other sizes of culturing dish) was applied onto the cells for 1.5 min at room temperature. Subsequently, the trypsin-solution was decanted and the fibroblasts were incubated for another 1.5 min at 37°C. Due to pitching the flask/dish onto a working bench the cells were finally detached and to stop trypsin reaction, cells were rinsed into an appropriate amount of 10% FCS-solution. Pelleting the cells was achieved by centrifugation at 808 g for 5 min. The pellet was then resuspended

in an appropriate amount of RPMI-complete medium. Cells were either split in a ratio of about 1:3 or seeded for experimental setting (see Pages 34 and 39).

### 2.7.1.3 Cryopreservation and thawing of primary cells

#### Media:

##### **Cryo medium**

Prepared in RPMI-complete or KGM2

FCS	10%
DMSO	10%

The medium was always prepared fresh before freezing the cells.

#### *Freezing*

Primary human cells were cryopreserved for storage over longer periods. Therefore the cells were trypsinised/detached (as described above). After pelleting, the cells were dissolved in an appropriate amount of cryo medium (3 ml per 10 cm petri dish). 1 ml of this cryo medium-cell-mix was transferred into cryo tubes and the tubes again were transferred into a special freezing container (Nalgene, “Mr. Frosty” Freezing Container Rack), which guaranteed a constant cooling process of about 1°C/min. Subsequently the containers were stored at -80°C for at least over night. The following day the tubes could be transferred into liquid nitrogen and the cells were maintained at -196°C.

#### *Thawing*

To reculture frozen cells, the tubes were first transferred from the liquid nitrogen into warm water (37°C) for 2-3 min. After mixing, the cryo medium-cell mix was given into 5 ml PBS (w/o Ca<sup>2+</sup>, Mg<sup>2+</sup>) to wash the cells. After pelleting by centrifugation at 808 g for 5 min the pellet was resuspended in an appropriate amount of particular culture medium and transferred into the desired cell culture dish to be maintained in the incubator until being either split or used for experimental setup.

### 2.7.1.4 Counting of cell suspensions

In experimental setups it is important to seed a certain amount of cells. Therefore cells were detached from the culture plate (as described above). After centrifugation the pellet was resuspended in the (for the particular assay) minimal necessary amount of particular medium to count the cells. Cells were counted with Countess Cell Counter according to manufacturer’s specifications. Hereupon the necessary dilutions were calculated and cells seeded in required densities.

## 2.7.2 Keratinocyte submerged culture

### Media:

#### EpiLife

EpiLife basal medium was prepared with supplements (HKGS) to obtain EpiLife according to manufacturer's specifications.

#### EpiLife high $\text{Ca}^{2+}$

Prepared with EpiLife (see above)

$\text{CaCl}_2$	1.8 mM
-----------------	--------

EpiLife and EpiLife high  $\text{Ca}^{2+}$  were stored at 4°C for up to 4 weeks.

To analyse specific TJ effects on NHEKs without a functional *Stratum corneum*, the submerged culture model was used. Therefore passage 3 NHEKs were seeded in EpiLife medium to a density of 40.000 cells in 200  $\mu\text{l}$  per insert on the apical part of 24 well transwell inserts (Costar Transwell, Corning Incorporated, New York, USA) (Figure 10). Subsequently, the basal compartment was filled up with 1000  $\mu\text{l}$  of EpiLife medium.

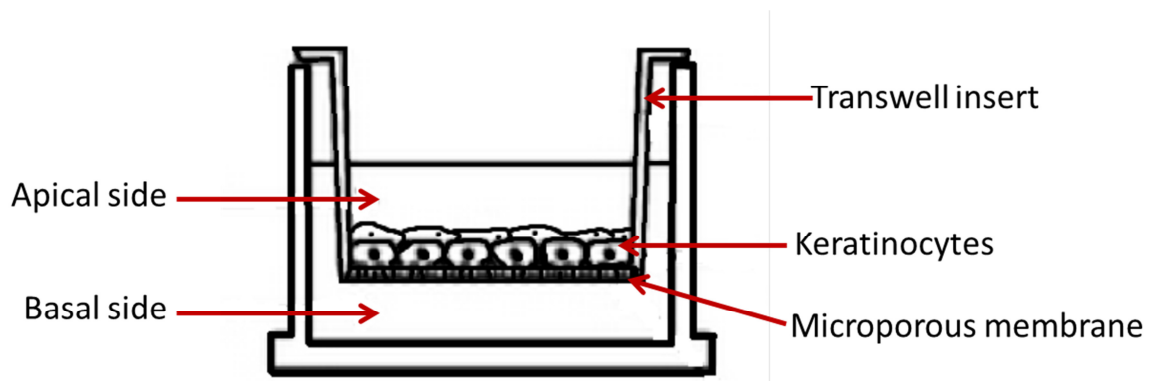


Figure 10: Schematic drawing of the submerged model.

For the usage of other dishes (12 or 24-well plates (for protein or mRNA isolation or letting the cells grow on cover slides)) the seeding density was adapted to the growth area.

After letting the cells attach and propagate to build a confluent monolayer for 3 days, the medium was shifted to EpiLife high  $\text{Ca}^{2+}$  in order to induce differentiation and TJ formation. Following this point, the medium was refreshed every 24 h. After 3 more days of maintenance the submerged model showed a proper TJ functionality ( $\text{TER} > 300 \Omega/\text{cm}^2$ ) and was used for bacterial inoculation approaches (see Page 43).

### 2.7.2.1 Cytokine culture

#### Media:

##### **IL-1 $\beta$ containing EpiLife**

Prepared with EpiLife high Ca<sup>2+</sup> (see above)

IL-1 $\beta$	100 ng/ml
--------------	-----------

The IL-1 $\beta$  containing medium was always prepared freshly.

##### **TNF $\alpha$ containing EpiLife**

Prepared with EpiLife high Ca<sup>2+</sup> (see above)

TNF $\alpha$	100 ng/ml
--------------	-----------

The TNF $\alpha$  containing medium was always prepared freshly.

In order to investigate the influence of parallel treatment with the proinflammatory cytokines IL-1 $\beta$  or TNF $\alpha$  to bacterial infection of submerged models, EpiLife containing the particular cytokine was applied at the time point of infection to the basal part of the model. Additionally, bacteria were diluted in the same particular cytokine containing medium and applied as described below.

### 2.7.2.2 Diseased culture (atopic dermatitis mimicking conditions)

#### Media:

##### **Cytokine and toll-like receptor agonist mix (CTM)**

Prepared with EpiLife high Ca<sup>2+</sup> (see above)

IL-1 $\beta$	60 ng/ml
Poly I:C	10 $\mu$ g/ml
Pam3CSK4	5 $\mu$ g/ml

The CTM containing medium was always prepared freshly.

In order to perform experiments in a diseased context and to mimic an AD background, submerged cultures were treated with a cytokine and toll-like receptor agonist mixture after instructions of Pierre Fabre Dermo-Cosmétique (Bernard et al., 2017). Thereby IL-1 $\beta$  represents a cytokine being enhanced in AD, and Poly I:C (TLR3) and Pam3CSK4 (TLR1/2) represent TLR activators as AD usually is associated with skin infections and due to the barrier decrease the contact of PRRs to their agonists is enhanced. Treatment of NHEKs in the submerged model with the CTM was performed 24 h after shifting the cells to high Ca<sup>2+</sup> for 24 h. CTM containing medium was only applied from the basal part of the submerged model, whereas the apical part was refreshed with EpiLife high Ca<sup>2+</sup>. After 24 h of treatment, CTM containing medium was replaced with EpiLife high Ca<sup>2+</sup>.



### 2.7.3 3D models

In order to perform investigations closer to the *in vivo* situation, two different types of 3D models have been used in this work. The first type was the reconstructed human epidermis (RHE) consisting of only keratinocytes on a microporous membrane building a multi-layered epithelium (Figure 11 A). RHEs used within this work have been built either after the protocol from CellnTec or Pierre Fabre (see below). The second type of 3D models that was used was a reconstructed human skin (RHS) model after the protocol from Mildner et al. (2006). This is a full skin model consisting of a dermal equivalent (with primary human fibroblasts embedded in a collagen matrix) and an epidermal part (with NHEKs) (Figure 11 B).

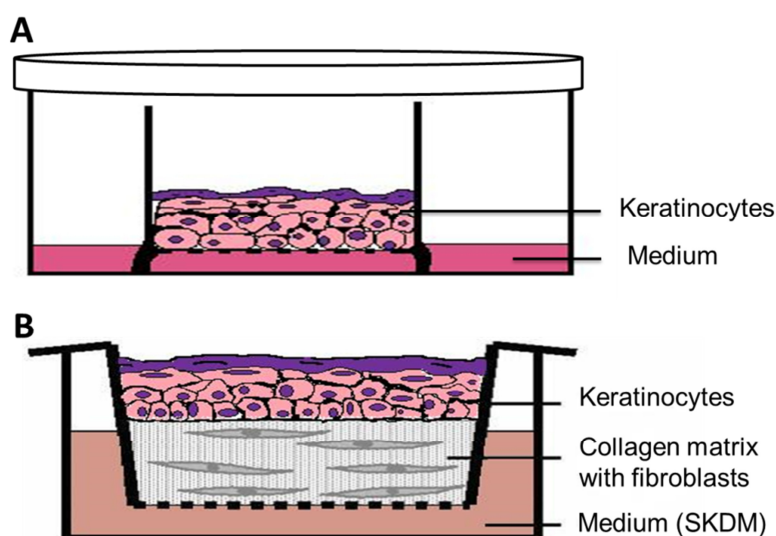


**Figure 11: Schematic drawing of the different types of 3D models used within this work.** Reconstructed human epidermis (RHE) (A) and reconstructed human skin (RHS) (B). SKDM - Serumfree defined keratinocyte medium.

#### 2.7.3.1 RHE according to protocol of CellnTec (CnTe3D)

##### Media:

##### 3D medium

Composed of basal medium (CnT-BM.3-500) and 3 supplements (A, B, and, C: CnT-02-3DP5.S).

Supplements were given into basal medium according to manufacturer's specifications.

The medium was stored at 4°C for up to 2 weeks.

##### *Preparation and seeding*

Millicell PCF inserts (0.4  $\mu$ m PCF, 12 mm diameter; Merck Millipore, Tullagreen, Ireland) were placed in 10 cm petri dishes with a maximum of 9 inserts per dish.  $5 \times 10^5$  keratinocytes/ml in passage 3 were prepared as described above in KGM2 (see Page 32) and 400  $\mu$ l of this solution (corresponding to  $2 \times 10^5$  cells) were given into each insert. Afterwards the basal part was carefully filled with KGM2 up to the volume of the apical liquid inside of the inserts ( $\sim 30$  ml) and incubated for 3 days.

*Medium change*

After 3 days the medium was replaced in the basal as well as apical compartment with 3D medium and the models were incubated for another night.

*Air-liquid-interface*

To initiate differentiation and 3D structure, NHEKs were then incubated under air-liquid-interface (ALI) conditions. Therefore apical as well as basal medium was removed and only the basal part was refilled with 3D medium up to the bottom of the inserts (~ 8 ml). The models were incubated and medium was changed every 2 days.

## 2.7.3.2 RHE according to protocol of Pierre Fabre (PFe3D)

**Media:**

**EpiLife (see Page 35) containing 1.5 mM CaCl<sub>2</sub>**

**PFe3D medium**

Prepared with EpiLife

CaCl <sub>2</sub>	1.44 mM
2-phospho-L-ascorbic acid	92 µg/ml
Recombinant human KGF/FGF-7	10 ng/ml

The supplements were kept in aliquots at -20°C and always added freshly directly before using the medium.

*Before*

One night before building the models, NHEKs (cultured in KGM2) were incubated with fresh EpiLife.

*Preparation and seeding*

Millicell PCF inserts were placed into one well of a 6-well plate each. Passage 3 keratinocytes were trypsinised (as described above) and prepared in EpiLife containing 1.5 mM CaCl<sub>2</sub>. From the moment of detachment, cells were kept on ice until seeding. 500 µl of a solution with 4 x 10<sup>5</sup> cells/ml were given into each insert with circulating movement of the pipette. Right after seeding, the basal part was filled up with 2.5 ml EpiLife containing 1.5 mM CaCl<sub>2</sub> (at room temperature). After controlling that no air bubbles formed under each model, incubation for 30 h followed.

*Air-liquid-interface*

The next day models were lifted to ALI. Therefore the medium was carefully removed from the apical as well as from the basal part. 1.5 ml of PFe3D medium was given under each

model thereby carefully avoiding air bubbles. Refreshment of the basal medium was repeated every second day.

### 2.7.3.3 Reconstructed human skin (RHS)

#### Media:

##### **Serumfree defined keratinocyte medium (SKDM)**

Prepared in KGM2 (see Page 32) without bovine pituitary extract (BPE)

CaCl <sub>2</sub>	1.3 mM
BSA	1 mg/ml
Ascorbic acid	50 µg/ml

The medium was filtered sterile and stored at 4°C for up to 2 weeks.

#### Solutions:

##### **Collagen-solution**

Preparation for 1 well (1 model)

PureCol (bovine collagen)	2 ml
HBSS (10x)	0.25 ml

Depending on the number of models this solution was prepared freshly in a 50 ml reaction tube on ice. With some drops of 1N NaOH solution the pH was adjusted to 7.4, which was easily confirmed with a change in colour of the whole solution from orange to pink.

RHS models were constructed as described before (Mildner et al., 2006). To build these models, passage 3 primary human keratinocytes and fibroblasts (in passages 2-5) were used. Directly before starting, a 37°C-incubator (without additional CO<sub>2</sub>) was sprayed with Aqua dest. to provide a humidified atmosphere and the amount of required 6-well membrane inserts (High Density Translucent PET Membranes; BD Biosciences, Bedford, UK) were placed into deep-well plates (Biocoat Deep-Well plate; BD Biosciences, Bedford, UK).

#### *Preparation of a collagen-fibroblast-mix (gel-matrix)*

First, the collagen solution was prepared as described above. Then fibroblasts were trypsinised and resuspended in 10% FCS solution (see Page 32). The cell suspension was counted and  $2.5 \times 10^5$  fibroblasts/model were pipetted into a new tube and cells were spun down at 808 g for 5 min. After discarding the supernatant the pellet was resuspended in 0.25 ml FCS/model. The fibroblasts in FCS and the collagen solution were mixed very carefully, avoiding bubbling. 2.5 ml of this mix were pipetted onto the membrane insert (again avoiding of bubbling) in the prepared deep-well plates. Subsequently, the collagen-fibroblast-gel-mix was incubated for 2 h at 37°C in humidified atmosphere without additional CO<sub>2</sub> (before sprayed incubator) where the mix could coagulate.

*Equilibration*

To equilibrate the gels 16 ml KGM2 (see Page 32) were used per model. 14 ml were given to the basal part and 2 ml to the apical part, followed by incubation for another 2 h at 37°C in a humidified atmosphere but 5% CO<sub>2</sub> in air.

*Addition of keratinocytes and ALI*

After equilibration, the apically applied 2 ml of KGM2 were replaced with the equal volume of KGM2 containing  $1.5 \times 10^6$  keratinocytes, followed by incubation for 24 h. At the next day, the basal and the apical medium were carefully replaced with SKDM to be incubated for another 24 h. Finally, the models were cultured at ALI conditions. Therefore the medium from the apical part was removed and the medium from the basal part was changed to 10 ml of fresh SKDM. From this on, the medium was refreshed every 2 days.

**2.7.4 Bacterial culture and inoculation****Media/Agar plates:****Brain-heart-infusion-agar (BHI)**

Prepared according to manufacturer's specifications.

Depending on bacterial strain antibiotics were added (10 µg/ml respectively).

**2.7.4.1 Bacterial culture and cryopreservation**

For cryopreservation Cryobank tubes (Mast group Ltd, Bootle, Great Britain) were used. Bacterial colonies from a fresh, pure culture were inoculated in a tube filled with glass beads and cryopreservative fluid (already filled by manufacturer). After mixing carefully, the fluid was removed and the tube was stored at -80°C. For thawing, one bead was removed from the vial and streaked immediately over appropriate agar surface. Bacterial colonies were grown over night at 37°C. To ensure the pureness, the streak plate isolation method was used for further cultivation on fresh agar plates. After the growth of bacterial strains at 37°C over night, the agar plates were kept at 4°C for up to 6 weeks and used to prepare fresh bacterial cultures when needed.

2.7.4.2 Generation of *S. aureus*  $\Delta agr$  strain**Media:****Softagar**

Prepared in Aqua dest.

Nutrient broth 2	20 g/l
NaCl	5 g/l
CaCl <sub>2</sub>	0.4 g/l
Bactoagar	7 g/l

After unsterile preparation, softagar was dissolved and sterilized via autoclavation (30 min at 125°C and 1.5 bar) and kept at room temperature for up to 2 weeks. Directly before usage it was liquidated by heating in the microwave (at 600 W) until cooking.

**NB<sup>2+</sup>-medium**

Prepared in Aqua dest.

Nutrient broth 2	20 g/l
CaCl <sub>2</sub>	0.4 g/l

NB<sup>2+</sup>-medium was sterilized by autoclavation (see above) and kept at room temperature for up to 2 weeks

**Brain heart infusion broth (BHI-broth)**

Prepared in Aqua dest. according to manufacturer's specifications.

SH1000 $\Delta agr$  strain was constructed using phage transduction from RN6390 $\Delta agr$  (Novick et al., 1993), where a tetracycline-resistance (tetM cassette) replaces the *arg* locus. An over night culture of *S. aureus* RN6390 $\Delta agr$  at an optical density at 600 nm (OD<sub>600</sub>) of 1.0 was infected with phage 11 (Sjöström and Philipson, 1974) (~ 10<sup>9</sup> plaque forming units) in softagar and incubated over night at 30°C. In order to resuspend the plaque containing softagar, 5 ml of NB<sup>2+</sup>-medium were added and the resulting suspension sonificated on ice (10 s at 35% amplitude; Branson sonifier). Subsequently the softagar was pelleted by centrifugation (30 min; 3913 g). The supernatant, which contained the plasmid-bearing phage particle lysate was filtrated with a 0.2 µm filter (Thermo Fischer, Rockford, USA). *S. aureus* SH1000 at an OD<sub>600</sub> of 8.0 in NB<sup>2+</sup>-medium was mixed 1:1 with the phage lysate and incubated for 30 min at 37°C allowing phage particle adsorption to bacterial host cells. After adding sodium citrate to a final concentration of 20 mM, bacteria were washed 3 times in BHI-broth and incubated for 1 h at 37°C in BHI-broth containing 10 µg/ml tetracycline. Afterwards, the suspension was plated onto agar plates with selective BHI-medium containing tetracycline (10 µg/ml) and incubated for 24 h at 37°C. Plates were screened for resistant colonies, which were transferred to BHI selective medium for further investigation.

*Confirmation of S. aureus  $\Delta$ agr mutants using PCR***Primer:****Primer for detection of the tetM cassette**

Oligoname	Sequence (5' → 3')
TetM_reverse	TAGGTATACAAGCATACAGATATTCTC
TetM_forward	TCGATGTATTCAAGAAGATTATCGC

The primer have been ordered at Eurofins Genomics (Ebersberg, DE)

**Buffer:****Trizma base-boric acid-EDTA buffer (TBE-buffer)**

Prepared in Aqua dest.

Trizma base	90 mM
Boric acid	90 mM
EDTA	2.5 mM

TBE-buffer was stored at room temperature for up to one year.

**Agarose-gel**

Prepared in TBE-buffer

SeaKem LE-Agarose	1%
-------------------	----

Agarose was dissolved in TBE-buffer by heating in the microwave oven at 600 W till TBE-buffer boiled. After a short cooling 5  $\mu$ l Red Safe solution was added. Liquid agarose-gel was poured into a gel-chamber system (MWG-Biotech, Ebersberg, DE) and coagulate for 1 h.

**Loading buffer**

Prepared in Aqua dest.

Glycerine	50%
EDTA	1 mM
Bromphenol blue	0.25%

Loading buffer was stored at -20°C.

*DNA-Isolation*

Bacterial DNA (template DNA) was isolated using an appropriate amount of bacterial material (approximately one inoculation loop) in 200  $\mu$ l of InstaGene matrix. After adding of 10  $\mu$ l Lysostaphin, an incubation for 60 min at 37°C followed. Next steps were vortexing for 2 min, 20 min at 56°C, vortexing for 2 min, 8 min at 100°C and again vortexing for 2 min. Following this, the resulting supernatant after centrifugation for 5 min at 16350 g contained the isolated DNA. The amount of total DNA was determined with NanoDrop machine and DNA was stored at -20°C.

*PCR*

The polymerase chain reaction (PCR) was performed with a Thermocycler. Reactions (25  $\mu$ l) contained 1 pmol/ $\mu$ l each primer, ~20 ng template DNA and included in Phusion high-Fidelity PCR kit: 2.5  $\mu$ l buffer, 0,5  $\mu$ l deoxynucleoside triphosphates, 1  $\mu$ l Polymerase (Phusion). Reactions were run for 30 cycles: 30 s at 98°C, 55 s at 55°C and 1 min at 72°C.

20  $\mu$ l of PCR products were mixed with 4  $\mu$ l of loading buffer, transferred onto an agarose-gel, and separated at 130 V for 45 min. As a positive control PCR products of RN6390 $\Delta$ agr

and as a negative control PCR products of SH1000 (WT) were analysed as well. Finally the PCR products were visualized using ChemiDoc XRS (BioRad, Hercules, USA) were at about 2300 base pairs a thick band was visible for both  $\Delta agr$  strains, while no band was visible for the wild-type control.

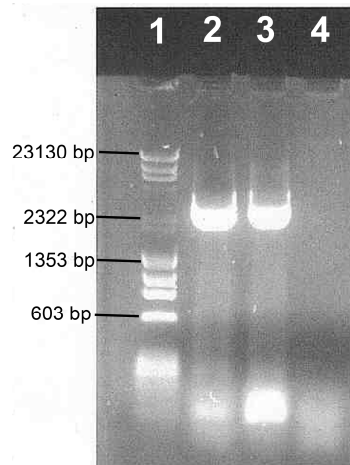


**Figure 12: Visualization of PCR products of TetM cassette in  $\Delta agr$  strains.** Line 1: DNA size standard representing fragment sizes in base pairs (bp); Line 2: PCR product of RN6390 $\Delta agr$  (positive control); Line 3: PCR product of SH1000 $\Delta agr$ ; Line 4: PCR product of SH100WT (negative control).

#### 2.7.4.3 Creation of bacterial suspensions

Bacterial strains were freshly transferred on specific agar plates with the help of an inoculation loop and incubated over night at 37°C.

The next day cultured strains were inoculated in 5 ml of either 0.9% NaCl solution or EpiLife high  $\text{Ca}^{2+}$  medium (see Page 35) to an  $\text{OD}_{600}$  of 1.0 (corresponding to  $\sim 10^9$  staphylococci/ml). For further usage 1:10 dilutions were prepared in the appropriate medium up to the bacterial concentration needed.

#### 2.7.4.4 Bacterial inoculation of submerged culture

For bacterial inoculation of the submerged culture, bacteria were diluted in EpiLife high  $\text{Ca}^{2+}$  medium (see Page 35) or cytokine containing medium (see Page 36) to the indicated concentrations ( $10^6$  or  $10^4$  bacteria/ml corresponding to  $6 \times 10^5$  bacteria  $\text{cm}^{-2}$  or  $6 \times 10^3$  bacteria  $\text{cm}^{-2}$ ). For treatment, first the basal medium was refreshed with particular sterile medium to avoid contamination. Afterwards the 200  $\mu\text{l}$  of apical medium were removed and replaced with either sterile medium as control or medium containing bacteria. Using the same bacterial concentrations compared to the growth area, this was also performed in well plates (12 or 24 well plates) for the incubation on cover slides or the isolation of mRNA and protein.

#### 2.7.4.5 Bacterial inoculation of PFe3D

For bacterial inoculation of PFe3D models, bacteria were diluted in 0.9% NaCl solution to a concentration of  $10^7$ /ml. On day 4 after lifting the models to ALI, the basal medium was refreshed first. Then the models were treated apically either with nothing (control), with 5  $\mu$ l of sterile NaCl solution or with 5  $\mu$ l of bacterial suspension (corresponding to  $5 \times 10^4$  bacteria  $\text{cm}^{-2}$ ). After transferring the 5  $\mu$ l onto the models, these were spread with small spatula (made out of Pasteur-pipettes by using a burner) (Figure 13) very carefully without touching the margins or the models surface. This was followed by incubation of the models for indicated time points. Medium refreshment was carried out after 48 h.

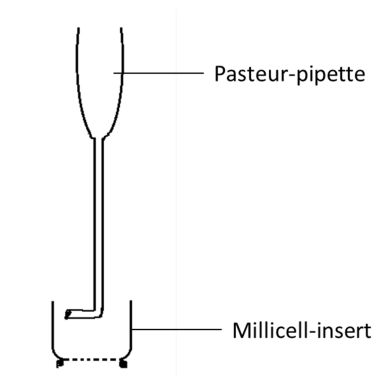


Figure 13: Schematic drawing of the small spatula made out of Pasteur-pipettes used for spreading of the bacteria on top of PFe3D models.

#### 2.7.4.6 Counting of bacterial growth on PFe3D models

For investigating whether the bacteria are able to grow/live on top of the models, the amount of living bacteria was evaluated by examining the colony forming units (CFU). Therefore models were cut very carefully out of the insert and placed together with the membrane in 2 ml reaction tubes filled with 500  $\mu$ l 0.9% NaCl solution and a metallic ball on ice. Using the TissueLyser for 2 min at 20 times per second, models were shred at 4°C. After a short centrifugation at 12280 g the suspension was placed for 1 min in an ultrasonic bath (Bandelin) in order to separate the bacteria that might have interconnected. Subsequently serial 1:10 dilutions of the bacterial suspension in NaCl solution were performed on ice and 100  $\mu$ l of appropriate and desired dilutions were plated evenly on BHI-Agar plates with a Drigalski spatula (dipped in 99% ethanol and flamed over a Bunsen burner before each plating). After incubation at 37°C for 48 – 72 h the CFU were counted and the CFU/model were calculated  $((\text{CFU} \times 10 \times \text{dilution factor}) / 2)$ .



#### 2.7.4.7 Visualization of the bacteria

For visualization of bacteria, GFP and RFP producing bacteria were used and incubated on the PFe3D as described above. After 0 or 24 h the models were cut out of the insert, placed on an object slide and covered with a cover slide. Fluorescent bacteria were visualized with an Axiophot II fluorescence microscope.

#### 2.7.5 Barrier assays

At indicated time points different assays in order to investigate barrier properties were performed with the models (submerged as well as 3D).

##### 2.7.5.1 Measurement of the transepithelial electrical resistance (TER)

The TER reflects the overall physical barrier function provided by the investigated test system cultured on a filter support. After TER measurement the culture was either further incubated or used for fixation. Before using the epithelial volttohmmeter, electrodes were equilibrated and sterilised according to the manufacturer's recommendations. Measuring the TER was carried out quite fast after taking the culture out of the incubator, as temperature shift does have an impact on the TER values. The ohmic resistance of the submerged models was measured by placing one electrode in the apical part and the other electrode in the basal part of the well and applying an electrical field (Figure 14). Also a blank (culture insert without cells) was measured in parallel and subtracted from the total resistance of the sample.

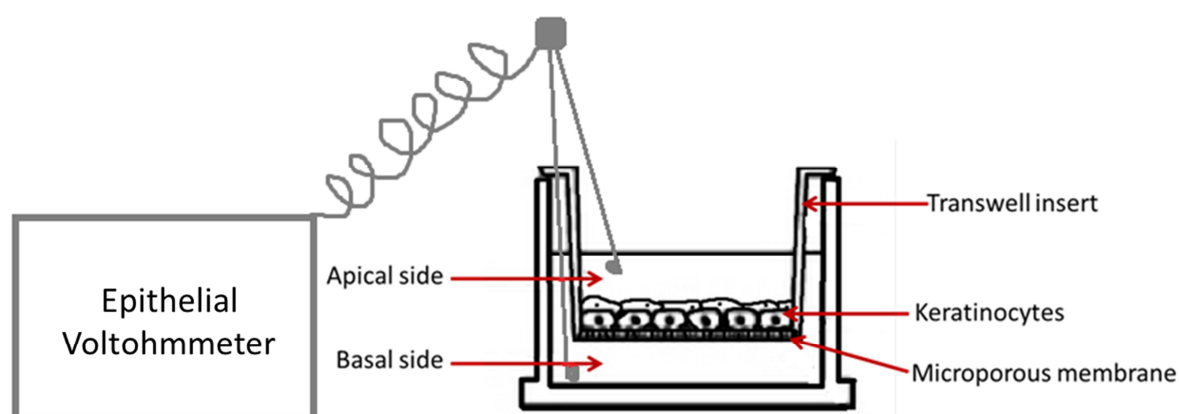


**Figure 14:** Exemplary schematic installation of transepithelial electrical resistance measurement with an epithelial volttohmmeter on submerged culture.

The ohmic resistance of RHE was measured by placing the models into one well of a 24-well plate and applying 600  $\mu$ l pre-warmed (37°C) PBS (w/o  $\text{Ca}^{2+}$ ,  $\text{Mg}^{2+}$ ) to the basal part and 400  $\mu$ l pre-warmed PBS (w/o  $\text{Ca}^{2+}$ ,  $\text{Mg}^{2+}$ ) onto the apical part. Electrodes were used as

described. The final unit area resistance ( $\Omega \cdot \text{cm}^2$ ) was calculated by subtracting the blank and multiplying the sample resistance with the area of the membrane system ( $0.33 \text{ cm}^2$  for 24-well transwell inserts and  $0.6 \text{ cm}^2$  for RHE inserts).

### 2.7.5.2 Tracer permeability assay for submerged models

#### Solution:

##### Fluorescein isothiocyanate dextran of 4 kDa solution (FD4 solution)

Prepared in EpiLife high  $\text{Ca}^{2+}$  (see Page 35)

FD4	312.5 $\mu\text{M}$
-----	---------------------

FD4 solution was prepared freshly from a stock solution of 2.5 mM in Aqua dest.

For measurement of paracellular permeability of submerged NHEKs, a 4 kDa tracer was used (FD4). Permeability was measured in the same context as TER measurement was performed. 200  $\mu\text{l}$  of FD4 solution were applied on the apical side directly after TER measurement, and incubated for 2 h. Subsequently the basal medium was collected in a 96 well plate (black, flat-bottom) and analysed with a Fluorescence reader. Permeability was compared to a calibration line and calculated as described before (Kirschner et al., 2013):  $P (10^{-6} \text{ cm/s}) = \text{flux (nmol} \times \text{h}^{-1} \times \text{cm}^{-2}) / \text{concentration (mmol/l)} \times 3.6$

### 2.7.5.3 Biotinylation assays

#### Biotinylation solution

Prepared in PBS (w/o  $\text{Ca}^{2+}$ ,  $\text{Mg}^{2+}$ )

EZ-Link Sulfo-NHS-LC-Biotin	0.5%
-----------------------------	------

$\text{CaCl}_2$	1 mM
-----------------	------

The solution was always prepared directly before usage.

The biotinylation assay is a well-known method used for analysing the inside out TJ barrier on 3D models and also on *ex vivo* skin (e.g. Yuki et al., 2007; Kirschner et al., 2010). RHE models were incubated with 200  $\mu\text{l}$  biotinylation solution from the basal part for 30 min (submerged models 20 min onto 25  $\mu\text{l}$  biotinylation solution and RHS models for 45 min onto 200  $\mu\text{l}$  biotinylation solution) at  $37^\circ\text{C}$ . During this time the tracer passed through the intercellular spaces thereby biotinylating cell surface molecules and being stopped at functional TJs. Afterwards the models were cut out of the insert and stored in Formafix solution up to 3 days at  $4^\circ\text{C}$  until they were embedded in paraffin (see Page 53). After cutting the paraffin sections, during immunohistochemical staining (see Page 54), together with the secondary antibody, streptavidin labelled with texas red was applied 1:700 in PBS\_IHC (see Page 54) on the sections to visualize the biotinylation for fluorescence microscopy. To evaluate the TJ functionality quantitatively, tracerstops per visual field were counted under the microscope (see below).

### Evaluation of Biotin-SH permeation stops

The amount of complete Biotin-SH permeation stops per visual field (Axiophot II microscope, 40x) were counted. In addition, also sites with a thin line of Biotin-SH right after the actual stop were counted. These sites were called “half stops” (Figure 15).

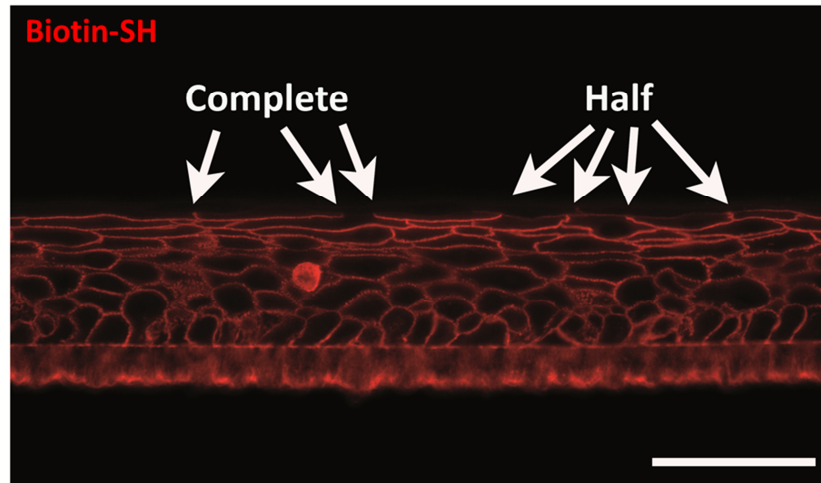


**Figure 15:** Examples for “complete stops” and “half stops” of Biotin-SH in PFe3D. Bar = 50  $\mu\text{m}$  (with permission from Bäsler et al. (2017)).

To calculate the permeability in control PFe3D models, complete stops and half stops were counted per visual field in 3 models per donor with at least 5 visual fields per model. Then mean amount of complete stops in control models was calculated and permeability of each individual control model determined by the formula:

**Mean of complete stops in control models – complete stops in an individual control model + half stops in an individual control model = amount of permeated TJs per visual field in a distinct control model**

For treated PFe3D (NaCl and *S. aureus* or *S. epidermidis* treatment) also 3 models per donor and treatment with at least 5 visual fields per model were counted and permeability was calculated as follows:

**Mean of complete stops in control models – complete stops in a treated model + half stops in a treated model = amount of permeated TJs per visual field in a treated model**

## 2.8 Molecular biological and biochemical analyses

### 2.8.1 Protein analyses by Western Blotting

#### Lysis buffer:

##### RIPA-buffer

Prepared in Aqua dest.

Tris	50 mM
NaCl	150 mM
NP40 (Igepal)	1%
Sodium deoxycholat	0.5%
EDTA	5 mM
Sodium dodecyl sulfate (SDS)	0.1%

The buffer was stored at 4°C for up to 6 months.

##### Proteinase-inhibitor-mix (100 x)

Prepared in Aqua dest.

Leupeptin	1 mg/ml
Pepstatin	mg/ml
Bacitracin	10 mg/ml
phenylmethane sulfonyl fluoride (PMSF)	10 mM

The mix was stored in aliquots at -20°C for up to one year.

#### Lysis-buffer:

98 parts of RIPA-buffer + 1 part of phosphatase inhibitor + 1 part of proteinase-inhibitor-mix.

The lysis-buffer was always prepared freshly.

#### Proteinquantification:

##### Bradford's reagent:

Prepared in Aqua dest.

Coomassie brilliant blue	0.01%
Orthophosphoric acid (88%)	1.6 M
Ethanol (99%)	0.8 M

The reagent was stored at 4°C for up to 3 months.

Before usage, the reagent was always filtered freshly.

#### SDS-PAGE:

##### Acrylamid-solution:

Prepared in Aqua dest.

Acrylamid	30%
Bis	0.8%

The solution was stored at 4°C for up to 6 months.

##### Separating gel buffer, pH 8.8

Prepared in Aqua dest.

Tris	1.5 M
SDS	0.4%

The solution was stored at 4°C for up to 6 months.

##### Stacking gel buffer, pH 6.8

Prepared in Aqua dest.

Tris	0.5 M
SDS	0.4%

The solution was stored at 4°C for up to 6 months.

**Ammonium persulfate (APS)**

Prepared in Aqua dest.

APS	10%
-----	-----

The solution was stored at -20°C for up to 6 months.

**Electrophoresis buffer, pH 8.8**

Prepared in Aqua dest.

Glycine	0.19 mM
Tris	23 mM
SDS	0.2%

The buffer was stored at room temperature for up to 1 year.

**Sodium dodecyl sulfate (SDS) sample buffer, pH 6.8**

Prepared in Aqua dest.

Tris	60 mM
Glycerine	10%
β-Mercaptoethanol	10%
SDS	5%
Bromphenolblue	0.5%

The buffer was stored at 4°C for up to 6 months.

**Protein transfer:****Transfer buffer**

Prepared in Aqua dest.

Methanol	20%
Glycine	192 mM
Tris	25 mM
SDS	0.02%

The buffer was stored at 4°C for up to 1 year.

**Protein detection:****Tris-buffered saline and Tween 20 for Western Blot (TBST\_WB), pH 7.4**

Prepared in Aqua dest.

Tris	10 mM
NaCl	150 mM
Tween 20	0.05%

The buffer was stored at room temperature for up to 1 year.

*Protein extraction and quantification*

Protein was extracted from submerged as well as 3D models. The submerged NHEKs were washed twice with cold PBS (w/o  $\text{Ca}^{2+}$ ,  $\text{Mg}^{2+}$ ). Depending on the size of the culture dish used, cells were incubated with 35-70  $\mu\text{l}$  of lysis buffer for 15 min on ice and shook with a shaker. Cells were then scraped into a 0.5 ml reaction tube and centrifuged for 15 min at 4°C and 12280 g. For lysis of 3D models, 70  $\mu\text{l}$  lysis buffers were used in 2 ml reaction tubes. Whole models were placed in these tubes together with a metallic ball. Using the TissueLyser for 3 min at 30 times per second, models were shred at 4°C followed by centrifugation for 15 min at 4°C and 12280 g. The resulting supernatant of submerged and 3D models contained soluble proteins and was kept for short-term (up to 4 weeks) at -20°C and for long-term storage at -80°C.

Quantification of protein concentration was performed using Bradford's assay (Bradford, 1976) in a 96 well plate. 1  $\mu$ l of protein samples was diluted with 19  $\mu$ l Aqua dest. After adding of 180  $\mu$ l Bradford's reagent, the absorption was measured at 595 nm in a plate reader. A calibration line was generated with bovine serum albumin at different dilutions, which were treated similar to the samples. Based on the calibration line, the amount of protein of each sample was calculated.

### *SDS Polyacrylamid gel electrophoresis (SDS-PAGE)*

After quantification of the protein amount, samples were diluted 1:1 in SDS sample buffer and denatured for 5 min at 95°C. The SDS polyacrylamide gel electrophoresis was then used to separate proteins according to their molecular weight in a discontinuous gel system by usage of the Mini-PROTEAN®3 System by BioRad. The system was used according to manufacturer's specifications. Basically, the percentage of SDS-Polyacrylamide Gel, according to protein molecular size of interest, was chosen (Table 9).

**Table 9: Composition of SDS-PAGE gels of different pore sizes.**

APS - Ammonium persulfate; TEMED - Tetramethylethylenediamine

Solution	Separating gel 8% (35-120 Da)	Separating gel 12% (15-60 kDa)	Separating gel 14% (12-50 kDa)	Stacking gel
Acylamid solution	8 ml	12 ml	14 ml	1.3 ml
Separating gel buffer	7.5 ml	7.5 ml	7.5 ml	-
Stacking gel buffer	-	-	-	2.5 ml
Aqua dest.	14.2 ml	12.2 ml	8.2 ml	5.9 ml
APS (10%)	300 $\mu$ l	300 $\mu$ l	300 $\mu$ l	300 $\mu$ l
TEMED	10 $\mu$ l	10 $\mu$ l	10 $\mu$ l	10 $\mu$ l

First, separating gel was prepared under stirring and immediately poured in the gel fixture. After solidifying for 30 min covered with 2-propanol, stacking gel was prepared and poured directly onto the separating gel after discarding the 2-propanol and washing with Aqua dest. Subsequently a comb with the necessary amount of pocket forming units (10 or 15) was placed in the liquid stacking gel allowing it to solidify for another 30 min. Gels and electrophoresis buffer were placed into an electrophoresis chamber and 10  $\mu$ g of denatured protein were applied into the gel pockets. As a molecular weight standard prestained SDS molecular weight marker was used. Finally, to separate the proteins, an electric field with 70 V for 15 min was applied first and increased to 180 V until the proteins were separated as wanted.

*Transfer of proteins*

The separated proteins were transferred afterwards onto a nitrocellulose membrane (0.45 µm; Bio-Rad, Hercules, USA). Therefore, the gels were carefully prepared out of the gel fixture and either placed with the membrane in a semi-dry-blot chamber for smaller molecules or in a maxi-wet tank for the blotting of larger proteins. Blotting was performed in blot buffer according to manufacturer's specifications.

To monitor transferred proteins and therefore to control the blotting, the membrane was incubated with Ponceau S solution for 5 min. After a short washing step in tap water red protein bands were visible. Washing the membrane 3 x 5 min in TBST\_WB resulted in discoloration of protein bands and the membrane was ready for antibody protein detection.

*Antibody protein detection*

To guarantee a specific detection, blots were washed in 5% non-fat milk in TBST\_WB for 1 h in order to block exposed hydrophobic sites and thereby inhibit unspecific binding. Protein specific antibodies were diluted in 5% non-fat milk in TBST\_WB and the blots were probed with the primary antibody over night at 4°C under rotation.

After removing unbound antibodies by washing the membrane three times 10 min in TBST\_WB, blots were incubated with horseradish peroxidase-conjugated secondary antibodies (diluted in 5% non-fat milk in TBST\_WB) directed against host species of the primary antibody for 30 min rotating at room temperature. Then the blots were washed three times 5 min in TBST\_WB. For visualisation, the blots were incubated with chemiluminescent substrate (ECL-system) for 5 min in the dark. Finally, the specific protein bands were detected by exposing the blot to an x-ray film for 30 sec to 15 min in the dark and developing the film afterwards according to manufacturer's specifications. For densitometric quantification ImageJ-software (Fiji) was used and bands were quantified relative to a loading control (β-actin) to correct for loading error.

**2.8.2 mRNA analyses by quantitative real-time PCR**

To investigate alterations in mRNA levels after bacterial inoculation quantitative real-time PCR was used. The mRNA was isolated from submerged NHEKs grown in 12- or 24- well plates with the RNeasy mini kit. After washing the cells twice with cold PBS (w/o Ca<sup>2+</sup>, Mg<sup>2+</sup>) on ice, the cells were lysed in 300 µl RLT buffer (included in the kit) containing 1%

$\beta$ -mercapthoethanol and mRNA was isolated according to the manufacturer's specifications. The final amount of RNA was measured using the NanoDrop machine.

Afterwards the 3  $\mu$ g mRNA were transcribed into cDNA by using Maxima First Strand cDNA Synthesis Kit for RT-qPCR according to the manufacturer's specifications. By incubation for 10 min at 25°C, 15 min at 50°C and 5 min at 85°C in a thermoblock (Biometra) cDNA was generated. 0.5  $\mu$ l of the cDNA (diluted 1:25 in Aqua dest.) was used as a template in real-time-PCR analysis with the FAM dye-labeled TaqMan MGB probes according to the protocol of Applied Biosystems. Quantitative real-time-PCRs were performed in a light cycler 96 under following conditions:

**1x Preincubation:**

50°C for 120 s  
95°C for 600 s

**45x 2 step amplification:**

95°C for 10 s  
60°C for 30 s

**1x Cooling:**

37°C for 30 s

All real-time-PCR analyses were performed in triplicates. Relative transcriptional levels within distinct experiments were determined by using the  $2^{-\Delta\Delta C_t}$  method (Livak and Schmittgen, 2001).

### 2.8.3 Analyses of protein levels of cytokines

Analyses on the protein level of cytokines was performed on sterile filtered apical supernatants of TER measurement assays with MILLIPLEX MAP Human Cytokine/Chemokine Magnetic Bead Panel - Immunology Multiplex Assay (Merck, Darmstadt, Germany) at Pierre Fabre Dermo-Cosmétique according to manufacturer's specifications.

## 2.9 Stainings/histological methods

### 2.9.1 Tissue-MTT

In order to investigate the tissue viability of submerged and 3D models, MTT staining was performed. Thereby NAD(P)H-dependent cellular oxidoreductase enzymes of living cells reduce the tetrazolium dye MTT (3-(4,5-dimethylthiazol-2-yl)-2,5-diphenyltetrazolium bromide) to the insoluble formazan, which appears deep purple. MTT solution (1 mg/ml in particular growth medium) was applied basically (600  $\mu$ l in a 24 well plate for 3D models and 1 ml for the submerged models) as well as apically (400  $\mu$ l on top of the 3D models and



200 µl to the submerged models). After incubation for 4 h at 37°C and 5% CO<sub>2</sub> in a humidified atmosphere, the models were cut out of their inserts, cut in two halves and placed vertically in a cryomold (Tissue-Tek; Torrance, USA) filled with cryomatrix. After freezing at -24°C, models were cut into 8 µm slices using a cryostat before light microscopic analyses.

### 2.9.2 Fixation in formalin and embedding in paraffin

Either RHS, RHE or NHEKs on transwell filters were used for fixation and embedding in paraffin. For fixation the models were cut out of the insert and placed into 1.8 ml Formafix-solution in a 2 ml reaction tube. The models were fixed either 1 h at room temperature or up to 72 h at 4°C in the Formafix-solution. Afterwards, models were placed between two filter sponges (soaked with Formafix-solution) in embedding cassettes (Tissue-Tek; Torrance, USA), which were subsequently positioned in the paraffin embedding automat using the following schedule:

1.	Tap water	20 min
2.	Ethanol 70%	20 min
3.	Ethanol 80%	20 min
4.	Ethanol 96%	20 min
5.	Ethanol 96%	20 min
6.	Ethanol 99%	20 min
7.	Ethanol 99%	20 min
8.	Xylol	20 min
9.	Xylol	30 min
10.	Xylol	30 min
11.	Paraffin 65°C	30 min
12.	Paraffin 65°C	30 min

After placing the cassettes into the liquid paraffin of the pouring station for additional 30 min, liquid paraffin was poured into a metal form and by the help of electric heated tweezers (Vogel; Gießen, DE), the models were placed in a 90° angle into the form and closed with its labelled lidless embedding cassette. On a cooling plate (-10°C) paraffin blocks could solidify for about 15 min.

For histochemical analyses, the paraffin embedded models were cut into 5 µm slices with a microtome. For fixation these paraffin sections were “baked” onto the objective slide over night at 60°C in an incubator.

### 2.9.3 Haematoxylin and Eosine (H&E) staining

HE-staining was performed on paraffin sections after deparaffinating by the following steps:

1.	Xylol	15 min
2.	Xylol	15 min
4.	Ethanol 99%	1 min
5.	Ethanol 99%	5 min
6.	Ethanol 96%	shortly dipping
7.	Ethanol 80%	shortly dipping
8.	Ethanol 70%	shortly dipping
9.	Aqua dest.	shortly dipping
10.	Haematoxylin	10 min
11.	Tap water	10 min rinsing
12.	Aqua dest.	shortly dipping
13.	Eosin	40 s
14.	Aqua dest.	shortly dipping
15.	Ethanol 70%	shortly dipping
16.	Ethanol 80%	shortly dipping
17.	Ethanol 96%	1 min
18.	Ethanol 96%	5 min
19.	Xylol	15 min
20.	Xylol	15 min

Afterwards, cover slides were applied by using Eukitt, allowing solidification and drying under a fume cupboard.

### 2.9.4 Immunohistochemical stainings

#### Solutions and buffer:

##### **PBS for Immunohistochemical stainings (PBS\_IHC), pH 7.4**

Prepared in Aqua dest.

NaCl	140 mM
KCl	2.7 mM
Na <sub>2</sub> HPO <sub>4</sub>	8.1 mM
KH <sub>2</sub> PO <sub>4</sub>	1.5 mM

The solution was stored at room temperature for up to 6 months.

##### **TBST for Immunohistochemical stainings (TBST\_IHC), pH 7.6**

Prepared in Aqua dest.

Tris	50 mM
NaCl	150 mM
Tween 20	0.05%

The solution was stored at room temperature for up to 6 months.

##### **Tris-EDTA-citrat-buffer (TEC-buffer), pH 7.8**

Prepared in Aqua dest.

Tris	2 mM
EDTA	1.7 mM
Tri-sodiumcitrat-dihydrate	1 mM

The solution was stored at room temperature for up to 6 months.

**Tris-HCl, pH 7.4**

Prepared in Aqua dest.

Tris	0.5 M
------	-------

The pH was adjusted with HCl-solution and was stored at room temperature for up to 6 months.

**Trypsin-solution**

Prepared in Aqua dest.

Trypsin	0.001%
CaCl <sub>2</sub>	1.2 mM
Tris-HCl	10%

The solution was used immediately.

**Normal goat serum-triton solution (NGS-T solution)**

Prepared in PBS\_IHC

NGS	2%
Triton	1%

The solution was used immediately.

*Immunohistochemical staining of paraffin sections*

For immunohistochemical stainings, the 5 µm paraffin sections were deparaffinised and rehydrated in following steps:

1.	Xylol	15 min
2.	Xylol	15 min
4.	Ethanol 99%	1 min
5.	Ethanol 99%	5 min
6.	Ethanol 96%	shortly dipping
7.	Ethanol 80%	shortly dipping
8.	Ethanol 70%	shortly dipping
9.	Aqua dest.	5 min

Then, the sections were heated in TEC-buffer 2 times for 10 min at 360 W in a microwave oven for antigen retrieval. After cooling for 30 min at room temperature, the sections were washed 3 times for 5 min with TBST\_IHC buffer followed by incubation with Trypsin-solution for 10 min at 37°C, which was stopped by dipping the slices into Aqua dest. Following washing 2 times for 5 min, unspecific-binding sites were blocked with a Protein Block for 30 min. Subsequently, primary antibodies were diluted in PBS\_IHC and applied to the sections over night at 4°C, followed by washing of the samples for 3 × 10 min in TBST\_IHC and Alexa 488- and Alexa 594- or Cy3-labeled secondary antibody incubation (diluted in PBS\_IHC) for 30 min at room temperature. This was followed by washing in PBS\_IHC once for 5 min and 1 min incubation with 4,6-diamidino-2-phenylindole (DAPI; 0.001 mg/ml PBS\_IHC). After washing in PBS\_IHC for 5 min and in aqua dest. twice for 3 min the sections were embedded with Fluoromount-G and covered with a cover slide, which was allowed to attach over night in the dark.

*Immunohistochemical staining of cover slides*

Also immunohistochemical staining of NHEKs grown on cover slides was performed. At specific time points, the cells grown on cover slides, were washed with PBS (w/o  $\text{Ca}^{2+}$ ,  $\text{Mg}^{2+}$ ) buffer and fixed in methanol for 10 min at  $-20^{\circ}\text{C}$  and subsequently in acetone for 15 sec at room temperature. After drying, cover slides were either directly stained or stored at  $-20^{\circ}\text{C}$ . By using a wet chamber, slides were incubated with NGS-T solution for 30 min at room temperature. This was followed by incubation with the specific primary antibodies in PBS\_IHC for another 30 min. After washing 3 times 5 min in PBS\_IHC the secondary antibodies in PBS\_IHC were allowed to connect with the primary antibodies for another 30 min at room temperature. This was followed by washing in PBS\_IHC once for 5 min and 1 min incubation with DAPI solution (see above). After washing in PBS\_IHC for 5 min and in aqua dest. twice for 3 min the cover slides were embedded with Fluoromount G upside-down on a glass slide, allowing attachment over night in the dark.

*2.9.4.1 Photographing and evaluation of intensity*

An Axiophot II microscope and the software Openlab 2.0.9 were used for taking pictures of the stainings. All images of stainings from a series of experiments were acquired and processed with the same settings, and representative areas were photographed. For quantification, ImageJ software version 1.41n was used. For measurement of “whole tissue” intensity, 3 regions of interest (ROIs) were defined per raw image (Cldn-1: from suprabasal to granular cell layer; width  $79.7\text{ }\mu\text{m}$ ; for Cldn-4 and Ocln: ROIs of  $1060\text{ }\mu\text{m}^2$  located in the granular cell layer) and at least 3 images were evaluated per model. For evaluating intensities of membrane staining 3 ROIs ( $90\text{ }\mu\text{m}^2$ ) within cells (excluding the plasma membranes) were defined and the mean intensity of these ROIs was subtracted from the intensity of the larger ROIs measuring the whole tissue. For general background subtraction two ROIs ( $1060\text{ }\mu\text{m}^2$ ) were defined at areas without tissue. Intensity measurements were then normalized to the mean of untreated models.

*2.10 Statistical analyses*

Statistical analyses were performed with paired Student's t-test or analysis of variance (ANOVA) with Bonferroni post-test of SPSS software. The specific tests are denoted in the figure legends. Values are shown as mean with standard error of mean (SEM).

### 3 RESULTS

---

#### *3.1 Results, Part 1: Investigation of different model systems in order to find those suited best for Tight Junction analyses and staphylococcal treatment*

Recent research suggests an important role of the TJ barrier in context of bacterial skin infection (Ohnemus et al., 2008; Yuki et al., 2011b; Kuo et al., 2013). However, these studies have on one hand only been performed with bacterial supernatants or bacterial cell wall components (Yuki et al., 2011b; Kuo et al., 2013) or on the other hand with HaCaT cells instead of normal human epidermal keratinocytes (NHEKs) (Ohnemus et al., 2008). TJ analyses on the interaction of NHEKs with live bacteria are missing. In order to investigate this influence, a keratinocyte model system that is concomitantly suitable for bacterial inoculation and investigation of the TJs had to be found.

Being already a highly established model, the submerge system was used for these approaches and will therefore only shortly be introduced. However, in order to perform analyses on a system more closely representing *in vivo* situations, a 3D system needed to be found. Therefore three different 3D systems, using NHEKs, were examined for their morphology, their TJ and overall barrier function.

##### **3.1.1 Submerged model**

The submerged culture already is a well-established model for investigating pure TJ effects in keratinocytes, as these models do not form a proper *Stratum corneum* (SC) because of the submerged conditions (Madison et al., 1989; Eckhart et al., 2000). In this model system confluent monolayers of NHEKs are 'switched' to high  $\text{Ca}^{2+}$  conditions, with refreshment of the medium every 24 h. This induces TJ formation and barrier properties, which are reflected by a constant increase in TER up to 3 days after  $\text{Ca}^{2+}$ -switch (Figure 16 A). After 3 days a plateau was reached (Figure 16 A). In principle, TER does not distinguish between transcellular and paracellular pathway of ions (Madara, 1998). However, it was shown before that resistance of submerged keratinocytes after  $\text{Ca}^{2+}$ -switch is mainly provided by the resistance of the paracellular pathway and thus by TJs (Kirschner et al., 2013). In general, the submerged model system already is well established in order to investigate TJ barrier function of keratinocytes

(Mertens et al., 2005; Helfrich et al., 2007; Ohnemus et al., 2008; Kirschner et al., 2013; Yuki et al., 2016).

In order to visualise functional TJs, a biotinylation assay was performed 72 h after  $\text{Ca}^{2+}$ -switch. In general, the 557 Da tracer (Biotin-SH) was applied from the basal part, moving upwards through the intercellular spaces, stopping at functional TJs (indicated by Cldn-1 co-localisation at the sites of the tracer stops) (Figure 16 B). However, even though biotinylation is a great tool for visualisation of functional TJs, in the submerged model this is hard to evaluate, because often the stops are not as clear and easy to see as in 3D experiments (see below). This makes a quantification of the Biotin-SH permeability within the submerged model very hard and complex. Therefore this method will not be used for further investigations of this work. Nevertheless, investigating tracer permeability using a fluorescent-labelled 4 kDa tracer (FD4) is a common method (Matsukawa et al., 1997; Kawedia et al., 2007; Kirschner et al., 2013) and will thereby be used instead.

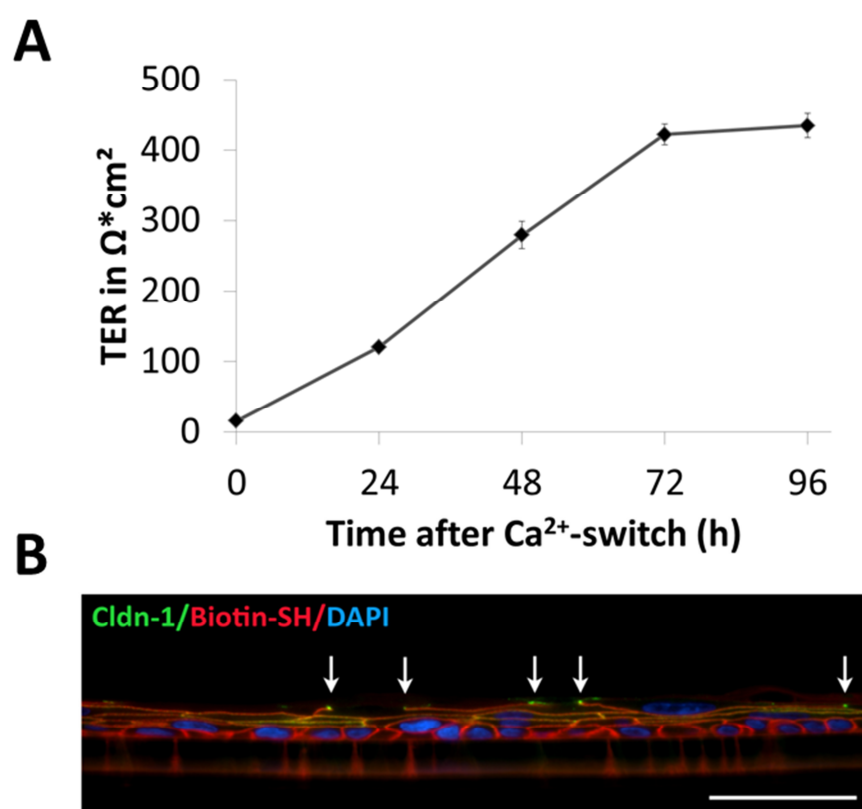


**Figure 16: Tight junction barrier properties of the submerged model.** Transepithelial electrical resistance (TER) of human keratinocytes in the submerged model in h after  $\text{Ca}^{2+}$ -switch (A). Immunohistochemical staining of claudin-1 (Cldn-1; green), the 557 Da tracer (Biotin-SH; red) and nuclei (DAPI; blue) (B). Mean  $\pm$  SEM; n = 3 donors in triplicates (0 h) or 8 donors in triplicates (24, 48, 72 and 96 h). Arrows denote Cldn-1 positive stops of Biotin-SH. Bar = 50  $\mu\text{m}$ .

Investigating the morphology at day 3 after  $\text{Ca}^{2+}$ -switch, when the plateau in TJ function was reached, revealed that the submerged model is not just a pure monolayer of cells, but consists of 2-3 keratinocyte layers, of which cells in the lower layer are shaped 'round' and provide some kind of a *Stratum basale* (SB), whereas the cells in the following 1-2 layers

strongly flatten like in *Stratum granulosum* (SG) of human epidermis (Figure 17 A). Immunohistochemical stainings of the TJ proteins Cldn-1, Cldn-4 and Occludin (Occludin) showed a mainly membrane associated localisation as reported in a normal human epidermis (Figure 17 B). For Occludin, this localisation was visible dotted in the uppermost cell layer, also comparable to human skin (Figure 17 B).

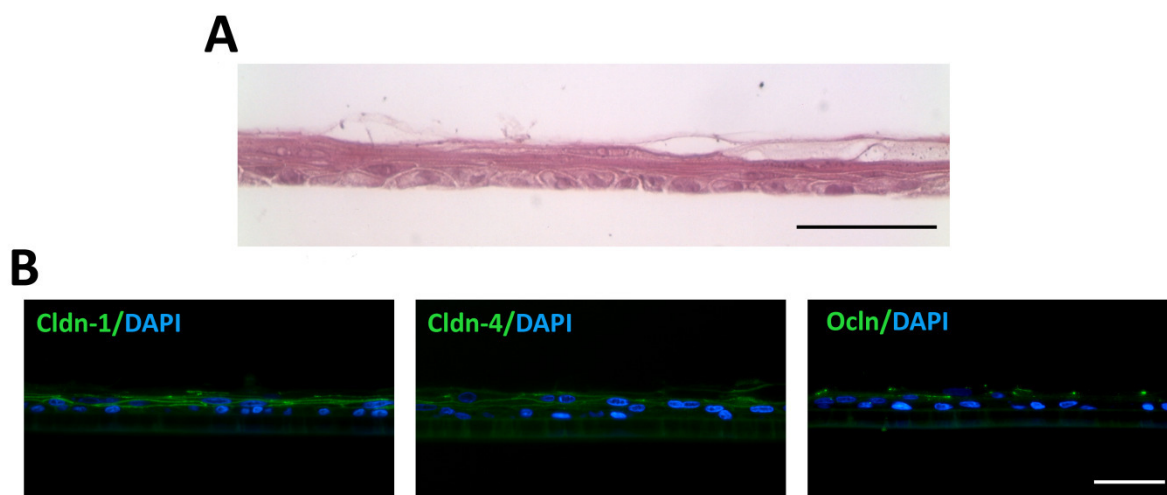


**Figure 17: Haematoxylin and eosin (H&E) staining and immunohistochemical stainings of the submerged model 3 days after  $\text{Ca}^{2+}$ -switch.** H&E staining of submerged keratinocytes after 3 days under high  $\text{Ca}^{2+}$  conditions (A). Immunohistochemical stainings of the tight junction proteins claudin-1 (Cldn-1), Cldn-4 and occludin (Occludin) (green) and of nuclei (DAPI; blue) (B). Bars = 50  $\mu\text{m}$ .

The submerged model has the advantage that pure TJ effects can be investigated without the impact of a barrier-forming SC. Nevertheless, the submerged system misses out physiological air-liquid-interface (ALI) conditions as well as the development of full stratification and interactions with a functional SC. These are important conditions when comparing to human skin. Therefore the submerged culture provides a very good additional system in order to analyse TJ interactions, but a system more closely to *in vivo* situations was necessary as well.

### 3.1.2 3D reconstruction

For 3D reconstruction, two different epidermal equivalents (reconstructed human epidermis (RHE)) and one full skin model (reconstructed human skin (RHS)) were analysed in order to find the model suited best for the approaches of this work.

#### 3.1.2.1 Reconstructed human epidermis (RHE)

The two different epidermal equivalents investigated were on the one hand a RHE after the protocol of CellnTec (CnTe3D) and on the other hand a RHE after the protocol of Pierre Fabre (PFe3D). Both models were built with equal amounts of NHEKs in the same inserts. The

usage of expensive collagen and fibroblasts was not necessary, when compared to RHS models. In addition, five times less numbers of NHEKs were needed.

#### 3.1.2.1.1 Reconstructed human epidermis after the protocol of CellnTec (CnTe3D)

Investigation of the histology of the CellnTec model showed a nice epidermal structuring comparable to human epidermis at day 7 after ALI (Figure 18 A). Palisade-like structures in SB, 2-3 layers of *Stratum spinosum* (SS), flattening cells with keratohyalin granules in SG, and some layers of SC (Figure 18 A) were present. This morphology still was observed after 14 days in ALI, however, with some more living cell layers as well as more layers of SC (Figure 18 B). Even though the model architecture was usually very nice in the middle of the model, coming closer to the margins often porous tissue or only a thin cell layer was observed (Figure 18 C). This was also mirrored by the fact that often the models did not stay completely dry on top after lifting them into ALI. Usually a liquid coat was visible, especially at the margins of the models, up to several days. This also resulted in very inconsistent model structure within a single model. Of note, these inconsistencies were not found in all models to the same extent, which makes the models even less reliable in their structure as well as less reproducible.

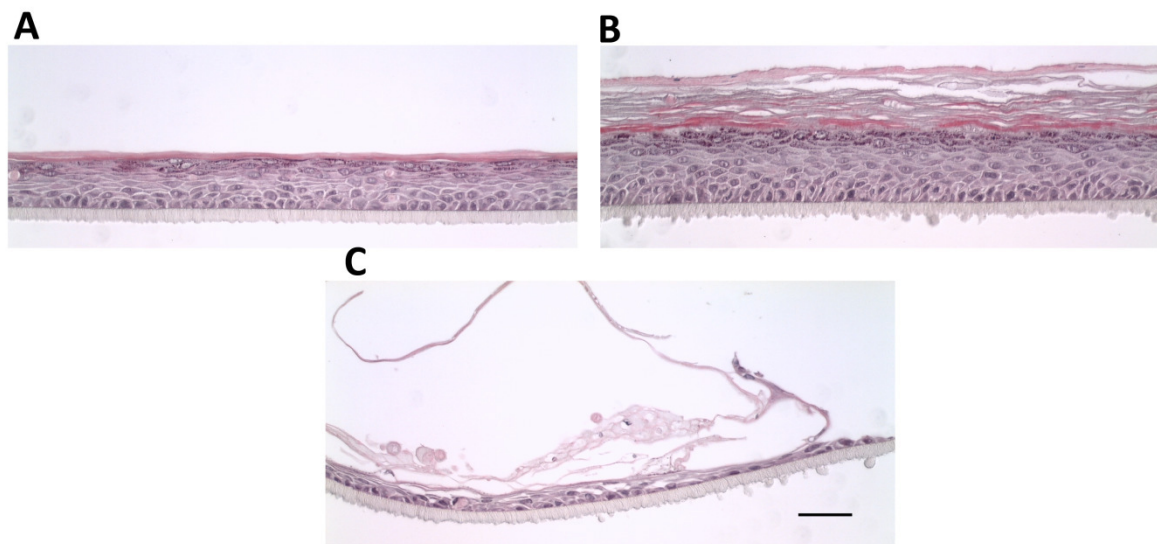


**Figure 18: Haematoxylin and eosin staining of reconstructed human epidermis after the protocol of CellnTec (CnTe3D).** Model architecture in the centre of CnTe3D models after 7 (A) and 14 (B) days under air-liquid-interface (ALI) conditions. Thin cell layer at the margin of a CnTe3D model after 7 days in ALI (C). Bar = 50  $\mu$ m.

In order to investigate distribution patterns of TJ proteins, immunohistochemical stainings were performed. Within CnTe3D models localisation pattern of TJ proteins after 7 and 14 days in ALI showed similar results at both time points and were mostly comparable to normal human epidermis. Cldn-1 was found mainly at the cellular membranes in all living cell



layers except of SB (Figure 19). Cldn-4 was found mainly membrane associated as well in SS and in SG (Figure 19). Of note, Cldn-4 immunolocalisation was broader than compared to normal human skin (see introduction, Figure 5). For Ocln, a dotted localisation at the cellular membranes was found in the SG (Figure 19).

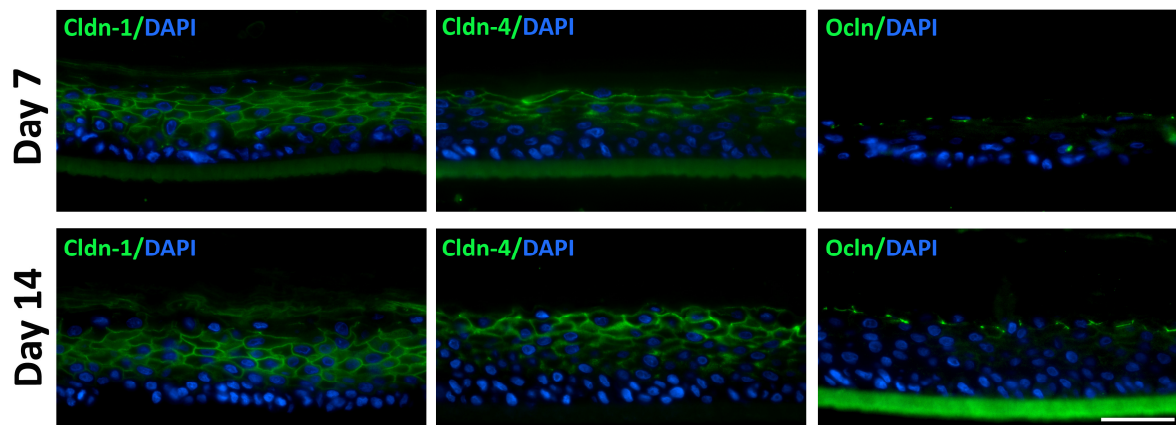


**Figure 19: Immunohistochemical stainings of tight junction proteins in reconstructed human epidermal models after the protocol of CellnTec.** Claudin-1 (Cldn-1), Cldn-4 and occludin (Ocln) (green) and nuclei (DAPI; blue) after 7 and 14 days under air-liquid-interface conditions. Bar = 50  $\mu$ m.

When investigating TJ functionality with Biotin-SH, it was observed that even though TJ proteins showed their correct localisation at day 7 and 14, the tracer was not 100% stopped (a thin line of Biotin-SH was still visible behind the actual stop) at day 7 and 14 (Figure 20). Within later development, e.g., on day 16, functional TJ were found (Figure 20). However, this was inconsistent within one model (some areas showed stops, others did not) as well as between different models.

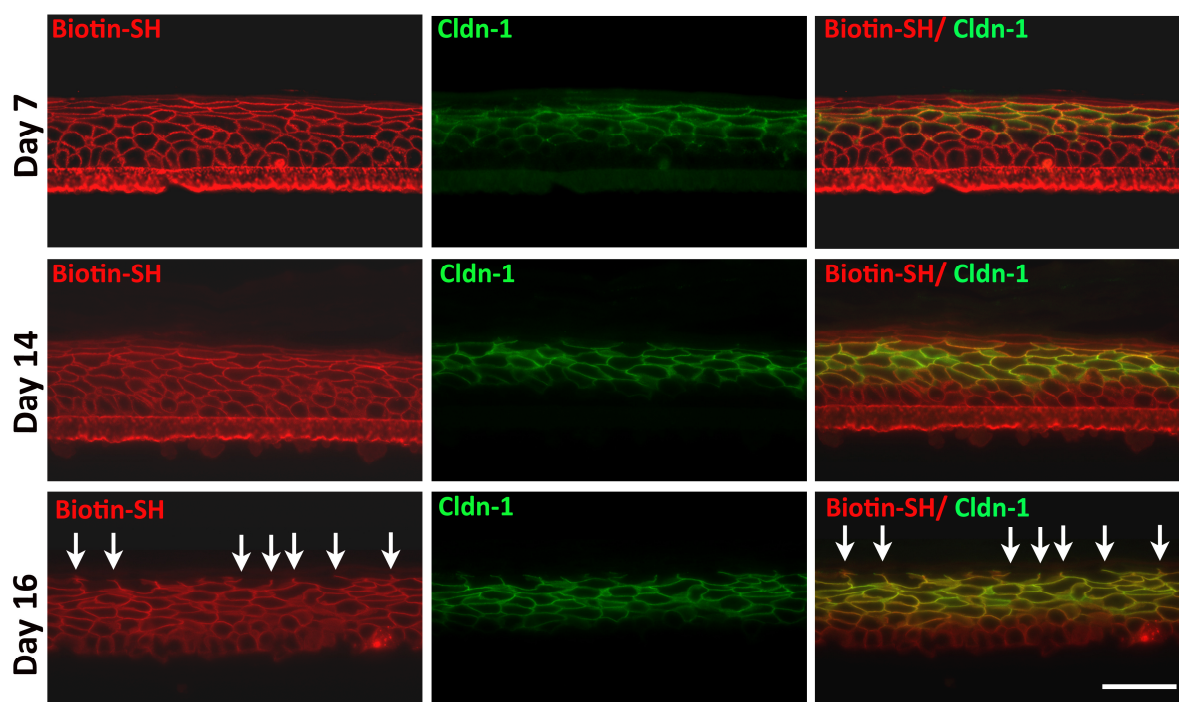


**Figure 20: Tight junction functionality of reconstructed human epidermal models after the protocol of CellnTec (CnTe3D).** Immunohistochemical staining of the 557 Da tracer (Biotin-SH; red) and claudin-1 (Cldn-1; green) on CnTe3D on days 7, 14 and 16 after lifting to air-liquid-interface. Arrows denote functional tight junctions indicated by complete tracerstops. Bar = 50  $\mu$ m.

Investigating overall barrier function by measurement of the TER, reflected observations already made in morphological analyses as well as in the tracer assay. TER values of CnTe3D models were very low (e.g., 780  $\Omega \cdot \text{cm}^2$  at day 14) (Figure 21) when compared to PFE3D models (6500  $\Omega \cdot \text{cm}^2$ , see below (Figure 26)). Even though an increase in the mean TER was observed at days 13 to 16 compared to days 7 to 12, the large standard deviations reveal huge differences between the models, which reflects the heterogeneity already described before. As the TER reflects the barrier function of the complete model area, these low TER values can be explained by the thin and leaky margins of CnTe3D models (Figure 18 C).

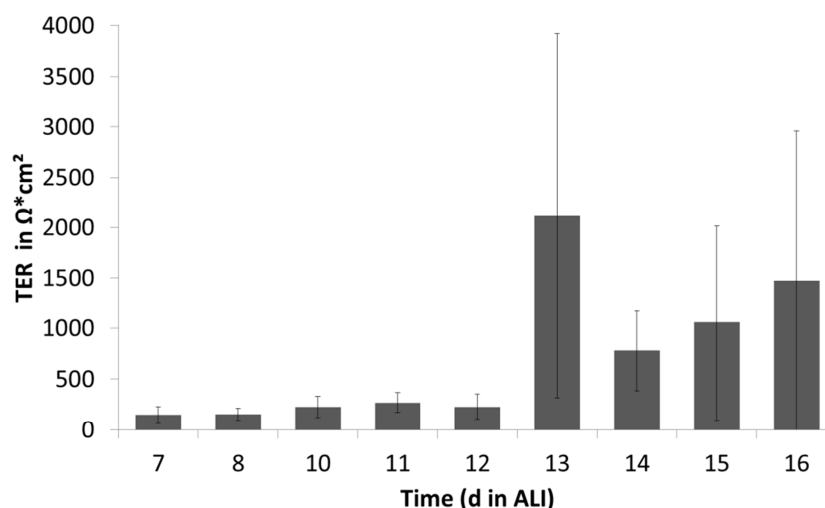


**Figure 21: Transepithelial electrical resistance (TER) of reconstructed human epidermal models after the protocol of CellnTec over time after lifting to air-liquid-interface (ALI).** Mean  $\pm$  SEM; n = 2 (day 7 and 8), 3 (day 10), 4 (days 12, 15 and 16), 5 (day 11) and 6 (days 13 and 14) donors.

Taken together, CnTe3D models were quite easy to build, showed nice epidermal structuring in certain areas, and TER measurement was effortless. However, they were heterogeneous in development (especially at the margins), TER values were very low, and even though functional TJs were found, these developed very late and also heterogeneous. Another negative point of these models is that the company did not state the supplements and their concentrations for the 3D medium, which is important to completely understand the models.

#### 3.1.2.1.2 Reconstructed human epidermis after protocol of Pierre Fabre (PFe3D)

The second RHE model analysed in this context was the RHE after the protocol provided by Pierre Fabre (PFe3D).

Examining the histology in the middle of these models revealed nice epidermal structuring similar to CnTe3D (Figure 22A, B). Also here a nice palisade-like SB, keratohyalin granules in SG and some layers of SC were already observed at day 7 after ALI (Figure 22 A), and were still present after 14 days in ALI, with a slight increase in viable cell layers and increased layers of SC (Figure 22 B), comparable to CnTe3D.

Interestingly, in difference to CnTe3D, the margins of PFe3D showed nice epidermal structuring as well. The margins were thick and consistent in development within different models as shown by a representative image of Figure 22 C. This was also reflected by the fact that PFe3D models did not show leakiness (indicated by wet margins on top of the model) already from the first day of ALI.

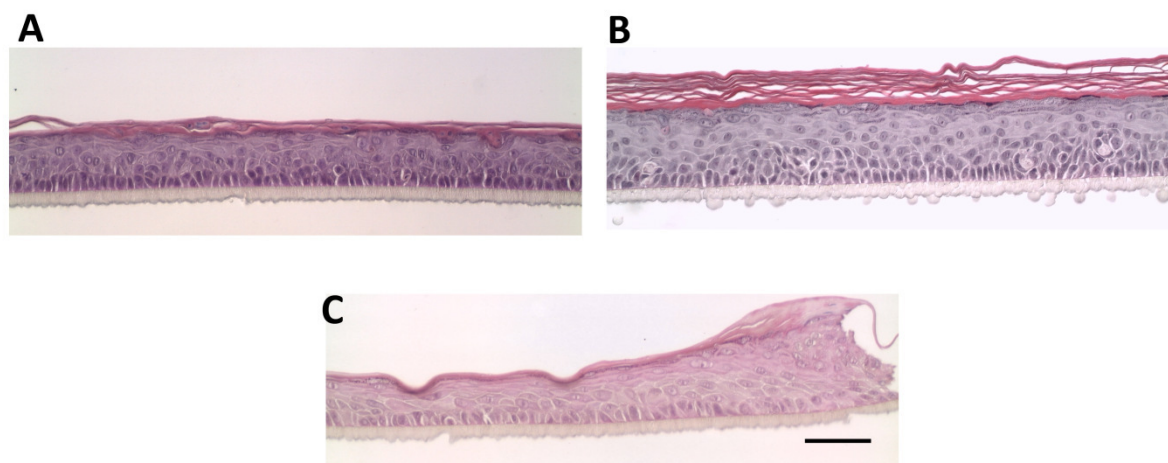


**Figure 22: Haematoxylin and eosin (H&E) stainings of reconstructed human epidermis after the protocol of Pierre Fabre (PFe3D).** Model architecture in the centre of PFe3D models after 7 (A) and 14 (B) days under air-liquid-interface (ALI) conditions and at the margin of PFe3D at day 7 of ALI (C). Bar = 50  $\mu$ m.

Inspecting TJ protein localisation revealed correct localisation of Cldn-1 as well as of Ocln, similar to CnTe3D and normal human skin, after 7 days of ALI (Figure 23) and still after 14 days (Figure 23). Additionally, Cldn-4 localisation revealed better parallels to normal human skin than in the CnTe3D models. Also here Cldn-1 was found mainly at the cellular membranes in all living cell layers except for SB. Cldn-4 was found mainly membrane associated as well, but only in the upper part of SS and in SG and for Ocln, a more dotted extracellular localisation was found in the SG (Figure 23).

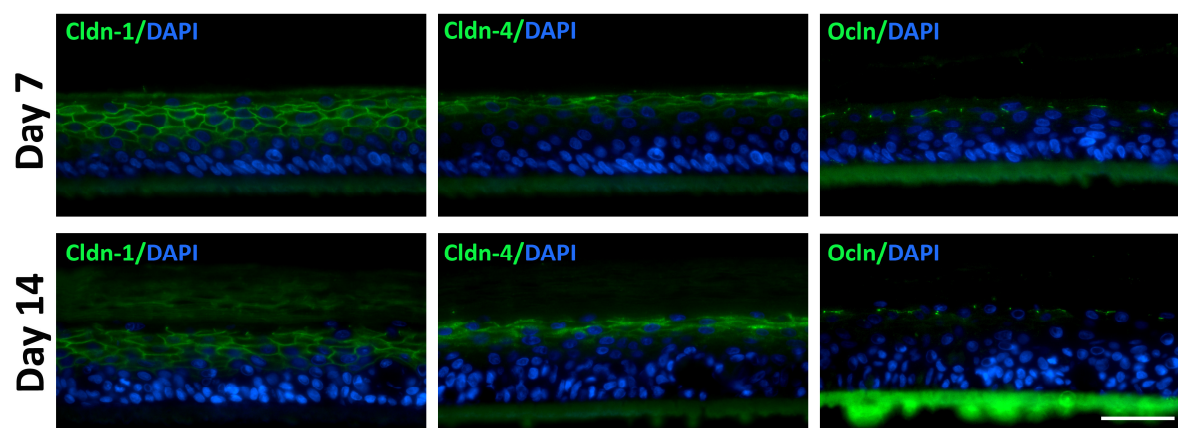


**Figure 23: Immunohistochemical stainings of tight junction proteins in reconstructed human epidermal models after the protocol of Pierre Fabre.** Claudin-1 (Cldn-1), Cldn-4 and occludin (Ocln) (green) and nuclei (DAPI; blue) after 7 and 14 days under air-liquid-interface conditions. Bar = 50  $\mu$ m.

When examining TJ barrier properties, PFe3D models showed pronounced tracerstops already at day 7 (see below). The stops were still present on day 14 (Figure 24) and co-localised with the uppermost localisation of Cldn-1 (Figure 24).

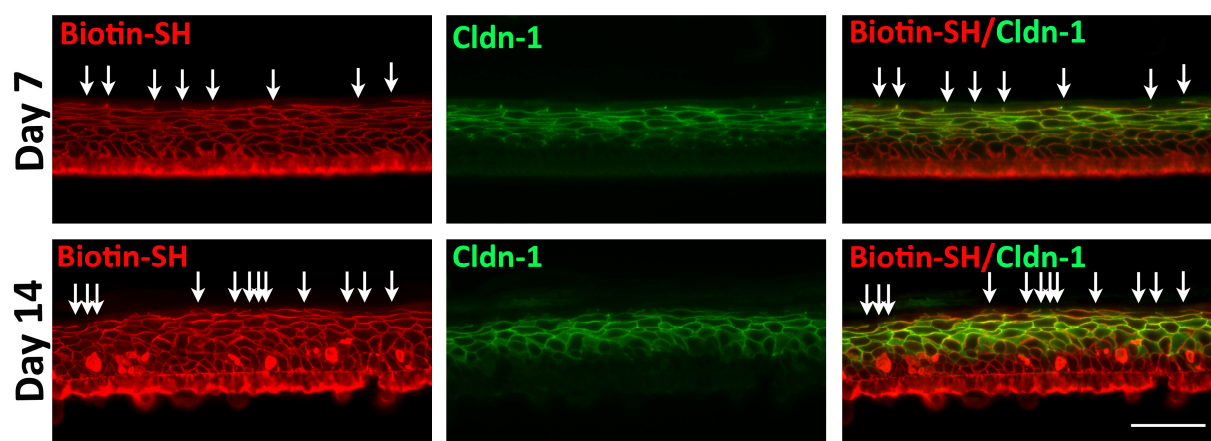


**Figure 24: Tight junction functionality of reconstructed human epidermal models after the protocol of Pierre Fabre (PFe3D).** Immunohistochemical staining of the 557 Da tracer (Biotin-SH; red) and claudin-1 (Cldn-1; green) on PFe3D on day 7 and day 14 after lifting to air-liquid-interface. Arrows denote functional tight junctions indicated by tracerstops. Bar = 50  $\mu$ m.

As the TJs already showed functionality at day 7 of ALI, it was of interest whether this happens already earlier in development. Indeed already on day 4 after lifting the models to the ALI functional TJs for Biotin-SH were formed (Figure 25 A). Additionally on this day the model architecture showed nice epidermal structuring by that time as well (Figure 25 B)

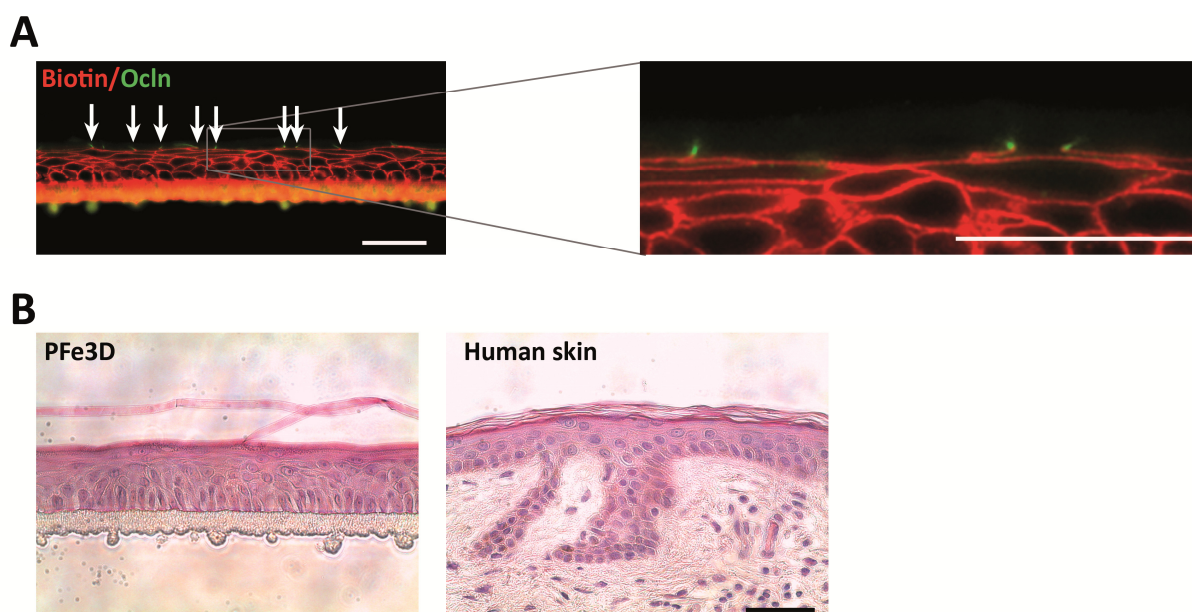


**Figure 25: Tight junction (TJ) functionality and Haematoxylin and eosin (H&E) staining of reconstructed human epidermal models after the protocol of Pierre Fabre (PFe3D) on day 4 of ALI.** Biotin-SH (red) being stopped at functional TJs (white arrows) indicated by co-localisation with occludin (Ocldn, green) (A). H&E staining of PFe3D at day 4 of ALI compared to normal human skin (B). Bars = 50  $\mu$ m.

When measuring the TER, already at day 4 a substantial TER of  $>2000 \text{ Ohm} \cdot \text{cm}^2$  was observed in PFe3D models which further increased over time (Figure 26).

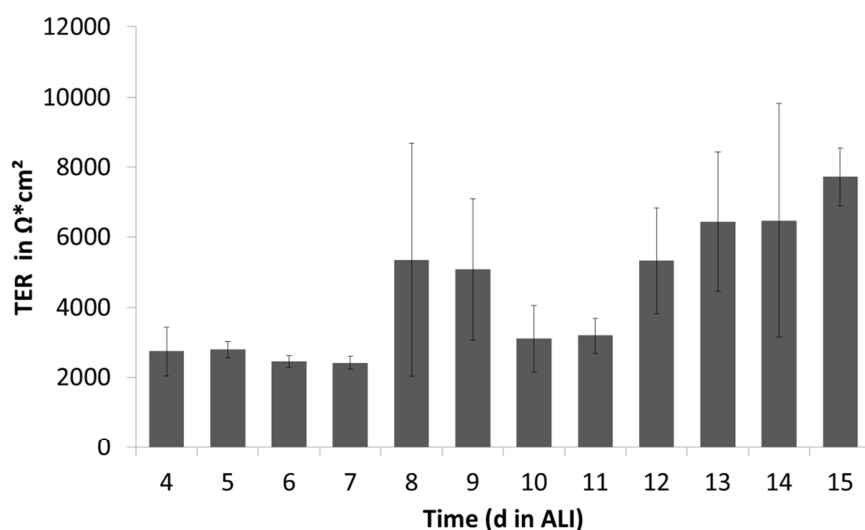


**Figure 26:** Transepithelial electrical resistance (TER) of reconstructed human epidermal models after the protocol of Pierre Fabre over time after lifting to air-liquid-interface (ALI). Mean  $\pm$  SEM; n = 2 (day 10 and 14), 3 (days 8, 11 and 15), 4 (days 5-7, 11 and 13), 5 (day 9), and 6 (day 4) donors.

Taken together, PFe3D models were easy to build, showed a nice and stable morphology, developed TJs early and pronounced, and TER measurement revealed reliable overall barrier results. In addition, in this case we prepared the supplements ourselves and concentrations of all ingredients were therefore known. However, using a 3D system even closer to *in vivo* situations might be of interest. Therefore, a full skin model was analysed in this context as well.

### 3.1.2.2 Reconstructed human skin (Mildner model)

The third 3D model examined was a RHS after Mildner et al. (2006). This full-skin-model consists of a dermal equivalent part (with primary human fibroblasts embedded in a bovine collagen matrix) and an epidermal part (consisting of NHEKs) and should represent a model system mirroring *in vivo* situations the closest of the investigated systems.

When investigating the morphology of these models at day 5 after lifting them to ALI, epidermal structuring was observed (Figure 27 A). However, this was not as nice as in the RHE models. In some areas a slight diffuse arrangement of the basal compartment was observed (Figure 27 A). Following the SB, several living cell layers were present, representing a SS as well as SG. Finally, a thin SC layer was observed as well (Figure 27 A, B).



At day 8 of ALI, epidermal structuring was similar to day 5 after ALI (Figure 27 B). However, at day 8 keratohyalin granules were more prominent in SG and more layers of SC were visible (Figure 27 B).

During further development (day 10 and day 14), the diffuse arrangement of the basal cell layer was more prominent (Figure 27 C, D). Additionally, continuing terminal differentiation of the models resulted in less living cell layers up to only two at day 14 after ALI, whereas a strong cornification (resulting in a very thick SC) was observed (Figure 27 D).

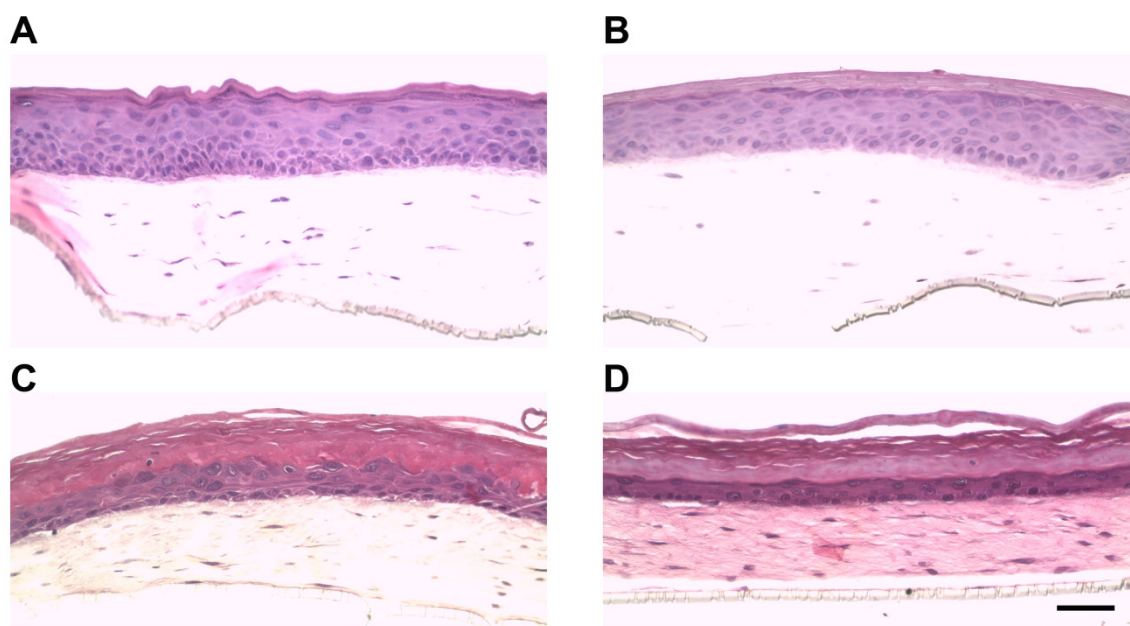


**Figure 27: Hematoxylin and eosin (H&E) stainings of reconstructed human skin (RHS) models.** RHS at day 5 (A), day 8 (B), day 10 (C) and day 14 (D) after air-liquid-interface. Bar = 50  $\mu$ m.

As day 8 of ALI showed the best epidermal structuring, further investigation of TJ protein localisation and function were performed at this day. This revealed similar results to PFe3D models and normal human skin. Cldn-1 was found at the cell-cell borders of all living layers of the epidermis, with a weaker expression in SB (Figure 28). Cldn-4 was found at the cell-cell borders in the upper part of the SS and in the SG (Figure 28). Ocln was observed in SG only in a dotted or whisker-like staining pattern (Figure 28).

Despite of different localisation patterns of Cldn-1, Cldn-4 and Ocln, all of them were found co-localised at the sites where the biotin tracer was stopped (Figure 28).

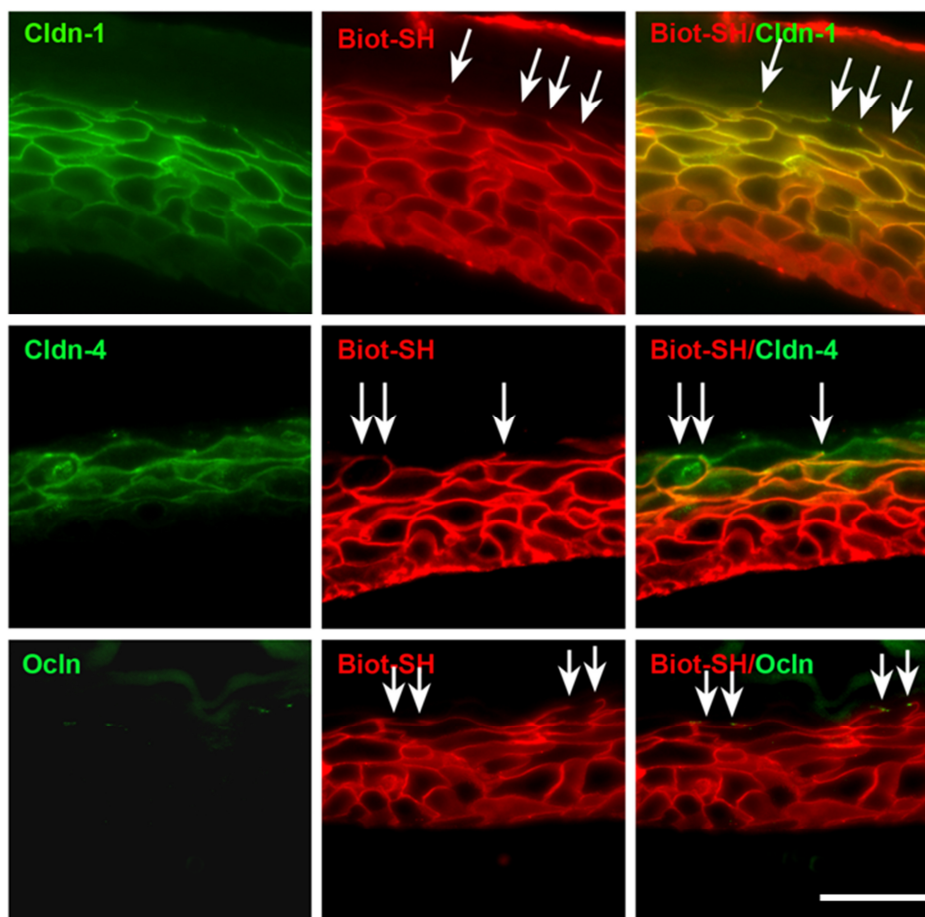


**Figure 28: Immunohistochemical stainings of tight junction proteins and tight junction functionality of reconstructed human skin on day 8 of air-liquid-interface (ALI).** Claudin-1 (Cldn-1), Cldn-4 and occludin (Ocln) (green) after 8 days under ALI conditions and the 557 Da tracer (Biot-SH). Arrows denote functional tight junctions indicated by tracerstops. Bar = 50  $\mu$ m.

Unfortunately, in the RHS model the development of a method to measure the overall barrier function by TER measurement failed. The problem with these models was that the collagen-gel contracted over time and in addition the keratinocytes only formed an epidermal structure right in the middle of the gel. Thus, at no time point there was an area of keratinocytes completely covering the whole surface of the insert, which is necessary to measure overall barrier function. Also the attempt to generate a measurable area by gluing small plastic rings on top of the RHS with either Vaseline or tissue glue failed. Additionally building these models was not very economic due to the usage of a huge amount of keratinocytes and fibroblasts as well as expensive collagen.

Taken together, within the 3 investigated 3D model systems PFe3D models were the best suited systems for the approach of this work and were therefore used in addition to the submerged model described above.



### 3.2 Results, Part 2: Investigation of the effect of staphylococcal inoculation on Tight Junctions in submerged models

#### 3.2.1 *S. epidermidis* and *S. aureus* first increase and later on decrease Tight Junction barrier function in submerged models

TER was investigated after bacterial inoculation of NHEKs in the submerged model 3 days after  $\text{Ca}^{2+}$ -switch, when proper TJ functionality was reached (reflected by TER values of  $>300 \Omega \cdot \text{cm}^2$ ). Inoculation was performed with *S. epidermidis* and *S. aureus* in two different concentrations reflecting a low ( $6 \times 10^3$  bacteria  $\text{cm}^{-2}$ ) and a high ( $6 \times 10^5$  bacteria  $\text{cm}^{-2}$ ) bacterial load.

Investigating *S. epidermidis* inoculation, NHEKs showed a temporary increase in TER during the first 12 h post infection (Figure 29 A). This TER increasing effect also demonstrated a slight dose-dependency, however not significant. The increase in TER after *S. epidermidis* inoculation was followed by a decrease to the same extent for both concentrations (Figure 29 A).

Also inoculation of the submerged models with *S. aureus* resulted similar to *S. epidermidis* inoculation, in an increase in TER during the first 12 hours (Figure 29 B). Comparing both concentrations used, *S. aureus* inoculation showed a significantly dose-dependent effect. The higher bacterial concentration ( $6 \times 10^5$  *S. aureus*  $\text{cm}^{-2}$ ) resulted in a faster and slightly stronger increase in TER (Figure 29 B). Comparable to *S. epidermidis*, the increase in TER after *S. aureus* inoculation was followed by a rapid dose-independent decrease (Figure 29 B). When comparing the results from both species (*S. epidermidis* and *S. aureus* inoculation) in the higher concentrations, it became obvious that the TER increasing effect of *S. aureus* was significantly stronger than the effect of *S. epidermidis* (Figure 29 C). Also, the TER decreasing effect was slightly more pronounced for *S. aureus* than for *S. epidermidis* (Figure 29 C).

As effects were the same, but more pronounced with the higher bacterial load, for most of the further investigations it was decided to work only with the higher bacterial concentration ( $6 \times 10^5$  bacteria  $\text{cm}^{-2}$ ) if not mentioned otherwise.

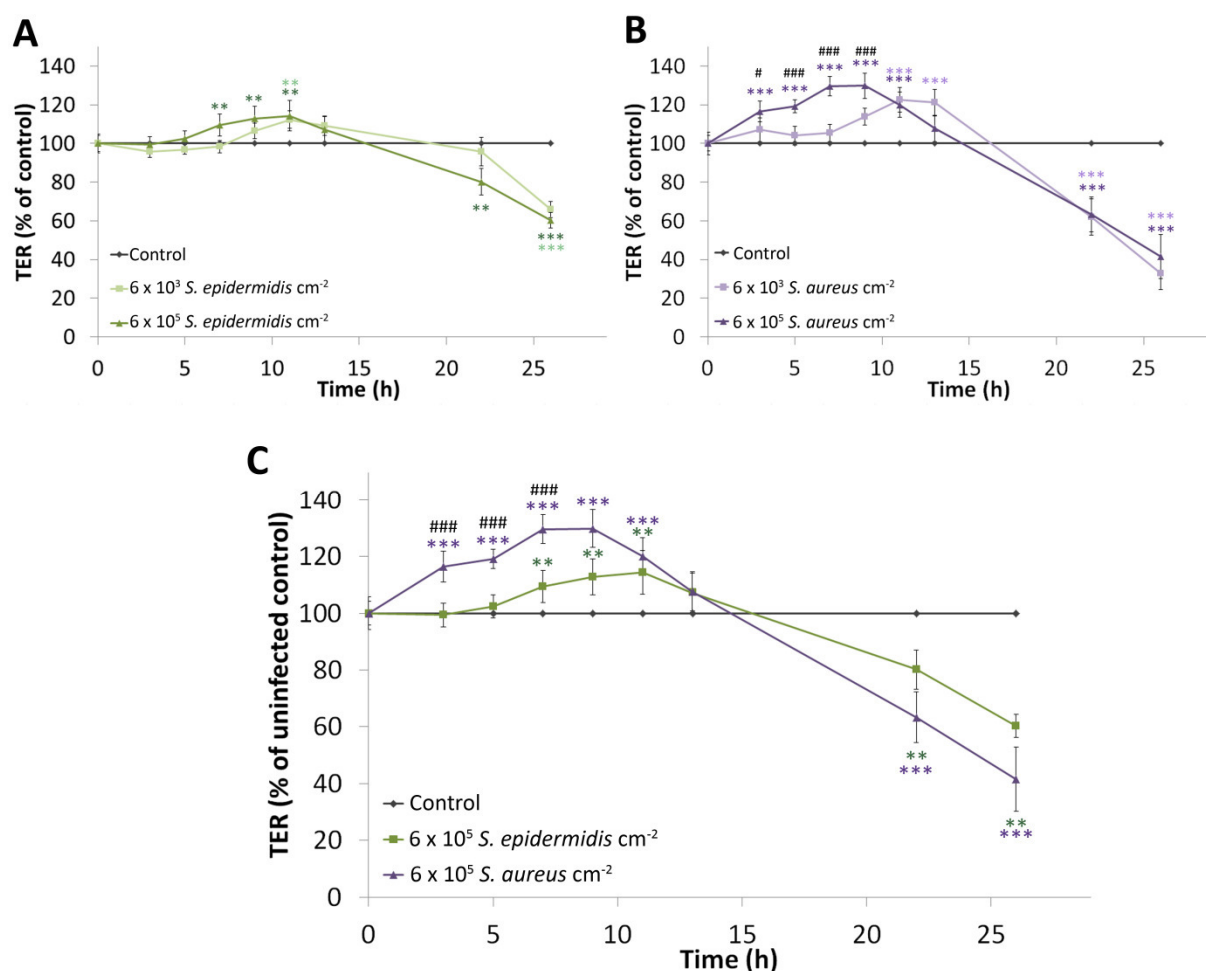


**Figure 29: Transepithelial electrical resistance (TER) of submerged models after staphylococcal inoculation.** TER of submerged models after inoculation with  $6 \times 10^3$  and  $6 \times 10^5$  *S. epidermidis*  $\text{cm}^{-2}$  in % of the untreated control (A). TER of submerged models after inoculation with  $6 \times 10^3$  and  $6 \times 10^5$  *S. aureus*  $\text{cm}^{-2}$  in % of the untreated control (B). TER of submerged models after inoculation with  $6 \times 10^5$  *S. aureus* or *S. epidermidis*  $\text{cm}^{-2}$  in % of the untreated control (C). Mean  $\pm$  SEM; n = 4 donors in triplicates, \*\* p<0.01, \*\*\* p<0.001 compared to uninfected control; # p<0.5, ## p<0.01, ### p<0.001 compared to the other bacterial concentration (A and B) or to the other species (C) using ANOVA (modified with permission from Bäsler et al. (2017))

In order to examine whether increase and decrease in TER after bacterial inoculation are really TJ specific effects, permeability for 4 kDa FITC dextran was investigated additionally. This tracer is commonly used to investigate the paracellular pathway of epithelial cell structures (Matsukawa et al., 1997; Kawedia et al., 2007; Kirschner et al., 2013).

Indeed, at early time points (12 h) after *S. epidermidis* as well as after *S. aureus* inoculation, when TER was increased significantly, a significant decrease in tracer permeability was found (Figure 30 A) and, in reversed orientation, at late time points (24 h), when TER was decreased, an increase in tracer permeability was observed (Figure 30 B). This clearly indicates that changes in TER measurement after bacterial inoculation are TJ specific. TJ barrier function is strengthened at the beginning of bacterial inoculation and impaired in the course of continuous infection.

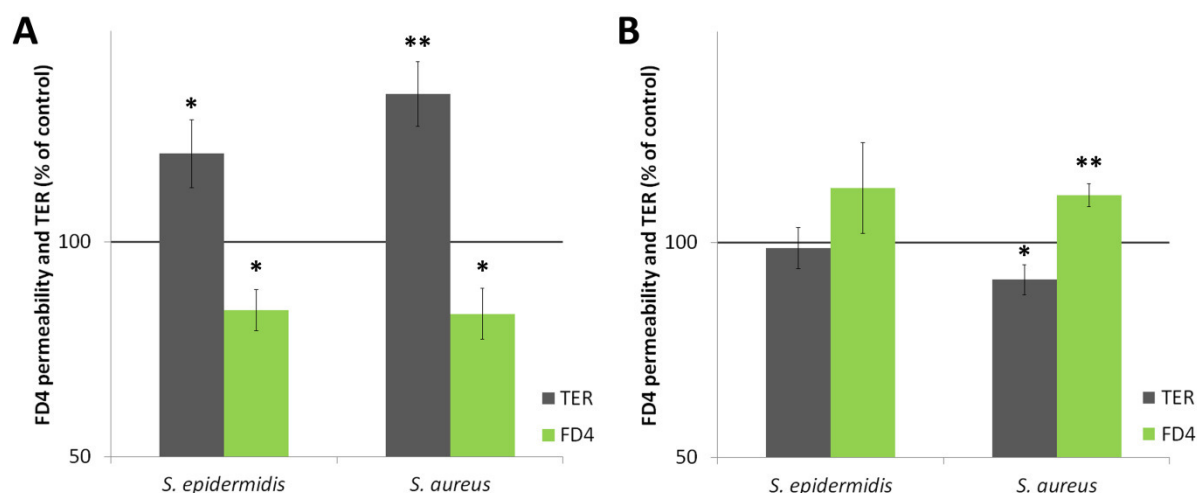


**Figure 30: Tight junction functionality after staphylococcal inoculation displayed by transepithelial electrical resistance (TER) and the permeability of a 4 kDa tracer (FD4).** TER (grey bars) and FD4 permeability (green bars) in % of the uninfected control after inoculation with  $6 \times 10^5$  *S. aureus* or *S. epidermidis* per  $\text{cm}^2$  after 12 h (A) and after 24 h (B). Mean  $\pm$  SEM;  $n = 5$  donors in triplicates; \*  $p < 0.05$ , \*\*  $p < 0.01$  compared to the uninfected control using paired Student's T-test. (Modified with permission from Bäsler et al. (2017))

### 3.2.2 Cell death is not the cause for decreased barrier function

In order to clarify whether the decreased barrier function after long-term inoculation with both bacterial species in the submerged model is just simply the result of cell death, a tissue-MTT assay (Herbig et al., 2015) was performed, because, as described above, NHEKs in this model build a thin tissue. This tissue-MTT assay was carried out on submerged models inoculated long-term (24 h) with either *S. aureus* or *S. epidermidis* using the higher bacterial concentration. Analysing long-term *S. aureus* and *S. epidermidis* inoculation, no differences in MTT colouration were observed when compared to the uninfected control (Figure 31) indicating no viability loss. As a positive control, submerged models were treated for 1 h with 1N HCl-solution before performing the tissue-MTT. In this positive control no colourisation was visible indicating dead tissue (Figure 31).

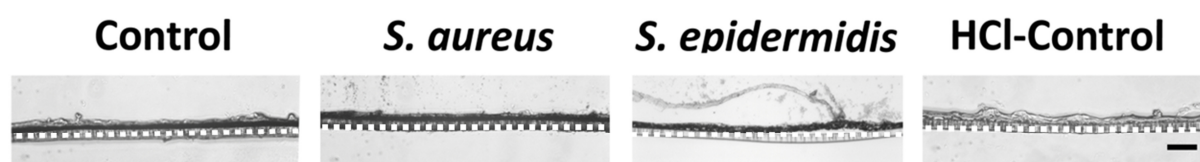


**Figure 31: Tissue viability of the submerged model after inoculation with  $6 \times 10^5$  *S. aureus* or *S. epidermidis*  $\text{cm}^{-2}$  compared to the uninfected control.** The dark staining denotes viable cell layers. As a positive control submerged models were treated for 1 h with 1 N HCl-solution, before performing the tissue-MTT. In this HCl-control no colourisation was visible indicating dead tissue. The white dotted line denotes the insert-membrane. Bar = 50  $\mu\text{m}$  (Modified with permission from (Bäsler et al., 2017)).

This shows that the decrease in barrier function after long-term inoculation with *S. aureus* or *S. epidermidis* is not due to cellular death, demonstrating that TJ specific mechanisms must play a role not only in TER increase after short-term inoculation, but also in TER decrease after long-term inoculation. Therefore investigations on the underlying mechanisms leading to TJ barrier strengthening and disruption have been performed.

### 3.2.3 Investigations on Tight Junction protein localisation patterns

Alterations in TJ functionality are often described to be associated with changes in TJ protein localisation patterns (Kirschner et al., 2009; Akiyama et al., 2014; Kiatsurayanon et al., 2014). In order to investigate putative causes for increased and decreased TJ barrier function immunofluorescence stainings of cover-slides as well as of cross sections of paraffin embedded cells on transwell-membranes, which had been used before for the TER measurements, were performed.

Indeed, short-term (12 h) inoculation with *S. epidermidis* and *S. aureus* resulted in a more pronounced localisation of Cldn-4 at the cell-cell membranes of the submerged models, which was observed on cover-slide as well as in cross section immunohistochemical stainings (Figure 32 A, B). For Cldn-1 no clear changes in protein localisation were detected either for *S. epidermidis* or for *S. aureus* infection (Figure 32 A, B).

Interestingly, also a more pronounced localisation of Occludin at the cell-cell membranes of the submerged models was found after short-term *S. aureus* inoculation, while this was not the case after short-term *S. epidermidis* inoculation (Figure 32 A, B).

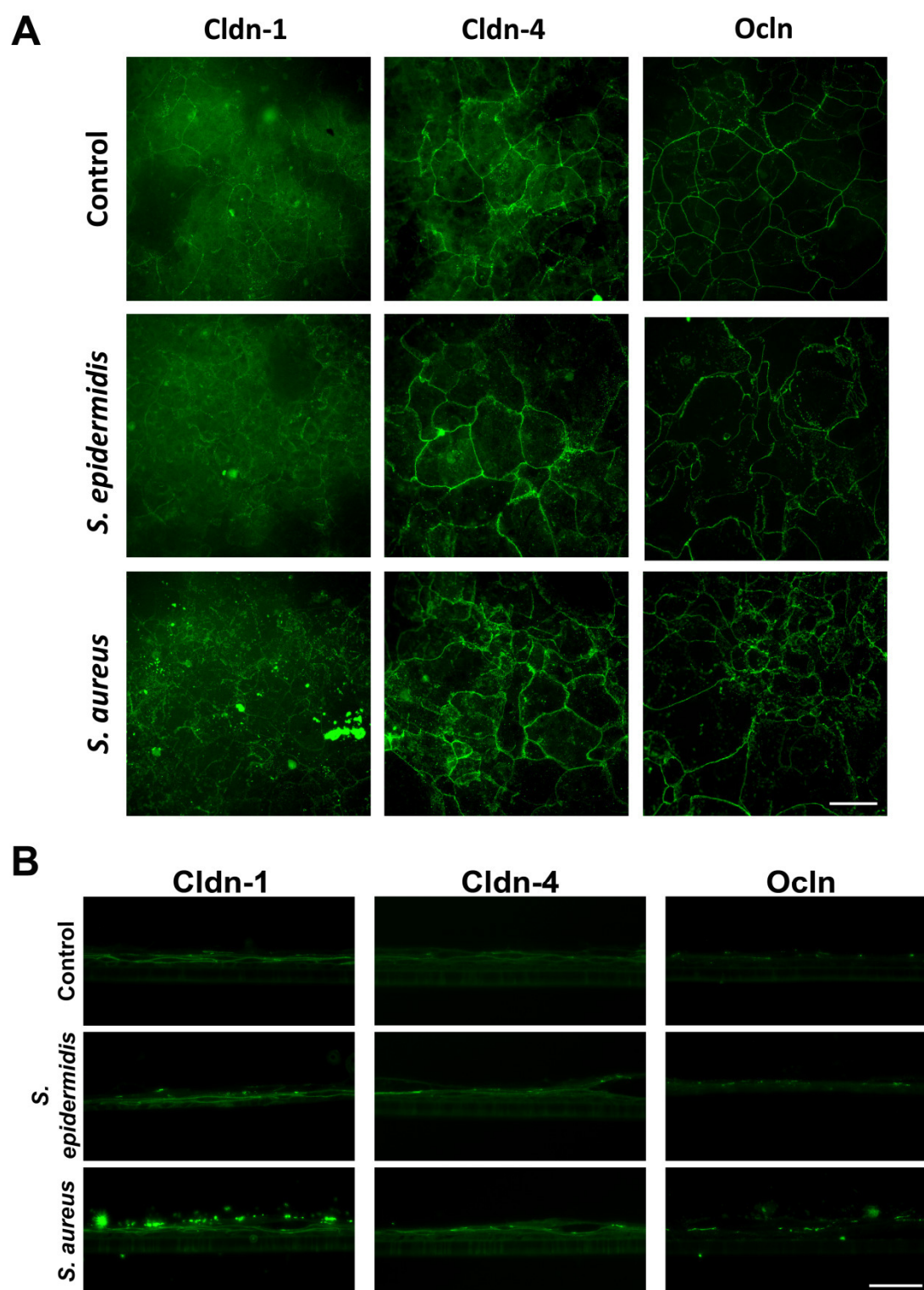


**Figure 32: Immunohistochemical stainings of tight junction proteins of the submerged model after 12 h of staphylococcal inoculation.** Immunohistochemical stainings (green) of claudin-1 (Cldn-1), Cldn-4 and occludin (Occludin) of the submerged culture after 12 h of inoculation with  $6 \times 10^5$  *S. epidermidis* or *S. aureus* per  $\text{cm}^2$  on cover slides (A) and on cross sections of paraffin embedded filter-membranes (B). Bright fluorescent green dots on top of *S. aureus* infected models represent a cross reaction of *S. aureus* with primary Cldn-1 antibody. Exemplary staining from  $n = 3$  donors. Bars =  $50 \mu\text{m}$  (modified with permission from Bäsler et al. (2017)).

Submerged models inoculated for long-term (24 h) with either *S. epidermidis* or *S. aureus* showed a decrease in immunointensity of the sealing claudins, Cldn-1 and Cldn-4, at the cell-

cell borders (Figure 33). While, for Ocln, a more pronounced localisation at the cell-cell borders was still evident after *S. aureus* infection (Figure 33). Interestingly, while there was no obvious increase in Ocln membrane localisation at early time points after *S. epidermidis* inoculation (in contrast to *S. aureus* inoculation), there was an increase after long-term inoculation (Figure 33).

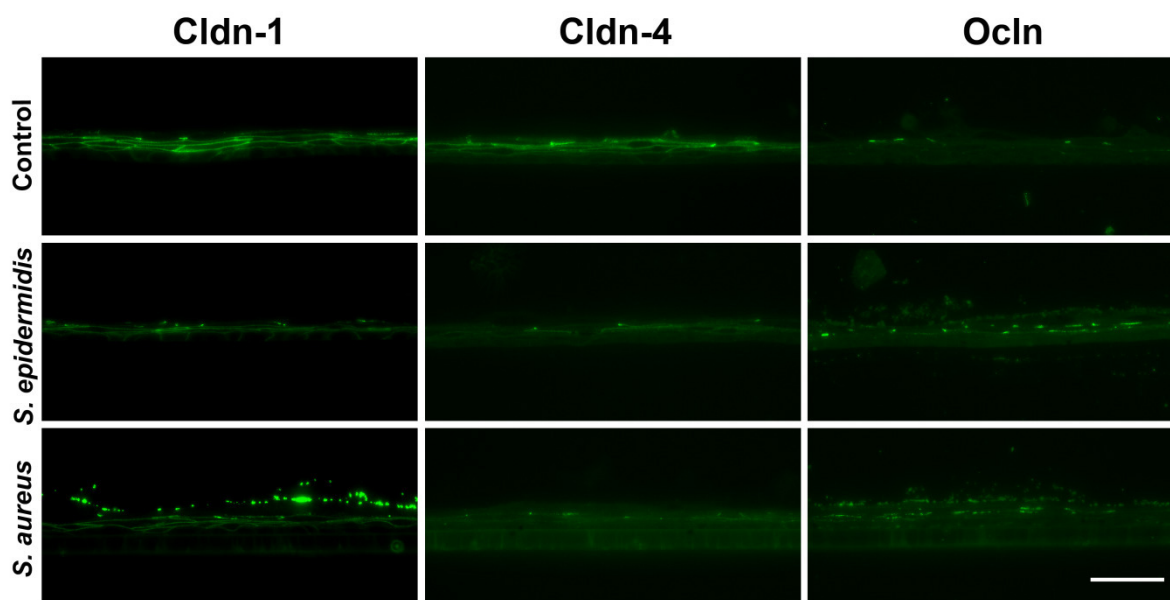


**Figure 33: Immunohistochemical stainings of tight junction proteins of the submerged model after 24 h of staphylococcal inoculation.** Immunohistochemical stainings (green) of claudin-1 (Cldn-1), Cldn-4 and occludin (Ocln) of the submerged culture after 24 h of inoculation with  $6 \times 10^5$  *S. epidermidis* or *S. aureus* per  $\text{cm}^2$  on cross sections of paraffin embedded filter-membranes. Bright fluorescent green dots on top of *S. aureus* infected models represent a cross reaction of *S. aureus* with primary Cldn-1 antibody. Exemplary staining from  $n = 3$  donors. Bars = 50  $\mu\text{m}$  (modified with permission from Bäsler et al. (2017)).

Because altered localisation patterns of TJ proteins were identified to be involved in increased as well as decreased TJ functionality after bacterial challenge the question arose: What are the mechanisms behind these changes?

### 3.2.4 Investigations on Tight Junction protein expression and protein levels

It has been shown that overexpression of e.g., Cldn-4 or Ocln results in relocalisation of the proteins to the cellular membranes and increasing TJ barrier function (McCarthy et al., 1996; Michikawa et al., 2008; Van Itallie et al., 2010). In order to clarify whether the increased localisation of Cldn-4 after *S. epidermidis* and of Cldn-4 and Ocln after *S. aureus* inoculation are the result of increased protein expression/levels, qPCR for mRNA analyses and Western Blot for protein level analyses were performed on the submerged models.

Investigation of mRNA expression levels of the TJ proteins Cldn-1, Cldn-4 and Ocln as well as the TJ associated plaque protein ZO-1 revealed no increased expression after 2, 4, 8 or 12 h

in NHEKs treated with either bacterial species (Figure 34). While only minor differences in mRNA levels were observed after 2 and 4 h of bacterial inoculation, even a decrease was found for Cldn-1, Cldn-4 and Occludin (Occludin) 8 and 12 h post staphylococcal challenge (Figure 34). Interestingly, a slight dose dependency was evident here as well, however not significant. No clear differences were found between the two species (Figure 34).

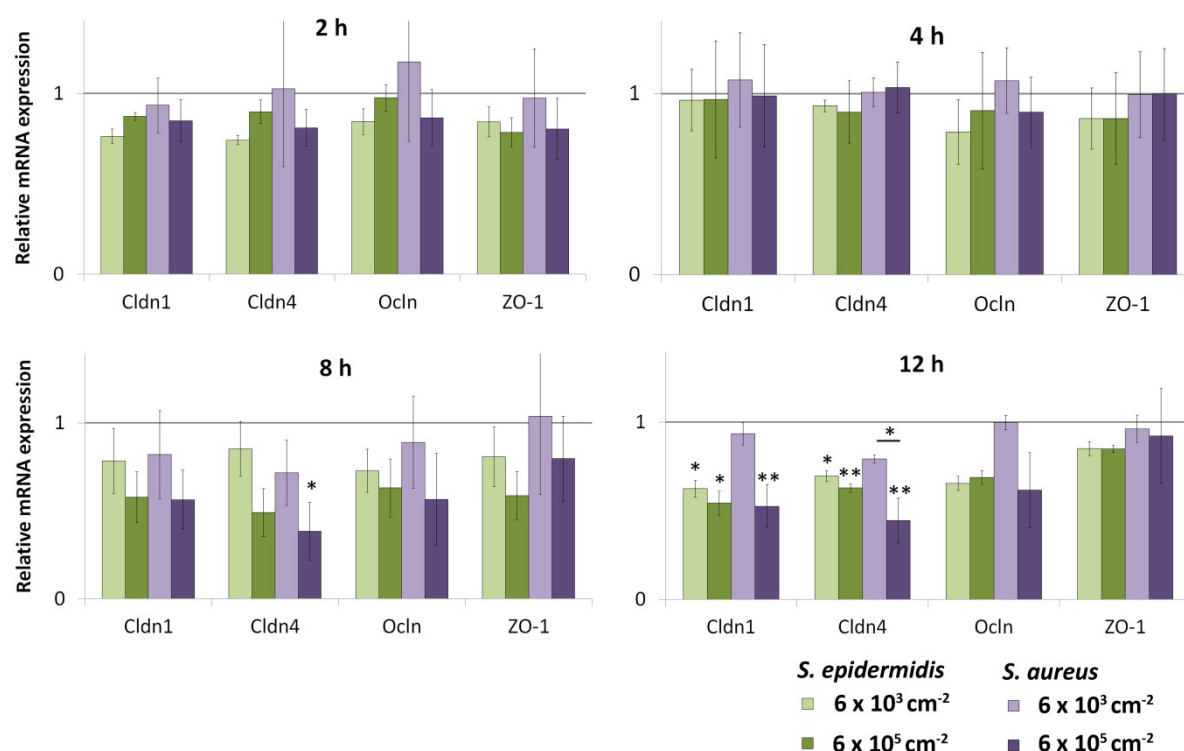


**Figure 34: Relative mRNA expression of tight junction proteins of the submerged model after staphylococcal inoculation.** Claudin-1 (Cldn-1), Cldn-4, Occludin (Occludin) and Zonula occludens-1 (ZO-1) of the submerged model inoculated with  $6 \times 10^3$  or  $6 \times 10^5$  *S. epidermidis* (green bars) or *S. aureus* (purple bars) per  $\text{cm}^2$  for the indicated time points. Mean  $\pm$  SEM;  $n = 3$  (2, 4 and 8 h) and 4 (12 h) donors in triplicates; \*  $p < 0.05$ , \*\*  $p < 0.01$  using ANOVA (modified from Bäsler et al. (2017)).

Thus, an increase in mRNA expression can be excluded as explanation for increased TJ protein at the cellular membranes. Still, the cell is a dynamic system and even though mRNA expression is unchanged or decreased, protein levels could be increased due to decreased protein degradation. Therefore, the protein levels of the sealing TJ proteins, Cldn-1 and Cldn-4, (Figure 35) as well as of Occludin (Figure 36) were analysed. After 12 h of inoculation with the *Staphylococcus* strains in the two doses no significant changes in protein levels of the sealing TJ proteins Cldn-1 and Cldn-4 were evident (Figure 35). Also, earlier time points (4 and 8 h) did not show differences in the protein levels of Cldn-1 and Cldn-4 (data not shown).



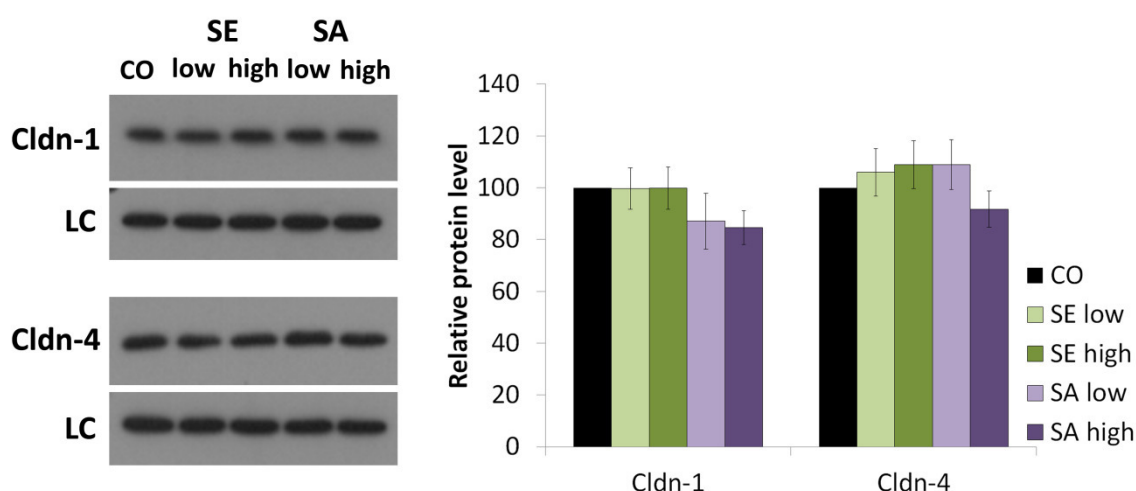


**Figure 35: Western Blot analysis of Claudin-1 (Cldn-1) and Cldn-4 in the submerged model after short-term bacterial challenge.** Representative Western Blots after 12 h of inoculation with  $6 \times 10^3$  (low) or  $6 \times 10^5$  (high) *S. epidermidis* (SE) or *S. aureus* (SA) per  $\text{cm}^2$  in comparison to the uninfected control (CO) and analyses of the relative protein levels. LC – loading control ( $\beta$ -actin). Mean  $\pm$  SEM;  $n = 5$  (SE low and high; SA low), 10 (SA high) donors (Modified with permission from Bäsler et al. (2017)).

In contrast, Western Blots of the infected submerged models for OcIn revealed clear changes for both bacterial strains, but differences between *S. epidermidis* and *S. aureus* short-term inoculation became apparent. Interestingly, while there was a dose-dependent decrease in overall OcIn after *S. epidermidis* inoculation, a dose-dependent increase in a higher phosphorylated form of OcIn was observed after *S. aureus* inoculation (Figure 36).

This could explain increased membrane localisation of OcIn after short-term *S. aureus* infection, because phosphorylation of OcIn is known to result in membrane accumulation of this protein (Sakakibara et al., 1997; Wong, 1997; Yuki et al., 2011b).

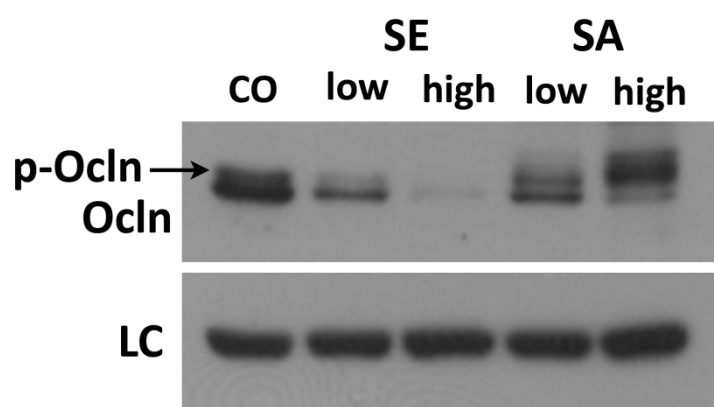


**Figure 36: Western Blot analysis of occludin (OcIn) in the submerged model after short-term bacterial challenge.** Representative Western Blot of Occludin (OcIn) in the submerged model after 12 h of inoculation with  $6 \times 10^3$  (low) or  $6 \times 10^5$  (high) *S. epidermidis* (SE) or *S. aureus* (SA) per  $\text{cm}^2$  in comparison to the uninfected control (CO). p-OcIn – higher phosphorylated form of OcIn; LC – loading control ( $\beta$ -actin) (modified with permission from Bäsler et al. (2017)).

The observation of OcIn phosphorylation after *S. aureus* inoculation while there was a decrease in overall OcIn level after *S. epidermidis* inoculation, indicates that the bacterial



strains are recognised in a different manner and that TJs react different depending on the species.

In order to investigate whether decreased Cldn-1 and Cldn-4 immuno-localisation after long-term staphylococcal inoculation was due to loss of protein, WB analyses were performed as well. As mRNA levels were already reduced at 8 and 12 h post inoculation, decreased protein levels are very likely to be involved in the loss of TJ integrity.

However, only a minor, non-significant decrease at the protein levels of the two sealing claudin could be found after long-term *S. aureus* infection (Figure 37), while for *S. epidermidis* even a slight increase was noticed (Figure 37). Thus, internalisation, but not degradation of Cldn-1 and Cldn-4 is the cause for the TJ barrier decrease.

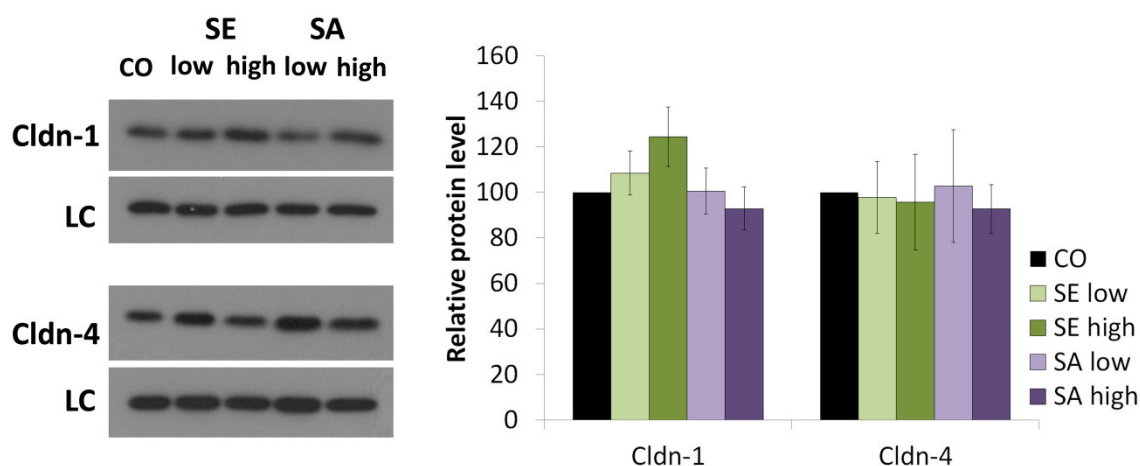


**Figure 37: Western Blot analysis of Claudin-1 (Cldn-1) and Cldn-4 in the submerged model after long-term bacterial challenge.** Representative Western Blots after 24 h of inoculation with  $6 \times 10^3$  (low) or  $6 \times 10^5$  (high) *S. epidermidis* (SE) or *S. aureus* (SA) per  $\text{cm}^2$  in comparison to the uninfected control (CO) and analyses of the relative protein levels. LC – loading control ( $\beta$ -actin). Mean  $\pm$  SEM; n = 5 (SE low and high; SA low), 10 (SA high) donors (Modified with permission from Bäsler et al. (2017)).

Interestingly, investigations on Ocln protein levels in WB revealed a strong decrease after long-term inoculation with either *S. epidermidis* or *S. aureus* independent from the initial concentration (Figure 38). This was a discrepancy to what has been observed in immunohistochemical stainings, where a strong increase in immunointensity was found.

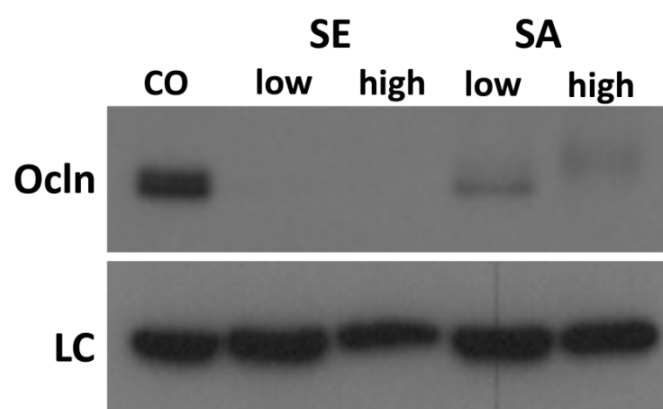


**Figure 38: Western Blot analysis of occludin (Ocln) in the submerged model after long-term bacterial challenge.** Representative Western Blot of Ocln in the submerged model after 24 h of inoculation with  $6 \times 10^3$  (low) or  $6 \times 10^5$  (high) *S. epidermidis* (SE) or *S. aureus* (SA) per  $\text{cm}^2$  in comparison to the uninfected control (CO). LC – loading control ( $\beta$ -actin) (modified with permission from Bäsler et al. (2017)).

### 3.2.5 Investigations of antimicrobial peptides and proinflammatory cytokines

Next the question arose whether the changes in TJ protein localisation are direct reactions on bacterial challenges or due to indirect mechanisms (e.g., inflammation), as the epidermal barrier is a dynamic system providing barrier function by interaction of different barrier components (see introduction).

It was shown in literature that NHEK treatment with antimicrobial peptides (AMPs) (Cathelicidin or h $\beta$ D3) (Akiyama et al., 2014; Kiatsurayanon et al., 2014) or with proinflammatory cytokines (IL-1 $\beta$  and TNF $\alpha$ ) (Kirschner et al., 2009) led to relocalisation of Ocln and/or Cldn-4 to the cellular membranes and increased TJ functionality. On the other hand, long-term treatment with IL-1 $\beta$  or TNF $\alpha$  has been shown to have a TJ function decreasing effect in NHEKs (Kirschner et al., 2009). Also other proinflammatory cytokines were described to decrease TJ functionality in NHEKs and other tissues (reviewed in e.g. Al-Sadi et al., 2009; Capaldo and Nusrat, 2009).

This suggests that an upregulation of AMPs or proinflammatory cytokines after bacterial inoculation could indirectly result in increased TJ functionality after short-term inoculation as well as a prolonged presence of proinflammatory cytokines could evoke decreasing TJ barrier function after long-term bacterial inoculation. Therefore the induction of these molecules was investigated together with other markers of inflammation by *S. epidermidis* or *S. aureus* inoculation in the submerged models.

Investigation of mRNA expression of Cathelicidin or h $\beta$ D3 revealed no upregulation of these two AMPs either after *S. epidermidis* or after *S. aureus* inoculation for 8 and 12 h. In contrast, there even was a significant decrease for h $\beta$ D3 (Figure 39). Thus, an indirect

involvement of an enhanced amount of AMPs in increasing TJ barrier function can be excluded.

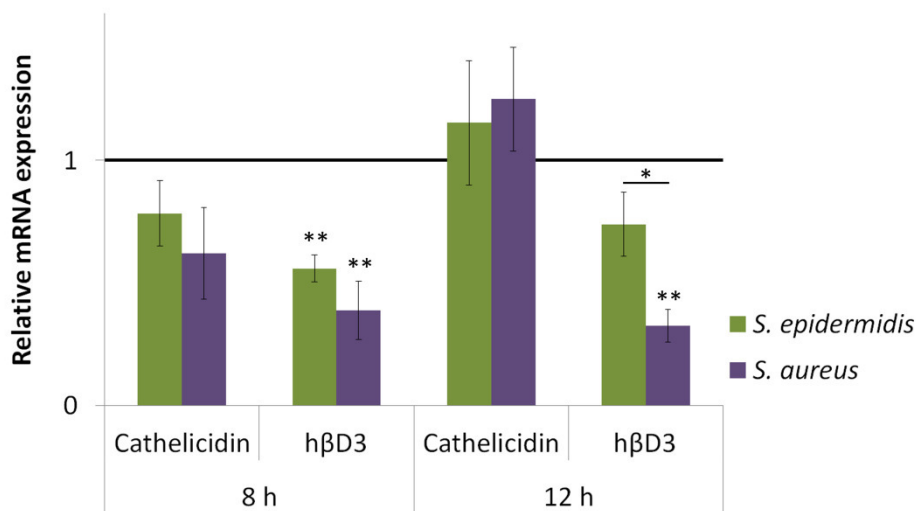


**Figure 39: Relative mRNA expression of antimicrobial peptides of the submerged culture after staphylococcal challenge.** Relative mRNA expression of Cathelicidin and human  $\beta$ -defensin-3 (h $\beta$ D3) in the submerged model 8 and 12 h post bacterial inoculation with  $6 \times 10^5$  *S. epidermidis* or *S. aureus* per cm<sup>2</sup>. Mean  $\pm$  SEM; n = 3 donors in triplicates; \* p < 0.05, \*\* p < 0.01 using ANOVA (modified with permission from Bäsler et al. (2017)).

Examination of proinflammatory cytokines revealed a substantial increase in IL-6, IL-8 and TNF $\alpha$  after 8 h of inoculation with *S. aureus*, while this was not the case after 4 h (Figure 40). Additionally, for *S. epidermidis* inoculation, an increase in TNF $\alpha$  and slightly in IL-6 and IL-8 mRNA was also visible 8 h post infection (for *S. epidermidis*, inoculation after 4 h was not investigated) (Figure 40).

This increase in proinflammatory cytokines was even more pronounced after 12 h of infection of the submerged model with *S. epidermidis* or *S. aureus*. A significant upregulation of IL-1 $\beta$  and IL-6 mRNA was detected for both species to the same extent. Also for IL-8 and TNF $\alpha$  mRNA a clear upregulation was evident (Figure 40).

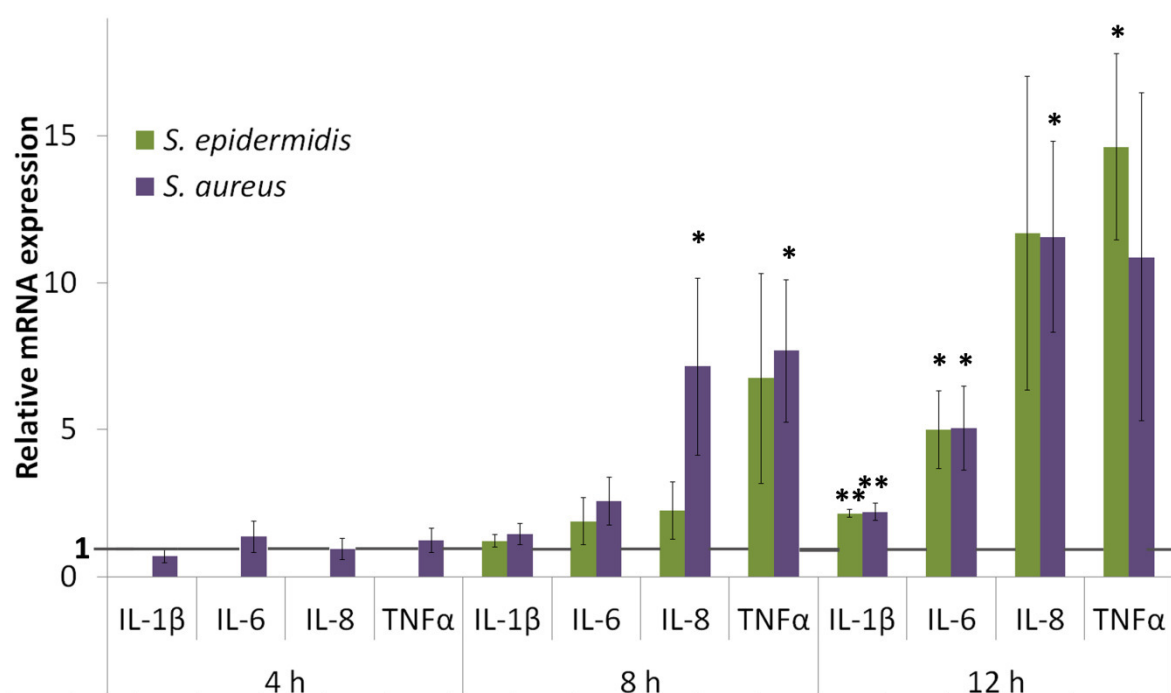


**Figure 40: Relative mRNA expression of proinflammatory cytokines of the submerged culture after staphylococcal challenge.** Relative mRNA expression of Interleukin-1β (IL-1β), IL-6, IL-8 and tumour necrosis factor-α (TNFα) in the submerged model 8 and 12 h post bacterial inoculation with  $6 \times 10^5$  *S. epidermidis* or *S. aureus* per cm<sup>2</sup>. Mean +/- SEM; n = 3 donors in triplicates; \* p<0.05, \*\* p<0.01 using ANOVA (modified with permission from Bäsler et al. (2017)).

As it is known that proinflammatory cytokines are stored in the cells in order to be released quickly (Latz et al., 2013), the release of cytokines during increase and decrease in TJ barrier function was investigated by protein analyses (Milliplex) of the supernatant of the infected submerged models 12 and 24 h post inoculation.

For the early time point (12 h), when TJ barrier was increased, a clear elevation in cytokine release of granulocyte-macrophage colony-stimulating factor (GM-CSF), IL-1β, IL-6, monocyte chemoattractant protein 1 (MCP-1) and TNFα and slight increase of IL-8 was detected for *S. aureus* inoculation (Figure 41). Interestingly, differences became evident between *S. epidermidis* and *S. aureus* short-term inoculation (Figure 41). The effect of *S. aureus* was more pronounced on most of the tested cytokines, except for IL-1α for which a small, but significantly stronger increase in the release after short-term *S. epidermidis* compared to *S. aureus* inoculation was observed (Figure 41).

Additionally, it was tested whether cytokines are prolonged upregulated after bacterial inoculation. A strong release of TNFα, GM-CSF, IL-1β and IL-6 and a slight increase of IL-8 were still observed 24 h after *S. aureus* inoculation (Figure 41). For *S. epidermidis*, there was still an increase in IL-1α and an additional increase in IL-1β and slightly in TNFα release (Figure 41). Also after long-term inoculation the release of all investigated cytokines was

more pronounced after *S. aureus* infection compared to *S. epidermidis* infection except of IL-1 $\alpha$ .

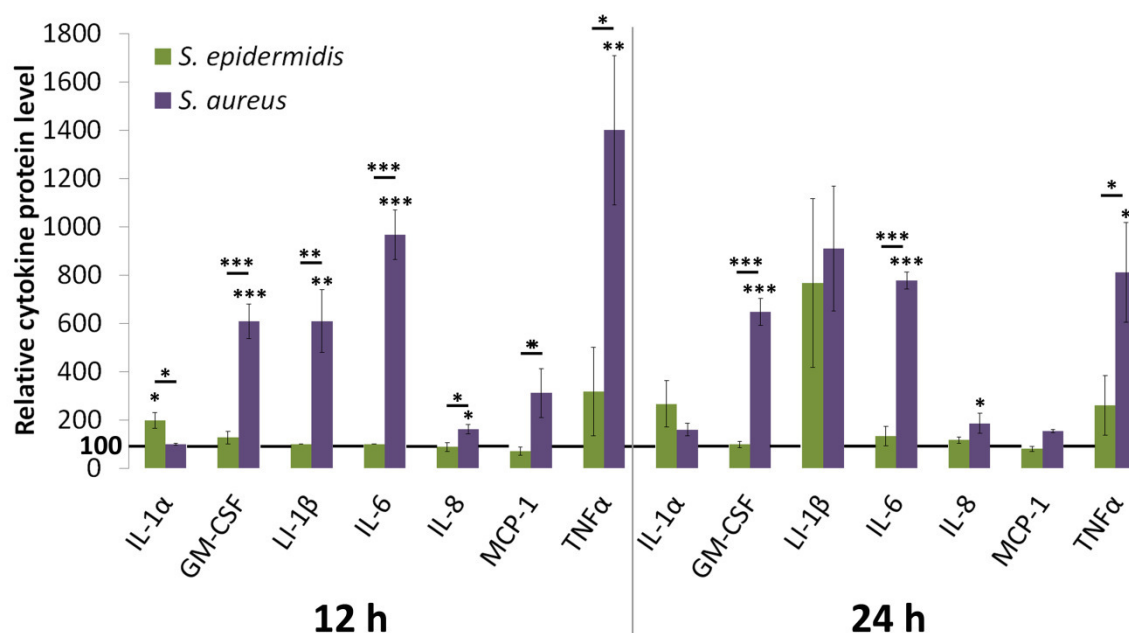


**Figure 41: Relative cytokine protein levels of the supernatant of submerged models after staphylococcal challenge.** Relative protein levels of interleukin-1 $\alpha$ , granulocyte-macrophage colony-stimulating factor (GM-CSF), IL-1 $\beta$ , IL-6, IL-8, monocyte chemoattractant protein 1 (MCP-1) and tumour necrosis factor- $\alpha$  (TNF $\alpha$ ) of the submerged model after inoculation for either 12 or 24 h with  $6 \times 10^5$  *S. epidermidis* or *S. aureus* per cm<sup>2</sup>. Mean  $\pm$  SEM; n = 3 donors; \* p<0.05, \*\* p<0.01, \*\*\* p<0.01 using ANOVA (modified with permission from Bäsler et al. (2017)).

If cytokines truly play a role during infection, than a dual effect – cytokines and bacteria – should influence the cells at the same time. To further test whether cytokines indeed can contribute to the increase and decrease of TJ barrier function in infected keratinocytes a combination of *S. aureus* infection and IL-1 $\beta$  as well as TNF $\alpha$  treatment was performed, as especially these two cytokines had been described before to influence TJ functionality

(Kirschner et al., 2009).

Indeed, parallel treatment of the submerged models with either IL-1 $\beta$  or TNF $\alpha$  and *S. aureus* inoculation showed an intensified increase in TER in short-term (8 h) investigation (Figure 42). Furthermore, parallel treatment with IL-1 $\beta$  resulted in an accelerated decrease after 15 h *S. aureus* inoculation, while there was only a slight tendency towards a faster decrease after TNF $\alpha$  treatment (Figure 42).

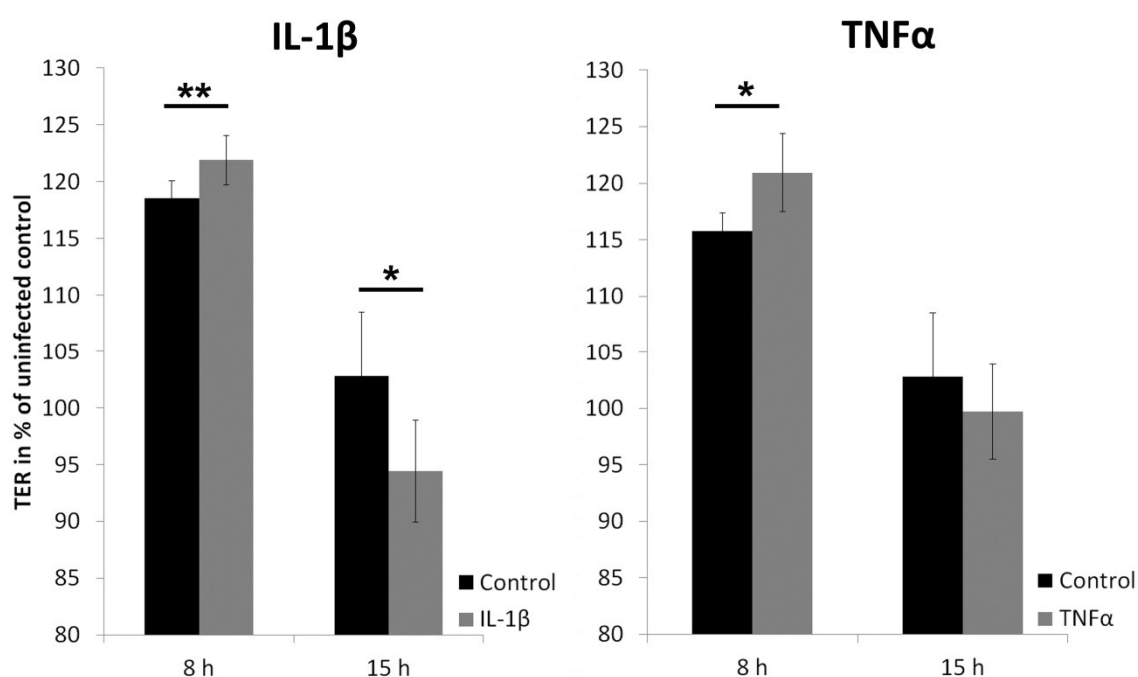


**Figure 42: Transepithelial electrical resistance (TER) of the submerged model after *S. aureus* inoculation and parallel treatment with proinflammatory cytokines.** TER in % of uninfected control of the submerged culture inoculated with  $6 \times 10^5$  *S. aureus* per  $\text{cm}^2$  either untreated (control) or treated in parallel with interleukin-1 $\beta$  (IL-1 $\beta$ ) or tumour necrosis factor- $\alpha$  (TNF $\alpha$ ). Mean  $\pm$  SEM; n = 4 donors in triplicates; \*  $p < 0.05$ , \*\*  $p < 0.01$  using Students T-test (modified with permission from Bäsler et al. (2017)).

The decrease in TJ barrier function after long-term infection with *S. epidermidis* or *S. aureus* could be a result of the increased inflammatory environment, but also other mechanisms might lead to TJ barrier breakdown, e.g., bacterial enzymes that destroy TJ structures or influence the cellular membranes.

### 3.2.6 Investigations on bacterial virulence factors

The question arose whether the internalisation of the two claudins might be triggered by bacterial enzymes, especially proteases or other virulence factors that are produced by the bacteria in order to destroy/open barrier systems. As already introduced, these bacterial proteases, as well as many other virulence factors are regulated via the accessory gene regulator (*agr*) system (Painter et al., 2014). To investigate the role of these virulence factors on TJ functionality, a *S. aureus* mutant strain was cloned, in which the *agr* regulon was not functional and secreted virulence factors could not be produced ( $\Delta$ *agr*). In addition, *Staphylococcus carnosus*, which is a completely apathogen strain and does not produce any virulence factors (Rosenstein et al., 2009; Rosenstein and Götz, 2010), was used in this approach as well.

Interestingly, TER measurements of submerged models after inoculation with these two strains showed no differences in decreasing TER after long-term (24 h) inoculation compared to wild type (WT) control (Figure 43).

Surprisingly, significant differences were observed between *S. aureus* WT and *S. aureus*  $\Delta agr$  or *S. carnosus* inoculation at early time points (Figure 43). While *S. aureus* WT inoculation resulted – as described before - in an accelerated increase in TER, the two strains lacking virulence factors, did not (Figure 43).

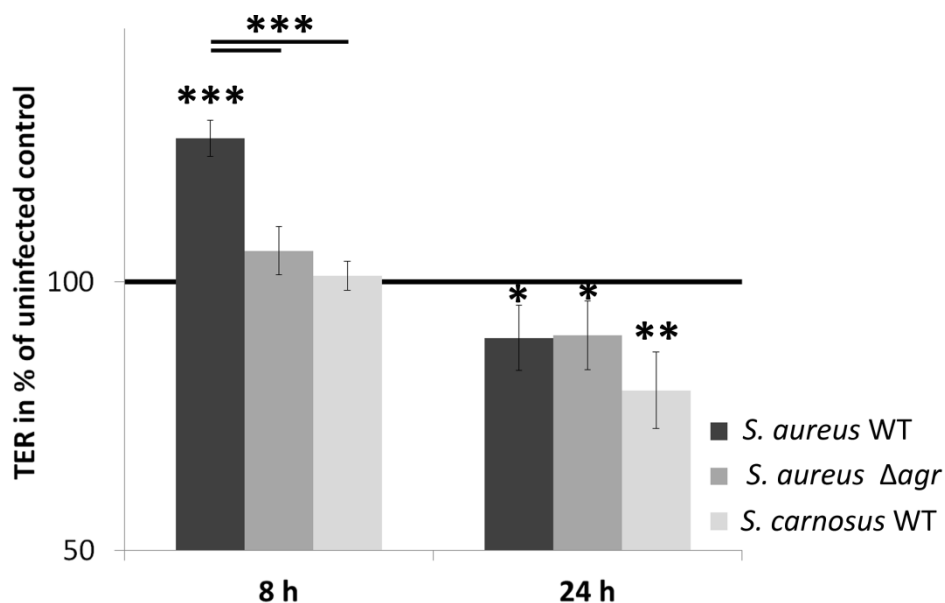


**Figure 43:** Transepithelial electrical resistance (TER) of the submerged model after inoculation with *S. aureus* wild-type (WT), a *S. aureus* mutant lacking the accessory gene reulator ( $\Delta agr$ ) or *S. carnosus*, representing an apathogenic strain. TER in % of the uninfected control after short-term (8 h) and long-term (24 h) inoculation with  $6 \times 10^5$  bacteria per  $\text{cm}^2$ . Mean  $\pm$  SEM; n = 5 donors in triplicates; \*  $p < 0.05$ , \*\*  $p < 0.01$ , \*\*\*  $p < 0.001$  using ANOVA (modified with permission from Bäsler et al. (2017)).

Thus, an involvement of bacterial proteases or other enzymes cannot be the reason for decreasing TJ barrier function. However, virulence factors seem to play an important role in the increase in TER.

### 3.3 Results, Part 3: Investigation of the effect of staphylococcal treatment on Tight Junctions in reconstructed human epidermis (PFe3D)

In order to bridge the gap between the results in submerged models and previous investigations made *in vivo/ex vivo*, the effects of bacterial treatment on epidermal TJs in a system closer to the *in vivo* situation, which also considers the influence of the SC and its interaction with TJs, i.e. 3D reconstructed human epidermis, was infected as well.

As already has been described, the 3D reconstruction after the protocol of Pierre Fabre (PFe3D) was found to be most suitable for these investigations.

For analysing the effect of Staphylococcal inoculation on PFe3D models, *Staphylococcus aureus* and *Staphylococcus epidermidis* were used in 5 µl of physiological NaCl solution at a concentration of  $5 \times 10^4$  bacteria  $\text{cm}^{-2}$ .

#### 3.3.1 *S. aureus* and *S. epidermidis* grow and live on top of the models

One hallmark of infection is the multiplication of the pathogenic organisms within or on their host (Miller and Cho, 2011). When developing a model of bacterial treatment in order to mimic skin infection on 3D models, it is important to investigate whether the used organism is able to multiply in this system.

PFe3D models at day 4 after ALI were incubated for 24, 48 and 72 h with *S. aureus* or *S. epidermidis*. After indicated time points the colony forming units (CFU) of both bacteria were investigated displaying the amount of living bacteria. Compared to the initial number of bacteria used, counts of CFU/model were strongly enhanced after 24, 48 and 72 h of *S. aureus* and *S. epidermidis* inoculation (Figure 44 A) with an especially strong rise after 24 h for both species, which was not only observed by counting, but also by examining fluorescent mutants on top of PFe3D (Figure 44 B-C'). While directly after application barely fluorescent bacteria were visible (Figure 44 B, C), after 24 h a strong increase in the amount of fluorescent bacteria was evident (Figure 44 B', C'). However, when comparing both strains, it became evident, that the growth of *S. aureus* was stronger than compared to *S. epidermidis* (Figure 44 A).



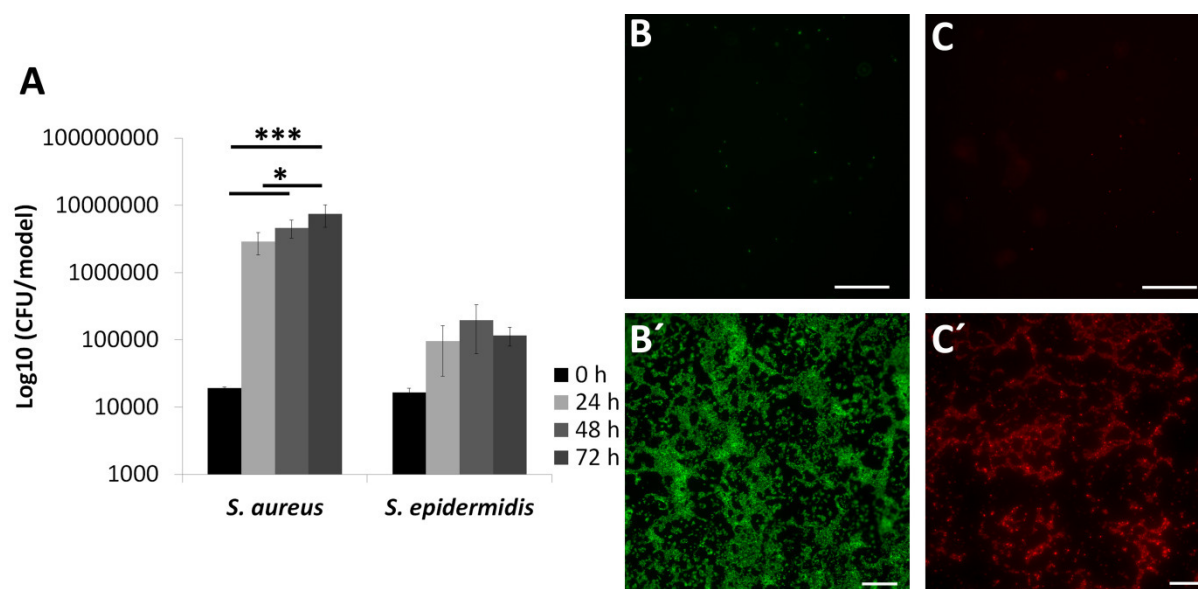


**Figure 44: Bacterial growth on top of PFe3D models.** Logarithmic diagram of the colony forming units (CFU) of *S. aureus* and *S. epidermidis* after inoculation of PFe3D at day 4 for 0, 24, 48 and 72h (A). Green-fluorescent mutant of *S. aureus* (B and B') and red-fluorescent mutant of *S. epidermidis* (C and C') directly (B and C) and 24 h (B' and C') after inoculation. Mean  $\pm$  SEM;  $n = 5$  (*S. aureus*) and 3 (*S. epidermidis*) donors in duplicates; \*  $p < 0.05$ , \*\*\*  $p < 0.01$  using ANOVA. Bars = 50  $\mu$ m (modified with permission from Bäsler et al. (2017)).

### 3.3.2 The growth of *S. aureus* can be reduced by *S. epidermidis*

Normal commensals on the skin, such as *S. epidermidis*, are known to provide a barrier against pathogen growth either directly, due to decreasing the amount of nutrients and space, or indirectly, due to the enhancement of host innate and adaptive immunity (Sanford and Gallo, 2013). In order to test this and to mimic colonisation with commensals, 3D models were pretreated with *S. epidermidis* for 24 h. Afterwards these models were incubated with *S. aureus* as well for another 48 h. Indeed, pretreatment with *S. epidermidis* significantly reduced the growth of *S. aureus* (Figure 45).

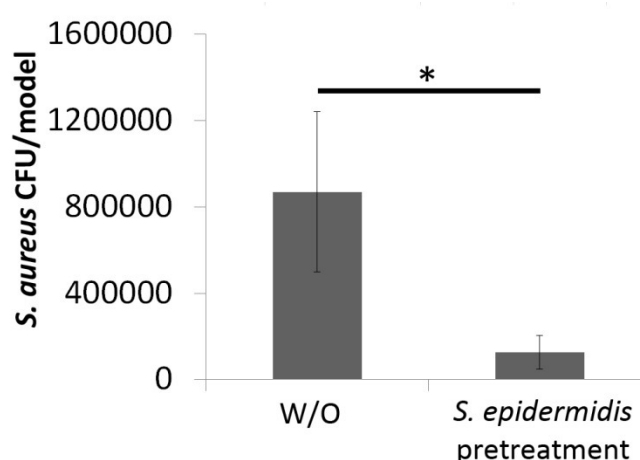


**Figure 45: Growth of *S. aureus* on PFe3D after *S. epidermidis* pretreatment.** Colony forming units (CFU) of *S. aureus* on PFe3D models on day 6 after 48 h without (W/O) and with pretreatment with *S. epidermidis* for 24 h. Mean  $\pm$  SEM;  $n = 3$  donors in duplicates; \*  $p < 0.05$  using Student's t-test (modified with permission from Bäsler et al. (2017)).

### 3.3.3 Morphological investigations of PFe3D after *S. epidermidis* or *S. aureus* inoculation

Examination of H&E staining of PFe3D incubated for 24, 48 and 72 h with either *S. epidermidis* or *S. aureus* did not reveal obvious morphological changes in epidermal structuring compared to the untreated control or NaCl-treated control (Figure 46).

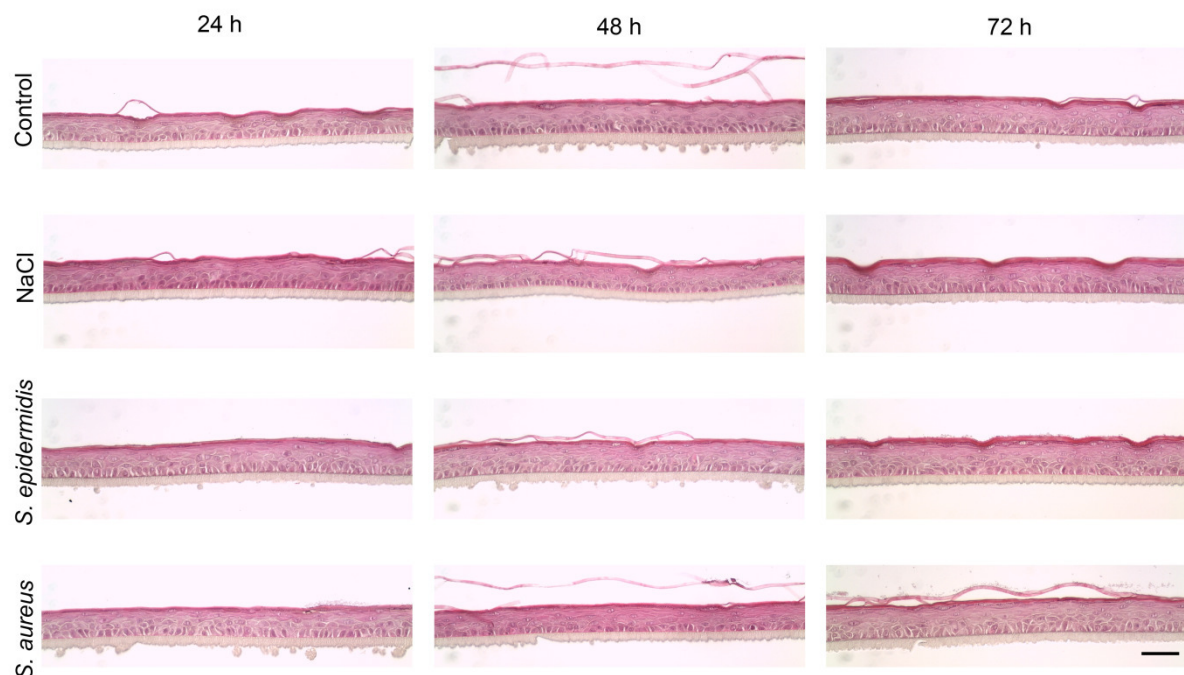


**Figure 46: Haematoxylin and eosin (H&E) staining of PFe3D after staphylococcal challenge.** PFe3D inoculated on day 4 of air-liquid-interface for indicated time points with either nothing (control), 5  $\mu$ l of 0.9% NaCl-solution (NaCl) or  $5 \times 10^4$  *S. epidermidis* or *S. aureus*  $\text{cm}^{-2}$  in 5  $\mu$ l of 0.9% NaCl-solution. Bar = 50  $\mu$ m.

### 3.3.4 Investigations on overall barrier function of PFe3D after *S. epidermidis* and *S. aureus* inoculation

Overall barrier function of PFe3D to ions was measured by determining TER, which comprises the barrier function of the SC and the TJs. As already described, PFe3D models in general provide a good overall barrier function. Infection of PFe3D with either *S. epidermidis* or *S. aureus* did not result in differences in overall barrier function, neither compared to the untreated nor to the NaCl-control (Figure 47). Additionally, no differences were observed for short-term (24 h) or long-term (72 h) inoculation (Figure 47).

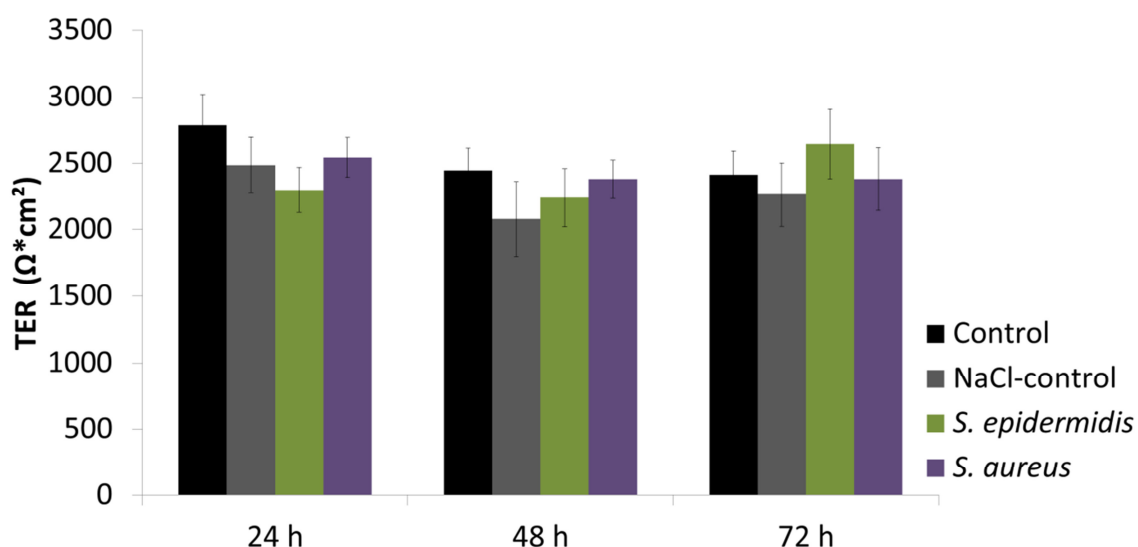


**Figure 47: Transepithelial electrical resistance (TER) of PFe3D after staphylococcal challenge.** TER of PFe3D models infected on day 4 of air-liquid-interface for indicated time points with  $5 \times 10^4$  *S. epidermidis* or *S. aureus*  $\text{cm}^{-2}$  in 5  $\mu\text{l}$  of 0.9% NaCl-solution compared to untreated or NaCl-control models. Mean  $\pm$  SEM; n = 4 donors in triplicates (modified with permission from Bäsler et al. (2017)).

### 3.3.5 Investigations on Tight Junction functionality of PFe3D after *S. epidermidis* and *S. aureus* inoculation

As already introduced, the biotinylation assay provides a good method to analyse TJ functionality in 3D systems. Following this, *S. epidermidis* and *S. aureus* infection of PFe3D models resulted in a decreased TJ barrier function starting at 48 h of inoculation in certain areas and being more pronounced after 72 h of inoculation with both species. There was no change after 24 h (Figure 48).

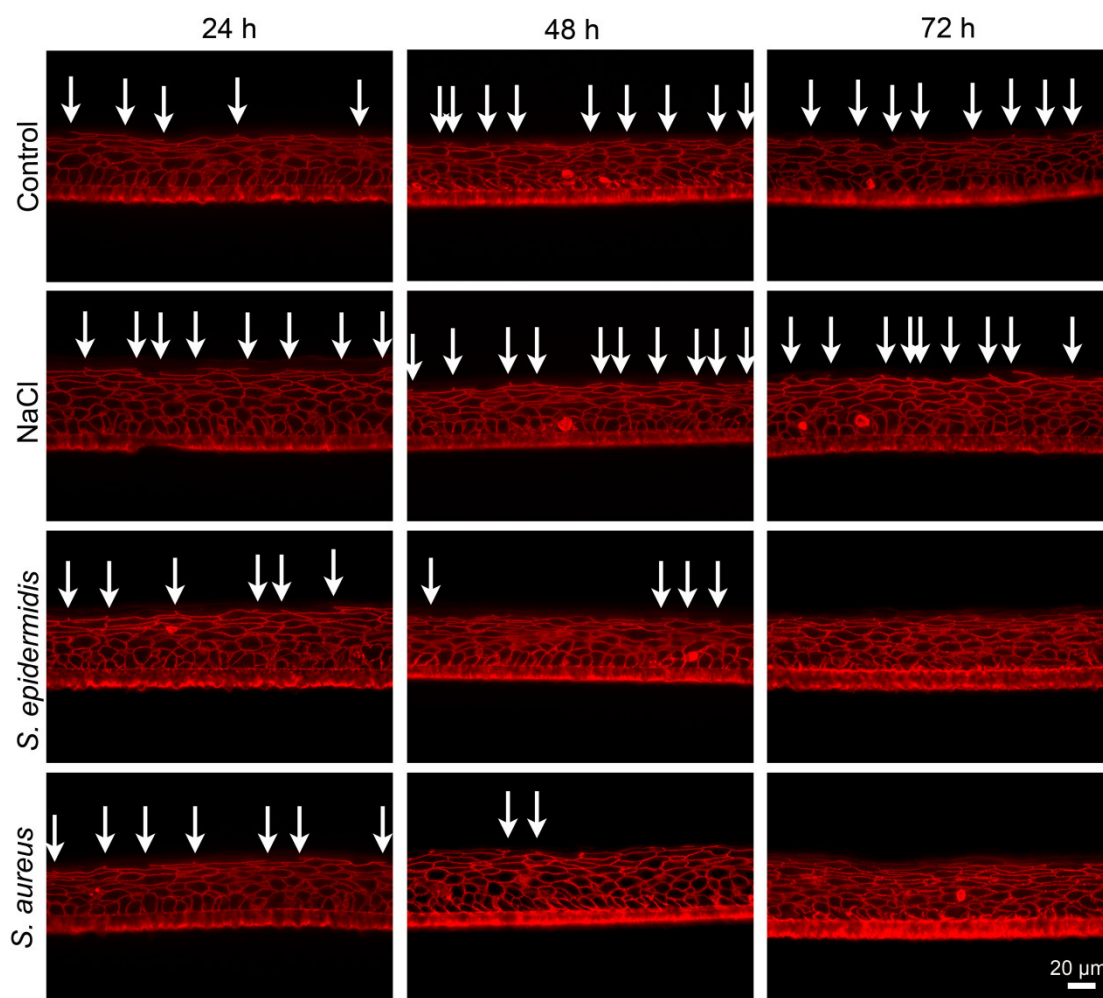


**Figure 48: Biotinylation assay of PFe3D models after staphylococcal inoculation.** Biotin tracer (red) in PFe3D models infected on day 4 of air-liquid-interface for the indicated time points with  $5 \times 10^4$  *S. epidermidis* or *S. aureus*  $\text{cm}^{-2}$  in 5  $\mu\text{l}$  of 0.9% NaCl-solution compared to untreated or NaCl-control models. White arrows denote complete stops of the tracer. Bar = 20  $\mu\text{m}$  (modified with permission from Bäsler et al. (2017)).

In order to quantify the increased permeability after long-term inoculation and in order to elucidate possible changes after short-term inoculation, counting of complete and half tracer stops was performed and the permeated TJs per visual field were evaluated. Indeed, this revealed a significant increase in TJ permeability, reflecting decreased TJ functionality, after 48 and 72 h of inoculation with *S. aureus* as well as with *S. epidermidis* (Figure 49). No changes in permeability were observed for the early time point (24 h).

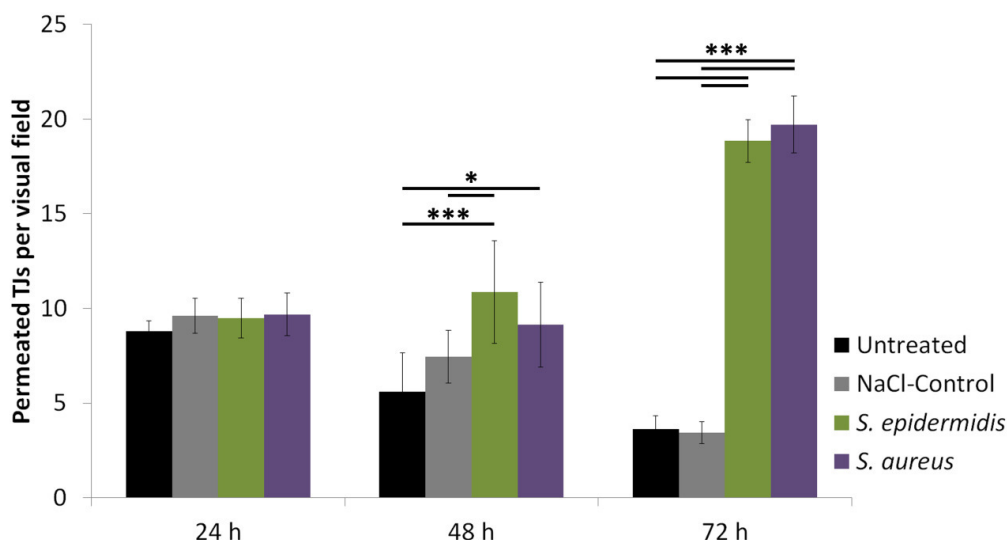


**Figure 49: Biotin tracer permeability of PFe3D models after staphylococcal inoculation.** Permeated tight junctions (TJs) per visual field after 24, 48 and 72 h of untreated, NaCl-treated (5  $\mu$ l) or infected PFe3D (5  $\mu$ l with either  $5 \times 10^4$  *S. epidermidis* or *S. aureus*). Mean  $\pm$  SEM; n = 3 (24 and 48 h) or 4 (72 h) donors in triplicates; \* p<0.05, \*\*\* p<0.01 using ANOVA (modified with permission from Bäsler et al. (2017)).

### 3.3.6 Infection of PFe3D with *S. aureus* did not result in cell death

Also for PFe3D models the tissue viability was analysed in context of long-term infection. As already indicated by H&E staining, infection of PFe3D for 72 h with *S. aureus* did not result in decreased tissue viability (Figure 50). This was investigated using tissue-MTT staining as described before. As a positive control for dead tissue, also PFe3D models were incubated with 1N HCl-solution for 1 h and subsequently stained with MTT. In these HCl-controls no positive staining was observed (Figure 50). These results were similar to observations made in submerged models. Of note, the viability of the tissue can also be observed in the biotinylation assays (see Figure 48). The tracer remains extracellular within viable cells, whereas it would penetrate into dead cells. For *S. epidermidis*, tissue-MTT was not performed, but viability was also observed in the biotinylation assays.

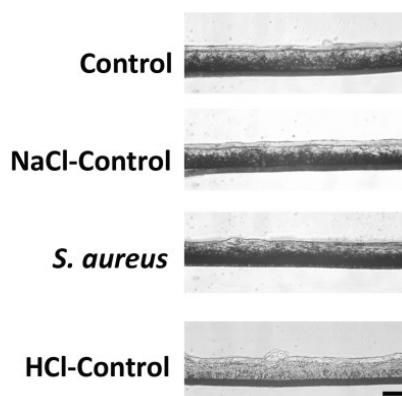


**Figure 50: Viability assay of long-term infected PFe3D with *S. aureus*.** Tissue-MTT of PFe3D infected on day 4 of air-liquid-interface for 72 h with  $5 \times 10^4$  *S. aureus* cm<sup>-2</sup> compared to untreated, NaCl- and HCl-control. The dark staining denotes viable cell layers. Unstained area on top of the models is the dead horny layer of SC. The darker line on the bottom displays the insert-membrane. Bar = 50  $\mu$ m (modified with permission from Bäsler et al. (2017)).

### 3.3.7 Investigations on Tight Junction protein localisation patterns

In the infected submerged models reduced TJ functionality after long-term inoculation was accompanied by a decrease in immunointensity of Cldn-1 and -4 and an increase in Ocln immunointensity. Therefore, also in PFe3D models, which also show decreased TJ functionality after long-term inoculation, immunofluorescence stainings were performed in order to analyse possible changes in TJ protein localisation.

Indeed, a decrease in immunointensity of Cldn-1 and Cldn-4 as well as an increased immunointensity of Ocln were observed after long-term (72 h) inoculation with *S. epidermidis* as well as *S. aureus* (see Figure 51 for Cldn-1, Figure 52 for Cldn-4, and Figure 53 for Ocln). There was no change after 24 and 48 h in Cldn-1 or Cldn-4 immunolocalisation/intensity (Figures 51 and 52). For Ocln, in certain areas a slight increase in immunointensity was observed after short-term (24 h) *S. aureus* inoculation and after 48 h of *S. aureus* as well as *S. epidermidis* inoculation (Figure 53).

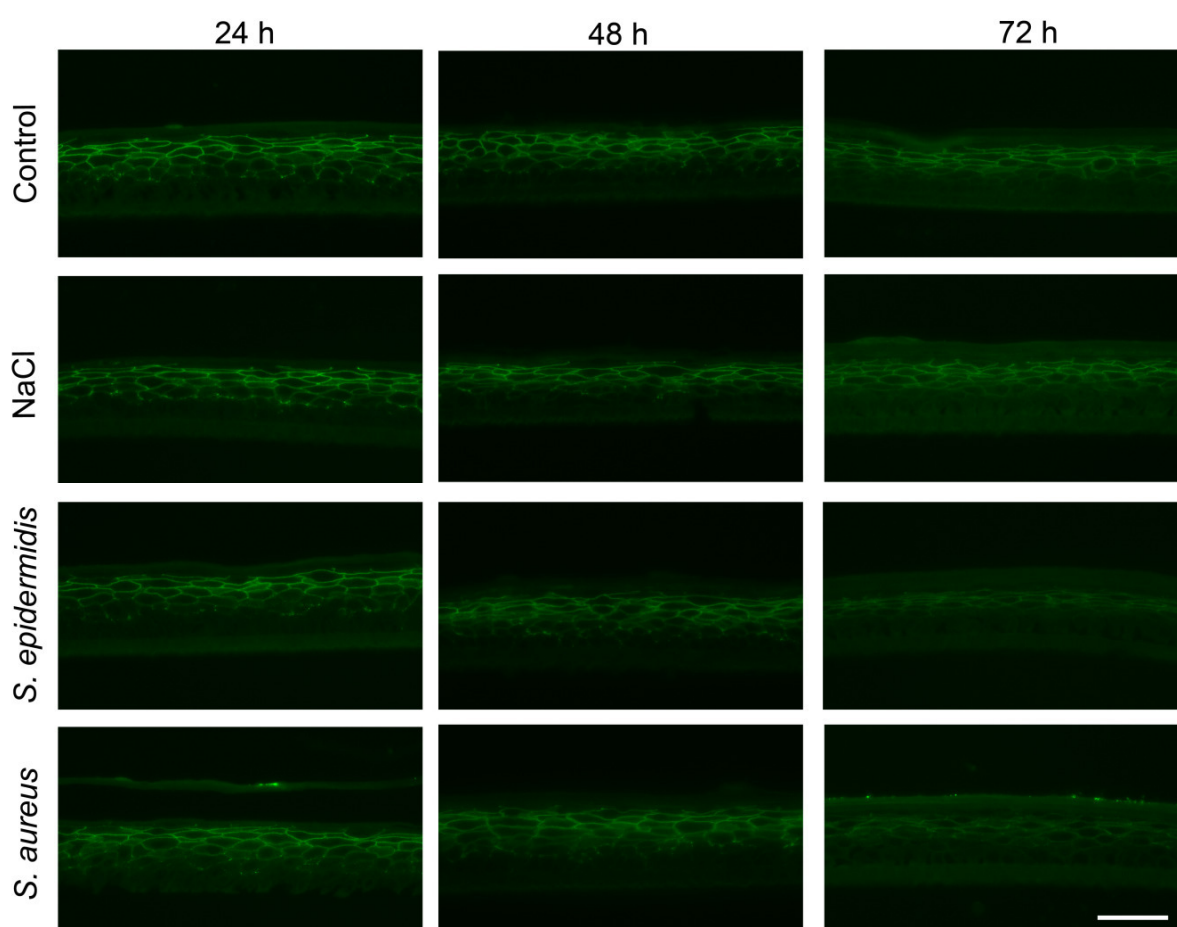


**Figure 51: Immunofluorescence staining of Claudin-1 (Cldn-1) in PFe3D models after staphylococcal challenge.** Cldn-1 (green) in PFe3D models infected on day 4 of air-liquid-interface for the indicated time points with  $5 \times 10^4$  *S. epidermidis* or *S. aureus*  $\text{cm}^{-2}$  in 5  $\mu\text{l}$  of 0.9% NaCl-solution compared to untreated or NaCl-control models. Bright fluorescent green dots on top of *S. aureus* infected models represent a cross reaction of *S. aureus* with primary Cldn-1 antibody. Exemplary staining from  $n = 3$  donors in triplicates. Bar = 50  $\mu\text{m}$  (modified with permission from Bäsler et al. (2017)).



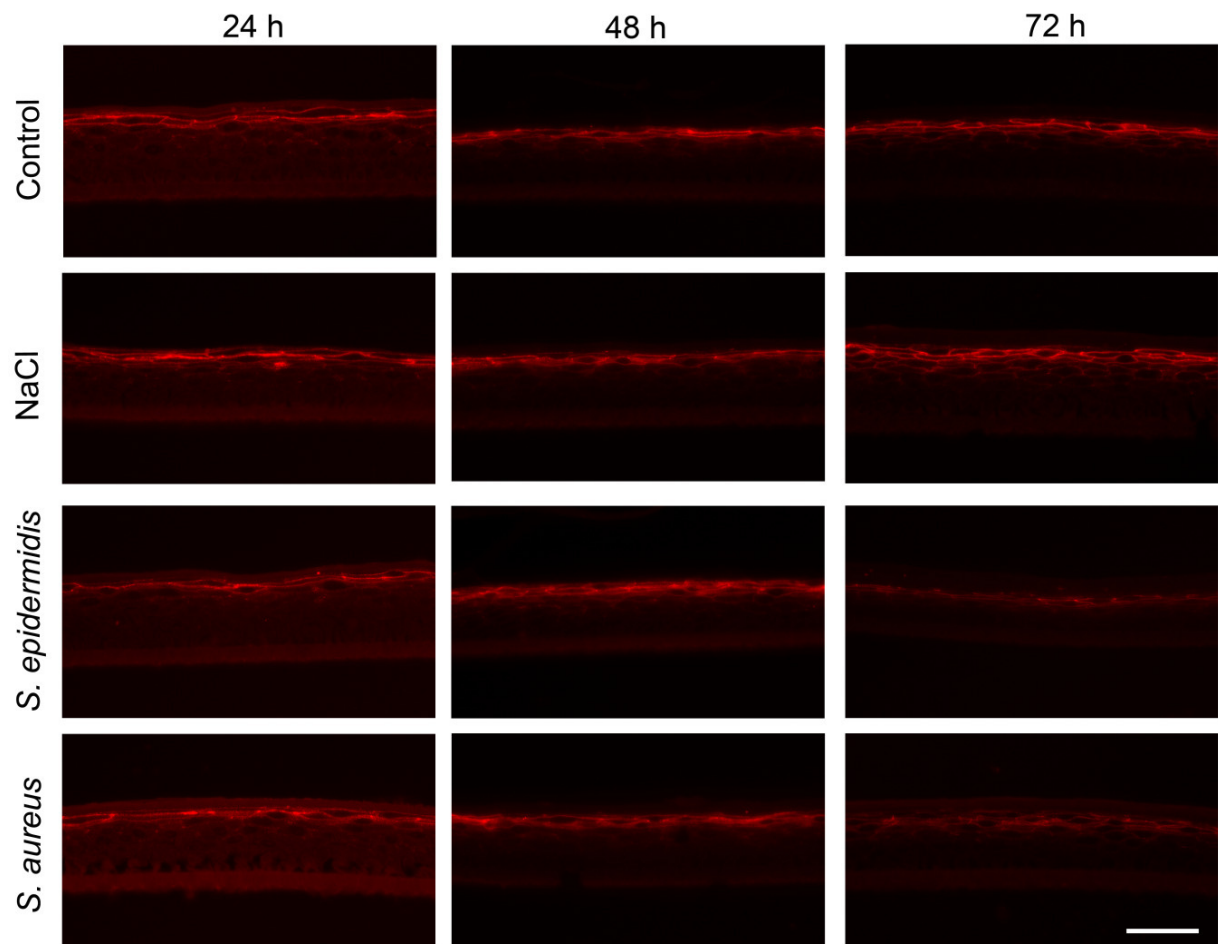


**Figure 52: Immunofluorescence staining of Claudin-4 (Cldn-4) in PFe3D models after staphylococcal challenge.** Cldn-4 (red) in PFe3D models infected on day 4 of air-liquid-interface for the indicated time points with  $5 \times 10^4$  *S. epidermidis* or *S. aureus*  $\text{cm}^{-2}$  in 5  $\mu\text{l}$  of 0.9% NaCl-solution compared to untreated or NaCl-control models. Exemplary staining from  $n = 3$  donors in triplicates. Bar = 50  $\mu\text{m}$  (modified with permission from Bäsler et al. (2017)).

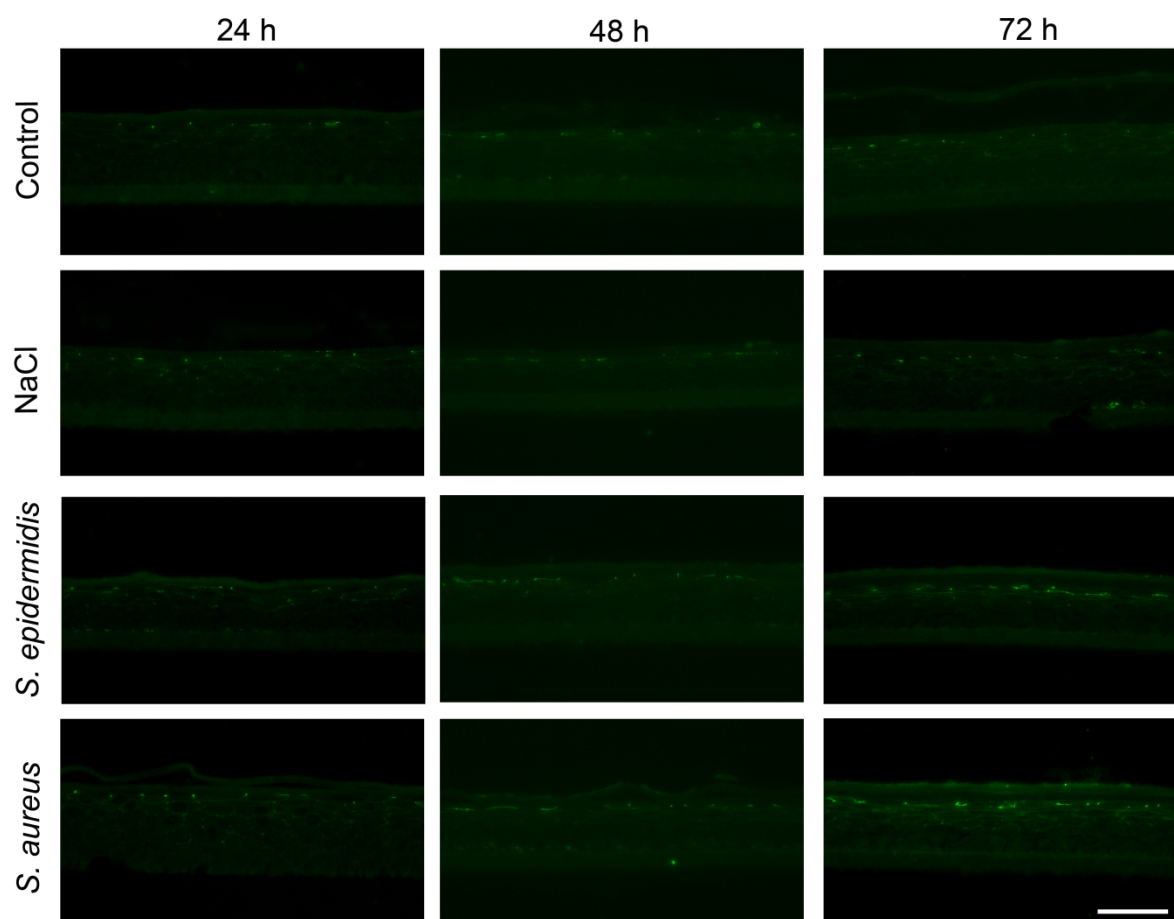


**Figure 53: Immunofluorescence staining of occludin (Ocln) in PFe3D models after staphylococcal challenge.** Ocln (green) in PFe3D models infected on day 4 of air-liquid-interface for the indicated time points with  $5 \times 10^4$  *S. epidermidis* or *S. aureus*  $\text{cm}^{-2}$  in 5  $\mu\text{l}$  of 0.9% NaCl-solution compared to untreated or NaCl-control models. Exemplary staining from  $n = 3$  donors in triplicates. Bar = 50  $\mu\text{m}$  (modified with permission from Bäsler et al. (2017)).

In order to analyse the decrease of Cldn-1 and Cldn-4 and the increase in Ocln after long-term inoculation in a more quantitative manner, fluorescence intensity was measured.

When evaluating overall intensity (whole tissue in SG), no changes were observed for Cldn-1 for both bacteria and a decrease for Cldn-4 (not significant) was evident only after *S. epidermidis* inoculation (Figure 54 A, B).

However, after subtraction of the intracellular intensity, the remaining intensity at the cellular membranes revealed a significant decrease in Cldn-1 (compared to NaCl-control) and Cldn-4 (compared to untreated control) at the membranes after long-term *S. aureus* as well as after *S. epidermidis* inoculation (Figure 54 A, B).

Measurement of Ocln immunointensity of PFe3D after long-term bacterial inoculation confirmed microscopic observation with a strong increase in Ocln staining, especially at the cellular membranes (Figure 54 C).



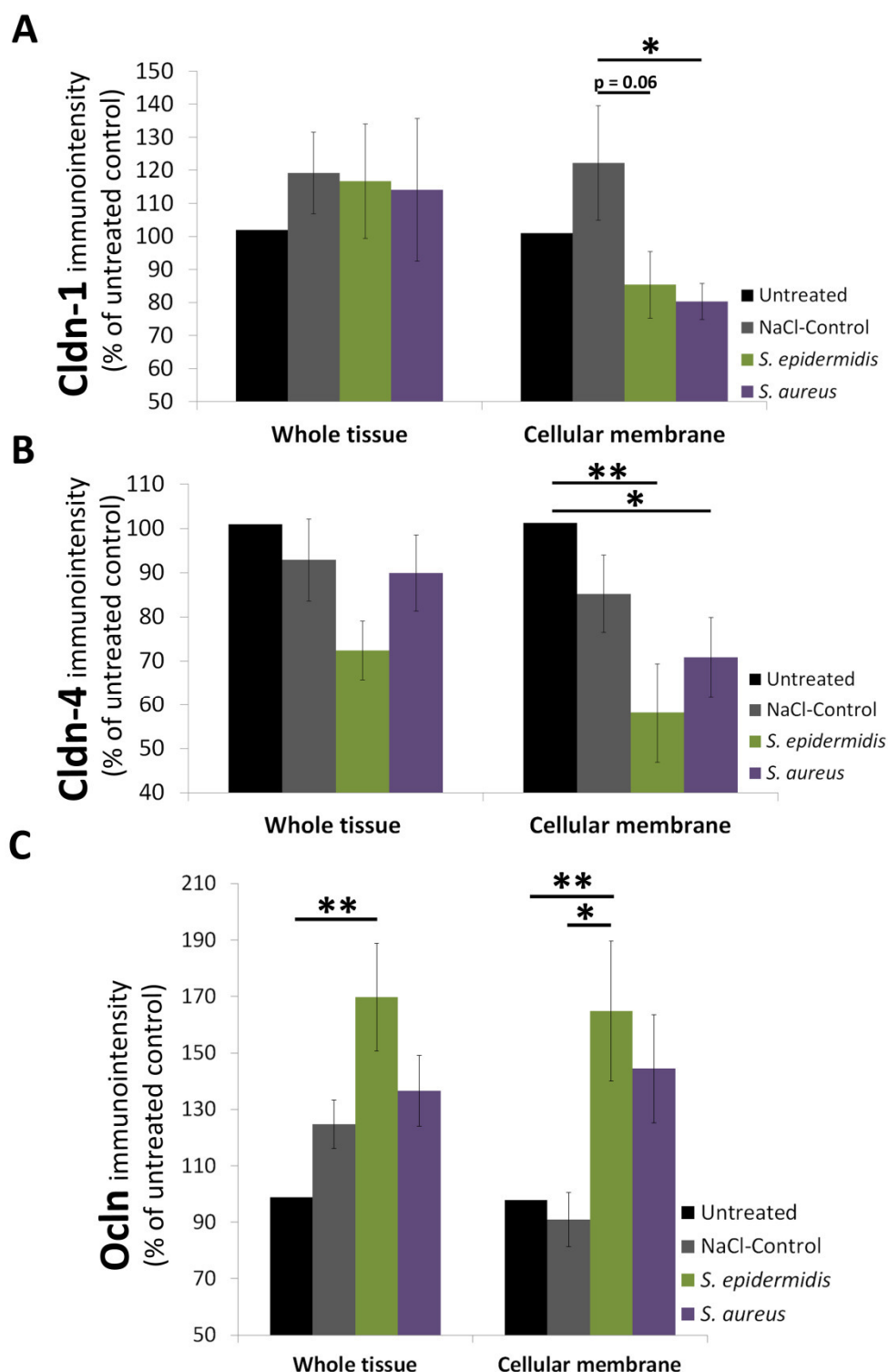


**Figure 54: Analyses of immunointensity of tight junction proteins on PFe3D models after long-term staphylococcal challenge.** Immunointensity of claudin-1 (Cldn-1; A), Cldn-4 (B) and occludin (Occludin; C) in % of untreated control of PFe3D models infected on day 4 of air-liquid-interface for 72 h with  $5 \times 10^4$  *S. epidermidis* or *S. aureus* cm<sup>-2</sup> in 5  $\mu$ l of 0.9% NaCl-solution compared to untreated or NaCl-control models. Mean  $\pm$  SEM; n = 3 different donors in triplicates; \* p<0.05, \*\* p<0.01 using ANOVA (modified with permission from Bäsler et al. (2017)).

### 3.3.8 Investigations on Tight Junction protein levels

WB analyses were performed on PFe3D models inoculated with *S. aureus* only. These revealed on protein level no changes in the overall amount of the two sealing claudins (Cldn-

1 and Cldn-4) after long-term inoculation (Figure 55). Also earlier time points (24 and 48 h) did not show differences (data not shown).

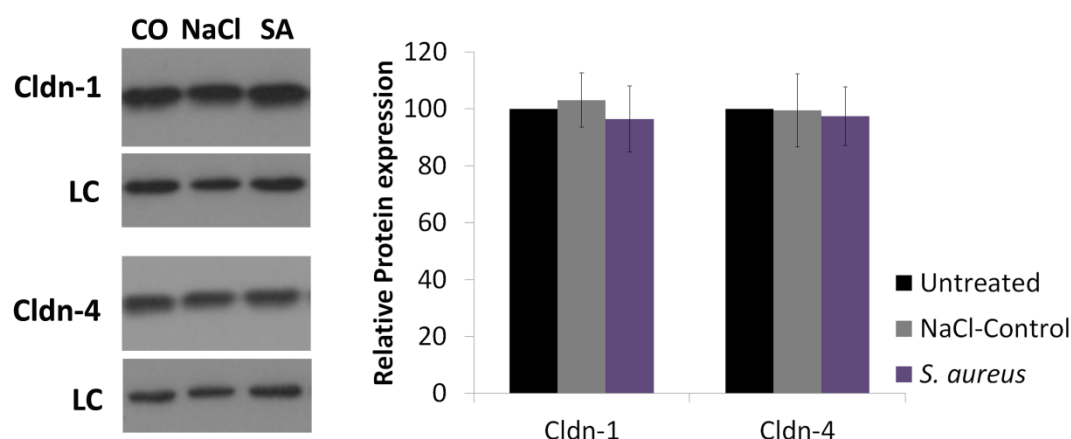


**Figure 55: Western Blot analyses of claudin-1 (Cldn-1) and Cldn-4 of PFe3D models after long-term *S. aureus* (SA) inoculation.** Cldn-1 and -4 protein levels in PFe3D models infected on day 4 of air-liquid-interface after inoculation for 72 h with  $5 \times 10^4$  *S. aureus*  $\text{cm}^{-2}$  in 5  $\mu\text{l}$  of 0.9% NaCl-solution compared to untreated or NaCl-control models. CO – untreated control; NaCl – NaCl-control; LC – loading control ( $\beta$ -Actin). Left side: exemplary Western-Blot; Right side: Semiquantitative evaluation of the Western Blot results. Mean  $\pm$  SEM;  $n = 3$  donors in duplicates (modified with permission from Bäsler et al. (2017)).

For Ocln, short-term inoculation with *S. aureus* resulted in a slight increase in phosphorylated Ocln (Figure 56). However, not as pronounced as in the submerged model. After long-term infection of PFe3D with *S. aureus* a slight decrease or no change (dependent on the donor) was observed in the total amount of Ocln in Western Blot (Figure 56).

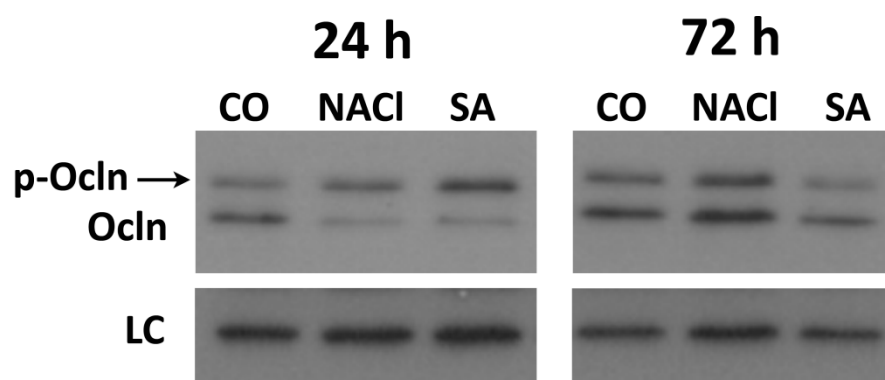


**Figure 56: Western Blot analyses of occludin (Ocln) of PFe3D models after *S. aureus* (SA) inoculation.** Exemplary Western Blot of Ocln protein levels in PFe3D models infected on day 4 of air-liquid-interface after inoculation for 24 and 72 h with  $5 \times 10^4$  *S. aureus*  $\text{cm}^{-2}$  in 5  $\mu\text{l}$  of 0.9% NaCl-solution compared to untreated (CO) or NaCl-control models. LC – loading control ( $\beta$ -Actin); p-Ocln – higher phosphorylated form of Ocln (modified with permission from Bäsler et al. (2017)).

Taken together, results obtained with long-term inoculated PFe3D nicely reflect observations made in submerged models. In both systems long-term inoculation with both staphylococcal species resulted in a decreased TJ barrier function, which was accompanied with delocalisation of Cldn-1 and -4 as well as a more pronounced localisation of Ocln.

For short-term inoculation, a TJ barrier increase, as it has been observed in the submerged models, could not be shown in 3D investigations. Nevertheless, also here Ocln phosphorylation as well as relocalisation was evident after *S. aureus* inoculation, while this early relocalisation was not observed in *S. epidermidis* infected PFe3D.

### 3.4 Results, Part 4: Atopic dermatitis mimicking conditions

Skin infections with especially *S. aureus* are the most common complication of AD (Huang et al., 2009). When developing a skin infection model, it is of great interest to also mimic diseased conditions and to investigate bacterial influences in this context.

In order to do so, a cytokine-toll-like-receptor-agonist-mix (CTM) was used, which was developed by Pierre Fabre Dermo-cosmétique (Bernard et al., 2017). This CTM mix was used to pretreat the NHEKs of the submerged model before infection (to first induce AD-like conditions). The CTM pretreatment was performed 48 h before bacterial inoculation for 24 h. The detailed experimental process of CTM-treatment and infection is visualised in the flow chart of Figure 57. In this context it is important to distinguish between treatment (with CTM or single components) and infection (with *S. aureus* or *S. epidermidis*).

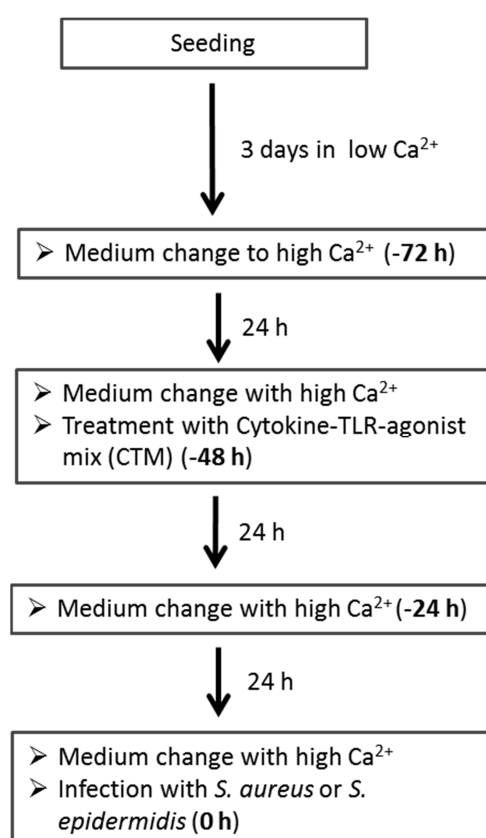
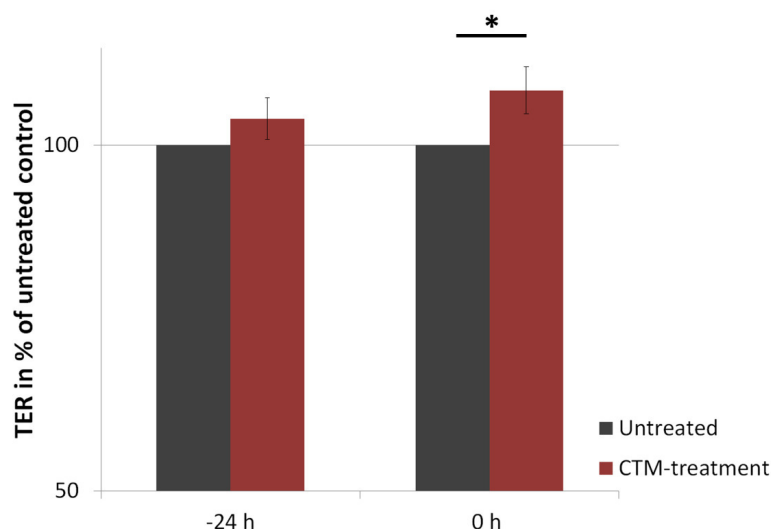


Figure 57: Flow chart of experimental procedure in order to mimick atopic dermatitis-like conditions in submerged models by pretreatment with a cytokine-toll-like-receptor-agonist-mix (CTM) before infection with *S. aureus* or *S. epidermidis*.

When investigating the effect of the CTM alone, a slight, but not significant increase was observed 24 h before infection (-24 h) (after 24 h of CTM-treatment) as well as a significant

increase in TER at the time point of infection (0 h) (after 24 h of CTM-treatment followed by 24 h without treatment) (Figure 58).



**Figure 58: Transepithelial electrical resistance (TER) of submerged model after induction of atopic dermatitis mimicking conditions (CTM-treatment).** TER of submerged models after CTM-treatment for 24 h (-24 h) and after following 24 h without treatment (0 h) in % of untreated control. Mean  $\pm$  SEM; n = 10 donors in triplicates; \*  $p < 0.05$  with paired Student's T-test.

This shows that the CTM treatment alone already influences TJ barrier function. At 0 h, infection was performed with *S. epidermidis* or *S. aureus*. This resulted in increased TER values in untreated and CTM-pretreated submerged models compared to the particular uninfected control (Figure 59).

There was no difference in TER increase after the pretreatment neither for *S. aureus* nor for *S. epidermidis* infection. However, CTM-pretreatment resulted in a faster TJ barrier breakdown after 12 h of *S. aureus* infection, but not after *S. epidermidis* infection (Figure 59 A). To verify whether this is a TJ effect, 4 kDa tracer-permeability was investigated as well for *S. aureus* infection and CTM treatment. The tracer-permeability was strongly increased for CTM-pretreated and *S. aureus* infected submerged models compared to untreated controls for all time points starting at 12 h (Figure 59 B). There was no change in decreased permeabilities for the early time point (8 h) (Figure 59 B).

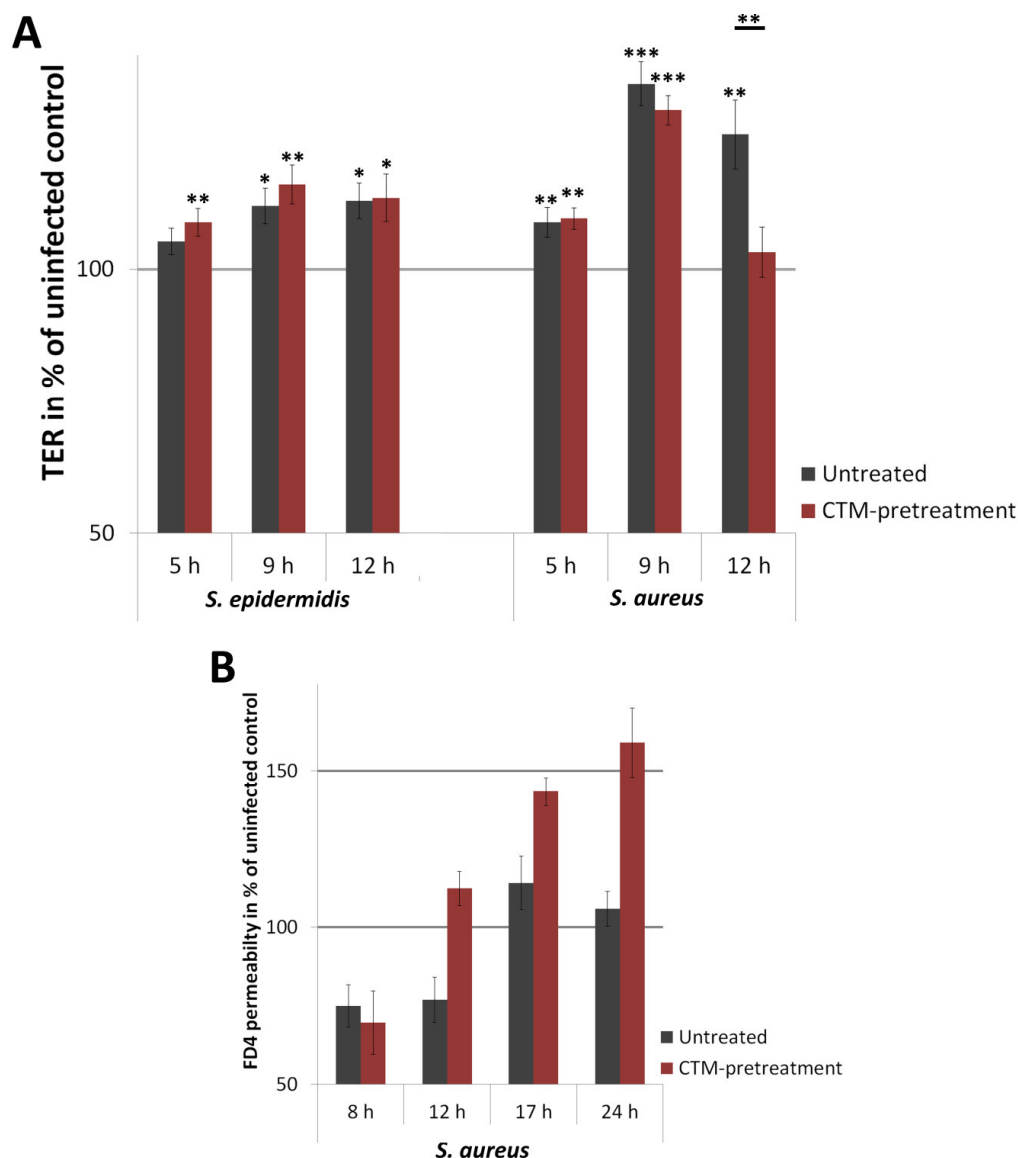


**Figure 59: Transepithelial electrical resistance (TER) of submerged models after induction of atopic dermatitis mimicking conditions (CTM-pretreatment) followed by staphylococcal challenge.** TER of submerged models either in CTM pretreated and infected (CTM-pretreatment) or in untreated but infected (untreated) models normalised to the particular uninfected control (A). Permeability of a 4 kDa tracer (FD4) after inoculation with *S. aureus* for indicated time points normalised to the specific uninfected control in CTM-pretreated or untreated conditions (B). Inoculation was performed with  $6 \times 10^5$  *S. aureus* or *S. epidermidis*  $\text{cm}^{-2}$ . Mean  $\pm$  SEM;  $n = 6$  (for *S. epidermidis*), 10 (for *S. aureus*) (A) and 2 (B) donors in triplicate; \*  $p < 0.05$ , \*\*  $p < 0.01$ , \*\*\*  $p < 0.001$  using ANOVA.

As the CTM-pretreatment resulted in TJ barrier disturbing effects after *S. aureus* inoculation, it was of great interest to figure out which ingredient of the CTM is responsible for the effect or whether it is the interaction of all components. Therefore CTM-pretreatment was compared to pretreatment with the single CTM components in context of *S. aureus* infection (Figure 60). Already for the time point directly before infection (0 h), it was quite obvious that IL-1 $\beta$  was mainly responsible for the increase in TER of the CTM as TER values of IL-1 $\beta$  pretreated NEHKs were very close to the CTM-pretreatment (Figure 60 A). However, also Pam3CSK4 pretreatment (TLR 1/2 agonist) resulted in a slight increase of barrier function,

while Poly I:C (TLR 3 agonist) treatment did not show alterations compared to the untreated control (Figure 60 A).

During *S. aureus* infection, these observations became even more evident. IL-1 $\beta$  was the main player of the CTM-effect on the TJ barrier breakdown. While no obvious differences were observed during TER increase (5 and 8 h), starting at 12 h, the effects of CTM or IL-1 $\beta$  pretreatment were very similar and both decreased the TER more pronounced when compared to the untreated control as well as to the other two components (Figure 60 B).

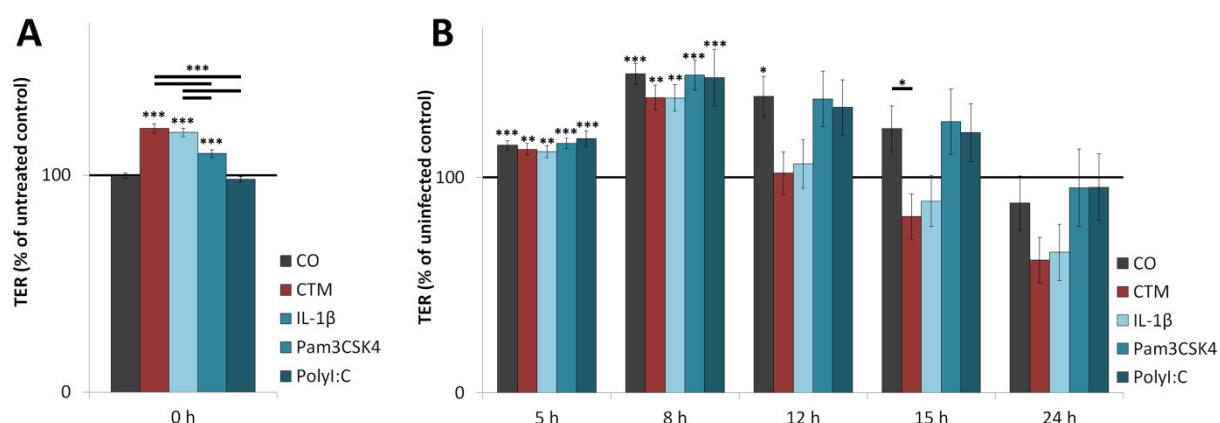


**Figure 60: Transepithelial electrical resistance (TER) of submerged models after treatment with an atopic dermatitis mimicking mix (CTM) or its single components upon *S. aureus* inoculation.** TER of submerged models pretreated with the CTM or its single components directly before the infection (0 h) normalised to the untreated control (A). TER of submerged models infected with  $6 \times 10^5$  *S. aureus* cm<sup>-2</sup> under either untreated or with CTM or its single components pretreated conditions (B). Mean  $\pm$  SEM; n = 4 donors in triplicates; \* p<0.05, \*\* p<0.01, \*\*\* p<0.01 using ANOVA.

In summary, mimicking AD conditions in the submerged model resulted in a faster decrease in TER upon *S. aureus* infection, while this was not the case after *S. epidermidis* infection. Key player of this effect is IL-1 $\beta$ .

First analyses on infected PFe3D with the CTM have been performed, but did not end in satisfactory results because the models reacted very heterogeneously on the CTM and often featured dead areas in the tissue after treatment. However, induction of these AD-like conditions on PFe3D in an infectious environment should to be analysed in the future in more detail.

## 4 DISCUSSION

---

### 4.1 Results, Part 1: Finding the right model system

Demand is increasing for *in vitro* skin modelling as these models provide a good alternative to animal experiments. However, many different models exist and it is necessary to find the right model/models for the specific investigations of interest. In order to do so, for this work, a model was needed with reliable results on barrier function, especially TJ barrier function with regard to live bacterial inoculation. In the skin, TJ barrier function has already been shown for the ion tracer Lanthanum (Baek et al., 2013) as well as for Biotin-SH (557 Da) (Kirschner et al., 2010; Yuki et al., 2011a) and for larger molecules (1.5 and 5000 Da, in mouse epidermis) (Yokouchi et al., 2015). In this work Biotin-SH is used as a tracer to visualise functional TJ structures, as it is a common method to analyse TJ function in 3D models and *ex vivo* skin (Kirschner et al., 2010; Yuki et al., 2011a; Yokouchi et al., 2015).

The submerged model was set to use in this work, as this system is already well established and accepted for analyses of “pure” TJ effects without the interference of SC (Mertens et al., 2005; Helfrich et al., 2007; Yuki et al., 2007; Kirschner et al., 2009; Kirschner et al., 2013). Investigating TJ protein expression with immunohistochemical staining of cross-sections of these models 3 days after  $\text{Ca}^{2+}$ -switch (when substantial TER values were reached) revealed localisation of Occludin, Cldn-1 and Cldn-4 at the cellular membranes with barrier formation for the 557 Da tracer Biotin-SH similar to SG of normal human skin.

The TJ barrier function of keratinocytes in submerged models already has been described for intermediate-sized molecules, as fluorescein (332 Da), as well as for macromolecules (3, 4 and 40 kDa FITC-Dextran) (Mertens et al., 2005; Yuki et al., 2007; Kirschner et al., 2013). Concerning the possibility of bacterial inoculation, the submerged model already was used before with HaCaT cells in context of life or heat-killed *S. aureus* or *S. epidermidis* infection (Ohnemus et al., 2008; Wang et al., 2017) as well as with NHEKs in context of *S. aureus* derived peptidoglycan treatment (Yuki et al., 2011b), treatment with lysates of *Bifidobacterium* and *Lactobacillus* (Menzies and Kenoyer, 2006) or treatment with bacterial supernatants (Wang et al., 2017), which indicated that bacterial inoculation is no problem using this system. This submerged system was quite easy to build due to the usage of only keratinocytes and the models were highly reproducible. Generally, fewer amounts of NHEKs are necessary for the submerged models compared to the 3D model systems, which makes a high throughput possible. Also TER measurements



were easily feasible in this model. As this was the simplest system being used in this study, costs were the lowest with the possibility of a high throughput. However, even though the submerged model was very promising for the analyses of TJs in context of bacterial inoculation, it is missing physiologic ALI conditions and thereby full stratification and the formation of a functional SC. In order to use a system representing the *in vivo* situation more closely and to analyse TJs effects with the interaction of a SC, a 3D system was needed as well.

In order to investigate this, analyses of three different 3D models were performed. These included two reconstructed human epidermis (RHE) models (one after the protocol of CellnTec (CnTe3D) and one after the protocol of Pierre Fabre (PFe3D)) and one reconstructed human skin (RHS) model.

Both RHE models were built in the same inserts with equal amounts of keratinocytes and TER measurement was feasible in both RHE systems.

CnTe3D models already have been used for analyses of SC lipid organisation (Thakoersing et al., 2013), for the development of siRNA based therapeutics (Hickerson et al., 2011) or lentiviral suppression of proteins (Robertson et al., 2012). The latter work also described a discrepancy in the expression of loricrin and filaggrin when compared to *in vivo* skin (Robertson et al., 2012). Even though the model architecture in the approach of this work revealed nice epidermal structuring in the centre of the models on days 7 and 14, very often leaky and thin margins or perforated areas were observed, which resulted in very low and non-reproducible TER values. Additionally, late and inhomogeneous TJ functionality was evident, even though TJ proteins were located correctly (except of a broader localization of Cldn-4). One other study exists where the TER development and TJ formation was analysed using CnTe3D models. In this study the authors demonstrated that in early development, the models provide a functional TJ barrier for the ion-tracer Lanthanum, which they stated to be replaced in later development by the lipid barrier of SC (Celli et al., 2012). The authors also described biotin-tracer stops at functional TJs even though Lanthanum is not blocked any more (Celli et al., 2012). They also measured the TER of these models, describing an increase in TER up to day 7, followed by a drop on day 9, increasing again after. However, also in this work, TER values barely reached levels above  $1500 \Omega \cdot \text{cm}^2$  (Celli et al., 2012). Generally, due to the inhomogeneous development of CnTe3D models (especially at the margins), infection would lead to unreliable results, as the bacteria would have an easy way into the models circumventing the

SC. There are different possible reasons underlying the problems regarding model architecture and barrier function of CnTe3D models. E.g., while building the models, the manufacturer recommended evaluating the amount of basal medium by eye depending on the amount of inserts in one petri dish, which is a source for non-reproducible results. Additionally, keratinocytes in CnTe3D models were seeded in a completely different medium than the one used later on for ALI. This might stress the cells. The supplements and their concentrations in the medium were not stated by the company, which would help to understand these models in a better/more scientific way. Interestingly, shortly after the decision not to use CnTe3D models for further investigations of this work, a new 3D medium was placed on the market by CellnTec, replacing the “old” medium, referring to induce better barrier properties compared to the medium used in this work (CellnTec homepage: <http://cellntec.com/products/cnt-pr-3d/>). Thus, insufficient supplementation could be the reason for unreliable results on (TJ) barrier function.

With respect to PFe3D models, there were more apparent advantages as compared to CnTe3D. To date, no report exists that uses PFe3D models, except for the publication of parts of this work (Bäsler et al., 2017). Generally, nice epidermal structuring was observed within the whole model already on day 4 being still present on days 7 and 14 comparable to human skin, which also was reflected by substantial TER values and reliable/reproducible results. TJ barrier function was established very early (already at day 4 and even earlier) and pronounced with correct localisation of TJ proteins as well as differentiation markers, comparable to human skin (see below). Even though no reports about PFe3D models exist, these models are only slightly modified from models that have been described before (Poumay et al., 2004). These also demonstrated similarity to histological features of human skin and correct localisation of various differentiation markers (Poumay et al., 2004). Regarding infection, the PFe3D models did not show leaky margins, where the bacteria would have an easy entry into the model. All supplements of the medium were known and costs in time and money were similar to CnTe3D models but lower than for RHS models (see below). As the supplements of CnTe3D were not known, it is hard to hypothesise whether the observed differences between the two RHE models are the result of the different media. But already in building the models differences were apparent. While for CnTe3D models the amount of medium was dependent on the amount of inserts in one petri dish (10 cm) and only evaluated by eye, for PFe3D models an exact amount of medium for one model in one well

of a 6 well plate was used. However, RHE models only provide epidermal structure, while missing a dermal part. Therefore a RHS model was investigated as well.

In general, RHS models represent a more physiological situation as being the system closest mirroring the *in vivo* situation because they comprise epidermis and dermis. It has been demonstrated that the existence of a dermal part influences barrier development (Thakorsing et al., 2011). The RHE model used in this work, after the protocol of Mildner et al., already were used for siRNA knock down of e.g., filaggrin (Mildner et al., 2006; Mildner et al., 2010). Morphologically, the models showed epidermal structuring, however not as nice as RHE models, due to a diffuse arrangement of cells in SB. Additionally, compared to RHE models, epidermal structuring was less stable over time and the models show very fast cornification, contemporaneously with the loss of living cell layers.

Concerning TJ barrier function, on day 8 of ALI, which revealed the best epidermal morphology, TJ proteins were localised correctly and functional TJ structures were established and proved possible to analyse with the biotinylation assay. Also before, biotinylation assay revealed functional TJ structures at day 7 (Gschwandtner et al., 2013). Unfortunately, the establishment of a method to measure overall barrier function by TER failed due to contraction of the collagen gel. Because this would also provide bacterial entry in case of infection, I decided to forgo bacterial inoculation with these models. Additionally, they were the most expensive in time and costs due to the usage of collagen and fibroblasts as well as due to the need of tremendous amounts of keratinocytes (5 times more than for RHE), which made a high throughput not possible.

In the end, the model system provided by Pierre Fabre (PFe3D) was revealed to be the best suited 3D model system for analyses of (TJ) barrier function in the context of bacterial infection. Together with the submerged model, PFe3D models were used for further investigations. The advantages and disadvantages of the different model-systems are listed in Table 10.

Table 10: Advantages and disadvantages of the different model systems investigated in this work.

Model-system	Advantages	Disadvantages
Submerged model	<ul style="list-style-type: none"> <li>• Due to the usage of only keratinocytes, the models are easy to build</li> <li>• Due to smaller inserts, less amount of cells / model is necessary compared to RHE and RHS → high throughput is possible</li> </ul> <u>Barrier properties:</u> <ul style="list-style-type: none"> <li>• Development of proper TER values, which are highly reproducible</li> <li>• No development of a functional SC (good to analyse “true” TJ effects)</li> </ul>	<ul style="list-style-type: none"> <li>• No stratified 3D structure which makes them less comparable to <i>in vivo</i> skin</li> </ul> <u>Barrier properties:</u> <ul style="list-style-type: none"> <li>• No functional SC which is an essential part of the overall skin barrier</li> </ul>
RHE 1: CnTe3D	<ul style="list-style-type: none"> <li>• Due to the usage of only keratinocytes, the models are easy to build</li> <li>• Due to smaller inserts, less amount of cells / model is necessary compared to RHS</li> <li>• Nice epidermal structuring in the middle of the models</li> </ul> <u>Barrier properties:</u> <ul style="list-style-type: none"> <li>• TER measurement is possible</li> <li>• Functional TJs for Biotin-SH are found in SG</li> <li>• SC is present</li> </ul>	<ul style="list-style-type: none"> <li>• The models often show leaky and thin margins without a SC</li> <li>• The company does not provide information about the medium supplements</li> <li>• Pure epidermal reconstruction, without a dermal compartment</li> </ul> <u>Barrier Properties:</u> <ul style="list-style-type: none"> <li>• No reliable TER, as values are very low, which probably originates from the thin and leaky margins</li> <li>• Even though functional TJs are found, tracer stops are not as clear and early as in other models → incomplete and late tracer stops</li> </ul>
RHE 2: PFe3D	<ul style="list-style-type: none"> <li>• Due to the usage of only keratinocytes, the models are easy to build</li> <li>• Due to smaller inserts, less amount of cells / model is necessary compared to RHS</li> <li>• Nice epidermal structuring all over the models</li> <li>• No leaky and thin margins</li> <li>• Compared to the medium of CellInTec all supplementation is known</li> </ul> <u>Barrier properties:</u> <ul style="list-style-type: none"> <li>• Development of proper TER values</li> <li>• Early and pronounced functional TJs for Biotin-SH in SG</li> <li>• SC is present</li> </ul>	<ul style="list-style-type: none"> <li>• Pure epidermal reconstruction, without a dermal compartment</li> </ul>
RHS (Mildner)	<ul style="list-style-type: none"> <li>• As a model consisting of a dermal and an epidermal compartment, this model mimics the <i>in vivo</i> situation the closest</li> <li>• Epidermal structuring is present</li> </ul> <u>Barrier properties:</u> <ul style="list-style-type: none"> <li>• Functional TJs for Biotin-SH are found in SG</li> <li>• SC is present</li> </ul>	<ul style="list-style-type: none"> <li>• Due to the usage of collagen and fibroblasts, the models are complicated to build and expensive</li> <li>• A large number of keratinocytes is necessary (limiting the number of models which can be built from one donor)</li> <li>• Compared to other models, epidermal structuring is less stable over time</li> <li>• The models show very fast cornification, contemporaneously with the loss of living cell layers</li> </ul> <u>Barrier properties:</u> <ul style="list-style-type: none"> <li>• The usage of collagen leads to shrinkage of the model, therefore it was not possible to measure overall barrier function (TER) in our hands</li> </ul>

## 4.2 Suitability of submerged and PFe3D models for bacterial infection approaches

The submerged system mirrors body conditions with a non-functional SC barrier, e.g., as in superficial wounds. As already discussed above, it is a well-established and accepted system in order to analyse pure TJ effects. Further, investigating the effect of live bacteria on NHEKs in submerged models shows the direct effect of the organisms on this cell type and delivers important information on general mechanisms of bacterial pathogenicity. Infection of these models was performed 3 days after  $\text{Ca}^{2+}$ -switch, when functional TJs had been established. The usage of an earlier time point would have been interesting in order to investigate the effect of a bacterial challenge on TJ development and should be further tested in the future. In order to exclude strain-dependent effects, TER measurement was performed additionally with another *S. aureus* strain, which was characterised to be methicillin-resistant (MRSA). Both *S. aureus* strains, 6820 (MRSA) and SH1000 (non-MRSA, used in this work) revealed similar effects on the TER of the submerged models (data not shown). Generally, results obtained after infection of the submerged models were highly reproducible not only in between technical replicates, but also in between different donors.

Even though the submerged models provide important information on the interplay of live bacteria on epidermal TJs, they lack the information about the interplay of TJs with the SC. Therefore additional experiments were performed with the 3D reconstruction PFe3D, which form a SC. The PFe3D models in the approach of this work were used for bacterial inoculation at day 4 of ALI. Generally speaking, it is still early days with respect to investigations of RHE models, but PFe3D models already expressed early (Keratin 10), intermediate (involucrin) as well as late (loricrin and filaggrin) differentiation markers at this time point, showing their correct localisation (Bäsler et al., 2017; Figure 61).

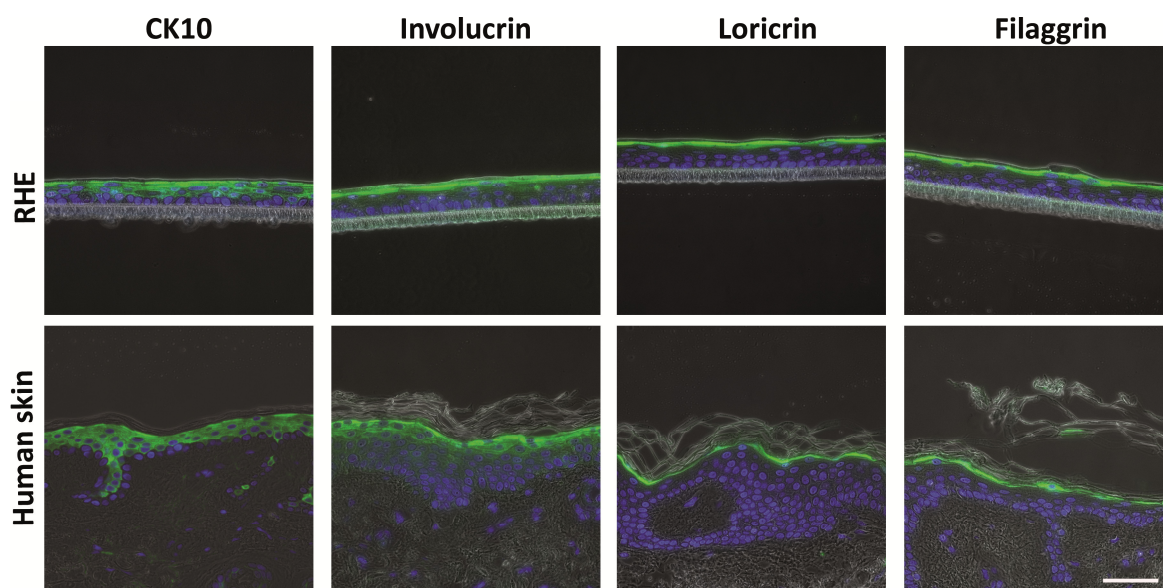


**Figure 61: Characterisation of PFe3D at day 4 of air-liquid-interface.** Immunohistological localisation of the denoted proteins (green) in the PFe3D (upper row) and in human skin (lower row). Blue: DAPI staining of nuclei; Overlay of epifluorescence pictures and phase contrast pictures. Bar = 50  $\mu$ m (modified with permission from [Bäsler et al. \(2017\)](#)).

Additionally, a good epidermal structuring was observed with palisade structure in the basal layer, functional TJs in the granular layer and some layers of SC, which was also reflected by a substantial TER. However, SC barrier was not fully developed at this time point, which can be seen by increased number of SC layers as well as increasing TER after day 4. Hence, this model mimics skin with compromised SC barrier function (as e. g. AD, bullous diseases or wounded and freshly regenerated skin), but not healthy skin. Bacterial inoculation was also tested at later time points (days 6, 8 or 11 after ALI), and still bacterial growth was observed (data not shown), but no decrease in TJ protein localisation and/or barrier function could be detected (data not shown). Nevertheless, this mirrors the *in vivo* situation of human skin, where under healthy conditions exfoliative toxin-negative *S. aureus* does not cause skin infections and it additionally confirms that the SC is of great importance for protection from bacterial infections. Collectively, when interpreting the data gained with infected submerged and PFe3D models, one has to keep in mind that both are model systems for skin conditions with compromised SC barrier function.

The usage of about  $5 \times 10^4$  bacteria  $\text{cm}^{-2}$  on top of the PFe3D and  $6 \times 10^3$  or  $6 \times 10^5$  bacteria  $\text{cm}^{-2}$  on submerged models nicely mirrors the number of bacteria found per  $\text{cm}^2$  on human skin, which fluctuates depending on the body side between  $10^2$  and  $10^6$  (Fredricks, 2001). The fact that the bacteria grow on top of the models up to a density of  $7 \times 10^6$  cfu  $\text{cm}^{-2}$  shows that they are able to live and multiply on PFe3D, which reflects an infectious environment. This

enhanced multiplication was also observed by the usage of fluorescent mutants. Even though bacterial growth was not investigated in the submerged model, a substantial growth of both species was visible by eye already after 12 h.

Pretreatment of PFe3D with *S. epidermidis* resulted in a significantly decreased growth of *S. aureus*. This shows the analogy of inoculated PFe3D to the normal skin flora. Also on normal human skin resident microbes (like *S. epidermidis*) are helping to inhibit the growth of pathogens (Sanford and Gallo, 2013). Some strains of *S. epidermidis* produce the serine protease Esp, which inhibits *S. aureus* colonisation in nares (Iwase et al., 2010). Also, germ free mice were more susceptible to cutaneous infection with the protozoan *Leishmania major*, whereas colonisation with *S. epidermidis* supported protective immunity against *L. major* (Naik et al., 2012).

### **4.3 Results, Parts 2 and 3: Biphasic influence of live *S. aureus* and *S. epidermidis* on epidermal Tight Junctions**

#### **4.3.1 *S. aureus* and *S. epidermidis* strengthen Tight Junction barrier function during short-term inoculation via different mechanisms**

For short-term bacterial challenge, this work revealed a dose-dependent TJ barrier strengthening effect in the submerged models with either *S. aureus* or *S. epidermidis*, while the effect of *S. aureus* was stronger. This was investigated using TER measurement and FD4 permeability. A TJ barrier function enforcing effect was also shown before for live *S. epidermidis* in the immortalised keratinocyte cell line HaCaT (Ohnemus et al., 2008) as well as for lysates of *Lactobacillus spp.* and *Bifidobacterium longum* in NHEKs (Sultana et al., 2013). Additionally, activation of several toll-like receptors (TLRs) in keratinocytes, resulted in increased TJ barrier function (Yuki et al., 2011b; Kuo et al., 2013). Further, a positive effect of bacteria or bacterial proteins on TJ barrier function was observed in simple epithelia (e.g., Seth et al., 2008; Miyauchi et al., 2012) and also the fungus *Candida albicans* increased TER values of an intestinal epithelial cell line (Böhringer et al., 2016). This indicates that strengthening the (skin) barrier via a fast response of the TJs on bacterial challenges might be the body's first protective reaction until further help by the innate and adaptive immunity has been recruited. However, this clearly is dependent on the tissue/cell type and the microbial species, as also reports exist, describing a direct decrease in TJ functionality after bacterial inoculation (e.g. *Escherichia*

*coli*, *Salmonella spp.* or *Shigella flexneri* directly decreased TER in intestinal epithelia cell lines (reviewed in Guttman and Finlay, 2009).

#### 4.3.1.1 Differences between NHEKs and HaCaT cells

Even though *S. epidermidis* inoculation of the submerged model with NHEKs resulted in an increase in TER comparable to descriptions made before for HaCaT cells, discriminative results were obtained after inoculation with *S. aureus*: While there was an immediate decrease in TER after *S. aureus* inoculation in HaCaT cells (Ohnemus et al., 2008), in NHEKs a temporary increase in TER was evident, comparable to *S. epidermidis* and even more pronounced (this work). The decrease in TER of HaCaT cells was accompanied by a decrease of Cldn-1 and Occludin localisation at the cell membranes already 5 h after *S. aureus* inoculation (Ohnemus et al., 2008), while in NHEKs these proteins were unchanged (Cldn-1) or concentrated at the membranes (Occludin) within the first 12 h. This could on the one hand be explained by the usage of different *S. aureus* strains (strain ATCC 29213 in Ohnemus et al. and strains SH1000 and 6820 in this work). However, also treatment of NHEKs with *S. aureus* derived peptidoglycan resulted in increased TER values (Yuki et al., 2011b; Kuo et al., 2013). Therefore another explanation is more likely, namely the different expression patterns of TLRs in NHEKs and HaCaTs. Köllisch et al. (2005) demonstrated that both cell types express TLR2, but only NHEKs also express TLR6. It has been shown before that TLR6 interacts with TLR2 in the recognition of *S. aureus* (Ozinsky et al., 2000), while for *S. epidermidis* up to now only TLR2 has been described, but other co-receptors are thought to be involved (Otto, 2009; Stevens et al., 2009). Interestingly, it has been shown that activation of TLR2/6 in human umbilical vein endothelial cells (HUVEC) resulted in an upregulation of GM-CSF (Grote et al., 2010), which also was observed in this work after *S. aureus* inoculation, while this was not the case after *S. epidermidis* inoculation. This and the fact that it is not quite sure whether HaCaT cells fully differentiate (Micallef et al., 2009), clearly shows that HaCaT cells are not the ideal test system for bacterial treatment approaches.



#### 4.3.1.2 Relocalisation of Tight Junction proteins accompanies the increased barrier function after short-term inoculation

The increase in TJ barrier function after staphylococcal inoculation of the submerged model was accompanied by relocalisation of Cldn-4 (both species) and Occludin (*S. aureus*) to the cellular membranes. Also, PFe3D models inoculated short-term with *S. aureus* showed a slight upregulation of Occludin immunointensity in some areas. For Occludin, this was consistent with what was observed *in vivo* and *ex vivo* as well, while Cldn-4 was not investigated (Ohnemus et al., 2008). Concerning this relocalisation, it was described before that overexpression of Occludin (which was accompanied by increased intensity of the protein at the cell-cell membranes) increased TER in MDCK cells (McCarthy et al., 1996; Van Itallie et al., 2010). In submandibular gland epithelial cells it was described that overexpression of Cldn-4 resulted in increased TER and decreased permeability for FITC dextran due to an increased Cldn-4 localisation at the cell-cell membranes (Michikawa et al., 2008). Additionally, NHEKs treated with antimicrobial peptides showed an increase in TJ barrier function accompanied by relocalisation of Cldn-4 (Akiyama et al., 2014; Kiatsurayanon et al., 2014) and Occludin (Akiyama et al., 2014) among others. In the course of investigating the TJ protein expression of Cldn-1, Cldn-4 and Occludin in this work, no increase could be detected, either on mRNA or on the protein level. Interestingly, phosphorylation of Occludin, which was evident after short-term *S. aureus* inoculation of both model systems, was shown before to result in such relocalisation to the membranes (Wong, 1997). This also fits to what has been observed with *S. aureus* derived peptidoglycan. It was shown that the increased TJ functionality after activation of TLR2 by *S. aureus* derived peptidoglycan was dependent on the kinase activity of atypical protein kinase C (aPKC), which phosphorylated Occludin (Yuki et al., 2011b).

Additionally, in this work an involvement of TLR2 was supported by some experimental data. Inoculation of NHEKs with the  $\Delta agr$  *S. aureus* strain resulted in a significantly diminished increase in TER compared to wild type *S. aureus* at early time points. It is known that the bacterial *agr* system, when activated due to quorum sensing, not only positively influences secreted virulence factors, but it also negatively regulates the production of Staphylococcal superantigen-like proteins (SSLs) (Painter et al., 2014), which means in reverse that SSLs are still produced by the bacterial  $\Delta agr$  strains. One of these SSLs is SSL-3, which is able to specifically bind to TLR2 and inhibit its activation as long as the bacteria have to hide from the cells recognition (Bardoel et al., 2012). This argues for the involvement of TLR2 activation in live

*S. aureus* induced TJ barrier increase, but, as discussed above, also TLR6 likely is involved. In order to investigate whether there indeed is an involvement of TLR2 and TLR6 in the recognition of live *S. aureus* in the submerged model, siRNA-knock down of TLR2 and TLR6 was performed in NHEKs. Unfortunately, even though proper knock down was achieved and the increase in TER after *S. aureus* inoculation was prevented by using TLR2 and TLR6 siRNAs, NHEKs treated with the negative control siRNA did not show an increase in TER either (data not shown). Thus, it was impossible to distinguish between knock-down specific and treatment-related effects.

#### 4.3.1.3 Indirect effects might additionally lead to Tight Junction protein relocalisation after short-term inoculation

The increase in TER due to the relocalisation of Cldn-4 and Occludin might not only be a direct effect via the activation of TLRs but also might be an indirect effect due to the upregulation of AMPs or proinflammatory cytokines.

It has been shown before that treatment with the AMPs cathelicidin or h $\beta$ D3 resulted in TER increase by relocalisation of Cldn-4 and Occludin (and others) to the cellular membranes (Akiyama et al., 2014; Kiatsurayanon et al., 2014). In the approach of this work, no upregulation, or even a downregulation on mRNA level was evident after 8 and 12 h of staphylococcal inoculation for cathelicidin and h $\beta$ D3. Of note, Menzies and colleagues reported an upregulation of h $\beta$ D3 in keratinocytes after live *S. aureus* inoculation or of Cathelicidin and h $\beta$ D3 after treatment with heat inactivated *S. aureus* (Menzies and Kenoyer, 2005; Menzies and Kenoyer, 2006). Furthermore, supernatants of *S. aureus* or *S. epidermidis* were shown to increase h $\beta$ D3 protein levels (Lai et al., 2010; Park et al., 2014). These different results might be a matter of different experimental setups and conditions. Nevertheless, an indirect involvement of these two AMPs (cathelicidin or h $\beta$ D3) in TER increase of this work can be excluded.

Concerning proinflammatory cytokines, it has been described that short-term treatment with IL-1 $\beta$  or TNF $\alpha$  enhanced TER of NHEKs (Kirschner et al., 2009). This was accompanied by increased localisation of Cldn-4 at the cell-cell membranes (Kirschner et al., 2009). In *ex vivo* skin, IL-1 $\beta$  treatment led to a broader localisation of Occludin at the cell-cell membranes (Kirschner et al., 2009). Moreover, IL-1 $\beta$  treatment of rat hepatocytes caused hyperphosphorylation of Occludin accompanied with an increased localisation of Occludin at the cell-cell borders (Yamamoto et al., 2004).

Interestingly, also IL-6 was shown to positively influence the intestinal epithelial barrier (reviewed in Al-Sadi et al., 2014).

Indeed, a strong upregulation of proinflammatory cytokines (IL-1 $\beta$ , IL-6, IL-8 and TNF $\alpha$ ) upon 12 h live *S. aureus* inoculation was evident on mRNA as well as protein level and on mRNA level upon 12 h live *S. epidermidis* inoculation. An involvement of these cytokines in *S. aureus* induced increase in TER is also supported by the fact that simultaneously addition of IL-1 $\beta$  or TNF $\alpha$  to *S. aureus* infected submerged models in this work showed a short-term TER increasing effect compared to *S. aureus* inoculation alone. Also in human epithelial keratinocytes treated with *S. aureus* biofilm secreted products an upregulation of IL-8, IL-6, IL-1 $\beta$  and TNF $\alpha$  (and many others) gene expression was reported already 2 h after treatment (Tankersley et al., 2014). This was also observed in another study where keratinocytes were treated with *S. aureus* biofilm conditioned medium or planktonic conditioned medium (Secor et al., 2011). Additionally, colonisation of vaginal epithelial cell multilayer cultures with *S. epidermidis* resulted in a significant increase in IL-1 $\beta$ , IL-8 and TNF $\alpha$  already after 6 h (Rose et al., 2012).

However, because TER increase starts almost immediately after *S. aureus* inoculation, while significant upregulation of inflammatory cytokines can only be detected after 8 h on mRNA level, these cytokines are probably not the initial causes for TER increase, but might supplement the effects. This is even more supported by the fact that after *S. epidermidis* inoculation – which results in upregulation of TER but later and to a lesser extent than *S. aureus* – significant upregulation of proinflammatory cytokines was only observed after 12 h on mRNA level (an increase after 8 h was seen, but not significant) and not on protein level, except for IL-1 $\alpha$ . Interestingly IL-1 $\alpha$  has been shown to positively influence skin barrier recovery in aged mice already after 3 and 6 h (measured by transepidermal water loss (TEWL) after tape-stripping) (Ye et al., 2002; Barland et al., 2004), but the authors concluded increased lipid synthesis to play a role (Barland et al., 2004). Tight junctions have not been analysed in this context.

#### 4.3.1.4 Differences between *S. epidermidis* and *S. aureus*

Even though both investigated staphylococcal species basically resulted in the same reaction of NHEKs, some differences became evident in short-term *S. epidermidis* and *S. aureus* inoculation. While both strains increased TER and decreased FD4 permeability, the effect of *S. aureus* was stronger. Also, the increase in TJ barrier function after short-term bacterial

inoculation of submerged models was accompanied by a relocalisation of Cldn-4 to the cellular membranes with both *Staphylococcus* species, but additionally to that, phosphorylation and relocalisation of Occludin (Occludin) was evident after *S. aureus* inoculation, while after *S. epidermidis* infection a decrease of Occludin was observed. This might explain the difference in the amount of barrier increase. In general, this strongly hints for differences in recognition of both species, which is also supported by the different results of NKEKs and HaCaT cells after inoculation with live *S. aureus* as discussed above. Additionally also different amounts of cytokine increase/release are evident and could explain partly the differences in TER values.

In order to sum up the results obtained during short-term inoculation with *S. aureus* and *S. epidermidis*, the schematic overview of Figure 62 illustrates possible effects on TJ barrier.

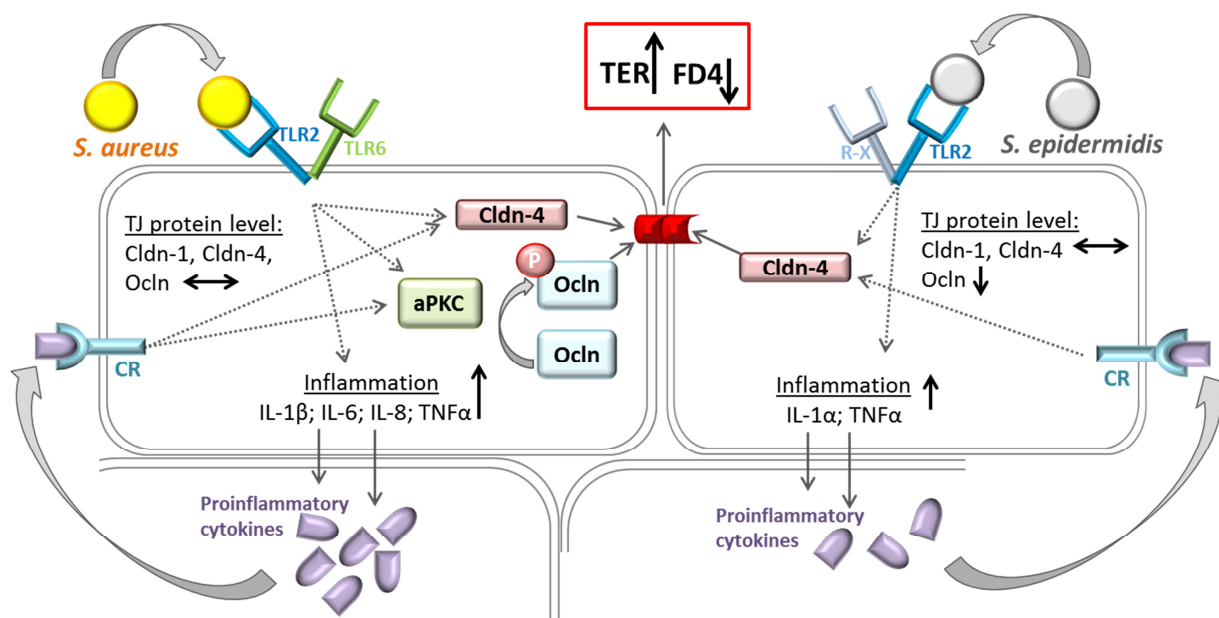


**Figure 62: Schematic overview of possible processes during short-term inoculation with *S. aureus* (left) or *S. epidermidis* (right) on tight junction (TJ) barrier increase in submerged models.** Left: *S. aureus* is recognised by toll-like-receptor 2 (TLR2), which interacts with TLR6. This leads to accumulation of claudin-4 (Cldn-4) at the cell-cell membranes and to activation of atypical protein kinase C (aPKC), which phosphorylates occludin (Occludin), which also accumulates at the cellular membranes as well. Right: *S. epidermidis* inoculation results in recognition via TLR2 dimerisation with a yet unknown receptor (R-X), leading to accumulation of Cldn-4 at the cellular membranes. Simultaneously, for both *Staphylococci*, increased expression and release of proinflammatory cytokines takes place, but to a lesser extent for *S. epidermidis*. Released proinflammatory cytokines bind to their specific cytokine receptors (CR), which also indirectly leads to TJ barrier strengthening. Grey arrows denote direct reactions; dotted grey lines denote reactions, which are likely the result of a cascade; black arrows denote increase/decrease/no changes. TER – transepithelial electrical resistance; FD4 – 4kDa tracer; IL – interleukin; TNFα – tumor necrosis factor-α.

#### 4.3.1.5 Differences between the two model systems for short-term inoculation

Important to mention, even though short-term inoculation of PFe3D with *S. aureus* did also result in phosphorylation and relocalisation of OcIn to the cellular membranes, this was not the case for Cldn-4. Additionally, bacterial inoculation of PFe3D with *S. aureus* or *S. epidermidis* did not result in changes in TJ functionality, neither measureable by biotinylation assay nor by TER. However, the detection threshold of the immunohistochemical staining of Biotin limits the evaluation method of Biotin-SH-stops in the epidermis. The stop of the tracer seems already to be clearly visible in control models and it is difficult to proof that there is an even “stronger” stop after bacterial treatment. Maybe the usage of tracer molecules smaller than 557 Da or the usage of an alternative method to evaluate Biotin-flux would reveal differences. E. g., a decrease of Biotin-SH permeability in RHE after TLR2 activation with *S. aureus* derived peptidoglycan has been shown by the usage of a dot blot system (Yuki et al., 2011b).

Also, measuring the TER of PFe3D post bacterial challenge did not reveal relevant differences. Generally, TER values were much higher in PFe3D compared to the submerged models at the time point of infection ( $1785 \pm 673 \text{ Ohm} \times \text{cm}^2$  compared to  $447 \pm 47 \text{ Ohm} \times \text{cm}^2$  ( $n = 6$  different donors for both)) (Bäsler et al., 2017). This clearly points out the contribution of the SC in PFe3D. A modification of about 30% in TJ derived TER, which was evident in submerged culture and which is approximately  $150 \text{ Ohm} \times \text{cm}^2$ , might simply not be noticed within the normal standard deviation of TER in PFe3D and might therefore be camouflaged by the SC. This also indicates a functional SC in PFe3D, even though the time point of infection was chosen quite early. However, this underlines the importance of investigating TJs not only in PFe3D but also in the submerged model in order to elucidate specific effects on TJs not covered by SC effects.

Another reason for different results in short-term inoculated PFe3D and submerged models might also be the difference in bacterial application. While in PFe3D the bacteria were applied in only 5  $\mu\text{l}$  of NaCl-solution, they were applied in 200  $\mu\text{l}$  of keratinocyte growth medium on the submerged models. This difference probably results in different induction of bacterial factors. On PFe3D it might be possible the bacteria produce a biofilm, while on submerged models, planktonic growth is very likely. It has been demonstrated that the

protein patterns of secreted proteins are different in biofilm and planktonic growth of *S. aureus* (Secor et al., 2011).

It might also be thinkable, that simply due to the existence of the SC in PFe3D, the TJs are not strengthened because it is not necessary. In the submerged models a functional SC is missing and the cells have to compensate this. It has been shown, e.g., that removing the SC via tape stripping results in an upregulation of TJ proteins (Kirschner et al., 2011; Baek et al., 2013), which clearly shows that skin barriers are interconnected tightly (reviewed in Bäsler et al., 2016). However, this theory is unlikely, as, as described above, a barrier strengthening effect in RHE already has been shown by Yuki et al with *S. aureus* derived peptidoglycan (Yuki et al., 2011b). Another aspect disfavouring this theory is that also inoculation of PFe3D already at day 1 or day 2 after ALI with *S. aureus* did not reveal increasing barrier function, neither using Biotin-SH nor in TER measurement (data not shown).

#### **4.3.2 Live *S. epidermidis* and *S. aureus* impair Tight Junction barrier function after long-term inoculation**

Investigation of the effect of long-term bacterial inoculation revealed a decrease in TJ functionality in both model systems (PFe3D and differentiated NHEKs in submerged culture) for both staphylococcal species to the same extent.

For the submerged model this decrease was detected by decreasing TER values as well as increased permeability in FD4 tracer flux, while for PFe3D this decrease was detected by an increased permeability of Biotin-SH. TER measurement of long-term inoculated PFe3D did not show any differences. As already discussed above, changes in TJ specific TER of PFe3D might be camouflaged by SC TER. The different time points representing long-term inoculation in PFe3D and the submerged models also reflect the functionality of the additional SC barrier in PFe3D. While in the submerged model the decrease in TJ function became evident between 17 and 24 h of inoculation, the TJ barrier loss in PFe3D was observed after 48-72 h of inoculation.

HaCaT cells inoculated with *S. aureus* also demonstrated a decrease in TER, but starting right after infection (Ohnemus et al., 2008). In ALI cultures of primary human nasal epithelial cells treated with conditioned media derived from *S. aureus* a decrease in TER was evident after 12 h (Malik et al., 2015).

#### 4.3.2.1 Delocalisation of Tight Junction proteins after long-term inoculation

In both analysed systems, this decreased TJ barrier function was not accompanied by cell death. The TJ barrier loss in both model systems was associated with a decreased membrane localisation of the sealing claudins, Cldn-1 and Cldn-4, even though protein levels in general did not change. Of note, as *S. epidermidis* was not analysed in Western Blot of PFe3D it cannot be excluded that a decrease in Cldn-4 protein might play a role in PFe3D. Internalisation of Cldn-1 and Cldn-4 (and many other TJ proteins) is known to disrupt the TJ barrier in various cell types (reviewed in Stamatovic et al., 2017). Even though the decrease in TJ functionality can be explained by internalisation of Cldn-1 and Cldn-4, a strong accumulation of Occludin at the cell-cell membranes was still evident after long-term bacterial challenge for both species in both systems. This will be discussed below (see Page 120).

This decreased immunointensity of the sealing Cldns nicely mirrors the observations made by Ohnemus et al. (2008) where a decreased immunointensity of Cldn-1 was reported *in vivo*, directly at sites of bacterial infection, as well as in an *ex vivo* porcine model infected with *S. aureus* for 24 h. Interestingly, while this work shows the same effects for long-term inoculation with *S. aureus* and *S. epidermidis*, in the porcine *ex vivo* model no decrease in Cldn-1 immunointensity was reported after *S. epidermidis* inoculation (Ohnemus et al., 2008). This could be explained by different reasons: First, the usage of different *S. epidermidis* strains (*S. epidermidis* strain 1457 was used by Ohnemus et al. and strain PIA97 was used in this work) or second, differences in the recognition of *S. epidermidis* in human and porcine skin. Additionally, the thicker SC in the porcine model might have prevented *S. epidermidis* breakthrough.

#### 4.3.2.2 The decrease in Tight Junction barrier function after long-term inoculation was independent from bacterial virulence factors

In order to elucidate the putative causes for the delocalisation of the two claudins, bacterial virulence factors were thought to play a role. These could be proteases that destroy protein structures leading to a disassembly of TJs. Also lipases may lead to changes in lipid structure and loosening of membrane associated TJ proteins. *S. aureus* and *S. epidermidis* are known to secrete multiple virulence factors such as proteases, lipases, nucleases and toxins. E.g., it has been shown that the serine protease V8 and serine-like protease exfoliative toxins of *S. aureus* are able to cleave corneodesmosome adhesion proteins (Hirasawa et al., 2010). Additionally,

V8 protease was shown to lead to decreased Cldn-1 levels in HaCaT cells (Wang et al., 2017). *S. aureus*  $\alpha$ -hemolysin has been shown to directly decrease TER in human squamous cell carcinoma cells (Inoshima et al., 2012).

The *agr* operon is the comprehensive regulon that controls cell-density dependent virulence factor expression and activates the production of secreted virulence factors within quorum sensing (Painter et al., 2014). Using a  $\Delta agr$  mutant of *S. aureus* or a *Staphylococcus* strain lacking virulence factors (*S. carnosus*), it was observed that the decreasing TJ functionality was independent from the *agr* regulon and therefore from bacterial virulence factors, such as proteases. This was investigated by TER measurement in submerged cultures, where no differences in decreasing TER values between wild-type,  $\Delta agr$  or *S. carnosus* were explored. Of note, it is known that *agr*-defective strains are as likely to lead to bloodstream infections as *agr*-competent strains (Smyth et al., 2012; Painter et al., 2014). They are even more likely to cause persistent infections, which result in an increased rate of secondary infections and mortality (Schweizer et al., 2011; Chong et al., 2013). However, in the blood stream the *agr* system is not a necessary mechanism as bacterial concentrations are simply too low to trigger quorum sensing and the serum component apolipoprotein B additionally sequesters auto inducing peptides (Peterson et al., 2008). Furthermore, as already described, *agr* negatively regulates the production of immune evasions, such as staphylococcal superantigen-like (SSL) proteins. Thus, lacking of *agr* helps the bacteria to hide from the immune recognition.

In a recent paper it was shown that *S. aureus* induces serine protease activity in the keratinocytes themselves (e.g., kallikreins and trypsin) (Williams et al., 2016). However, the authors concluded not TLR activation, but other virulence factors to be involved in the induction (Williams et al., 2016). If this is the case, also an enhanced intrinsic proteolytic activity can be excluded to be involved in decreasing TJ function.

#### 4.3.2.3 Inflammation likely leads to barrier disruption

Driving force for decreased TJ barrier function putatively is inflammation as a strong and prolonged upregulation of proinflammatory cytokines and chemokines was found on mRNA as well as protein level (IL-1 $\beta$ , TNF $\alpha$ , IL-6 and IL-8). Proinflammatory cytokines are known to decrease TJ barrier function in different tissues/cells. Several studies are engaged in the investigation of the regulation of the TJ barrier by cytokines. In intestinal epithelium most proinflammatory cytokines (e.g., IFN $\gamma$ , TNF $\alpha$ , IL-1 $\beta$ ) were shown to cause a decrease in TJ



functionality (reviewed in Al-Sadi et al., 2009) and as already described, treatment of NHEKs with IL-1 $\beta$  or TNF $\alpha$  resulted in an increase of TER at first, but in a decrease after long-term treatment (Kirschner et al., 2009). In several mouse models for inflammatory skin diseases it was shown that inflammation results in down-regulation of Cldn-1 while there were varying results for other TJ proteins (Gruber et al., 2015; Yokouchi et al., 2015; Yu et al., 2015). In one of these models this decrease in Cldn-1 was accompanied with an increase of TJ permeability for molecules from 557-5000 Da (Yokouchi et al., 2015). Additionally, dermal injection of IL-1 $\beta$  into healthy volunteers resulted in down-regulation of Cldn-1 (Watson et al., 2007). In porcine *ex vivo* models, decreased Cldn-1 immunointensity was reported after IL-1 $\beta$  injection (Kirschner et al., 2009). Also, in intestinal epithelium IL-1 $\beta$  has been shown to cause decreased TJ functionality, i.e. it has been shown to cause a time-dependent drop in TER of Caco-2 cells (Al-Sadi and Ma, 2007).

In Caco-2 cells, also TNF $\alpha$  has been described to increase TJ permeability, starting after 12 h and dropping TER maximal at 48-72 h (Al-Sadi et al., 2009). Interestingly, treatment of intestinal epithelial cells with TNF $\alpha$ /IFN $\gamma$  caused a drop in TER, being associated with internalisation of Cldn-1, Cldn-4 (and other TJ proteins) (Ivanov et al., 2008). Even though IL-6 is described to have a barrier protective role in intestinal epithelium, long-term treatment (72 h) of Caco-2 cells was shown to decrease TER and increase permeability (Tazuke et al., 2003). Also other proinflammatory cytokines (e.g., IL-4, IL-13, IL-31 or IL-17) have been shown to negatively influence epidermal TJs (Gutowska-Owsiak et al., 2012; Gruber et al., 2015; Hönzke et al., 2016; Niehues et al., 2016; Yuki et al., 2016). These studies demonstrate that decreased TJ barrier properties are likely due to long-term inflammation.

This inflammation-theory is also highly supported by results of this work, which show that a co-treatment of the submerged model with IL-1 $\beta$  and *S. aureus* infection resulted in a faster decrease in TER. Additionally, the diseased models (discussed below) showed an accelerated decrease after *S. aureus* inoculation as well, mainly induced by IL-1 $\beta$ . The possible events that happen after long-term staphylococcal inoculation are illustrated in the schematic overview of Figure 63.

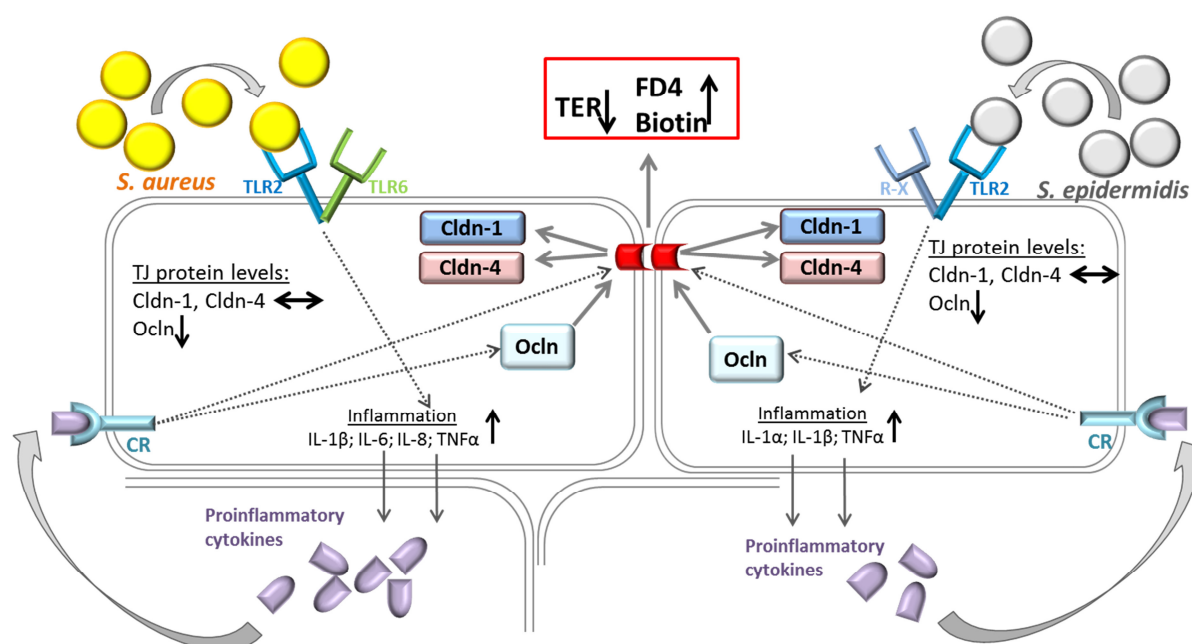


**Figure 63: Schematic overview of possible processes in tight junction (TJ) barrier breakdown during long-term inoculation with *S. aureus* or *S. epidermidis* of PFe3D and submerged models.** Both Staphylococci are recognised via toll-like receptors (TLRs). This leads to an increase in inflammation. Released proinflammatory cytokines bind to their special cytokine receptors (CR), which indirectly leads to TJ barrier disruption via internalisation of claudin-1 (Cldn-1) and Cldn-4. On the other hand, a relocalisation of occludin (Occludin) to the cellular membranes is evident. Grey arrows denote direct reactions; dotted grey lines denote reactions, which are likely the result of a cascade; black arrows denote increase/decrease/no changes. TER – transepithelial electrical resistance; FD4 – 4kDa tracer; IL – interleukin; TNF $\alpha$  – tumor necrosis factor- $\alpha$ ; R-X – yet unknown receptor.

#### 4.3.2.4 Why is opening the TJ barrier beneficial?

The question arises what might be the biological benefit to down-regulate TJ functionality in the course of infection if it is not a virulence mechanism actively performed by the bacteria themselves?

A hallmark of, e.g., *S. aureus* infection is neutrophil abscess formation. This is mediated by proinflammatory cytokines (IL-1 $\beta$ , TNF- $\alpha$ , or IL-6) and especially by chemokines like CXCL2 or IL-8 (Miller and Cho, 2011). Interestingly, also in this work IL-8 was significantly upregulated after *S. aureus* inoculation. It is known that IL-8 is a strong chemoattractant for neutrophil recruitment (Kunkel et al., 1991). Neutrophils can be seen as the “body’s soldiers” as they are able to phagocyte and kill invading pathogens (Thammavongsa et al., 2015). It might be thinkable, that the opening of the TJ barrier after long-term inoculation can be seen as an “opening of the gates” in order to clear the way for a fast neutrophil recruitment. Neutrophils play a central role in protecting humans against *S. aureus* infection. Staphylococcal entry and replication in host tissues leads to the release of bacterial products (pathogen-associated molecular patterns) and to damaged tissues (damage-associated molecular patterns), which are detected via TLRs and G protein-coupled receptors leading to cytokine release. Neutrophils

answer this call, emigrate from blood vessels, and migrate towards the site of infection in order to phagocyte and kill bacteria or to immobilise and damage the pathogens through the release of neutrophil extracellular traps (NETs) comprising DNA and antimicrobial peptides

(Thammavongsa et al., 2015).

As Cldn-1 is expressed in all viable layers, localised mainly at the cell-cell borders and is decreased especially in immunointensity at the cell-cell borders in our approach, this might indicate a possible involvement in “opening the gates” for neutrophil invasion and recruitment to infected sites. Even though it has been shown that in endothelia TJs remain intact during neutrophil adhesion and transmigration (Burns et al., 2000), decreasing TJ barrier function might result in a faster neutrophil recruitment in case of an infectious event especially in the multilayered epithelium of the skin.

The schematic overview in Figure 64 summarises the events that happen over time after bacterial skin infection.

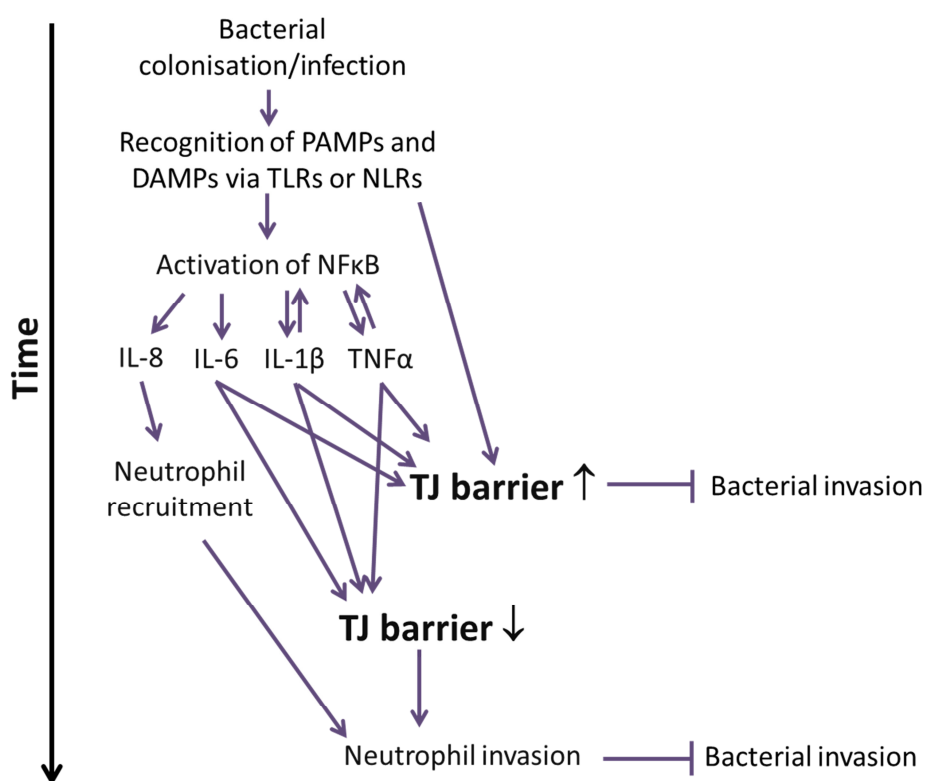


**Figure 64: Schematic overview on putative events that happen in the epidermis after bacterial challenge in the course of time.** Staphylococcal entry and replication in host tissues leads to the release of bacterial products (pathogen-associated molecular patterns (PAMPs)) and to damaged tissues (damage-associated molecular patterns (DAMPs)), which are detected via toll-like receptors (TLRs) or nod-like receptors (NLRs). These activate the nuclear factor  $\kappa$ -light-chain-enhancer of activated B cells (NF $\kappa$ B), which induces the production of several cytokines. These enhance tight junction (TJ) barrier function in short-term while neutrophils are recruited in order to reduce bacterial invasion. At later time points, when neutrophils are recruited, the decreased TJ barrier opens the way for neutrophil invasion, which clears the bacterial infection.

Also, other parts of the immune system might benefit from decreasing TJ function in order to react faster. E.g., dendrites of epidermal Langerhans cells are penetrating from inside-out through TJs to take up external antigens in order to present those to T cells in the secondary lymphatic organs (Kubo et al., 2009; Kubo et al., 2012). These dendrites have been shown to form functional TJs with the keratinocytes (Kubo et al., 2009). Once the TJ barrier is abrogated, antigens are able to penetrate the dermis, where they are taken up by dermal dendritic cells (Kubo et al., 2012; Yokouchi et al., 2015). So, it is postulated that impaired epidermal TJ function might affect the mode of immune reaction for distinct populations of dendritic cells that take up antigens (Yokouchi et al., 2015). Saying that opening the TJ barrier leads to a better/faster certain immune reaction.

#### 4.3.3 *S. epidermidis* – commensal or not?

The inoculation with *S. epidermidis* also resulted in a TJ barrier breakdown in both model systems. Under healthy conditions, *S. epidermidis* acts as a symbiotic commensal on the skin (Sanford and Gallo, 2013). However, *S. epidermidis* is also described as an opportunistic/"accidental" pathogen (Otto, 2009). The *S. epidermidis* strain PIA97 used within this work actually is a clinical isolate from a prosthetic infection (Rohde et al., 2007). In the submerged model, where the cells are not protected by a SC, as well as in PFe3D at day 4, where a SC is present but still weaker than in healthy skin, situations are represented, where *S. epidermidis* can get access to the cells and express its pathogenic character. Up to now, a negative effect of *S. epidermidis* on tight junction functionality has not been described.

#### 4.3.4 The occludin discrepancies

The function of Occludin in general still remains unclear, even though it was the first transmembrane TJ protein being discovered (Furuse et al., 1993). In Occludin deficient mice, TJ strands are visible and barrier function is not affected (Saitou et al., 2000), which shows that Occludin is not necessary for formation of TJ structure and barrier function, but it seems to play an important role in TJ regulation. Indeed, phenotypically these mice are characterised by developmental delay, infertility and gastritis (Saitou et al., 2000).

The first discrepancy concerning Occludin was the fact, that Occludin immunointensity was enhanced quite strongly, while in Western Blot analyses a decrease was evident. One explanation for this discrepancy is that Occludin after long-term incubation is very stably integrated into the cell

membrane and thus cannot be dissolved during the routine procedure of protein preparation. This should be further tested in future investigations.

Another contrariety concerning Occludin (Occludin) was, that even though the TJ functionality is decreased after long-term inoculation, which can be explained by a decrease in Cldn-1 and Cldn-4 at the cell-cell borders, Occludin immunointensity remains strongly increased. This shows that Occludin cannot compensate for the loss of other TJ components and is likely to have other functions.

Interestingly, Occludin has been shown to modulate transepithelial migration of neutrophils (Huber et al., 2000). Thus, the more pronounced localisation of Occludin at the cell membranes after long-term inoculation with *S. aureus* as well as with *S. epidermidis* might support the neutrophil migration into the epidermis in addition to the decrease in TJ barrier function discussed above. Hereby the increase in Occludin might also have an anchoring effect in order not to completely loose cell-cell adhesion during TJ opening, because Rachow et al. revealed that Occludin downregulation resulted in decreased epithelial cell-cell adhesion (Rachow et al., 2013), which implicates that increased Occludin membrane localisation might have the opposite effect. Also in fibroblasts it has been shown that Occludin is involved in cell-cell adhesion (Van Itallie and Anderson, 1997). However, this has to be evaluated in future studies.

Interestingly, it has also been shown that Occludin is required for cytokine-induced regulation of the TJ barrier. In MDCK II cells an overexpression of Occludin resulted in a more sensitive reaction of these cells to IFN $\gamma$  and TNF $\alpha$  and Occludin knock down in a less sensitive reaction (Van Itallie et al., 2010). Also, in intestinal epithelial cells, Occludin knock down prevented TNF $\alpha$  induced barrier disruption (Buschmann et al., 2013). This role of Occludin might explain why more Occludin is present at the cell-cell borders after bacterial inoculation, while other TJ proteins show a decrease in immunointensity. However, also the opposite effect was described: In *in vivo* mouse jejunal epithelia, Occludin overexpression prevented TNF $\alpha$  induced barrier disruption (Marchiando et al., 2010). Inflammation might be a cause for the increased Occludin localisation at the cell-cell borders. Yamamoto and colleagues showed that IL-1 $\beta$  caused hyperphosphorylation of Occludin in rat hepatocytes accompanied with an increased localisation of Occludin at the cell-cell borders (Yamamoto et al., 2004). Additionally, in *ex vivo* skin, IL-1 $\beta$  treatment also led to a broader localisation of Occludin (Kirschner et al., 2009). This also underlines the theory that alterations of TJ proteins after inoculation might be a reaction on increased inflammation. In human brain endothelial cells enhanced barrier tightness (measured by TER) was achieved by the

inactivation of glycogen synthase kinase 3 $\beta$  (Ramirez et al., 2013), which has an anti-inflammatory effect (Ramirez et al., 2010). In this study the half-life of OcIn was extended 2.7 times (Ramirez et al., 2013). Under steady-state conditions OcIn undergoes continuous endocytosis (Fletcher et al., 2014). Occludin degradation is enforced due to ubiquitination. TNF $\alpha$ -induced protein 3 (TNFAIP3 or A20) acts as a negative feedback loop as an inhibitor of TNF $\alpha$  and also IL-1 $\beta$  dependent NF $\kappa$ B activation. A20 was originally characterised as a protein protecting cells from TNF-induced cytotoxicity (Opipari et al., 1992). In a human intestinal epithelium cell line it has been shown that A20 deubiquitinates polyubiquitinated occludin and inhibits thereby the loss of occludin from the cell membrane (Kolodziej et al., 2011). Treatment of human keratinocytes with *S. aureus* biofilm secreted products resulted already after 2 h in an upregulation of TNFAIP3 (A20) (Tankersley et al., 2014). Interestingly, Cldn-1 is not ubiquitinated during its internalisation (Asaka et al., 2010). This might be a reason why occludin still is present and also more occludin is present at the cell-cell borders, because it's deubiquitinated due to an upregulation of TNFAIP3 / A20 and therefore not endocytosed like Cldn-1 and Cldn-4. If this truly is the case in the approach of this work, it needs to be investigated in the future.

It might be worth considering that different forms of OcIn exist that have a tightening or opening function or sensing function, e.g., depending on the phosphorylation status, as the increase in TJ barrier function after short-term *S. aureus* inoculation was associated with a higher phosphorylated form of OcIn and increased immunolocalisation at the cell-cell borders, which was not observed at later time points after *S. epidermidis* inoculation even though immunolocalisation was increased as well.

#### 4.3.5 Summary and future prospective of Results, Part 2 and 3

In conclusion, inoculation with *S. aureus* as well as with *S. epidermidis* resulted in a biphasic influence on epidermal TJs.

Concerning the mechanism underlying this biphasic influence of Staphylococci on TJs several hypotheses have been tested in this work and combined with knowledge from literature. The outcome is summarised in Figure 65. During the early phase of bacterial inoculation *S. aureus* as well as *S. epidermidis* are recognised via TLR2 and/or other PRRs, which finally results in relocation of TJ proteins and in an increased TJ functionality. During this process, inflammation is likely to play a role, as well as the activation of aPKC after *S. aureus*

inoculation, while an increase in the amount of TJ proteins or an increase in AMP production can be excluded. However, also other, not yet known, mechanisms could play a role.

Longer inoculation with the bacteria results in delocalisation of sealing TJ proteins, which ends in decreased TJ functionality. Thereby also inflammation seems to be strongly involved, while cell death or the involvement of bacterial proteases can be excluded. Still, also here the participation of other, yet unknown, mechanisms is thinkable.

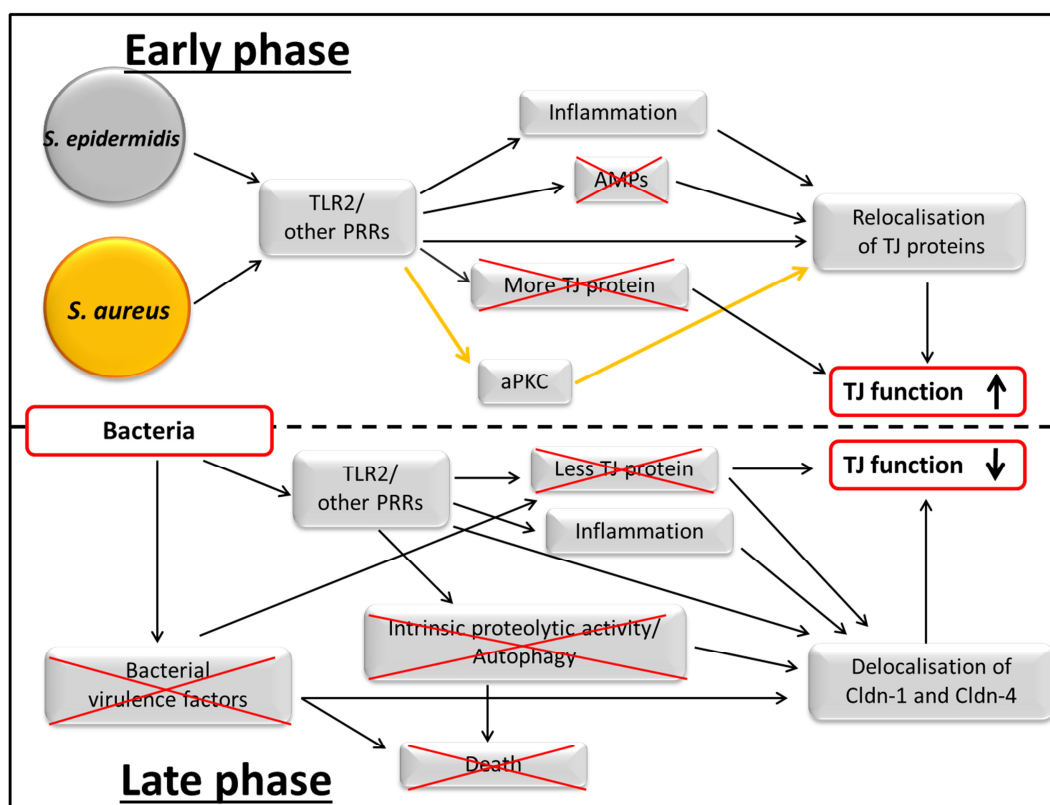


**Figure 65: Schematic overview of possible interactions that could lead to an increased tight junction (TJ) barrier function in the early phase of bacterial inoculation and to a TJ barrier breakdown during later treatment.** Red crosses denote mechanisms that could be excluded within this work; black arrows denote interactions with both *Staphylococcus* (*S.*) species; yellow arrows denote interactions with *S. aureus*. TLR2 – Toll-like receptor 2; PRRs – pattern recognition receptors; AMPs – antimicrobial peptides; aPKC – atypical protein kinase C; Cldn – claudin.

This biphasic influence on TJs indicates at first a strengthening of barrier properties until further help is recruited and an opening of the barrier in order to let the recruited help find a faster way to the sides of infection. Clearly this only is a theory and has to be investigated further in the future.

In general this work gives hint at an involvement of inflammation in infection-dependent TJ barrier increase or decrease. However, more experiments would be necessary in order to completely elucidate to what extent and in which context the inflammatory environment is

involved. This might be possible due to further experiments, inhibiting cytokine release or NF $\kappa$ B pathway.

#### 4.4 Results, Part 4: Atopic dermatitis mimicking conditions

Bacterial infections, in particular with *S. aureus*, are one of the most common complications in the pathogenesis of AD (Huang et al., 2009). In general *S. aureus* is not only a complication, but also strongly associated with AD. The skin of about 90% of AD patients is colonised (Breuer et al., 2002; Gong et al., 2006), whereas only 20% of healthy individuals are carrying *S. aureus* (Wertheim et al., 2005). While carrying *S. aureus* does not mean, that they show any clinical signs of infections, the amount of *S. aureus* however, is associated with an increased disease severity (Higaki et al., 1999). Treatment of *S. aureus* on the skin of AD patients resulted in a decreased disease severity (Huang et al., 2009).

AD is characterised by skin inflammation and the susceptibility to cutaneous viral and bacterial infections. In order to induce an AD-like environment, the submerged models were treated with a cytokine-toll-like-receptor-agonist-mix (CTM), containing the proinflammatory cytokine IL-1 $\beta$ , the TLR1/2 agonist Pam3CSK4 and the TLR3 agonist Poly I:C. In AD, a contribution of IL-1 $\beta$  to the development of the skin inflammation is suggested as e.g., in the serum of AD patients high levels of IL-1 $\beta$  have been recorded with a direct correlation to the disease severity (Nutan et al., 2012; Bernard et al., 2017). Additionally to IL-1 $\beta$ , the release of thymic stromal lymphopoietin (TSLP) of keratinocytes plays a key role in allergic diseases. It was demonstrated that poly I:C, a TLR3 ligand mimicking viral double-stranded RNA, triggers the release of TSLP in primary human keratinocytes and induces the gene expression of various other proinflammatory molecules (Vu et al., 2011). PolyI:C already has been used (together with TNF $\alpha$ , IL-4 and IL-13) for treatment of a RHE model in order to induce AD-related inflammation (Rouaud-Tinguely et al., 2015). Also, the TLR1/2 agonist Pam3CSK4 is known to result in upregulating an proinflammatory response (Aliprantis et al., 1999).

Generally, CTM already was shown to induce an AD-like epidermal inflammation and phenotype after treatment for 24 h of hair follicle derived RHE (Bernard et al., 2017).

Here the submerged models were pretreated with the CTM one day after lifting to high Ca<sup>2+</sup> for 24 h (-24 h), followed by incubation without the CTM for another 24 h (0 h). Then they



were infected. Interestingly, CTM treatment alone already resulted in a slight increase in TER at -24 h and significantly at 0 h.

IL-1 $\beta$  seems to be the main component of the CTM being responsible for the observed effects, while Pam3CSK4 and Poly I:C only seemed to play a minor role. This also confirms results obtained in RHE, where IL-1 $\beta$  was responsible for the main response, however co-activation with the TLR1/2 and 3 agonists boosted the release of inflammatory mediators (Bernard et al., 2017). Concerning barrier properties, as discussed above, it already has been shown that IL-1 $\beta$  is able to enhance TJ barrier function (Kirschner et al., 2009). Of note, IL-1 $\beta$  treatment in this approach differed from the treatment parallel to infection (discussed above) (in concentration and time). Even though IL-1 $\beta$  seems to be the main player of the CTM, also the TLR1/2 agonist Pam3CSK4 alone resulted in a significant increase in TER. Pam3CSK4 has been shown to significantly increase TER in a non-transformed porcine jejunum epithelial cell line (IPEC-J2) (Gu et al., 2016) as well as in NHEKs (Kuo et al., 2013).

Interestingly, CTM pretreatment with following infection accelerated the decrease in TER after *S. aureus* inoculation, while this was not the case after *S. epidermidis* inoculation. This indicates that increased AD-like conditions favour the breakthrough of *S. aureus*. This faster decrease in TER after CTM pretreatment after *S. aureus* inoculation could be on the one hand caused by the bacteria themselves, as being more active due to somehow sensing inflammatory signals. On the other hand, and being more likely, the keratinocytes could already be adjusted/prewarned on inflammatory stimuli after CTM treatment and thereby react faster. As the results of the non-CTM treated submerged models already indicated, the NHEKs react faster to *S. aureus* than to *S. epidermidis* with activation of proinflammatory cytokines. Thus, the interplay between being pre-activated and faster reaction on *S. aureus* inoculation could explain this result and also supports the inflammation theory for decreasing TER values. However, this only scratches the surface and clearly needs to be investigated in more detail in order to elucidate the initial steps.

In order to induce AD in PFe3D for later infection, models were incubated for 24 h with the CTM and another 72 h without CTM (the period of infection). Unfortunately, this did not work very well, as the models reacted very heterogeneously on this mix and often showed areas with dead tissue already after 24 h, being more pronounced over time. Even though the usage of older PFe3D (day 11) for CTM treatment was more promising, also here results

were not satisfactory enough for further investigations. The CTM already has been used for treatment of RHE models before (Bernard et al., 2017). However, analyses were performed already after 24 h of treatment on models at day 14 and additionally a different RHE system has been used in this work (Bernard et al., 2017). In order to investigate CTM pretreatment and infection on RHE, it might be beneficial to use a different RHE system (e.g., the one used by Bernard et al. (2017)) than the PFe3D models or to retry different time points.

Nevertheless, results obtained with the CTM on the submerged models have been very promising. Future investigations should concentrate on the reasons of the faster breakdown of the TJ barrier after *S. aureus* inoculation. Additionally, experimental settings on investigations using a 3D tissue should be evaluated.

## ABSTRACT

---

The skin is a pivotal barrier against the invasion of pathogens and allergens and the skin barrier is part of the innate immune system. Tight junctions (TJs) contribute to the overall skin barrier by forming a physical barrier and interacting with the other components of the skin barrier. Previously, *in vivo* analyses of infected skin and a porcine *ex vivo* infection model with *Staphylococcus aureus* (*S. aureus*) revealed changes in immunolocalisation of TJ proteins. As a change of proteins does not necessarily reflect alterations in the functionality of TJs, the aim of this study was to investigate the influence of *S. epidermidis* and *S. aureus* on TJ functionality and to elucidate the underlying mechanisms on TJ functionality in normal human epidermal keratinocytes (NHEKs) in a submerged model and in reconstructed human epidermis (RHE).

By using NHEKs under submerged conditions, a dose dependent increase of transepithelial electrical resistance (TER) and decrease of paracellular permeability for a 4 kDa tracer during short-term incubation with *S. epidermidis* and *S. aureus* was observed. This argues for a prevention mechanism by strengthening of the innate immune system via tightening the TJ barrier to reduce/delay pathogen uptake. The usage of bacterial mutants revealed that the accessory gene regulator (*agr*) plays a role in this effect. However, even though the outcome is similar, mechanisms are different between *S. epidermis* and *S. aureus*. Short-term inoculation with both bacteria resulted in relocalisation of claudin-4 to the cellular membranes, while for *S. aureus* additionally increased levels of phosphorylated occludin were evident, which also resulted in an increase of this protein at the cell-cell borders. Experimental data hint for a role of Toll-like receptors (TLR) and cytokines for these differences. Investigation of RHE confirmed the phosphorylation and relocalisation of Occludin to the cell membranes after *S. aureus* inoculation. However, the TJ barrier-tightening effect could not be measured in this system, putatively due to camouflaging effects by the *Stratum corneum*.

At later time points of incubation with both bacteria in both model systems, a decreased TJ barrier was found. This was not accompanied by increased cell death, but by internalisation of TJ proteins. Bacterial virulence factors of the *agr*-regulon are not responsible for this internalisation, but inflammation seems to be involved.

A pretreatment of the submerged culture with an Atopic Dermatitis mimicking mix consisting of cytokines and TLR agonists followed by infection also resulted in a short-term increase in TER for both bacteria, but for *S. aureus* a subsequent accelerated decrease was observed, hinting for a supporting effect of AD conditions on *S. aureus* infection.

In conclusion, this work demonstrates that infection of primary keratinocytes not only with the commensal *S. epidermidis*, but also with the pathogen *S. aureus* results in a transient upregulation of TJ functionality, hinting for a prevention mechanism of keratinocytes against invasion of pathogens. However, long-term infection results in a TJ barrier breakdown. In AD related conditions, the TJ barrier breakdown is intensified after *S. aureus* but not *S. epidermidis* infection.

## ZUSAMMENFASSUNG

---

Die Haut bildet eine zentrale Barriere gegen das Eindringen von pathogenen Organismen und Allergenen und ist daher ein Teil der angeborenen Immunabwehr. Tight Junctions (TJs) spielen für die Gesamthautbarriere eine wichtige Rolle, denn sie bilden eine physikalische Grenze und interagieren mit den anderen Komponenten der Hautbarriere. *In vivo* Analysen infizierter Haut, sowie ein porcines *ex vivo* Infektionsmodell mit *Staphylococcus aureus* (*S. aureus*) haben Veränderungen in der Immunlokalisation von TJ proteinen gezeigt. Da Veränderungen von Proteinen nicht zwangsläufig eine veränderte Funktionalität der TJs widerspiegeln, war es das Ziel dieser Arbeit den Einfluss von *S. epidermidis* und *S. aureus* auf die TJ Funktionalität von primären humanen Keratinozyten (NHEKs) in einem überfluteten Modell sowie einer epidermalen Hautrekonstruktion (RHE) zu untersuchen und die zu Grunde liegenden Mechanismen zu analysieren.

NHEKs im überfluteten Modell zeigten nach kurzzeitiger Inkubation mit *S. epidermidis* und *S. aureus*. einen dosisabhängigen Anstieg des transepithelialen Widerstandes (TER) sowie einen Abfall der parazellulären Permeabilität für ein 4 kDa großes Tracermolekül. Diese Beobachtung spricht für einen Schutzmechanismus, in dem die angeborene Immunabwehr durch eine Verdichtung der TJ Barriere gestärkt wird um das Eindringen Pathogener zu verhindern/verzögern. Die Verwendung bakterieller Mutanten zeigte, dass der „accessory gene regulator“ (*agr*) bei diesem Effekt eine Rolle spielt. Jedoch obwohl das Ergebnis ähnlich ist, gibt es verschiedene Mechanismen zwischen *S. epidermidis* und *S. aureus*. Kurzzeitige

Inokulation mit beiden Bakterien zeigte eine Relokalisation von Claudin-4 zu den Zellmembranen, wohingegen für *S. aureus* zusätzlich höhere Level von phosphoryliertem Occludin ersichtlich waren, was auch zu einer verstärkten Lokalisation dieses Proteins an die Zellgrenzen führte. Experimentelle Ergebnisse deuten auf eine Rolle von Toll-like-Rezeptoren (TLR) und Zytokinen für diese Unterschiede hin. Untersuchungen an RHE bestätigten die Phosphorylierung und Relokalisierung von Occludin zu den Zellgrenzen nach *S. aureus* Inokulation. Trotzdem konnte der TJ-Barriere stärkende Effekt in RHE nicht gezeigt werden, was vermutlich an einem Tarneffekt des Statum corneum liegt.

Zu späteren Zeitpunkten der Inkubation mit beiden Bakterien wurde in beiden Modellsystemen eine Schwächung der TJ Barriere festgestellt, was nicht durch Zelltod hervorgerufen wurde, sondern durch eine Internalisierung von TJ Proteinen. Hierbei spielen bakterielle Virulenzfaktoren des *agr*-Regulons keine Rolle, aber eine Inflamationsreaktion scheint ein Trigger zu sein.

Die Vorbehandlung der überfluteten Kultur mit einem atopische Dermatitis nachahmenden Mix aus Zytokinen und TLR-Agonisten gefolgt von einer Infektion zeigte nach kurzzeitiger Inokulation auch einen Anstieg des TERs, allerdings führte *S. aureus* zu einem schnelleren und stärkeren Abfall des TERs, was auf eine Begünstigung atopischer Umstände für eine *S. aureus* Infektion hindeutet.

Zusammenfassend zeigt diese Arbeit, dass eine Infektion von primären Keratinozyten nicht nur mit dem Kommensalen *S. epidermidis*, sondern auch mit dem Pathogenen *S. aureus*, in einer transienten hochregulation der TJ Funktionalität endet. Dies spricht für einen Schutzmechanismus gegen das Eindringen von Pathogenen. Dennoch führt eine längerfristige Infektion zu einem Verlust der TJ Barriere. Unter atopischen Umständen ist dieser Barriereverlust durch *S. aureus*, aber nicht durch *S. epidermidis*, verstärkt.

## REFERENCES

---

- Abrahamsson, T. R., H. E. Jakobsson, A. F. Andersson, B. Björkstén, L. Engstrand and M. C. Jenmalm (2012).** "Low diversity of the gut microbiota in infants with atopic eczema." *Journal of Allergy and Clinical Immunology* 129(2): 434-440.e432.
- Akiyama, T., F. Niyonsaba, C. Kiatsurayanon, T. T. Nguyen, H. Ushio, T. Fujimura, T. Ueno, K. Okumura, H. Ogawa and S. Ikeda (2014).** "The Human Cathelicidin LL-37 Host Defense Peptide Upregulates Tight Junction-Related Proteins and Increases Human Epidermal Keratinocyte Barrier Function." *Journal of Innate Immunity*.
- Al-Sadi, R., M. Boivin and T. Ma (2009).** "Mechanism of cytokine modulation of epithelial tight junction barrier." *Frontiers in bioscience : a journal and virtual library* 14: 2765-2778.
- Al-Sadi, R., D. Ye, M. Boivin, S. Guo, M. Hashimi, L. Ereifej and T. Y. Ma (2014).** "Interleukin-6 modulation of intestinal epithelial tight junction permeability is mediated by JNK pathway activation of claudin-2 gene." *PLoS One* 9(3): e85345.
- Al-Sadi, R. M. and T. Y. Ma (2007).** "IL-1 $\beta$  Causes an Increase in Intestinal Epithelial Tight Junction Permeability." *Journal of immunology (Baltimore, Md. : 1950)* 178(7): 4641-4649.
- Aliprantis, A. O., R.-B. Yang, M. R. Mark, S. Suggett, B. Devaux, J. D. Radolf, G. R. Klimpel, P. Godowski and A. Zychlinsky (1999).** "Cell Activation and Apoptosis by Bacterial Lipoproteins Through Toll-like Receptor-2." *Science* 285(5428): 736.
- Anderson, J. M. (2001).** "Molecular structure of tight junctions and their role in epithelial transport." *News in Physiological Sciences* 16: 126-130.
- Asad, S., M. C. G. Winge, C. F. Wahlgren, K. D. Bilcha, M. Nordenskjöld, F. Taylan and M. Bradley (2016).** "The tight junction gene Claudin-1 is associated with atopic dermatitis among Ethiopians." *Journal of the European Academy of Dermatology and Venereology* 30(11): 1939-1941.
- Asaka, M., T. Hirase, A. Hashimoto-Komatsu and K. Node (2010).** "Rab5a-mediated localization of claudin-1 is regulated by proteasomes in endothelial cells." *American Journal of Physiology - Cell Physiology* 300(1): C87.
- Baek, J. H., S. E. Lee, K. J. Choi, E. H. Choi and S. H. Lee (2013).** "Acute modulations in stratum corneum permeability barrier function affect claudin expression and epidermal tight junction function via changes of epidermal calcium gradient." *Yonsei Medical Journal* 54(2): 523-528.
- Bardoel, B. W., R. Vos, T. Bouman, P. C. Aerts, J. Bestebroer, E. G. Huizinga, T. H. C. Brondijk, J. A. G. van Strijp and C. J. C. de Haas (2012).** "Evasion of Toll-like receptor 2 activation by staphylococcal superantigen-like protein 3." *Journal of Molecular Medicine* 90(10): 1109-1120.

- Barland, C. O., E. Zettersten, B. S. Brown, J. Ye, P. M. Elias and R. Ghadially (2004).** "Imiquimod-Induced Interleukin-1 $\alpha$  Stimulation Improves Barrier Homeostasis in Aged Murine Epidermis." *Journal of Investigative Dermatology* 122(2): 330-336.
- Barnes, K. C. (2010).** "An update on the genetics of atopic dermatitis: Scratching the surface in 2009." *Journal of Allergy and Clinical Immunology* 125(1): 16-29.e11.
- Bäsler, K., S. Bergmann, M. Heisig, A. Naegel, M. Zorn-Kruppa and J. M. Brandner (2016).** "The role of tight junctions in skin barrier function and dermal absorption." *Journal of Controlled Release*.
- Bäsler, K. and J. M. Brandner (2016).** "Tight junctions in skin inflammation." *Pflügers Archiv: European journal of physiology*.
- Bäsler, K., M.-F. Galliano, S. Bergmann, H. Rohde, E. Wladykowski, S. Vidal-y-Sy, B. Guiraud, P. Houdek, G. Schüring, T. Volksdorf, A. Caruana, S. Bessou-Touya, S. W. Schneider, H. Duplan and J. M. Brandner (2017).** "Biphasic influence of Staphylococcus aureus on human epidermal tight junctions." *Annals of the New York Academy of Sciences* 1405(1): 53-70.
- Batista, D. I., L. Perez, R. L. Orfali, M. C. Zaniboni, L. P. Samorano, N. V. Pereira, M. N. Sotto, A. S. Ishizaki, L. M. Oliveira, M. N. Sato and V. Aoki (2015).** "Profile of skin barrier proteins (filaggrin, claudins 1 and 4) and Th1/Th2/Th17 cytokines in adults with atopic dermatitis." *Journal of the European Academy of Dermatology and Venereology : JEADV* 29(6): 1091-1095.
- Bernard, M., C. Carrasco, L. Laoubi, B. Guiraud, A. Rozières, C. Goujon, H. Duplan, S. Bessou-Touya, J.-F. Nicolas, M. Vocanson and M.-F. Galliano (2017).** "IL-1 $\beta$  induces thymic stromal lymphopoietin and an atopic dermatitis-like phenotype in reconstructed healthy human epidermis." *The Journal of Pathology* 242(2): 234-245.
- Böhringer, M., S. Pohlers, S. Schulze, D. Albrecht-Eckardt, J. Piegsa, M. Weber, R. Martin, K. Hünninger, J. Linde, R. Guthke and O. Kurzai (2016).** "Candida albicans infection leads to barrier breakdown and a MAPK/NF- $\kappa$ B mediated stress response in the intestinal epithelial cell line C2BB $\epsilon$ 1." *Cellular microbiology*: n/a-n/a.
- Borkowski, A. W., I. H. Kuo, J. J. Bernard, T. Yoshida, M. R. Williams, N. J. Hung, B. D. Yu, L. A. Beck and R. L. Gallo (2015).** "Toll-like receptor 3 activation is required for normal skin barrier repair following UV damage." *Journal of Investigative Dermatology* 135(2): 569-578.
- Boyce, S. T. and R. G. Ham (1983).** "Calcium-Regulated Differentiation of Normal Human Epidermal Keratinocytes in Chemically Defined Clonal Culture and Serum-Free Serial Culture." *Journal of Investigative Dermatology* 81(1, Supplement): S33-S40.
- Bradford, M. M. (1976).** "A rapid and sensitive method for the quantitation of microgram quantities of protein utilizing the principle of protein-dye binding." *Analytical Biochemistry* 72(1): 248-254.

- Brandner, J. M., S. Kief, C. Grund, M. Rendl, P. Houdek, C. Kuhn, E. Tschachler, W. W. Franke and I. Moll (2002).** "Organization and formation of the tight junction system in human epidermis and cultured keratinocytes." *European Journal of Cell Biology* 81(5): 253-263.
- Breuer, K., S. HÄussler, A. Kapp and T. Werfel (2002).** "Staphylococcus aureus: colonizing features and influence of an antibacterial treatment in adults with atopic dermatitis." *British Journal of Dermatology* 147(1): 55-61.
- Bunikowski, R., M. E. A. Mielke, H. Skarabis, M. Worm, I. Anagnostopoulos, G. Kolde, U. Wahn and H. Renz (2000).** "Evidence for a disease-promoting effect of Staphylococcus aureus-derived exotoxins in atopic dermatitis." *Journal of Allergy and Clinical Immunology* 105(4): 814-819.
- Burns, A. R., R. A. Bowden, S. D. MacDonell, D. C. Walker, T. O. Odebunmi, E. M. Donnachie, S. I. Simon, M. L. Entman and C. W. Smith (2000).** "Analysis of tight junctions during neutrophil transendothelial migration." *Journal of Cell Science* 113(1): 45.
- Buschmann, M. M., L. Shen, H. Rajapakse, D. R. Raleigh, Y. Wang, Y. Wang, A. Lingaraju, J. Zha, E. Abbott, E. M. McAuley, L. A. Breskin, L. Wu, K. Anderson, J. R. Turner and C. R. Weber (2013).** "Occludin OCEL-domain interactions are required for maintenance and regulation of the tight junction barrier to macromolecular flux." *Molecular Biology of the Cell* 24(19): 3056-3068.
- Candi, E., R. Schmidt and G. Melino (2005).** "The cornified envelope: a model of cell death in the skin." *Nature Reviews Molecular Cell Biology* 6(4): 328-340.
- Capaldo, C. T. and A. Nusrat (2009).** "Cytokine regulation of tight junctions." *Biochimica et biophysica acta* 1788(4): 864-871.
- Celli, A., Y. Zhai, Y. J. Jiang, D. Crumrine, P. M. Elias, K. R. Feingold and T. M. Mauro (2012).** "Tight junction properties change during epidermis development." *Experimental Dermatology* 21(10): 798-801.
- Chong, Y. P., S.-J. Park, H. S. Kim, E. S. Kim, M.-N. Kim, K.-H. Park, S.-H. Kim, S.-O. Lee, S.-H. Choi, J.-Y. Jeong, J. H. Woo and Y. S. Kim (2013).** "Persistent Staphylococcus aureus Bacteremia: A Prospective Analysis of Risk Factors, Outcomes, and Microbiologic and Genotypic Characteristics of Isolates." *Medicine* 92(2): 98-108.
- Claude, P. and D. A. Goodenough (1973).** "Fracture faces of zonulae occludentes from "tight" and "leaky" epithelia." *The Journal of Cell Biology* 58(2): 390-400.
- Costello, E. K., C. L. Lauber, M. Hamady, N. Fierer, J. I. Gordon and R. Knight (2009).** "Bacterial Community Variation in Human Body Habitats Across Space and Time." *Science* 326(5960): 1694-1697.
- Danso, M. O., V. van Drongelen, A. Mulder, J. van Esch, H. Scott, J. van Smeden, A. El Ghalbzouri and J. A. Bouwstra (2014).** "TNF- $\alpha$  and Th2 Cytokines Induce Atopic Dermatitis-Like Features on Epidermal Differentiation Proteins and Stratum Corneum Lipids in Human Skin Equivalents." *Journal of Investigative Dermatology* 134(7): 1941-1950.



- De Benedetto, A., N. M. Rafaels, L. Y. McGirt, A. I. Ivanov, S. N. Georas, C. Cheadle, A. E. Berger, K. Zhang, S. Vidyasagar, T. Yoshida, M. Boguniewicz, T. Hata, L. C. Schneider, J. M. Hanifin, R. L. Gallo, N. Novak, S. Weidinger, T. H. Beaty, D. Y. Leung, K. C. Barnes and L. A. Beck (2011a).** "Tight junction defects in patients with atopic dermatitis." *The Journal of allergy and clinical immunology* 127(3): 773-786 e771-777.
- De Benedetto, A., M. K. Slifka, N. M. Rafaels, I. H. Kuo, S. N. Georas, M. Boguniewicz, T. Hata, L. C. Schneider, J. M. Hanifin, R. L. Gallo, D. C. Johnson, K. C. Barnes, D. Y. Leung and L. A. Beck (2011b).** "Reductions in claudin-1 may enhance susceptibility to herpes simplex virus 1 infections in atopic dermatitis." *The Journal of allergy and clinical immunology*.
- Dörfel, M. J. and O. Huber (2012).** "Modulation of Tight Junction Structure and Function by Kinases and Phosphatases Targeting Occludin." *Journal of Biomedicine and Biotechnology* 2012: 14.
- Dufour, P., S. Jarraud, F. Vandenesch, T. Greenland, R. P. Novick, M. Bes, J. Etienne and G. Lina (2002).** "High Genetic Variability of the agr Locus in Staphylococcus Species." *Journal of Bacteriology* 184(4): 1180-1186.
- Eberlein-König, B., T. Schafer, J. Huss-Marp, U. Darsow, M. Mohrenschlager, O. Herbert, D. Abeck, U. Kramer, H. Behrendt and J. Ring (2000).** "Skin surface pH, stratum corneum hydration, trans-epidermal water loss and skin roughness related to atopic eczema and skin dryness in a population of primary school children." *Acta Dermato-Venereologica* 80(3): 188-191.
- Eckhart, L., W. Declercq, J. Ban, M. Rendl, B. Lengauer, C. Mayer, S. Lippens, P. Vandenabeele and E. Tschachler (2000).** "Terminal Differentiation of Human Keratinocytes and Stratum Corneum Formation is Associated with Caspase-14 Activation." *Journal of Investigative Dermatology* 115(6): 1148-1151.
- Elias, P. M. and M. Schmuth (2009).** "Abnormal skin barrier in the etiopathogenesis of atopic dermatitis." *Current allergy and asthma reports* 9(4): 265-272.
- Enikanolaiye, A., N. Lariviere, T. C. Troy, A. Arabzadeh, E. Atasoy and K. Turksen (2010).** "Involucrin-claudin-6 tail deletion mutant (CDelta206) transgenic mice: a model of delayed epidermal permeability barrier formation and repair." *Disease Models & Mechanisms* 3(3-4): 167-180.
- Eyerich, K. and N. Novak (2013).** "Immunology of atopic eczema: overcoming the Th1/Th2 paradigm." *Allergy* 68(8): 974-982.
- Farquhar, M. G. and G. E. Palade (1963).** "Junctional complexes in various epithelia." *Journal of Cell Biology* 17: 375-412.
- Feuchter, D., M. Heisig and G. Wittum (2006).** "A Geometry Model for the Simulation of Drug Diffusion through the Stratum Corneum." *Computing and Visualization in Science* 9(2): 117-130.
- Fletcher, S. J., M. Iqbal, S. Jabbari, D. Stekel and J. Z. Rappoport (2014).** "Analysis of Occludin Trafficking, Demonstrating Continuous Endocytosis, Degradation, Recycling and Biosynthetic Secretory Trafficking." *PLoS One* 9(11): e111176.

- Foolad, N., E. A. Brezinski, E. P. Chase and A. W. Armstrong (2013).** "Effect of nutrient supplementation on atopic dermatitis in children: A systematic review of probiotics, prebiotics, formula, and fatty acids." *JAMA Dermatology* 149(3): 350-355.
- Fredricks, D. N. (2001).** "Microbial Ecology of Human Skin in Health and Disease." *Journal of Investigative Dermatology Symposium Proceedings* 6(3): 167-169.
- Furuse, M., K. Fujita, T. Hiiragi, K. Fujimoto and S. Tsukita (1998).** "Claudin-1 and -2: Novel integral membrane proteins localizing at Tight Junctions with no sequence similarity to occludin." *Journal of Cell Biology* 141(1539-1550).
- Furuse, M., M. Hata, K. Furuse, Y. Yoshida, A. Haratake, Y. Sugitani, T. Noda, A. Kubo and S. Tsukita (2002).** "Claudin-based tight junctions are crucial for the mammalian epidermal barrier: a lesson from claudin-1-deficient mice." *Journal of Cell Biology* 156: 1099-1111.
- Furuse, M., T. Hirase, M. Itoh, A. Nagafuchi, S. Yonemura and S. Tsukita (1993).** "Occludin: a novel integral membrane protein localizing at tight junctions." *Journal of Cell Biology* 123: 1777-1788.
- Garnacho-Saucedo, G., R. Salido-Vallejo and J. C. Moreno-Gimenez (2013).** "Atopic dermatitis: update and proposed management algorithm." *Actas Dermosifiliogr* 104(1): 4-16.
- Garrido-Urbani, S., P. F. Bradfield and B. A. Imhof (2014).** "Tight junction dynamics: the role of junctional adhesion molecules (JAMs)." *Cell and tissue research* 355(3): 701-715.
- Gong, J. Q., L. Lin, T. Lin, F. Hao, F. Q. Zeng, Z. G. Bi, D. Yi and B. Zhao (2006).** "Skin colonization by *Staphylococcus aureus* in patients with eczema and atopic dermatitis and relevant combined topical therapy: a double-blind multicentre randomized controlled trial." *British Journal of Dermatology* 155(4): 680-687.
- Grice, E. A. (2014).** "The skin microbiome: potential for novel diagnostic and therapeutic approaches to cutaneous disease." *Seminars in Cutaneous Medicine and Surgery* 33(2): 98-103.
- Grice, E. A. and J. A. Segre (2011).** "The skin microbiome." *Nature Reviews Microbiology* 9(4): 244-253.
- Grote, K., H. Schuett, G. Salguero, C. Grothusen, J. Jagielska, H. Drexler, P. F. Mühlradt and B. Schieffer (2010).** "Toll-like receptor 2/6 stimulation promotes angiogenesis via GM-CSF as a potential strategy for immune defense and tissue regeneration." *Blood* 115(12): 2543.
- Gruber, R., C. Bornchen, K. Rose, A. Daubmann, T. Volksdorf, E. Wladykowski, Y. S. S. Vidal, E. M. Peters, M. Danso, J. A. Bouwstra, H. C. Hennies, I. Moll, M. Schmuth and J. M. Brandner (2015).** "Diverse regulation of claudin-1 and claudin-4 in atopic dermatitis." *American Journal of Pathology* 185(10): 2777-2789.
- Gschwandtner, M., M. Mildner, V. Mlitz, F. Gruber, L. Eckhart, T. Werfel, R. Gutzmer, P. M. Elias and E. Tschachler (2013).** "Histamine suppresses epidermal keratinocyte differentiation and impairs skin barrier function in a human skin model." *Allergy* 68(1): 37-47.

- Gu, M. J., S. K. Song, I. K. Lee, S. Ko, S. E. Han, S. Bae, S. Y. Ji, B.-C. Park, K.-D. Song, H.-K. Lee, S. H. Han and C.-H. Yun (2016).** "Barrier protection via Toll-like receptor 2 signaling in porcine intestinal epithelial cells damaged by deoxynivalnol." *Veterinary Research* 47(1): 25.
- Guillemot, L., S. Paschoud, P. Pulimeno, A. Foglia and S. Citi (2008).** "The cytoplasmic plaque of tight junctions: a scaffolding and signalling center." *Biochimica et biophysica acta* 1778(3): 601-613.
- Günzel, D. and A. S. L. Yu (2013).** "Claudins and the Modulation of Tight Junction Permeability." *Physiological Reviews* 93(2): 525-569.
- Gutowska-Owsiak, D., A. L. Schaupp, M. Salimi, T. A. Selvakumar, T. McPherson, S. Taylor and G. S. Ogg (2012).** "IL-17 downregulates filaggrin and affects keratinocyte expression of genes associated with cellular adhesion." *Experimental Dermatology* 21(2): 104-110.
- Guttman, J. A. and B. B. Finlay (2009).** "Tight junctions as targets of infectious agents." *Biochimica et Biophysica Acta (BBA) - Biomembranes* 1788(4): 832-841.
- Hashimoto, K. (1971).** "Intercellular spaces of the human epidermis as demonstrated with lanthanum." *Journal of Investigative Dermatology* 57: 17-31.
- Hattori, F., C. Kiatsurayanon, K. Okumura, H. Ogawa, S. Ikeda, K. Okamoto and F. Niyonsaba (2014).** "The antimicrobial protein S100A7/psoriasin enhances expression of keratinocyte differentiation markers and strengthens the skin tight junction barrier." *British Journal of Dermatology*.
- Helfrich, I., A. Schmitz, P. Zigrino, C. Michels, I. Haase, A. le Bivic, M. Leitges and C. M. Niessen (2007).** "Role of aPKC isoforms and their binding partners Par3 and Par6 in epidermal barrier formation." *Journal of Investigative Dermatology* 127(4): 782-791.
- Hennings, H., D. Michael, C. Cheng, P. Steinert, K. Holbrook and S. H. Yuspa (1980).** "Calcium regulation of growth and differentiation of mouse epidermal cells in culture." *Cell* 19(1): 245-254.
- Herbig, M. E., P. Houdek, S. Gorissen, M. Zorn-Kruppa, E. Wladykowski, T. Volksdorf, S. Grzybowski, G. Kolios, C. Willers, H. Mallwitz, I. Moll and J. M. Brandner (2015).** "A custom tailored model to investigate skin penetration in porcine skin and its comparison with human skin." *European journal of pharmaceuticals and biopharmaceutics : official journal of Arbeitsgemeinschaft fur Pharmazeutische Verfahrenstechnik e.V* doi: 10.1016/j.ejpb.2015.03.030. [Epub ahead of print].
- Hickerson, R. P., M. A. Flores, D. Leake, M. F. Lara, C. H. Contag, S. A. Leachman and R. L. Kaspar (2011).** "Use of Self-Delivery siRNAs to Inhibit Gene Expression in an Organotypic Pachyonychia Congenita Model." *Journal of Investigative Dermatology* 131(5): 1037-1044.
- Higaki, S., M. Morohashi, T. Yamagishi and Y. Hasegawa (1999).** "Comparative study of staphylococci from the skin of atopic dermatitis patients and from healthy subjects." *International Journal of Dermatology* 38(4): 265-269.

- Hirasawa, Y., T. Takai, T. Nakamura, K. Mitsuishi, H. Gunawan, H. Suto, T. Ogawa, X.-L. Wang, S. Ikeda, K. Okumura and H. Ogawa (2010). "Staphylococcus aureus Extracellular Protease Causes Epidermal Barrier Dysfunction." *Journal of Investigative Dermatology* 130(2): 614-617.
- Holtfreter, S., D. Grumann, M. Schmudde, H. T. T. Nguyen, P. Eichler, B. Strommenger, K. Kopron, J. Kolata, S. Giedrys-Kalemba, I. Steinmetz, W. Witte and B. M. Bröker (2007). "Clonal Distribution of Superantigen Genes in Clinical Staphylococcus aureus Isolates." *Journal of Clinical Microbiology* 45(8): 2669-2680.
- Hönzke, S., L. Wallmeyer, A. Ostrowski, M. Radbruch, L. Mundhenk, M. Schafer-Korting and S. Hedtrich (2016). "Influence of Th2 Cytokines on the Cornified Envelope, Tight Junction Proteins, and  $\alpha$ -Defensins in Filaggrin-Deficient Skin Equivalents." *Journal of Investigative Dermatology* 136(3): 631-639.
- Horsburgh, M. J., J. L. Aish, I. J. White, L. Shaw, J. K. Lithgow and S. J. Foster (2002). " $\sigma$ B Modulates Virulence Determinant Expression and Stress Resistance: Characterization of a Functional rsbU Strain Derived from Staphylococcus aureus 8325-4." *Journal of Bacteriology* 184(19): 5457-5467.
- Howell, M. D., B. E. Kim, P. Gao, A. V. Grant, M. Boguniewicz, A. DeBenedetto, L. Schneider, L. A. Beck, K. C. Barnes and D. Y. M. Leung (2007). "Cytokine modulation of atopic dermatitis filaggrin skin expression." *Journal of Allergy and Clinical Immunology* 120(1): 150-155.
- Huang, J. T., M. Abrams, B. Tloutan, A. Rademaker and A. S. Paller (2009). "Treatment of Staphylococcus aureus Colonization in Atopic Dermatitis Decreases Disease Severity." *Pediatrics* 123(5): e808-e814.
- Huber, D., M. S. Balda and K. Matter (2000). "Occludin modulates transepithelial migration of neutrophils." *The Journal of Biological Chemistry* 275(8): 5773-5778.
- Igawa, S., M. Kishibe, M. Murakami, M. Honma, H. Takahashi, H. Iizuka and A. Ishida-Yamamoto (2011). "Tight junctions in the stratum corneum explain spatial differences in corneodesmosome degradation." *Experimental Dermatology* 20(1): 53-57.
- Inoshima, N., Y. Wang and J. B. Wardenburg (2012). "Genetic Requirement for ADAM10 in Severe Staphylococcus aureus Skin Infection." *The Journal of investigative dermatology* 132(5): 1513-1516.
- Ivanov, A. I., A. Nusrat and C. Parkos (2008). "The Epithelium in Inflammatory Bowel Disease: Potential Role of Endocytosis of Junctional Proteins in Barrier Disruption." *Novartis Foundation Symposium* 263: 115-132.
- Iwase, T., Y. Uehara, H. Shinji, A. Tajima, H. Seo, K. Takada, T. Agata and Y. Mizunoe (2010). "Staphylococcus epidermidis Esp inhibits Staphylococcus aureus biofilm formation and nasal colonization." *Nature* 465(7296): 346-349.
- Jakasa, I., C. M. De Jongh, M. M. Verberk, J. D. Bos and S. Kežić (2006). "Percutaneous penetration of sodium lauryl sulphate is increased in uninvolved skin of patients with atopic dermatitis compared with control subjects." *British Journal of Dermatology* 155(1): 104-109.

**Jakasa, I., E. S. Koster, F. Calkoen, W. H. Irwin McLean, L. E. Campbell, J. D. Bos, M. M. Verberk and S. Kezic (2011).** "Skin Barrier Function in Healthy Subjects and Patients with Atopic Dermatitis in Relation to Filaggrin Loss-of-Function Mutations." *Journal of Investigative Dermatology* 131(2): 540-542.

**Jakasa, I., M. M. Verberk, M. Esposito, J. D. Bos and S. Kezic (2007).** "Altered Penetration of Polyethylene Glycols into Uninvolved Skin of Atopic Dermatitis Patients." *Journal of Investigative Dermatology* 127(1): 129-134.

**Jarraud, S., C. Mougel, J. Thioulouse, G. Lina, H. Meugnier, F. Forey, X. Nesme, J. Etienne and F. Vandenesch (2002).** "Relationships between *Staphylococcus aureus* genetic background, virulence factors, agr groups (alleles), and human disease." *Infection and Immunity* 70(2): 631 - 641.

**Jung, E. G., M. Augustin, F. A. Bahmer, J. A. Bahmer, C. Bayerl, H. P. J. Boonen, E. Coors, M. Fischer, M. Grimm, I. Hadshiew, U. Hauswirth, H. Hofmann, E. G. Jung, W. Kimmig, E. Knußmann-Hartig, M. Köberle, K. Kohrmeyer, M. Meissner, X. Miller, I. Moll, M.-A. Radtke, A. Rauterberg, C. Rose, D. Schoch, W. Schulze, U. Siemann-Harms, S. Stangl, A. Tsianakas, D. Varwig-Janßen, V. Voigtländer, J. Weiß, R. Weißbecher and J. Witte (2016).** *Dermatologie*. Stuttgart, New York, Georg Thieme Verlag.

**Jungersted, J. M., H. Scheer, M. Mempel, H. Baurecht, L. Cifuentes, J. K. Høgh, L. I. Hellgren, G. B. E. Jemec, T. Agner and S. Weidinger (2010).** "Stratum corneum lipids, skin barrier function and filaggrin mutations in patients with atopic eczema." *Allergy* 65(7): 911-918.

**Kachar, B. and T. S. Reese (1982).** "Evidence for the lipidic nature of tight junction strands." *Nature* 296(5856): 464-466.

**Kawasaki, H., K. Nagao, A. Kubo, T. Hata, A. Shimizu, H. Mizuno, T. Yamada and M. Amagai (2012).** "Altered stratum corneum barrier and enhanced percutaneous immune responses in filaggrin-null mice." *The Journal of allergy and clinical immunology* 129(6): 1538-1546 e1536.

**Kawedia, J. D., M. L. Nieman, G. P. Boivin, J. E. Melvin, K.-I. Kikuchi, A. R. Hand, J. N. Lorenz and A. G. Menon (2007).** "Interaction between transcellular and paracellular water transport pathways through Aquaporin 5 and the tight junction complex." *Proceedings of the National Academy of Sciences* 104(9): 3621-3626.

**Kenshalo, D. R. (1970).** Psychophysical Studies of Temperature Sensitivity. *Contributions to Sensory Physiology*. N. William D, Elsevier. **Volume 4**: 19-74.

**Kiatsurayanon, C., F. Niyonsaba, R. Smithrithee, T. Akiyama, H. Ushio, M. Hara, K. Okumura, S. Ikeda and H. Ogawa (2014).** "Host Defense (Antimicrobial) Peptide, Human beta-Defensin-3, Improves the Function of the Epithelial Tight-Junction Barrier in Human Keratinocytes." *Journal of Investigative Dermatology* 134(8): 2163-2173.

**Kirschner, N. and J. M. Brandner (2012).** "Barriers and more: functions of tight junction proteins in the skin." *Annals of the New York Academy of Sciences* 1257: 158-166.

- Kirschner, N., M. Haftek, C. M. Niessen, M. J. Behne, M. Furuse, I. Moll and J. M. Brandner (2011). "CD44 regulates tight-junction assembly and barrier function." *Journal of Investigative Dermatology* 131(4): 932-943.
- Kirschner, N., P. Houdek, M. Fromm, I. Moll and J. M. Brandner (2010). "Tight junctions form a barrier in human epidermis." *European Journal of Cell Biology* 89(11): 839-842.
- Kirschner, N., C. Poetzel, P. von den Driesch, E. Wladykowski, I. Moll, M. J. Behne and J. M. Brandner (2009). "Alteration of tight junction proteins is an early event in psoriasis: putative involvement of proinflammatory cytokines." *American Journal of Pathology* 175(3): 1095-1106.
- Kirschner, N., R. Rosenthal, M. Furuse, I. Moll, M. Fromm and J. M. Brandner (2013). "Contribution of Tight Junction Proteins to Ion, Macromolecule, and Water Barrier in Keratinocytes." *Journal of Investigative Dermatology* 133 1161-1169. .
- Kirschner, N., R. Rosenthal, D. Günzel, I. Moll and J. M. Brandner (2012). "Tight junctions and differentiation – a chicken or the egg question?" *Experimental Dermatology* 21(3): 171-175.
- Kloos, W. E. and M. S. Musselwhite (1975). "Distribution and Persistence of Staphylococcus and Micrococcus Species and Other Aerobic Bacteria on Human Skin." *Applied Microbiology* 30(3): 381-395.
- Kobayashi, S. D., K. R. Braughton, A. M. Palazzolo-Ballance, A. D. Kennedy, E. Sampaio, E. Kristosturyan, A. R. Whitney, D. E. Sturdevant, D. W. Dorward, S. M. Holland, B. N. Kreiswirth, J. M. Musser and F. R. DeLeo (2010). "Rapid Neutrophil Destruction following Phagocytosis of Staphylococcus aureus." *Journal of Innate Immunity* 2(6): 560-575.
- Köllisch, G., B. N. Kalali, V. Voelcker, R. Wallich, H. Behrendt, J. Ring, S. Bauer, T. Jakob, M. Mempel and M. Ollert (2005). "Various members of the Toll-like receptor family contribute to the innate immune response of human epidermal keratinocytes." *Immunology* 114(4): 531-541.
- Kolodziej, L. E., J. P. Lodolce, J. E. Chang, J. R. Schneider, W. A. Grimm, S. J. Bartulis, X. Zhu, J. S. Messer, S. F. Murphy, N. Reddy, J. R. Turner and D. L. Boone (2011). "TNFAIP3 Maintains Intestinal Barrier Function and Supports Epithelial Cell Tight Junctions." *PLoS One* 6(10): e26352.
- Kong, H. H., J. Oh, C. Deming, S. Conlan, E. A. Grice, M. A. Beatson, E. Nomicos, E. C. Polley, H. D. Komarow, N. C. S. Program, P. R. Murray, M. L. Turner and J. A. Segre (2012). "Temporal shifts in the skin microbiome associated with disease flares and treatment in children with atopic dermatitis." *Genome Res* 22(5): 850-859.
- Kubo, A., K. Nagao and M. Amagai (2012). "Epidermal barrier dysfunction and cutaneous sensitization in atopic diseases." *The Journal of Clinical Investigation* 122(2): 440-447.
- Kubo, A., K. Nagao, M. Yokouchi, H. Sasaki and M. Amagai (2009). "External antigen uptake by Langerhans cells with reorganization of epidermal tight junction barriers." *The Journal of Experimental Medicine* 206(13): 2937-2946.

- Kubo, T., K. Sugimoto, T. Kojima, N. Sawada, N. Sato and S. Ichimiya (2014).** "Tight junction protein claudin-4 is modulated via DeltaNp63 in human keratinocytes." *Biochemical and biophysical research communications* 455(3-4): 205-211.
- Kunkel, S. L., T. Standiford, K. Kasahara and R. M. Strieter (1991).** "Interleukin-8 (IL-8): The Major Neutrophil Chemotactic Factor in the Lung." *Experimental Lung Research* 17(1): 17-23.
- Kuo, I. H., A. Carpenter-Mendini, T. Yoshida, L. Y. McGirt, A. I. Ivanov, K. C. Barnes, R. L. Gallo, A. W. Borkowski, K. Yamasaki, D. Y. Leung, S. N. Georas, A. De Benedetto and L. A. Beck (2013).** "Activation of epidermal toll-like receptor 2 enhances tight junction function: implications for atopic dermatitis and skin barrier repair." *J Invest Dermatol* 133(4): 988-998.
- Lai, Y., A. L. Cogen, K. A. Radek, H. J. Park, D. T. MacLeod, A. Leichtle, A. F. Ryan, A. Di Nardo and R. L. Gallo (2010).** "Activation of TLR2 by a Small Molecule Produced by *Staphylococcus epidermidis* Increases Antimicrobial Defense against Bacterial Skin Infections." *Journal of Investigative Dermatology* 130(9): 2211-2221.
- Latz, E., T. S. Xiao and A. Stutz (2013).** "Activation and regulation of the inflammasomes." *Nature reviews. Immunology* 13(6): 10.1038/nri3452.
- Lee, C. H., H. Y. Chuang, C. C. Shih, S. B. Jong, C. H. Chang and H. S. Yu (2006).** "Transepidermal water loss, serum IgE and  $\beta$ -endorphin as important and independent biological markers for development of itch intensity in atopic dermatitis." *British Journal of Dermatology* 154(6): 1100-1107.
- Leung, D. Y. M., M. Boguniewicz, M. D. Howell, I. Nomura and Q. A. Hamid (2004).** "New insights into atopic dermatitis." *The Journal of Clinical Investigation* 113(5): 651-657.
- Leyden, J. J., R. R. Marples and A. M. Kligman (1974).** "Staphylococcus aureus in the lesions of atopic dermatitis." *British Journal of Dermatology* 90(5): 525-525.
- Li, A., P. J. Simmons and P. Kaur (1998).** "Identification and isolation of candidate human keratinocyte stem cells based on cell surface phenotype." *Proceedings of the National Academy of Sciences* 95(7): 3902-3907.
- Limbago, B., G. E. Fosheim, V. Schoonover, C. E. Crane, J. Nadle, S. Petit, D. Heltzel, S. M. Ray, L. H. Harrison, R. Lynfield, G. Dumyati, J. M. Townes, W. Schaffner, Y. Mu, S. K. Fridkin and f. t. A. B. C. s. M. Investigators (2009).** "Characterization of Methicillin-Resistant *Staphylococcus aureus* Isolates Collected in 2005 and 2006 from Patients with Invasive Disease: a Population-Based Analysis." *Journal of Clinical Microbiology* 47(5): 1344-1351.
- Livak, K. J. and T. D. Schmittgen (2001).** "Analysis of Relative Gene Expression Data Using Real-Time Quantitative PCR and the 2- $\Delta\Delta$ CT Method." *Methods* 25(4): 402-408.
- Madara, J. L. (1998).** "Regulation of the Movement of Solutes across Tight Junctions." *Annual Review of Physiology* 60(1): 143-159.

- Madison, K. C., D. C. Swartzendruber, W. Wertz and D. T. Downing (1989).** "Murine Keratinocyte Cultures Grown at the Air/Medium Interface Synthesize Stratum Corneum Lipids and "Recycle" Linoleate During Differentiation." *Journal of Investigative Dermatology* 93(1): 10-17.
- Malik, Z., E. Roscioli, J. Murphy, J. Ou, A. Bassiouni, P.-J. Wormald and S. Vreugde (2015).** "Staphylococcus aureus impairs the airway epithelial barrier in vitro." *International Forum of Allergy & Rhinology* 5(6): 551-556.
- Marchiando, A. M., L. Shen, W. V. Graham, C. R. Weber, B. T. Schwarz, J. R. Austin, 2nd, D. R. Raleigh, Y. Guan, A. J. Watson, M. H. Montrose and J. R. Turner (2010).** "Caveolin-1-dependent occludin endocytosis is required for TNF-induced tight junction regulation in vivo." *The Journal of Cell Biology* 189(1): 111-126.
- Matsukawa, Y., V. H. L. Lee, E. D. Crandall and K.-J. Kim (1997).** "Size-Dependent Dextran Transport across Rat Alveolar Epithelial Cell Monolayers." *Journal of pharmaceutical sciences* 86(3): 305-309.
- Matter, K., S. Aijaz, A. Tsapara and M. S. Balda (2005).** "Mammalian tight junctions in the regulation of epithelial differentiation and proliferation." *Current Opinion in Cell Biology* 17(5): 453-458.
- McCarthy, K. M., I. B. Skare, M. C. Stankewich, M. Furuse, S. Tsukita, R. A. Rogers, R. D. Lynch and E. E. Schneeberger (1996).** "Occludin is a functional component of the tight junction." *Journal of Cell Science* 109 ( Pt 9): 2287-2298.
- Menzies, B. E. and A. Kenoyer (2005).** "Staphylococcus aureus Infection of Epidermal Keratinocytes Promotes Expression of Innate Antimicrobial Peptides." *Infection and Immunity* 73(8): 5241-5244.
- Menzies, B. E. and A. Kenoyer (2006).** "Signal transduction and nuclear responses in Staphylococcus aureus-induced expression of human beta-defensin 3 in skin keratinocytes." *Infection and Immunity* 74.
- Mertens, A. E., T. P. Rygiel, C. Olivo, R. van der Kammen and J. G. Collard (2005).** "The Rac activator Tiam1 controls tight junction biogenesis in keratinocytes through binding to and activation of the Par polarity complex." *Journal of Cell Biology* 170(7): 1029-1037.
- Micallef, L., F. Belaubre, A. Pinon, C. Jayat-Vignoles, C. Delage, M. Charveron and A. Simon (2009).** "Effects of extracellular calcium on the growth-differentiation switch in immortalized keratinocyte HaCaT cells compared with normal human keratinocytes." *Experimental Dermatology* 18(2): 143-151.
- Michikawa, H., J. Fujita-Yoshigaki and H. Sugiya (2008).** "Enhancement of barrier function by overexpression of claudin-4 in tight junctions of submandibular gland cells." *Cell and tissue research* 334(2): 255-264.
- Mildner, M., C. Ballaun, M. Stichenwirth, R. Bauer, R. Gmeiner, M. Buchberger, V. Mlitz and E. Tschachler (2006).** "Gene silencing in a human organotypic skin model." *Biochemical and biophysical research communications* 348(1): 76-82.
- Mildner, M., J. Jin, L. Eckhart, S. Kezic, F. Gruber, C. Barresi, C. Stremnitzer, M. Buchberger, V. Mlitz, C. Ballaun, B. Sterniczky, D. Födinger and E. Tschachler (2010).** "Knockdown of Filaggrin Impairs Diffusion Barrier



Function and Increases UV Sensitivity in a Human Skin Model." *Journal of Investigative Dermatology* 130(9): 2286-2294.

**Miller, L. S. and J. S. Cho (2011).** "Immunity against *Staphylococcus aureus* cutaneous infections." *Nature Reviews Immunology* 11(8): 505-518.

**Mineta, K., Y. Yamamoto, Y. Yamazaki, H. Tanaka, Y. Tada, K. Saito, A. Tamura, M. Igarashi, T. Endo, K. Takeuchi and S. Tsukita (2011).** "Predicted expansion of the claudin multigene family." *FEBS Letters* 585(4): 606-612.

**Miyauchi, E., J. O'Callaghan, L. F. Butto, G. Hurley, S. Melgar, S. Tanabe, F. Shanahan, K. Nally and P. W. O'Toole (2012).** "Mechanism of protection of transepithelial barrier function by *Lactobacillus salivarius*: strain dependence and attenuation by bacteriocin production." *American journal of physiology. Gastrointestinal and liver physiology* 303(9): G1029-1041.

**Moll, I. (2016).** Dermatologie Stuttgart, Thieme.

**Monteiro, A. C. and C. A. Parkos (2012).** "Intracellular mediators of JAM-A-dependent epithelial barrier function." *Annals of the New York Academy of Sciences* 1257: 115-124.

**Morita, K., M. Itoh, M. Saitou, Y. Ando-Akatsuka, M. Furuse, K. Yoneda, S. Imamura, K. Fujimoto and S. Tsukita (1998).** "Subcellular distribution of tight junction-associated proteins (occludin, ZO-1, ZO-2) in rodent skin." *Journal of Investigative Dermatology* 110: 862-866.

**Naik, S., N. Bouladoux, C. Wilhelm, M. J. Molloy, R. Salcedo, W. Kastenmuller, C. Deming, M. Quinones, L. Koo, S. Conlan, S. Spencer, J. A. Hall, A. Dzutsev, H. Kong, D. J. Campbell, G. Trinchieri, J. A. Segre and Y. Belkaid (2012).** "Compartmentalized Control of Skin Immunity by Resident Commensals." *Science* 337(6098): 1115-1119.

**Neis, M. M., B. Peters, A. Dreuw, J. Wenzel, T. Bieber, C. Mauch, T. Krieg, S. Stanzel, P. C. Heinrich, H. F. Merk, A. Bosio, J. M. Baron and H. M. Hermanns (2006).** "Enhanced expression levels of IL-31 correlate with IL-4 and IL-13 in atopic and allergic contact dermatitis." *Journal of Allergy and Clinical Immunology* 118(4): 930-937.

**Niehues, H., J. Schalkwijk, I. M. van Vlijmen-Willems, D. Rodijk-Olthuis, M. M. van Rossum, E. Wladykowski, J. M. Brandner, E. H. van den Bogaard and P. L. Zeeuwen (2016).** "Epidermal equivalents of filaggrin null keratinocytes do not show impaired skin barrier function." *The Journal of allergy and clinical immunology*.

**Niessen, C. M. (2007).** "Tight junctions/adherens junctions: basic structure and function." *Journal of Investigative Dermatology* 127(11): 2525-2532.

**Novick, R. P., H. F. Ross, S. J. Projan, J. Kornblum, B. Kreiswirth and S. Moghazeh (1993).** "Synthesis of staphylococcal virulence factors is controlled by a regulatory RNA molecule." *The EMBO Journal* 12(10): 3967-3975.

- Nutan, F. N. U., A. J. Kanwar and D. Parsad (2012).** "The effect of topically applied corticosteroids on interleukin 1 $\beta$  levels in patients with atopic dermatitis." *Journal of the European Academy of Dermatology and Venereology* 26(8): 1020-1022.
- O'Neill, C. A. and D. Garrod (2011).** "Tight junction proteins and the epidermis." *Experimental Dermatology* 20(2): 88-91.
- Ogston, A. (1882).** "Micrococcus Poisoning." *Journal of Anatomy and Physiology* 17(Pt 1): 24-58.
- Ohnemus, U., K. Kohrmeyer, P. Houdek, H. Rohde, E. Wladykowski, S. Vidal, M. A. Horstkotte, M. Aepfelbacher, N. Kirschner, M. J. Behne, I. Moll and J. M. Brandner (2008).** "Regulation of epidermal tight-junctions (TJ) during infection with exfoliative toxin-negative Staphylococcus strains." *Journal of Investigative Dermatology* 128(4): 906-916.
- Opipari, A. W., H. M. Hu, R. Yabkowitz and V. M. Dixit (1992).** "The A20 zinc finger protein protects cells from tumor necrosis factor cytotoxicity." *Journal of Biological Chemistry* 267(18): 12424-12427.
- Orenstein, A. (2011).** "The Discovery and Naming of Staphylococcus aureus." *Periodical [serial online]. Date. Available from.*
- Otto, M. (2009).** "Staphylococcus epidermidis - the 'accidental' pathogen." *Nature Reviews Microbiology* 7(8): 555-567.
- Otto, M. (2013).** "Community-associated MRSA: what makes them special?" *International journal of medical microbiology : IJMM* 303(0): 324-330.
- Ozinsky, A., D. M. Underhill, J. D. Fontenot, A. M. Hajjar, K. D. Smith, C. B. Wilson, L. Schroeder and A. Aderem (2000).** "The repertoire for pattern recognition of pathogens by the innate immune system is defined by cooperation between Toll-like receptors." *Proceedings of the National Academy of Sciences* 97(25): 13766-13771.
- Painter, K. L., A. Krishna, S. Wigneshweraraj and A. M. Edwards (2014).** "What role does the quorum-sensing accessory gene regulator system play during Staphylococcus aureus bacteremia?" *Trends in Microbiology* 22(12): 676-685.
- Palmer, C. N., A. D. Irvine, A. Terron-Kwiatkowski, Y. Zhao, H. Liao, S. P. Lee, D. R. Goudie, A. Sandilands, L. E. Campbell, F. J. Smith, G. M. O'Regan, R. M. Watson, J. E. Cecil, S. J. Bale, J. G. Compton, J. J. DiGiovanna, P. Fleckman, S. Lewis-Jones, G. Arseculeratne, A. Sergeant, C. S. Munro, B. El Houate, K. McElreavey, L. B. Halkjaer, H. Bisgaard, S. Mukhopadhyay and W. H. McLean (2006).** "Common loss-of-function variants of the epidermal barrier protein filaggrin are a major predisposing factor for atopic dermatitis." *Nature genetics* 38(4): 441-446.
- Park, K., R. Ommori, K. Imoto and H. Asada (2014).** "Epidermal growth factor receptor inhibitors selectively inhibit the expressions of human  $\beta$ -defensins induced by Staphylococcus epidermidis." *Journal of Dermatological Science* 75(2): 94-99.

- Peterson, M. M., J. L. Mack, P. R. Hall, A. A. Alsup, S. M. Alexander, E. K. Sully, Y. S. Sawires, A. L. Cheung, M. Otto and H. D. Gresham (2008). "Apolipoprotein B Is an Innate Barrier against Invasive *Staphylococcus aureus* Infection." *Cell Host & Microbe* 4(6): 555-566.
- Poumay, Y. and A. Coquette (2007). "Modelling the human epidermis in vitro: tools for basic and applied research." *Archives of Dermatological Research* 298(8): 361-369.
- Poumay, Y., F. Dupont, S. Marcoux, M. Leclercq-Smekens, M. Hérin and A. Coquette (2004). "A simple reconstructed human epidermis: preparation of the culture model and utilization in in vitro studies." *Archives of Dermatological Research* 296(5): 203-211.
- Priest, N. K., J. K. Rudkin, E. J. Feil, J. M. H. van den Elsen, A. Cheung, S. J. Peacock, M. Laabei, D. A. Lucks, M. Recker and R. C. Massey (2012). "From genotype to phenotype: can systems biology be used to predict *Staphylococcus aureus* virulence?" *Nature Reviews Microbiology* 10(11): 791-797.
- Pruniéras, M., M. Régnier and D. Woodley (1983). "Methods for Cultivation of Keratinocytes with an Air-Liquid Interface." *Journal of Investigative Dermatology* 81(1, Supplement): S28-S33.
- Pummi, K., M. Malminen, H. Aho, S.-L. Karvonen, J. Peltonen and S. Peltonen (2001). "Epidermal tight junctions: ZO-1 and occludin are expressed in mature, developing, and affected skin and in vitro differentiating keratinocytes." *Journal of Investigative Dermatology* 117: 1050-1058.
- Rachow, S., M. Zorn-Kruppa, U. Ohnemus, N. Kirschner, S. Vidal-y-Sy, P. von den Driesch, C. Bornchen, J. Eberle, M. Mildner, E. Vettorazzi, R. Rosenthal, I. Moll and J. M. Brandner (2013). "Occludin is involved in adhesion, apoptosis, differentiation and Ca<sup>2+</sup>-homeostasis of human keratinocytes: implications for tumorigenesis." *PLoS One* 8(2): e55116.
- Radoja, N., A. Gazel, T. Banno, S. Yano and M. Blumenberg (2006). "Transcriptional profiling of epidermal differentiation." *Physiological Genomics* 27(1): 65.
- Rahn, E., K. Thier, P. Petermann, M. Rübsam, P. Staeheli, S. Iden, C. M. Niessen and D. Knebel-Mörsdorf (2017). "Epithelial Barriers in Murine Skin during Herpes Simplex Virus 1 Infection: The Role of Tight Junction Formation." *Journal of Investigative Dermatology* 137(4): 884-893.
- Ramirez, S. H., S. Fan, H. Dykstra, S. Rom, A. Mercer, N. L. Reichenbach, L. Gofman and Y. Persidsky (2013). "Inhibition of Glycogen Synthase Kinase 3 $\beta$  Promotes Tight Junction Stability in Brain Endothelial Cells by Half-Life Extension of Occludin and Claudin-5." *PLoS One* 8(2): e55972.
- Ramirez, S. H., S. Fan, M. Zhang, A. Papugani, N. Reichenbach, H. Dykstra, A. J. Mercer, R. F. Tuma and Y. Persidsky (2010). "Inhibition of Glycogen Synthase Kinase 3 $\beta$  (GSK3 $\beta$ ) Decreases Inflammatory Responses in Brain Endothelial Cells." *The American Journal of Pathology* 176(2): 881-892.
- Rassner, G. (2009). *Dermatologie : Lehrbuch und Atlas (Dermatology, Textbook and Atlas)*. München, Elsevier, Urban & Fischer.

- Rheinwald, J. G. and H. Green (1975a).** "Formation of a keratinizing epithelium in culture by a cloned cell line derived from a teratoma." *Cell* 6(3): 317-330.
- Rheinwald, J. G. and H. Green (1975b).** "Serial cultivation of strains of human epidermal keratinocytes: the formation of keratinizing colonies from single cells." *Cell* 6(3): 331-342.
- Robertson, E. D., L. Weir, M. Romanowska, I. M. Leigh and A. A. Panteleyev (2012).** "ARNT controls the expression of epidermal differentiation genes through HDAC- and EGFR-dependent pathways." *Journal of Cell Science* 125(14): 3320.
- Rohde, H., E. C. Burandt, N. Siemssen, L. Frommelt, C. Burdelski, S. Wurster, S. Scherpe, A. P. Davies, L. G. Harris, M. A. Horstkotte, J. K. M. Knobloch, C. Rangunath, J. B. Kaplan and D. Mack (2007).** "Polysaccharide intercellular adhesin or protein factors in biofilm accumulation of *Staphylococcus epidermidis* and *Staphylococcus aureus* isolated from prosthetic hip and knee joint infections." *Biomaterials* 28(9): 1711-1720.
- Rose, W. A., II, C. L. McGowin, R. A. Spagnuolo, T. D. Eaves-Pyles, V. L. Popov and R. B. Pyles (2012).** "Commensal Bacteria Modulate Innate Immune Responses of Vaginal Epithelial Cell Multilayer Cultures." *PLoS One* 7(3): e32728.
- Rosenbach, A. J. F. (1884).** Mikro-organismen bei den Wund-infections-krankheiten des Menschen, JF Bergmann.
- Rosenstein, R. and F. Götz (2010).** "Genomic differences between the food-grade *Staphylococcus carnosus* and pathogenic staphylococcal species." *International Journal of Medical Microbiology* 300(2): 104-108.
- Rosenstein, R., C. Nerz, L. Biswas, A. Resch, G. Raddatz, S. C. Schuster and F. Götz (2009).** "Genome Analysis of the Meat Starter Culture Bacterium *Staphylococcus carnosus* TM300." *Applied and Environmental Microbiology* 75(3): 811-822.
- Ross-Hansen, K., A. Linneberg, J. D. Johansen, L. G. Hersoug, C. Brasch-Andersen, T. Menne and J. P. Thyssen (2013).** "The role of glutathione S-transferase and claudin-1 gene polymorphisms in contact sensitization: a cross-sectional study." *British Journal of Dermatology* 168(4): 762-770.
- Rothman, P. F. (1944).** "The physiology of the skin." *Annual Review of Physiology* 6: 195-224.
- Rouaud-Tinguely, P., D. Boudier, L. Marchand, V. Barruche, S. Bordes, H. Coppin, M. P. Roth and B. Closs (2015).** "From the morphological to the transcriptomic characterization of a compromised three-dimensional in vitro model mimicking atopic dermatitis." *British Journal of Dermatology* 173(4): 1006-1014.
- Saitou, M., M. Furuse, H. Sasaki, J. D. Schulzke, M. Fromm, H. Takano, T. Noda and S. Tsukita (2000).** "Complex phenotype of mice lacking occludin, a component of tight junction strands." *Molecular Biology of the Cell* 11(12): 4131-4142.

- Sakakibara, A., M. Furuse, M. Saitou, Y. Ando-Akatsuka and S. Tsukita (1997).** "Possible Involvement of Phosphorylation of Occludin in Tight Junction Formation." *The Journal of Cell Biology* 137(6): 1393-1401.
- Sánchez-Pulido, L., F. Martín-Belmonte, A. Valencia and M. A. Alonso (2002).** "MARVEL: a conserved domain involved in membrane apposition events." *Trends in Biochemical Sciences* 27(12): 599-601.
- Sanford, J. A. and R. L. Gallo (2013).** "Functions of the skin microbiota in health and disease." *Seminars in immunology* 25(5): 370-377.
- Sator, P.-G., J. B. Schmidt and H. Hönigsmann (2003).** "Comparison of epidermal hydration and skin surface lipids in healthy individuals and in patients with atopic dermatitis." *Journal of the American Academy of Dermatology* 48(3): 352-358.
- Scheuplein, R. J. and I. H. Blank (1971).** "Permeability of the skin." *Physiological Reviews* 51(4): 702.
- Schneeberger, E. E. and R. D. Lynch (2004).** "The tight junction: a multifunctional complex." *American Journal of Physiology - Cell Physiology* 286(6): C1213-1228.
- Schweizer, M. L., J. P. Furuno, G. Sakoulas, J. K. Johnson, A. D. Harris, M. D. Shardell, J. C. McGregor, K. A. Thom and E. N. Perencevich (2011).** "Increased Mortality with Accessory Gene Regulator (agr) Dysfunction in *Staphylococcus aureus* among Bacteremic Patients." *Antimicrobial Agents and Chemotherapy* 55(3): 1082-1087.
- Secor, P. A., J. A. Garth, P. Fleckman, J. E. Olerud, K. McInnemei and P. S. Stewart (2011).** "Staphylococcus aureus biofilm and planktonic cultures differentially impact gene expression, mapk phosphorylation, and cytokine production in human keratinocytes." *BMC Microbiology* 11.
- Serre, G., V. Mils, M. Haftek, C. Vincent, F. Croute, A. Réano, J.-P. Ouhayoun, S. Bettinger and J.-P. Soleihavoup (1991).** "Identification of Late Differentiation Antigens of Human Cornified Epithelia, Expressed in Re-Organized Desmosomes and Bound to Cross-Linked Envelope." *Journal of Investigative Dermatology* 97(6): 1061-1072.
- Seth, A., F. Yan, D. B. Polk and R. K. Rao (2008).** "Probiotics ameliorate the hydrogen peroxide-induced epithelial barrier disruption by a PKC- and MAP kinase-dependent mechanism." *American journal of physiology. Gastrointestinal and liver physiology* 294(4): G1060-1069.
- Shen, L., C. R. Weber, D. R. Raleigh, D. Yu and J. R. Turner (2011).** "Tight junction pore and leak pathways: a dynamic duo." *Annual Review of Physiology* 73: 283-309.
- Shompole, S., K. T. Henon, L. E. Liou, K. Dziewanowska, G. A. Bohach and K. W. Bayles (2003).** "Biphasic intracellular expression of *Staphylococcus aureus* virulence factors and evidence for Agr-mediated diffusion sensing." *Molecular Microbiology* 49(4): 919-927.

- Sjöström, J.-E. and L. Philipson (1974).** "Role of the  $\phi$ 11 Phage Genome in Competence of *Staphylococcus aureus*." *Journal of Bacteriology* 119(1): 19-32.
- Smyth, D. S., J. M. Kafer, G. A. Wasserman, L. Velickovic, B. Mathema, R. S. Holzman, T. A. Knipe, K. Becker, C. von Eiff, G. Peters, L. Chen, B. N. Kreiswirth, R. P. Novick and B. Shopsin (2012).** "Nasal Carriage as a Source of agr-Defective *Staphylococcus aureus* Bacteremia." *The Journal of Infectious Diseases* 206(8): 1168-1177.
- Soter, N. A. (1989).** "Morphology of atopic eczema." *Allergy* 44(s9): 16-19.
- Stamatovic, S. M., A. M. Johnson, N. Sladojevic, R. F. Keep and A. V. Andjelkovic (2017).** "Endocytosis of tight junction proteins and the regulation of degradation and recycling." *Annals of the New York Academy of Sciences* 1397(1): 54-65.
- Stevens, N. T., I. Sadovskaya, S. Jabbouri, T. Sattar, J. P. O'Gara, H. Humphreys and C. M. Greene (2009).** "Staphylococcus epidermidis polysaccharide intercellular adhesin induces IL-8 expression in human astrocytes via a mechanism involving TLR2." *Cellular microbiology* 11(3): 421-432.
- Stevenson, B. R., J. D. Silicano, M. Mooseker and D. A. Goodenough (1986).** "Identification of ZO-1: a high molecular weight polypeptide associated with the tight junction (zonula occludens) in a variety of epithelia." *Journal of Cell Biology* 103: 755-766.
- Sugawara, T., N. Iwamoto, M. Akashi, T. Kojima, J. Hisatsune, M. Sugai and M. Furuse (2013).** "Tight junction dysfunction in the stratum granulosum leads to aberrant stratum corneum barrier function in claudin-1-deficient mice." *Journal of Dermatological Science* 70(1): 12-18.
- Sully, E. K., N. Malachowa, B. O. Elmore, S. M. Alexander, J. K. Femling, B. M. Gray, F. R. DeLeo, M. Otto, A. L. Cheung, B. S. Edwards, L. A. Sklar, A. R. Horswill, P. R. Hall and H. D. Gresham (2014).** "Selective Chemical Inhibition of agr Quorum Sensing in *Staphylococcus aureus* Promotes Host Defense with Minimal Impact on Resistance." *PLOS Pathogens* 10(6): e1004174.
- Sultana, R., A. J. McBain and C. A. O'Neill (2013).** "Strain-Dependent Augmentation of Tight-Junction Barrier Function in Human Primary Epidermal Keratinocytes by *Lactobacillus* and *Bifidobacterium* Lysates." *Applied and Environmental Microbiology* 79(16): 4887-4894.
- Sun, F., H. Liang, X. Kong, S. Xie, H. Cho, X. Deng, Q. Ji, H. Zhang, S. Alvarez, L. M. Hicks, T. Bae, C. Luo, H. Jiang and C. He (2012).** "Quorum-sensing agr mediates bacterial oxidation response via an intramolecular disulfide redox switch in the response regulator AgrA." *Proceedings of the National Academy of Sciences* 109(23): 9095-9100.
- Tal-Gan, Y., D. M. Stacy, M. K. Foegen, D. W. Koenig and H. E. Blackwell (2013).** "Highly Potent Inhibitors of Quorum Sensing in *Staphylococcus aureus* Revealed Through a Systematic Synthetic Study of the Group-III Autoinducing Peptide." *Journal of the American Chemical Society* 135(21): 7869-7882.

- Tankersley, A., M. B. Frank, M. Bebak and R. Brennan (2014).** "Early effects of *Staphylococcus aureus* biofilm secreted products on inflammatory responses of human epithelial keratinocytes." *Journal of Inflammation* 11(1): 17.
- Tazuke, Y., R. A. Drongowski, D. H. Teitelbaum and A. G. Coran (2003).** "Interleukin-6 changes tight junction permeability and intracellular phospholipid content in a human enterocyte cell culture model." *Pediatric Surgery International* 19(5): 321-325.
- Thakoersing, V. S., G. S. Gooris, A. Mulder, M. Rietveld, A. El Ghalbzouri and J. A. Bouwstra (2011).** "Unraveling Barrier Properties of Three Different In-House Human Skin Equivalents." *Tissue Engineering Part C: Methods* 18(1): 1-11.
- Thakoersing, V. S., J. van Smeden, A. A. Mulder, R. J. Vreeken, A. El Ghalbzouri and J. A. Bouwstra (2013).** "Increased Presence of Monounsaturated Fatty Acids in the Stratum Corneum of Human Skin Equivalents." *Journal of Investigative Dermatology* 133(1): 59-67.
- Thammavongsa, V., H. K. Kim, D. Missiakas and O. Schneewind (2015).** "Staphylococcal manipulation of host immune responses." *Nature reviews. Microbiology* 13(9): 529-543.
- Tokumasu, R., K. Yamaga, Y. Yamazaki, H. Murota, K. Suzuki, A. Tamura, K. Bando, Y. Furuta, I. Katayama and S. Tsukita (2016).** "Dose-dependent role of claudin-1 in vivo in orchestrating features of atopic dermatitis." *Proceedings of the National Academy of Sciences* 113(28): E4061-E4068.
- Tsukita, S., M. Furuse and M. Itoh (2001).** "Multifunctional strands in tight junctions." *Nature Reviews Molecular Cell Biology* 2: 285-293.
- Turksen, K. and T. C. Troy (2002).** "Permeability barrier dysfunction in transgenic mice overexpressing claudin 6." *Development* 129(7): 1775-1784.
- Turnbaugh, P. J., R. E. Ley, M. Hamady, C. Fraser-Liggett, R. Knight and J. I. Gordon (2007).** "The human microbiome project: exploring the microbial part of ourselves in a changing world." *Nature* 449(7164): 804-810.
- Van Itallie, C. M. and J. M. Anderson (1997).** "Occludin confers adhesiveness when expressed in fibroblasts." *Journal of Cell Science* 110(9): 1113.
- Van Itallie, C. M., A. S. Fanning, J. Holmes and J. M. Anderson (2010).** "Occludin is required for cytokine-induced regulation of tight junction barriers." *Journal of Cell Science* 123(16): 2844-2852.
- Van Itallie, C. M., J. Holmes, A. Bridges, J. L. Gookin, M. R. Coccaro, W. Proctor, O. R. Colegio and J. M. Anderson (2008).** "The density of small tight junction pores varies among cell types and is increased by expression of claudin-2." *Journal of Cell Science* 121(3): 298-305.
- van Rensburg, J. J., L. Dbeibo and S. M. Spinola (2016).** The Cutaneous Microbiota as a Determinant of Skin Barrier Function: Molecular Interactions and Therapeutic Opportunities. *Skin Stress Response Pathways*:

*Environmental Factors and Molecular Opportunities*. G. T. Wondrak. Cham, Springer International Publishing: 379-401.

**van Smeden, J., M. Janssens, E. C. J. Kaye, P. J. Caspers, A. P. Lavrijsen, R. J. Vreeken and J. A. Bouwstra (2014)**. "The importance of free fatty acid chain length for the skin barrier function in atopic eczema patients." *Experimental Dermatology* 23(1): 45-52.

**Vu, A. T., X. Chen, Y. Xie, S. Kamijo, H. Ushio, J. Kawasaki, M. Hara, S. Ikeda, K. Okumura, H. Ogawa and T. Takai (2011)**. "Extracellular Double-Stranded RNA Induces TSLP via an Endosomal Acidification- and NF- $\kappa$ B-Dependent Pathway in Human Keratinocytes." *Journal of Investigative Dermatology* 131(11): 2205-2212.

**Vuong, C. and M. Otto (2002)**. "Staphylococcus epidermidis infections." *Microbes and infection / Institut Pasteur* 4(4): 481-489.

**Wang, B., B. J. McHugh, A. Qureshi, D. J. Campopiano, D. J. Clarke, J. R. Fitzgerald, J. R. Dorin, R. Weller and D. J. Davidson (2017)**. "IL-1 $\beta$ -Induced Protection of Keratinocytes against Staphylococcus aureus-Secreted Proteases Is Mediated by Human  $\beta$ -Defensin 2." *Journal of Investigative Dermatology* 137(1): 95-105.

**Watson, R. E., R. Poddar, J. M. Walker, I. McGuill, L. M. Hoare, C. E. Griffiths and A. O'Neill C (2007)**. "Altered claudin expression is a feature of chronic plaque psoriasis." *The Journal of Pathology* 212(4): 450-458.

**Wertheim, H. F. L., D. C. Melles, M. C. Vos, W. van Leeuwen, A. van Belkum, H. A. Verbrugh and J. L. Nouwen (2005)**. "The role of nasal carriage in Staphylococcus aureus infections." *The Lancet Infectious Diseases* 5(12): 751-762.

**Williams, A. F. and A. N. Barclay (1988)**. "The immunoglobulin superfamily—domains for cell surface recognition." *Annual review of immunology* 6(1): 381-405.

**Williams, M. R., T. Nakatsuji, J. A. Sanford, A. F. Vrbanc and R. L. Gallo (2016)**. "Staphylococcus aureus Induces Increased Serine Protease Activity in Keratinocytes." *Journal of Investigative Dermatology*.

**Williams, R. E. A., A. G. Gibson, T. C. Aitchison, R. Lever and R. M. Mackie (1990)**. "Assessment of a contact-plate sampling technique and subsequent quantitative bacterial studies in atopic dermatitis." *British Journal of Dermatology* 123(4): 493-501.

**Winge, M. C. G., K. D. Bilcha, A. Liedén, D. Shibeshi, A. Sandilands, C. F. Wahlgren, W. H. I. McLean, M. Nordenskjöld and M. Bradley (2011)**. "Novel filaggrin mutation but no other loss-of-function variants found in Ethiopian patients with atopic dermatitis." *British Journal of Dermatology* 165(5): 1074-1080.

**Wong, V. (1997)**. "Phosphorylation of occludin correlates with occludin localization and function at the tight junction." *American Journal of Physiology - Cell Physiology* 273(6): C1859-C1867.



- Yamamoto, T., T. Kojima, M. Murata, K.-i. Takano, M. Go, H. Chiba and N. Sawada (2004).** "IL-1 $\beta$  regulates expression of Cx32, occludin, and claudin-2 of rat hepatocytes via distinct signal transduction pathways." *Experimental Cell Research* 299(2): 427-441.
- Yarwood, J. M. and P. M. Schlievert (2003).** "Quorum sensing in Staphylococcus infections." *The Journal of Clinical Investigation* 112(11): 1620-1625.
- Ye, J., A. Garg, C. Calhoun, K. R. Feingold, P. M. Elias and R. Ghadially (2002).** "Alterations in cytokine regulation in aged epidermis: implications for permeability barrier homeostasis and inflammation." *Experimental Dermatology* 11(3): 209-216.
- Yokouchi, M., A. Kubo, H. Kawasaki, K. Yoshida, K. Ishii, M. Furuse and M. Amagai (2015).** "Epidermal tight junction barrier function is altered by skin inflammation, but not by filaggrin-deficient stratum corneum." *Journal of Dermatological Science* 77(1): 28-36.
- Yoshida, K., A. Kubo, H. Fujita, M. Yokouchi, K. Ishii, H. Kawasaki, T. Nomura, H. Shimizu, K. Kouyama, T. Ebihara, K. Nagao and M. Amagai (2014).** "Distinct behavior of human Langerhans cells and inflammatory dendritic epidermal cells at tight junctions in patients with atopic dermatitis." *The Journal of allergy and clinical immunology* 134(4): 856-864.
- Yoshida, K., M. Yokouchi, K. Nagao, K. Ishii, M. Amagai and A. Kubo (2013).** "Functional tight junction barrier localizes in the second layer of the stratum granulosum of human epidermis." *Journal of Dermatological Science* 71(2): 89-99.
- Yoshida, Y., K. Morita, A. Mizoguchi, C. Ide and Y. Miyachi (2001).** "Altered expression of occludin and tight junction formation in psoriasis." *Archives of Dermatological Research* 293: 239-244.
- Yu, H. S., M. J. Kang, J. W. Kwon, S. Y. Lee, E. Lee, S. I. Yang, Y. H. Jung, K. Hong, Y. J. Kim, S. H. Lee, H. J. Kim, H. Y. Kim, J. H. Seo, B. J. Kim, H. B. Kim and S. J. Hong (2015).** "Claudin-1 polymorphism modifies the effect of mold exposure on the development of atopic dermatitis and production of IgE." *The Journal of allergy and clinical immunology* 135(3): 827-830 e825.
- Yuki, T., A. Hachiya, A. Kusaka, P. Sriwiriyanont, M. O. Visscher, K. Morita, M. Muto, Y. Miyachi, Y. Sugiyama and S. Inoue (2011a).** "Characterization of tight junctions and their disruption by UVB in human epidermis and cultured keratinocytes." *Journal of Investigative Dermatology* 131(3): 744-752.
- Yuki, T., A. Haratake, H. Koishikawa, K. Morita, Y. Miyachi and S. Inoue (2007).** "Tight junction proteins in keratinocytes: localization and contribution to barrier function." *Experimental Dermatology* 16(4): 324-330.
- Yuki, T., M. Tobiiishi, A. Kusaka-Kikushima, Y. Ota and Y. Tokura (2016).** "Impaired Tight Junctions in Atopic Dermatitis Skin and in a Skin-Equivalent Model Treated with Interleukin-17." *PLoS One* 11(9): e0161759.
- Yuki, T., H. Yoshida, Y. Akazawa, A. Komiya, Y. Sugiyama and S. Inoue (2011b).** "Activation of TLR2 enhances tight junction barrier in epidermal keratinocytes." *The Journal of Immunology* 187(6): 3230-3237.

## LISTS OF FIGURES AND TABLES

---

### *List of Figures*

#### *Introduction*

**Figure 1:** Schematic overview on the skin composition, in particular the epidermal composition.

**Figure 2:** Reconstructed human epidermis under air-liquid-interface conditions.

**Figure 3:** Ultrathin sectional view of tight junctions.

**Figure 4:** Schematic overview of the basic structural transmembrane components of tight junctions.

**Figure 5:** Schematic overview of distribution patterns of tight junction proteins within the epidermis and immunohistochemical stainings of claudin-1 (Cldn-1), occludin, Cldn-4 and zonula-occludens-1 in normal human skin.

**Figure 6:** Schematic drawing denoting the different barriers in the epidermis and their interaction with the tight junction barrier.

**Figure 7:** The influence of Staphylococci on epidermal tight junctions.

**Figure 8:** Alteration of tight junction proteins in skin diseases.

**Figure 9:** The vicious cycle in atopic dermatitis.

#### *Material and methods*

**Figure 10:** Schematic drawing of the submerged model.

**Figure 11:** Schematic drawing of the different types of 3D models used within this work.

**Figure 12:** Visualization of PCR products of TetM cassette in  $\Delta agr$  strains.

**Figure 13:** Schematic drawing of the small spatula made out of Pasteur-pipettes used for spreading of the bacteria on top of PFe3D models.

**Figure 14:** Exemplary schematic installation of transepithelial electrical resistance measurement with an epithelial voltohmmeter on submerged culture.

**Figure 15:** Examples for “complete stops” and “half stops” of Biotin-SH in PFe3D.

#### *Results*

**Figure 16:** Tight junction barrier properties of the submerged model.

**Figure 17:** Haematoxylin and eosin staining and immunohistochemical stainings of the submerged model 3 days after  $\text{Ca}^{2+}$ -switch.

**Figure 18:** Haematoxylin and eosin staining of reconstructed human epidermis after the protocol of CellnTec (CnTe3D).

**Figure 19:** Immunohistochemical stainings of tight junction proteins in reconstructed human epidermal models after the protocol of CellnTec.

**Figure 20:** Tight junction functionality of reconstructed human epidermal models after the protocol of CellnTec (CnTe3D).

**Figure 21:** Transepithelial electrical resistance of reconstructed human epidermal models after the protocol of CellnTec over time after lifting to air-liquid-interface.

**Figure 22:** Haematoxylin and eosin stainings of reconstructed human epidermis after the protocol of Pierre Fabre (PFe3D).

**Figure 23:** Immunohistochemical stainings of tight junction proteins in reconstructed human epidermal models after the protocol of Pierre Fabre (PFe3D).

**Figure 24:** Tight junction functionality of reconstructed human epidermal models after the protocol of Pierre Fabre (PFe3D).

**Figure 25:** Tight junction functionality and Haematoxylin and eosin staining of reconstructed human epidermal models after the protocol of Pierre Fabre (PFe3D) on day 4 of ALI.

**Figure 26:** Transepithelial electrical resistance of reconstructed human epidermal models after the protocol of Pierre Fabre over time after lifting to air-liquid-interface.

**Figure 27:** Hematoxylin and eosin stainings of reconstructed human skin models.

**Figure 28:** Immunohistochemical stainings of tight junction proteins and tight junction functionality of reconstructed human skin on day 8 of air-liquid-interface.

**Figure 29:** Transepithelial electrical resistance of submerged models after staphylococcal inoculation.

**Figure 30:** Tight junction functionality after staphylococcal inoculation displayed by transepithelial electrical resistance and the permeability of a 4 kDa tracer (FD4).

**Figure 31:** Tissue viability of the submerged model after inoculation with  $6 \times 10^5$  *S. aureus* or *S. epidermidis*  $\text{cm}^{-2}$  compared to the uninfected control.

**Figure 32:** Immunohistochemical stainings of tight junction proteins of the submerged model after 12 h of staphylococcal inoculation.

**Figure 33:** Immunohistochemical stainings of tight junction proteins of the submerged model after 24 h of staphylococcal inoculation.

**Figure 34:** Relative mRNA expression of tight junction proteins of the submerged model after staphylococcal inoculation.

**Figure 35:** Western Blot analysis of Claudin-1 (Cldn-1) and Cldn-4 in the submerged model after short-term bacterial challenge.

**Figure 36:** Western Blot analysis of occludin in the submerged model after short-term bacterial challenge.

**Figure 37:** Western Blot analysis of Claudin-1 (Cldn-1) and Cldn-4 in the submerged model after long-term bacterial challenge.

**Figure 38:** Western Blot analysis of occludin in the submerged model after long-term bacterial challenge.

**Figure 39:** Relative mRNA expression of antimicrobial peptides of the submerged culture after staphylococcal challenge.

**Figure 40:** Relative mRNA expression of proinflammatory cytokines of the submerged culture after staphylococcal challenge.

**Figure 41:** Relative cytokine protein levels of the supernatant of submerged models after staphylococcal challenge.

**Figure 42:** Transepithelial electrical resistance of the submerged model after *S. aureus* inoculation and parallel treatment with proinflammatory cytokines.

**Figure 43:** Transepithelial electrical resistance of the submerged model after inoculation with *S. aureus* wild-type (WT), a *S. aureus* mutant lacking the accessory gene reulator ( $\Delta agr$ ) or *S. carnosus*, representing an apathogenic strain.

**Figure 44:** Bacterial growth on top of PFe3D models.

**Figure 45:** Growth of *S. aureus* on PFe3D after *S. epidermidis* pretreatment.

**Figure 46:** Haematoxylin and eosin staining of PFe3D after staphylococcal challenge.

**Figure 47:** Transepithelial electrical resistance of PFe3D after staphylococcal challenge.

**Figure 48:** Biotinylation assay of PFe3D models after staphylococcal inoculation.

**Figure 49:** Biotin tracer permeability of PFe3D models after staphylococcal inoculation.

**Figure 50:** Viability assay of long-term infected PFe3D with *S. aureus*.

**Figure 51:** Immunofluorescence staining of Claudin-1 in PFe3D models after staphylococcal challenge.

**Figure 52:** Immunofluorescence staining of Claudin-4 in PFe3D models after staphylococcal challenge.

**Figure 53:** Immunofluorescence staining of occludin in PFe3D models after staphylococcal challenge.

**Figure 54:** Analyses of immunointensity of tight junction proteins on PFe3D models after long-term staphylococcal challenge.

**Figure 55:** Western Blot analyses of claudin-1 (Cldn-1) and Cldn-4 of PFe3D models after long-term *S. aureus* inoculation.

**Figure 56:** Western Blot analyses of occludin of PFe3D models after *S. aureus* inoculation.

**Figure 57:** Flow chart of experimental procedure in order to mimick atopic dermatitis-like conditions in submerged models by pretreatment with a cytokine-toll-like-receptor-agonist-mix (CTM) before infection with *S. aureus* or *S. epidermidis*.

**Figure 58:** Transepithelial electrical resistance of submerged model after induction of atopic dermatitis mimicking conditions (CTM-treatment).

**Figure 59:** Transepithelial electrical resistance of submerged models after induction of atopic dermatitis mimicking conditions (CTM-pretreatment) followed by staphylococcal challenge.

**Figure 60:** Transepithelial electrical resistance of submerged models after treatment with an atopic dermatitis mimicking mix (CTM) or its single components upon *S. aureus* inoculation.

## Discussion

**Figure 61:** Characterisation of PFe3D at day 4 of air-liquid-interface.

**Figure 62:** Schematic overview of possible processes during short-term inoculation with *S. aureus* or *S. epidermidis* on tight junction barrier increase in submerged models.

**Figure 63:** Schematic overview of possible processes in tight junction barrier breakdown during long-term inoculation with *S. aureus* or *S. epidermidis* of PFe3D and submerged models.

**Figure 64:** Schematic overview on putative events that happen in the epidermis after bacterial challenge in the course of time.

**Figure 65:** Schematic overview of possible interactions that could lead to an increased tight junction barrier function in the early phase of bacterial inoculation and to a TJ barrier breakdown during later treatment.

## *List of Tables*

**Table 1:** List of abbreviations used in this work.

**Table 2:** List of measurement units and symbols used in this work.

**Table 3:** Listing of chemicals and their origins used within this work.

**Table 4:** Listing of the devices and their origins used within this work.

**Table 5:** Antibodies and dilutions used within this work for Western Blot and immunohistochemical stainings.

**Table 6:** FAM dye-labeled real-time PCR (qRT–PCR) TaqMan MGB probes and their catalogue numbers.

**Table 7:** Software and its origin used during this work.

**Table 8:** Listing of bacterial strains that have been used during this work.

**Table 9:** Composition of SDS-PAGE gels of different pore sizes.

**Table 10:** Advantages and disadvantages of the different model systems investigated in this work.

## DANKSAGUNG

---

Diese Arbeit hätte nicht entstehen können ohne die Unterstützung, die ich von vielen Seiten erfahren habe. Dafür möchte ich mich herzlich bedanken.

Mein besonderer Dank geht an Frau Prof. Dr. Johanna Brandner nicht nur für die Bereitstellung des spannenden und vielseitigen Themas, sondern insbesondere für die engagierte und herzliche Betreuung. Durch das entgegengebrachte Vertrauen hatte ich die Möglichkeit mich selbständig, wissenschaftlich zu entfalten, aber dennoch durch konstruktive Kritik und die ständige Ansprechbarkeit (auch in stressigen Zeiten) in die richtige Richtung gelenkt zu werden. Auch für die aufmunternden Worte und das Verständnis in Phasen des Zweifels sowie persönlicher Krisen bin ich sehr dankbar.

Ich danke Herrn Prof. Dr. Thorsten Burmester für die Zweitbetreuung seitens des Fachbereichs Biologie der Universität Hamburg.

Frau Prof. Dr. Ingrid Moll und Herrn Prof. Dr. Stefan W. Schneider danke ich für die Möglichkeit, meine Dissertation im Zellbiologischen Labor der Klinik und Poliklinik für Dermatologie und Venerologie des UKE anfertigen zu können.

Der Firma Pierre Fabre Dermo-cosmétique danke ich für die finanzielle Unterstützung meiner Arbeit und die Bereitstellung ihres epidermalen 3D-Modells. Dabei möchte ich insbesondere Frau Dr. Hélène Duplan, Frau Dr. Marie-Florence Galliano sowie Herrn Antony Caruana für anregende Diskussionen und die nette Zusammenarbeit danken.

Herrn Prof. Dr. Holger Rohde danke ich für die Bereitstellung der Bakterien-Stämme und die Möglichkeit zur Nutzung der Laborräume. Sowie Frau Gesche Kroll und Samira Weißelberg für die freundliche Anleitung und Unterstützung.

Des Weiteren danke ich allen Mitarbeitern des zellbiologischen Labors der Klinik und Poliklinik für Dermatologie und Venerologie des UKE für das freundschaftliche Miteinander, das tolle Arbeitsklima und die hilfreichen Diskussionen (und auch das Ertragen meiner Gesangseinlagen). Vor allem möchte ich mich hier bei den technischen Assistentinnen Pia Houdek, Sabine Vidal-y-sy und Ewa Wladykowski bedanken, die mir immer mit Rat und Tat beruflich, wie privat zur Seite standen. Außerdem danke ich Herrn Dr. Thomas Volksdorf für die Hilfestellung bei der statistischen Auswertung.

Ganz besonders herzlich möchte ich mich bei meinen Freunden und meiner Familie – meinen Eltern und verstorbenen Großeltern – bedanken, die mich mit viel Ausdauer und Verständnis begleitet haben. Vielen Dank für euer Vertrauen, eure Liebe und Unterstützung in jeglicher Art!

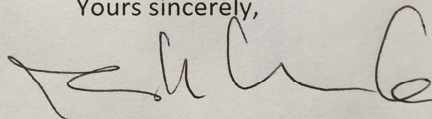
## CERTIFICATE OF LANGUAGE PROOF

---

### Certificate of Language Proof

I, Mark Kanak, am a native English speaker and hereby confirm that this PhD thesis by Katja Bäsler has been written in acceptable English and has been reviewed and approved by me.

Yours sincerely,

A handwritten signature in black ink, appearing to read 'Mark Kanak', written in a cursive style.

Mark Kanak

## DECLARATION OF AUTHORSHIP

### EIDESSTATTLICHE VERSICHERUNG

---

I hereby declare, on oath, that I have written the present dissertation by my own and have not used other than the acknowledged resources and aids.

Hiermit erkläre ich an Eides statt, dass ich die vorliegende Dissertationsschrift selbst verfasst und keine anderen als die angegebenen Quellen und Hilfsmittel benutzt habe.

Hamburg, 08<sup>th</sup> of October 2017



---

Katja Bäsler